RIGHT VENTRICULAR ADAPTATION

in conditions of **increased pressure load**

Anne-Marie C. Koop

RIGHT VENTRICULAR ADAPTATION

in conditions of increased pressure load

ANNE-MARIE C. KOOP

Right ventricular adaptation in conditions of increased pressure load
PhD thesis, University of Groningen

Author:	Anne-Marie Koop
Cover design:	Stefan Heinrich & Willemijn Vismans
Text lay-out:	Stefan Heinrich | www.publiss.nl
Printing:	Ridderprint | www.ridderprint.nl
ISBN (printed book):	978-94-6416-264-6
ISBN (e-book):	978-94-6416-265-3

Financial support for the publication of this thesis was kindly provided by:

ABN Amro
Chipsoft
Guerbet Nederland
Koop Communicatie
Medis Medical Imaging Systems
Pfizer
Rijksuniversiteit Groningen
Salveo Medical
Spinalis ergonomische stoelen

Financial support by the Dutch Heart Foundation for the publication of this thesis is gratefully acknowledged.

rijksuniversiteit
groningen

Right ventricular adaptation

In conditions of increased pressure load

Proefschrift

ter verkrijging van de graad van doctor aan de
Rijksuniversiteit Groningen
op gezag van de
rector magnificus prof. dr. C. Wijmenga
en volgens besluit van het College voor Promoties.

De openbare verdediging zal plaatsvinden op

woensdag 25 november 2020 om 09.00 uur

door

Anne-Marie Catherine Koop

geboren op 7 september 1990
te Houten

Promotor
Prof. dr. R.M.F. Berger
Dr. H.H.W. Silljé

Copromotores
Dr. D.P.Y. Koonen
Dr. B. Bartelds

Beoordelingscommissie
Prof. dr. F. Kuipers
Prof. dr. T. Ebels
Prof. dr. H.J. Bogaard

CONTENT

1

CHAPTER 1

INTRODUCTION

A.M.C. Koop

Nowadays, heart failure affects more than 26 million people worldwide and is an important cause of morbidity and mortality.[1] Heart failure can result from various pathologic conditions, including sustained abnormal loading conditions due to valve abnormalities, septal defects or pulmonary hypertension.[2] Deterioration of left ventricular (LV) function has long been considered as the leading determining factor of well-being and survival in this group of patients. However, over the last decades, it has become increasingly clear that in patients with congenital heart defects[3], pulmonary hypertension[3,4] and LV disease[5–9], the right ventricular (RV) function is an important determinant of outcome. RV adaptation is a continuum from beneficial to pathologic remodelling, accompanied with metabolic and hemodynamic changes, which eventually contributes to clinical right sided heart failure. In the last years, scientific statements have been published regarding RV disease, aiming at better guidance to clinical management.[10,11] These statements report that interventions targeting RV failure have not been well investigated yet and RV specific therapies are still unavailable. After years of ignoring the relevance of the RV in cardiac disease, it is time to rapidly expand the knowledge of RV adaptation to pathological conditions. This will improve the identification of patients affected by RV disease and optimize their treatment options.

Definition of right ventricular failure

Right sided heart failure is a clinical syndrome with sypmtoms as epigastric fullness, ankle swelling and fatigue.(see **table 1**) as a result of changes in structure and function of the right heart circulatory system.[12] The right ventricle plays a central role in the development of right sided heart failure. The inability to adequately pump blood into the lungs and the increased stiffness of the RV leads to increased central venous pressure (CVP) and reduced LV filling.[2,13] This results from the reduced RV stroke volume and the interventricular dependence as a consequence of RV dilatation. Both congestion (backward failure) and reduced cardiac output (forward failure) contribute to impaired organ function. RV failure may lead to hepatic congestion with subsequent laboratory abnormalities in the liver integral.[14,15] Renal function is predominantly affected by the increase of CVP,[16] but also by the insufficient circulation as a result of forward failure, leading to fluid retention and reduced urine output.[13] Reduced gastrointestinal absorption and malnutrition can be the consequence of both reduced CO and increased CVP, where the latter contributes to deficient abdominal lymph flow leading to interstitial and visceral oedema.[17] This mechanism also applies to the lung, where decreased lymphatic drainage contributes to pulmonary oedema and pleural effusions.[2]

Table 1. Clinical presentation of RV failure.

Symptoms, e.g.:	Signs, e.g.:
- epigastric fullness,	- jugular venous distention,
- right upper abdominal discomfort,	- third heart sound,
- ankle swelling,	- hepatomegaly,
- dyspnea or tachypnea, and	- ascites, and
- fatigue.	- peripheral oedema.

Determination of RV dysfunction

RV dysfunction precedes RV failure and is reflected by worsening of RV hemodynamic parameters derived by echocardiography, cardiac magnetic resonance imaging (CMR) or heart catheterization. Early recognition of RV dysfunction is important to halt further deterioration of RV function and clinical status. Contraction of the RV is a movement against the septum, ending with a wringing movement in longitudinal direction. Most frequently used parameter of RV systolic function is based on this longitudinal function derived by echocardiography: the tricuspid annular plane systolic excursion (TAPSE). Although this marker may be of prognostic value in various diseases,[18,19] it incompletely reflects RV systolic function. In addition,

Early recognition of RV dysfunction is important to halt further deterioration of RV function and clinical status.

RV function encompasses also RV diastolic function. Parameters reflecting diastolic dysfunction are E/A ratio[1], deceleration time[2] and E/e' ratio[3] derived by echocardiography and the slope of the end diastolic pressure volume relationship, i.e. the end-diastolic elastance (Eed), derived by heart catheterization. However, RV diastolic function is still insufficiently considered in both clinical practice and scientific research. In **chapter 2** we will carefully look into the role of diastolic dysfunction in the progression towards RV failure.

In the last decades, CMR is being progressively used to characterize cardiac disease. CMR enables tissue characterization, and may be especially of added value in determining dimensions and function used in more complex RV morphology as in CHD.[20,21] A great advantage is the opportunity for 3D approach instead of the echocardiographic 2D approach. Because of the complex RV anatomy, quality of the views and parameters are dependent of the echocardiographic skills of the executor. In **chapter 6** and **7** we illustrate the use of CMR in experimental setting of increased RV pressure overload, as has been described in the protocol presented in **chapter 5.**

Right ventricular physiology

Although in utero the LV and RV are exposed to a similar pressure load, in the post-natal period rapid unloading of the RV takes place.[22] Under normal conditions, the adult RV pumps blood into the lung circulation which has a relatively low resistance. In pathologic conditions, RV afterload may increase up to five times, while in pathologic conditions of the LV, i.e. systemic hypertension, afterload will maximally increase up to 50% (**figure 1**).[23]

1 E/A ratio: where E represents the RV pressure during early diastolic filling and A represents the RV pressure during late diastolic filling, caused by the atrial contraction
2 deceleration time: time taken from the maximum E point to baseline
3 E/e' ratio: where E represents the RV pressure during early diastolic filling and e' represents myocardial relaxation

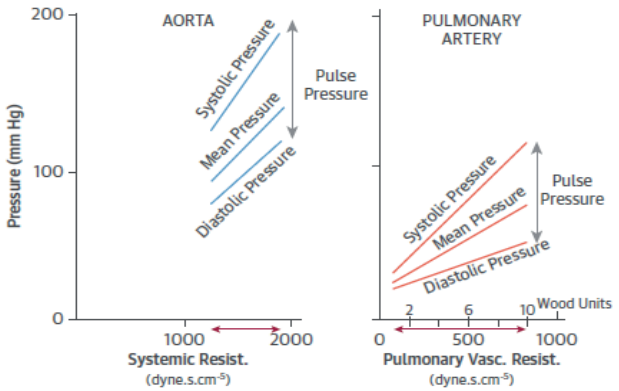

Figure 1. Relative increases in aorta versus pulmonary artery pressure in case of increasing afterload. Vonk Noordegraaf et al. JACC 2017.

The term "cardiac dysfunction" often refers to systolic dysfunction. However, also diastolic function significantly affects cardiac function. RV diastolic dysfunction not only reduces stroke volume, but is also an important indicator of outcome.[24–26]

Right ventricular diastolic function is still insufficiently considered clinical practice and scientific research, while it is an important indicator of outcome.

Furthermore, because of the emergence of asynchronic contraction of the ventricles, the synergy of the RV with the LV will be lost.[27] In response to increased ventricular load, the RV is able to increase contractility four to five times to meet the increased afterload conditions with preservation of ventriculoarterial coupling. Moreover, in progressive RV disease the ventricular thickening will be halted and RV dilatation will occur. This dilatation attempts to retain stroke volume (SV) and, together with increase of heart rate, to maintain adequate cardiac output, but will eventually lead to ventriculoarterial uncoupling.[23,28] Ventriculoarterial uncoupling reflects the imbalance between the myocardial oxygen consumption and mechanical energy,[29] eventually leading to right sided heart failure.

Right ventricular remodelling

RV remodelling includes the presence of hypertrophy, altered angiogenesis and fibrosis.[30–33] In conditions of increased pressure load, the initial response will be the development of concentric hypertrophy, which will progress towards eccentric hypertrophy (dilatation) in case of persistent abnormal loading.[34,35] Concentric hypertrophy (wall thickening) aims to reduce wall stress and preserves the force development of the ventricle,[23] but will eventually lead to diminished diastolic function and contribution to Right ventricular remodelling processes aim to withstand the

increased pressure load of the right ventricle. However, these processes eventually leads to pathologic alternations contributing to the development of right ventricular failure..[31] In the process of adaptive towards maladaptive hypertrophy, several signalling pathways are involved. Activation of Akt (also known as protein kinase B) is associated with a physiological hypertrophic response,[36,37] whereas activation of the calcineurin/nuclear factor activated T-cells (NFAT)-signaling predominantly induces pathological features.[38–42] The hypertrophic response may be accompanied by a shift in type of myosin heavy chains. In particular, slow twitch -myosin heavy chains, which are more energy efficient, will relatively increase as compared to the fast twitch -myosin heavy chains.[43] This resembles the fetal situation, but in the adult heart this finally contributes to maladaptation. Due to the increased afterload, more nutrients and oxygen will be required in order to meet the increased energy demand for contraction.[23] Contrary, increased pressure load impairs angiogenesis, with subsequent capillary rarefaction which is associated with RV failure.[44,45] Angiogenesis involves signalling cascades including vascular endothelial growth factor (VEGF), forkhead transcription factor (FOXO1) and hypoxia inducible factor 1 (HIF1), which may be initiated by metabolic remodelling.[46] In the pressure loaded RV specifically, activation of angiogenic signalling differs in various pressure overload animal models.[45,47,48] Also fibrosis is a characteristic feature of RV adaptation due to increased pressure load conditions.[33,49,50] Fibrosis embodies collagen disposition induced by fibroblasts activated by macrophages via transforming growth factor , and affects cardiac stiffness, promotes arrhythmias and impairs oxygen diffusion to cardiomyocytes.[51–53] Fibrosis is in general considered as a pathological sign and contributes to further pathological remodelling. Hereby, the progression of remodelling correlates not only with the quantity but also the quality of fibrosis, expressed by type of fibrillar collagen and the degree of cross-linking.[54,55] Troughout the thesis, we have characterized various remodelling processes by the use of experimental models. Where previous studies mostly focussed on one particular time point, we aimed to characterize different stages of RV disease. In **chapter 2** we demonstrate the differences between compensated RV dysfunction and clinical RV failure, whereas **chapter 4** focusses on different timepoints in compensated RV dysfunction. Proper characterization at different time points and standardized methods will be pivotal for proper RV investigation.

Right ventricular metabolism

RV pressure load is accompanied with metabolic derangements.[56–58] RV metabolism may fulfil a central role in RV adaptation due to the interactions with various processes of RV remodelling.[2,57,59,60] In the healthy adult heart, fatty acid metabolism is the primary source of energy (60-90%), whereas glucose metabolism is present in lesser extent (10-40%).[61] During RV stress a fetal switch takes place, which incorporates altered metabolism.[43,62–66] Metabolism during fetal life relies predominantly on the substrates glucose and lactate, due to substrate availability and a greater efficiency in a low oxygen environment.[43,67] As result of the reactivation of the fetal program in the stressed adult myocardium, the oxidative metabolism of fatty acids switches back to glucose metabolism with predominance of glycolysis, which has been associated with high proliferative processes in various organs and tissues.[68–70] Next to increased use of glucose and lactate, also ketones and amino acids serve

Pressure load induces metabolic shifts associated with high proliferative processes.

as substrates in the stressed myocardium.[71] The role of fatty acid metabolism in the pressure loaded RV has been differently described in various models of RV pressure overload, and inhibition of fatty acid metabolism has been considered as a therapeutic option.[72–76] Therefore, we systematically reviewed glucose and fatty acid metabolism in the pressure loaded RV encompassing various models of increased RV pressure load in **chapter 3**. In addition, in **chapter 4**, we assessed the course of mitochondrial respiratory capacity in a model of fixed increased afterload over time. The roles of lipids in the RV, other than serving as a substrate, lipotoxic compound, anti-oxidant, or as part of the mitochondrial membrane, are sparsely studied.[77,78] We performed lipidomics to map alternations in intracardiac lipids in the pressure loaded RV in **chapter 4**.

Right ventricular molecular mechanisms

Recent work indicates that transcription factors may be differently regulated in the RV compared to the LV.[66] This stems from the different embryonic origin of the two ventricles. Regulatory mechanism in right ventricular adaptation may be different regulated compared to left ventricular adaptation because the different embryonic origin of both ventricles. The heart is formed out of two types of progenitor cells representing the primary and secondary heart field. The primary heart field forms the LV and the atria, whereas the second heart field forms the RV, the outflow tract and the atria.[79,80] Genetic transcription in the myocardium is regulated by transcription factors. Where some factors can be found in both heart fields, other transcription

factors are heart field specific. In fetal development of the heart, certain transcription factors are essential for RV development, i.e. islet 1, Nkx-2.5, GATA4, -5 or -6, and the embryonic basic helix-loop-helix transcription factor heart and neural crest derivatives expressed-2 (Hand2).[79,81–85] Deletion of these genes will be lethal or induce severe RV pathology.[86] On the other hand, some of these transcription factors contribute to pathologic remodelling in the stressed adult LV.[87] This raises the question what the role will be in the stressed adult RV. In the current thesis (**chapter 7**), we studied the role of Hand2 in the pressure loaded RV. Next to transcriptional activation, gene expression is also regulated at post-transcriptional level. In general, non-coding microRNA's (miR's) are progressively studied.[88–90] Studies in cardiac tissue show ventricular specific assessments expression levels of miR's.[91] However, the role of many of these miR's in the stressed RV still needs to be unravelled. This emphasizes the different origin of both ventricles and hereby the relevance of research clarifying the RV specific factors during post-fetal life in order to develop therapy targeting RV disease. In **chapter 6** we studied the role of miR-199b in the pressure loaded RV.

SCOPE OF THE THESIS

The general aim of this thesis was to investigate RV adaptation due to increased pressure load, at both molecular and functional level. Hereby, we specifically focused on RV metabolism and we tested whether previous identified molecular mechanisms of ventricular remodelling in the LV also apply to the RV.

OUTLINE OF THE THESIS

- **Chapter 2** Here we characterized a rat model of chronic pressure overload induced by pulmonary artery banding at different time points (at five weeks and time of termination) and disease severity (RV dysfunction versus clinical RV failure). In this model we assessed RV function by echocardiography and right heart catheterization, and molecular changes using RT-PCR, histological techniques and microarray analysis.
- **Chapter 3** In this chapter we describe metabolism in the pressure loaded RV by providing an overview of current available literature, specifically focusing on glucose and fatty acid metabolism. In this systematic review and meta-analysis both animal experiments and clinical studies were included.
- **Chapter 4** Temporal changes of RV function, remodelling and metabolism at two, five and twelve weeks were assessed in a rat model of RV pressure load. Furthermore, we performed lipidomics to assess the effect of pressure overload on the RV lipid content.

- **Chapter 5** Here describe a protocol for proper assessment of RV function and morphology by CMR in mice subjected to pulmonary artery banding.
- **Chapter 6** By using transgenic mice with miR-199b overexpression, it was tested whether miR-199b also accounts as a pro-hypertrophic factor in the RV subjected to pressure overload, as has been previously described in LV remodelling. In addition, we tested the role of miR-199b in the LV during RV pressure load.
- **Chapter 7** Hand2$^{F/F}$ and MCM-Hand2$^{F/F}$ mice were treated with tamoxifen and subjected to pulmonary artery banding to assess the role of Hand2 in adult RV remodelling in response to pressure overload. Since the role of Hand2 in the RV appeared to be different from the LV, we performed RNA sequence analysis in order to identify downstream targets of Hand2 in the pressure loaded RV specifically.
- **Chapter 8** We aimed to identify early stages of RV disease in children with a history of congenital heart disease or pulmonary hypertension using a multi-biomarker approach. Eight blood plasma derived biomarkers were taken of 125 children and correlated to the type and degree of RV loading, RV remodelling and RV function.
- **Chapter 9** This chapter discusses the main findings of this thesis and the subsequent future prospects in the field of RV adaptation due to increased pressure load.

REFERENCES

1. Ambrosy AP, Fonarow GC, Butler J, Chioncel O, Greene SJ, Vaduganathan M, Nodari S, Lam CSP, Sato N, Shah AN, Gheorghiade M. The global health and economic burden of hospitalizations for heart failure: Lessons learned from hospitalized heart failure registries. *J Am Coll Cardiol* Elsevier Inc; 2014;63:1123–1133.
2. Haddad F, Doyle R, Murphy DJ, Hunt SA. Right ventricular function in cardiovascular disease, part II: Pathophysiology, clinical importance, and management of right ventricular failure. *Circulation* 2008;117:1717–1731.
3. Norozi K, Wessel A, Alpers V, Arnhold JO, Geyer S, Zoege M, Buchhorn R. Incidence and Risk Distribution of Heart Failure in Adolescents and Adults With Congenital Heart Disease After Cardiac Surgery. *Am J Cardiol* 2006;97:1238–1243.
4. Wolferen SA Van, Marcus JT, Boonstra A, Marques KMJ, Bronzwaer JGF, Spreeuwenberg MD, Postmus PE, Vonk-Noordegraaf A. Prognostic value of right ventricular mass, volume, and function in idiopathic pulmonary arterial hypertension. *Eur Heart J* 2007;28:1250–1257.
5. Ghio S, Gavazzi A, Campana C, Inserra C, Klersy C, Sebastiani R, Arbustini E, Recusani F, Tavazzi L. Independent and Additive Prognostic Value of Right Ventricular Systolic Function and Pulmonary Artery Pressure in Patients With Chronic Heart Failure. *J Am Coll Cardiol* Elsevier Masson SAS; 2001;37:183–188.
6. Haddad F, Hunt SA, Rosenthal DN, Murphy DJ. Right ventricular function in cardiovascular disease, part I: Anatomy, physiology, aging, and functional assessment of the right ventricle. *Circulation* 2008;117:1436–1448.
7. Meyer P, Filippatos GS, Ahmed MI, Iskandrian AE, Bittner V, Perry GJ, White M, Aban IB, Mujib M, Italia LJD, Ahmed A. Effects of Right Ventricular Ejection Fraction on Outcomes in Chronic Systolic Heart Failure. 2010;252–259.
8. Mohammed SF, Hussain I, Abou Ezzeddine OF, Takahama H, Kwon SH, Forfia P, Roger VL, Redfield MM. Right ventricular function in heart failure with preserved ejection fraction: A community-based study. *Circulation* 2014;130:2310–2320.
9. Melenovsky V, Hwang SJ, Lin G, Redfield MM, Borlaug BA. Right heart dysfunction in heart failure with preserved ejection fraction. *Eur Heart J* 2014;35:3452–3462.
10. Konstam MA, Kiernan MS, Bernstein D, Bozkurt B, Jacob M, Kapur NK, Kociol RD, Lewis EF, Mehra MR, Pagani FD, Raval AN, Ward C. Evaluation and Management of Right-Sided Heart Failure: A Scientific Statement From the American Heart Association. Circulation. 2018.
11. Gorter TM, Veldhuisen DJ van, Bauersachs J, Borlaug BA, Celutkiene J, Coats AJS, Crespo-Leiro MG, Guazzi M, Harjola VP, Heymans S, Hill L, Lainscak M, Lam CSP, Lund LH, Lyon AR, Mebazaa A, Mueller C, Paulus WJ, Pieske B, Piepoli MF, Ruschitzka F, Rutten FH, Seferovic PM, Solomon SD, Shah SJ, Triposkiadis F, Wachter R, Tschöpe C, Boer RA de. Right heart dysfunction and failure in heart failure with preserved ejection fraction: mechanisms and management. Position statement on behalf of the Heart Failure Association of the European Society of Cardiology. *Eur J Heart Fail* 2018;20:16–37.
12. Mehra MR, Park MH, Landzberg MJ, Lala A, Waxman AB. Right heart failure: Toward a common language. *J Hear Lung Transplan*t 2014;33:123–126.
13. Harjola VP, Mebazaa A, Čelutkiene J, Bettex D, Bueno H, Chioncel O, Crespo-Leiro MG, Falk V, Filippatos G, Gibbs S, Leite-Moreira A, Lassus J, Masip J, Mueller C, Mullens W, Naeije R, Nordegraaf AV, Parissis J, Riley JP, Ristic A, Rosano G, Rudiger A, Ruschitzka F, Seferovic

P, Sztrymf B, Vieillard-Baron A, Yilmaz MB, Konstantinides S. Contemporary management of acute right ventricular failure: A statement from the Heart Failure Association and the Working Group on Pulmonary Circulation and Right Ventricular Function of the European Society of Cardiology. *Eur J Heart Fa*il 2016;18:226–241.

14. Poelzl G, Ess M, Mussner-Seeber C, Pachinger O, Frick M, Ulmer H. Liver dysfunction in chronic heart failure: Prevalence, characteristics and prognostic significance. *Eur J Clin Invest* 2012;42:153–163.
15. Allen LA, Felker GM, Pocock S, McMurray JJV, Pfeffer MA, Swedberg K, Wang D, Yusuf S, Michelson EL, Granger CB. Liver function abnormalities and outcome in patients with chronic heart failure: Data from the Candesartan in Heart Failure: Assessment of Reduction in Mortality and Morbidity (CHARM) program. *Eur J Heart Fail* 2009;11:170–177.
16. Damman K, Deursen VM van, Navis G, Voors AA, Veldhuisen DJ van, Hillege HL. Increased Central Venous Pressure Is Associated With Impaired Renal Function and Mortality in a Broad Spectrum of Patients With Cardiovascular Disease. *J Am Coll Cardiol* 2009;53:582–588.
17. Verbrugge FH, Dupont M, Steels P, Grieten L, Malbrain M, Tang WHW, Mullens W. Abdominal contributions to cardiorenal dysfunction in congestive heart failure. *J Am Coll Cardiol* 2013;62:485–495.
18. Mathai SC, Sibley CT, Forfia PR, Mudd JO, Fisher MR, Tedford RJ, Lechtzin N, Boyce D, Hummers LK, Housten T, Zaiman AL, Girgis RE, Hassoun PM. Tricuspid annular plane systolic excursion is a robust outcome measure in systemic sclerosis-associated pulmonary arterial hypertension. *J Rheumatol* 2011;38:2410–2418.
19. Mazurek JA, Vaidya A, Mathai SC, Roberts JD, Forfia PR. Follow-up tricuspid annular plane systolic excursion predicts survival in pulmonary arterial hypertension. *Pulm Circ* 2017;**7**:361–371.
20. Lu X, Nadvoretskiy V, Bu L, Stolpen A, Ayres N, Pignatelli RH, Kovalchin JP, Grenier M, Klas B, Ge S. Accuracy and Reproducibility of Real-Time Three-Dimensional Echocardiography for Assessment of Right Ventricular Volumes and Ejection Fraction in Children. *J Am Soc Echocardiogr* 2008;21:84–89.
21. Soriano BD, Hoch M, Ithuralde A, Geva T, Powell AJ, Kussman BD, Graham DA, Tworetzky W, Marx GR. Matrix-array 3-dimensional echocardiographic assessment of volumes, mass, and ejection fraction in young pediatric patients with a functional single ventricle: A comparison study with cardiac magnetic resonance. *Circulation* 2008;117:1842–1848.
22. Rudolph AM. The changes in the circulation after birth. Their importance in congenital heart disease. *Circulatio*n 1970;41:343–359.
23. Vonk Noordegraaf A, Westerhof BE, Westerhof N. The Relationship Between the Right Ventricle and its Load in Pulmonary Hypertension. *J Am Coll Cardiol* 2017;69:236–243.
24. Borgdorff M a J, Bartelds B, Dickinson MG, Steendijk P, Vroomen M de, Berger RMF. Distinct loading conditions reveal various patterns of right ventricular adaptation. *Am J Physiol Heart Circ Physiol* 2013;305:H354-64.
25. Yu CM, Sanderson JE, Chan S, Yeung L, Hung YT, Woo KS. Right Ventricular Diastolic Dysfunction in Heart Failure. p. 1509–1514.
26. Trip P, Rain S, Handoko ML, DerBruggen C Van, Bogaard HJ, Marcus JT, Boonstra A, Westerhof N, Vonk-Noordegraaf A, S De Man F. Clinical relevance of right ventricular diastolic stiffness in pulmonary hypertension. *Eur Respir J* 2015;45:1603–1612.

27. Marcus JT, Gan CTJ, Zwanenburg JJM, Boonstra A, Allaart CP, Götte MJW, Vonk-Noordegraaf A. Interventricular Mechanical Asynchrony in Pulmonary Arterial Hypertension. Left-to-Right Delay in Peak Shortening Is Related to Right Ventricular Overload and Left Ventricular Underfilling. *J Am Coll Cardiol* 2008;51:750–757.

28. Lahm T, Douglas IS, Archer SL, Bogaard HJ, Chesler NC, Haddad F, Hemnes AR, Kawut SM, Kline JA, Kolb TM, Mathai SC, Mercier O, Michelakis ED, Naeije R, Tuder RM, Ventetuolo CE, Vieillard-Baron A, Voelkel NF, Vonk-Noordegraaf A, Hassoun PM. Assessment of right ventricular function in the research setting: Knowledge gaps and pathways forward an official American thoracic society research statement. *Am J Respir Crit Care Med* 2018;198:e15–e43.

29. Vonk-Noordegraaf A, Haddad F, Chin KM, Forfia PR, Kawut SM, Lumens J, Naeije R, Newman J, Oudiz RJ, Provencher S, Torbicki A, Voelkel NF, Hassoun PM. Right heart adaptation to pulmonary arterial hypertension: Physiology and pathobiology. *J Am Coll Cardiol* 2013;62:22–33.

30. Correia-Pinto J, Henriques-Coelho T, Roncon-Albuquerque R, Leite-Moreira AF. Differential right and left ventricular diastolic tolerance to acute afterload and NCX gene expression in wistar rats. *Physiol Res* 2006;55:513–526.

31. Rain S, Handoko ML, Trip P, Gan CT-J, Westerhof N, Stienen GJ, Paulus WJ, Ottenheijm CAC, Marcus JT, Dorfmüller P, Guignabert C, Humbert M, Macdonald P, Remedios C Dos, Postmus PE, Saripalli C, Hidalgo CG, Granzier HL, Vonk-Noordegraaf A, Velden J Van Der, Man FS De. Right ventricular diastolic impairment in patients with pulmonary arterial hypertension. *Circulation* F.S. De Man, Department of Pulmonology, VU University Medical Center, Institute for Cardiovascular Research, 1081 HV Amsterdam, Netherlands; 2013;128:2016–2025.

32. Rain S, Andersen S, Najafi A, Schultz JG, Silva Gonçalves Bós D Da, Handoko ML, Bogaard H-J, Vonk-Noordegraaf A, Andersen A, Velden J Van Der, Ottenheijm CAC, Man FS De. Right ventricular myocardial stiffness in experimental pulmonary arterial hypertension. *Circ Hear Fail* F.S. De Man, Department of Pulmonology, Vrije Universiteit University Medical Center, Amsterdam, Netherlands; 2016;9.

33. Bartelds B, Borgdorff M a., Smit-Van Oosten A, Takens J, Boersma B, Nederhoff MG, Elzenga NJ, Gilst WH Van, Windt LJ De, Berger RMF. Differential responses of the right ventricle to abnormal loading conditions in mice: Pressure vs. volume load. *Eur J Heart Fail* 2011;13:1275–1282.

34. Rossi MA, Carillo S V. Cardiac hypertrophy due to pressure and volume overload: distinctly different biological phenomena? *Int J Cardiol* 1991;31:133–141.

35. Grossman W. Cardiac hypertrophy: Useful adaptation or pathologic process? *Am J Med* 1980;69:576–584.

36. Yeves AM, Villa-Abrille MC, Pérez NG, Medina AJ, Escudero EM, Ennis IL. Physiological cardiac hypertrophy: Critical role of AKT in the prevention of NHE-1 hyperactivity. *J Mol Cell Cardiol* Elsevier Ltd; 2014;76:186–195.

37. DeBosch B, Treskov I, Lupu TS, Weinheimer C, Kovacs A, Courtois M, Muslin AJ. Akt1 is required for physiological cardiac growth. *Circulation* 2006;113:2097–2104.

38. Zou Y, Hiroi Y, Uozumi H, Takimoto E, Toko H, Zhu W, Kudoh S, Mizukami M, Shimoyama M, Shibasaki F, Nagai R, Yazaki Y, Komuro I. Calcineurin plays a critical role in the development of pressure overload-induced cardiac hypertrophy. *Circulation* 2001;104:97–101.

39. Wilkins BJ, Windt LJ De, Bueno OF, Braz JC, Glascock BJ, Kimball TF, Molkentin JD. Targeted Disruption of NFATc3, but Not NFATc4, Reveals an Intrinsic Defect in Calcineurin-Mediated Cardiac Hypertrophic Growth. *Mol Cell Biol* 2002;22:7603–7613.

40. Molkentin JD, Lu JR, Antos CL, Markham B, Richardson J, Robbins J, Grant SR, Olson EN. A calcineurin-dependent transcriptional pathway for cardiac hypertrophy. *Cell* 1998;**93**:215–228.

41. Dolinsky VW, Soltys CLM, Rogan KJ, Chan AYM, Nagendran J, Wang S, Dyck JRB. Resveratrol prevents pathological but not physiological cardiac hypertrophy. *J Mol Med* 2015;**93**:413–425.

42. Wilkins BJ, Dai YS, Bueno OF, Parsons SA, Xu J, Plank DM, Jones F, Kimball TR, Molkentin JD. Calcineurin/NFAT Coupling Participates in Pathological, but not Physiological, Cardiac Hypertrophy. *Circ Res* 2004;94:110–118.

43. Taegtmeyer H, Sen S, Vela D. Return to the fetal gene program: A suggested metabolic link to gene expression in the heart. *Ann N Y Acad Sci* 2010;1188:191–198.

44. Archer SL, Fang Y-H, Ryan JJ, Piao L. Metabolism and bioenergetics in the right ventricle and pulmonary vasculature in pulmonary hypertension. *Pulm Circ* 2013;3:144–152.

45. Bogaard HJ, Natarajan R, Henderson SC, Long CS, Kraskauskas D, Smithson L, Ockaili R, McCord JM, Voelkel NF. Chronic pulmonary artery pressure elevation is insufficient to explain right heart failure. *Circulation* 2009;120:1951–1960.

46. Ryan JJ, Archer SL. The right ventricle in pulmonary arterial hypertension: Disorders of metabolism, angiogenesis and adrenergic signaling in right ventricular failure. *Circ Res* S.L. Archer, Department of Medicine, Queen's University, Kingston, ON K7L 3N6, Canada; 2014;115:176–188.

47. Redout EM, Wagner MJ, Zuidwijk MJ, Boer C, Musters RJP, Hardeveld C van, Paulus WJ, Simonides WS. Right-ventricular failure is associated with increased mitochondrial complex II activity and production of reactive oxygen species. *Cardiovasc Res* W.S. Simonides, Laboratory for Physiology, Institute for Cardiovascular Research, VU University Medical Center, Amsterdam, Netherlands; 2007;75:770–781.

48. Partovian C, Adnot S, Eddahibi S, Teiger E, Levame M, Dreyfus P, Raffestin B, Frelin C. Heart and lung VEGF mRNA expression in rats with monocrotaline- or hypoxia-induced pulmonary hypertension. *Am J Physiol - Hear Circ Physiol* 1998;275:1948–1956.

49. Borgdorff MA, Bartelds B, Dickinson MG, Steendijk P, Berger RMF. A cornerstone of heart failure treatment is not effective in experimental right ventricular failure. *Int J Cardiol* Elsevier Ireland Ltd; 2013;169:183–189.

50. Paulin R, Sutendra G, Gurtu V, Dromparis P, Haromy A, Provencher S, Bonnet S, Michelakis ED. A miR-208-Mef2 axis drives the decompensation of right ventricular function in pulmonary hypertension. *Circ Res* 2015;116:56–69.

51. Westermann D, Lindner D, Kasner M, Zietsch C, Savvatis K, Escher F, Schlippenbach J Von, Skurk C, Steendijk P, Riad A, Poller W, Schultheiss HP, Tschöpe C. Cardiac inflammation contributes to changes in the extracellular matrix in patients with heart failure and normal ejection fraction. *Circ Hear Fail* 2011;4:44–52.

52. Harvey PA, Leinwand LA. Cellular mechanisms of cardiomyopathy. *J Cell Biol* 2011;194: 355–365.

53. Piek A, Boer RA de, Silljé HHW. The fibrosis-cell death axis in heart failure. *Heart Fail Rev* 2016;21:199–211.

54. Paulin R, Sutendra G, Gurtu V, Dromparis P, Haromy A, Provencher S, Bonnet S, Michelakis ED. A miR-208-Mef2 axis drives the decompensation of right ventricular function in pulmonary hypertension. *Circ Res* 2015;116:56–69.

55. Koshy SKG, Reddy HK, Shukla HH. Collagen cross-linking: New dimension to cardiac remodeling. *Cardiovasc Res* 2003;57:594–598.

56. Gomez-Arroyo J, Mizuno S, Szczepanek K, Tassell B Van, Natarajan R, Remedios CG Dos, Drake JI, Farkas L, Kraskauskas D, Wijesinghe DS, Chalfant CE, Bigbee J, Abbate A, Lesnefsky EJ, Bogaard HJ, Voelkel NF. Metabolic gene remodeling and mitochondrial dysfunction in failing right ventricular hypertrophy secondary to pulmonary arterial hypertension. *Circ Hear Fail* N.F. Voelkel, Victoria Johnson Center for Lung Obstructive Disease Research, Virginia Commonwealth University, Richmond, VA 23298, United States; 2013;6:136–144.

57. Sutendra G, Dromparis P, Paulin R, Zervopoulos S, Haromy A, Nagendran J, Michelakis ED. A metabolic remodeling in right ventricular hypertrophy is associated with decreased angiogenesis and a transition from a compensated to a decompensated state in pulmonary hypertension. *J Mol Med* E.D. Michelakis, Department of Medicine, University of Alberta, Edmonton, AB T6G 2B7, Canada; 2013;91:1315–1327.

58. Nagendran J, Gurtu V, Fu DZ, Dyck JRB, Haromy A, Ross DB, Rebeyka IM, Michelakis ED. A dynamic and chamber-specific mitochondrial remodeling in right ventricular hypertrophy can be therapeutically targeted. *J Thorac Cardiovasc Surg* E.D. Michelakis, Pulmonary Hypertension Program, Department of Medicine, University of Alberta, Edmonton, Alta., Canada; 2008;136:168-178.e3.

59. Voelkel NF, Quaife RA, Leinwand LA, Barst RJ, McGoon MD, Meldrum DR, Dupuis J, Long CS, Rubin LJ, Smart FW, Suzuki YJ, Gladwin M, Denholm EM, Gail DB. Right ventricular function and failure: Report of a National Heart, Lung, and Blood Institute working group on cellular and molecular mechanisms of right heart failure. *Circulation* 2006;114:1883–1891.

60. Nagendran J, Michelakis ED. Mitochondrial NOS is upregulated in the hypoxic heart: implications for the function of the hypertrophied right ventricle. *Am J Physiol Heart Circ Physi*ol 2009;296:H1723-6.

61. Neubauer S. The Failing Heart — An Engine Out of Fuel. *N Engl J Med* 2007;356:1140–1151.

62. Ryan JJ, Huston J, Kutty S, Hatton ND, Bowman L, Tian L, Herr JE, Johri AM, Archer SL. Right Ventricular Adaptation and Failure in Pulmonary Arterial Hypertension. *Can J Cardiol* Canadian Cardiovascular Society; 2015;31:391–406.

63. Ahmadi A, Ohira H, Mielniczuk LM. FDG PET imaging for identifying pulmonary hypertension and right heart failure. *Curr Cardiol Rep* 2015;17:555.

64. Archer SL, Fang Y-H, Ryan JJ, Piao L. Metabolism and bioenergetics in the right ventricle and pulmonary vasculature in pulmonary hypertension. *Pulm Circ* United States; 2013;3:144–152.

65. Bruns DR, Dale Brown R, Stenmark KR, Buttrick PM, Walker LA. Mitochondrial integrity in a neonatal bovine model of right ventricular dysfunction. *Am J Physiol - Lung Cell Mol Physiol* L.A. Walker, Univ. of Colorado-Denver, Dept. of Medicine, Cardiology, Aurora, United States; 2015;308:L158–L167.

66. Drake JI, Bogaard HJ, Mizuno S, Clifton B, Xie B, Gao Y, Dumur CI, Fawcett P, Voelkel NF, Natarajan R. Molecular signature of a right heart failure program in chronic severe pulmonary hypertension. *Am J Respir Cell Mol Bi*ol 2011;45:1239–1247.

67. Bartelds B, Knoester H, Smid GB, Takens J, Visser GH, Penninga L, Leij FR van der, Beaufort-Krol GC, Zijlstra WG, Heymans HS, Kuipers JR. Perinatal changes in myocardial metabolism in lambs. *Circulation* 2000;102:926–931.

68. Greiner EF, Guppy M, Brand K. Glucose is essential for proliferation and the glycolytic enzyme induction that provokes a transition to glycolytic energy production. *J Biol Chem* 1994;269:31484–31490.

69. Marsboom G, Toth PT, Ryan JJ, Hong Z, Wu X, Fang Y-H, Thenappan T, Piao L, Zhang HJ, Pogoriler J, Chen Y, Morrow E, Kenneth Weir E, Rehman J, Archer SL. Dynamin-related protein 1-mediated mitochondrial mitotic fission permits hyperproliferation of vascular smooth muscle cells and offers a novel therapeutic target in pulmonary hypertension. *Circ Res* S.L. Archer, Department of Medicine, Section of Cardiology, Chicago, IL 60637, United States; 2012;110:1484–1497.

70. Allard MF, Schonekess BO, Henning SL, English DR, Lopaschuk GD. Contribution of oxidative metabolism and glycolysis to ATP production in hypertrophied hearts. *Am J Physiol - Hear Circ Physiol* 1994;267.

71. Lopaschuk GD. Metabolic Modulators in Heart Disease – Past, Present and Future. *Can J Cardiol* Canadian Cardiovascular Society; 2017;33:838–849.

72. Piao L, Sidhu VK, Fang YH, Ryan JJ, Parikh KS, Hong Z, Toth PT, Morrow E, Kutty S, Lopaschuk GD, Archer SL. FOXO1-mediated upregulation of pyruvate dehydrogenase kinase-4 (PDK4) decreases glucose oxidation and impairs right ventricular function in pulmonary hypertension: therapeutic benefits of dichloroacetate. *J Mol Med (Berl)* L. Piao, Section of Cardiology, Department of Medicine, University of Chicago, Chicago, IL, USA.; 2013;91:333–346.

73. Liu A, Philip J, Vinnakota KC, Bergh F Van den, Tabima DM, Hacker T, Beard DA, Chesler NC. Estrogen maintains mitochondrial content and function in the right ventricle of rats with pulmonary hypertension. *Physiol Rep* 2017;5:1–12.

74. Fang Y-H, Piao L, Hong Z, Toth PT, Marsboom G, Bache-Wiig P, Rehman J, Archer SL. Therapeutic inhibition of fatty acid oxidation in right ventricular hypertrophy: Exploiting Randle's cycle. *J Mol Med* S.L. Archer, Medicine/Cardiology, University of Chicago, Chicago, IL 60637, United States; 2012;90:31–43.

75. Rumsey WL, Abbott B, Bertelsen D, Mallamaci M, Hagan K, Nelson D, Erecinska M. Adaptation to hypoxia alters energy metabolism in rat heart. *Am J Physiol - Hear Circ Physiol* W.L. Rumsey, Zeneca Pharmaceuticals, Wilmington, DE 19850-5437, United States; 1999;276:H71–H80.

76. Nouette-Gaulain K, Malgat M, Rocher C, Savineau J-P, Marthan R, Mazat J-P, Sztark F. Time course of differential mitochondrial energy metabolism adaptation to chronic hypoxia in right and left ventricles. *Cardiovasc Res* F. Sztark, Laboratoire d'Anesthésiologie, E.A. Physiologie Mitochondriale, Universite Bordeaux 2, 33076 Bordordeaux, France; 2005;66:132–140.

77. Hemnes AR, Brittain EL, Trammell AW, Fessel JP, Austin ED, Penner N, Maynard KB, Gleaves L, Talati M, Absi T, Disalvo T, West J. Evidence for right ventricular lipotoxicity in heritable pulmonary arterial hypertension. *Am J Respir Crit Care Med* 2014;189:325–334.

78. Brittain EL, Talati M, Fessel JP, Zhu H, Penner N, Calcutt MW, West JD, Funke M, Lewis GD, Gerszten RE, Hamid R, Pugh ME, Austin ED, Newman JH, Hemnes AR. Fatty acid metabolic defects and right ventricular lipotoxicity in human pulmonary arterial hypertension. *Circulation* E.L. Brittain, Division of Cardiovascular Medicine, Vanderbilt University Medical School, Nashville, United States; 2016;133:1936–1944.

79. Zaffran S, Kelly RG, Meilhac SM, Buckingham ME, Brown NA. Right ventricular myocardium derives from the anterior heart field. *Circ Res* 2004;95:261–268.

80. Dyer LA, Kirby ML. The role of secondary heart field in cardiac development. *Dev Biol* Elsevier Inc.; 2009;336:137–144.

81. McFadden DG, Charité J, Richardson JA, Srivastava D, Firulli AB, Olson EN. A GATA-dependent right ventricular enhancer controls dHAND transcription in the developing heart. *Development* 2000;127:5331–5341.

82. Sun Y-M, Wang J, Qiu X-B, Yuan F, Li R-G, Xu Y-J, Qu X-K, Shi H-Y, Hou X-M, Huang R-T, Xue S, Yang Y-Q. A HAND2 loss-of-function mutation causes familial ventricular septal defect and pulmonary stenosis. *G3 Genes, Genomes, Genet* J. Wang, Department of Cardiology, Jing'an District Central Hospital, Shanghai, China; 2016;6:987–992.

83. Kolwicz SC, Tian R. Glucose metabolism and cardiac hypertrophy. *Cardiovasc Res* 2011;90:194–201.

84. Kelly RG, Brown NA, Buckingham ME. The Arterial Pole of the Mouse Heart Forms from Fgf10-Expressing Cells in Pharyngeal Mesoderm. *Dev Cell* 2001;1:435–440.

85. Cai CL, Liang X, Shi Y, Chu PH, Pfaff SL, Chen J, Evans S. Isl1 identifies a cardiac progenitor population that proliferates prior to differentiation and contributes a majority of cells to the heart. *Dev Cel*l 2003;5:877–889.

86. Srivastava D, Thomas T, Lin Q, Kirby ML, Brown D, Olson EN. Regulation of cardiac mesodermal and neural crest development by the bHLH transcription factor, dHAND. *Nat Genet* 1997;16:154–160.

87. Dirkx E, Gladka MM, Philippen LE, Armand A, Kinet V, Leptidis S, Azzouzi H, Salic K, Bourajjaj M, Silva GJJ, Olieslagers S, Nagel R Van Der, Weger R De, Bitsch N, Kisters N, Seyen S, Morikawa Y, Chanoine C, Heymans S, Volders PGA, Thum T, Dimmeler S, Cserjesi P, Eschenhagen T, Paula A, Martins C, Windt LJ De, Azzouzi H El, Salic K, Bourajjaj M, et al. Nfat and miR-25 cooperate to reactivate the transcription factor Hand2 in heart failure. *Nat Cell Biol* Nature Publishing Group; 2013;15:1282–1293.

88. Wallace E, Morrell NW, Yang XD, Long L, Stevens H, Nilsen M, Loughlin L, Mair KM, Baker AH, MacLean MR. A sex-specific microRNA-96/5-hydroxytryptamine 1B axis influences development of pulmonary hypertension. *Am J Respir Crit Care Med* 2015;**191**:1432–1442.

89. Caruso P, Dempsie Y, Stevens HC, McDonald RA, Long L, Lu R, White K, Mair KM, McClure JD, Southwood M, Upton P, Xin M, Rooij E Van, Olson EN, Morrell NW, MacLean MR, Baker AH. A role for miR-145 in pulmonary arterial hypertension: Evidence from mouse models and patient samples. *Circ Res* 2012;111:290–300.

90. Gou D, Ramchandran R, Peng X, Yao L, Kang K, Sarkar J, Wang Z, Zhou G, Usha Raj J. Mir-210 has an antiapoptotic effect in pulmonary artery smooth muscle cells during hypoxia. *Am J Physiol - Lung Cell Mol Physi*ol 2012;303:682–691.

91. Reddy S, Bernstein D. Molecular mechanisms of right ventricular failure. *Circulation* S. Reddy, Department of Pediatrics (Cardiology), Stanford Cardiovascular Institute, Stanford University, Lucile Packard Children's Hospital, Palo Alto, United States; 2015;132:1734–1742.

1

2

CHAPTER 2

Clinical symptoms of right ventricular failure in experimental chronic pressure load are associated with progressive diastolic dysfunction

M.A.J. Borgdorff, A.M.C. Koop, V.W. Bloks, M.G. Dickinson, P. Steendijk, H.H.W. Silljé, M.P.H. van Wiechen, R.M.F. Berger, B. Bartelds. - Journal of Molecular and Cellular Cardiology. 2015; 79:244-253.

ABSTRACT

Background

Right ventricular failure (RVF) due to pressure load is a major cause of death in congenital heart diseases and pulmonary hypertension. The mechanisms of RVF are unknown. We used an experimental approach based upon clinical signs of RVF to delineate functional and biological processes associated with RVF.

Methods and results

Wistar rats were subjected to a pulmonary artery banding (PAB n=12) or sham surgery (CON, n=7). After 52±5 days, 5/12 PAB rats developed clinical symptoms of RVF (inactivity, ruffled fur, dyspnea, ascites) necessitating termination (PAB+CF). We compared these to PAB rats with RVF without clinical symptoms (PAB-). PAB resulted in reduced cardiac output, RV stroke volume, TAPSE, and increased end diastolic pressure (all $p<0.05$ vs. CON) in all rats, but PAB+CF rats were significantly more affected than PAB-, despite similar pressure load (p=ns). Pressure-volume analysis showed enhanced contractility (end systolic elastance) in PAB- and PAB+CF, but diastolic function (end diastolic elastance, end diastolic pressure) deteriorated especially in PAB+CF. In PAB+CF capillary density was lower than in PAB-. Gene-array analysis revealed downregulation of both fatty acid oxidation and carbohydrate metabolism in PAB+CF.

Conclusion

Chronic PAB led to different degrees of RVF, with half of the rats developing severe clinical symptoms of RVF, associated with progressive deterioration of diastolic function, hypoxia-prone myocardium, increased response to oxidative stress and suppressed myocardial metabolism. This model represents clinical RVF and allows for unraveling of mechanisms involved in the progression from RV adaptation to RV failure and the effect of intervention on these mechanisms.

INTRODUCTION

Right ventricular failure (RVF) due to increased pressure load is a primary risk factor for morbidity and mortality in patients with congenital heart diseases as well as in patients with pulmonary hypertension (PH).[1,2] Moreover, RV dysfunction has also been demonstrated to be an important prognostic determinant in left ventricular failure.[3]

Unfortunately, the pathophysiology of RV failure is yet insufficiently understood,[4] which precludes the development of RV specific treatments. Research into these mechanisms is hampered by the lack of a model reflecting clinical RVF. It is in this perspective that a National Heart, Lung and Blood Institute working group on cellular and molecular mechanisms of right heart failure stated that *'researchers must develop reliable, reproducible and relevant animal models of RV failure'.*[5]

Since RV function is a critical prognostic determinant in PH,[2] RV dysfunction has often been studied in animal models of PH, such as the monocrotaline rat model.[6] Although these models have proven to be valuable, they have two important disadvantages: direct therapeutic effects on the RV cannot be distinguished from (afterload-reducing) effects on the pulmonary vasculature and the used 'hits' necessary to induce PH may affect the RV.[7] The use of a pulmonary artery banding (PAB) to inflict chronic pressure load on the RV circumvents these limitations. However, it has been debated whether the phenotype of the chronic PAB model represents compensated adaptation instead of RV failure.[8–10] Heart failure is defined as the inability to meet the metabolic requirements of the tissues of the body. Heart failure is not an entity as such but a continuum of disease severity, graded according to the NYHA class. RV failure is defined similarly, but the clinical signs and symptoms differ from those in LV failure. The cardinal clinical characteristics of RV failure are fluid retention (presenting as peripheral edema, effusion, ascites) and low cardiac output (evident in decreased exercise tolerance, fatigue, dyspnea and poor peripheral circulation).[11,12]

Previously described PAB models showed features of chronic adaptation and mild RV dysfunction, e.g. RV dilatation, reduced TAPSE and hypertrophy,[8,9,13] but whether these represent the clinical phenotype of RV failure is unclear because the studies with hemodynamical analyses lack data on clinical symptoms of RVF[14,15] and conversely, the studies reporting on the clinical phenotype of RV failure lack (extensive) hemodynamical data.[8,10]

The clinical phenotype of RV failure consists of signs and symptoms as dyspnea at rest, hepatomegaly, ascites, pleural effusion and mortality.[5,12]

In the current study we aimed to characterize a phenotype of clinical RVF in rats with a tighter PAB (1.1 mm) than described before,[8,9,16,17] using clinical symptoms in

the rats (ABCDE-system), as reported previously.[6,18] We further aimed to relate the presence of clinical symptoms of RVF to specific hemodynamic, pathophysiologic and molecular patterns of RV function, using echocardiography, pressure-volume analysis and transcriptome-wide expression profiling in the RV. While a number of previous studies have compared different phenotypes, these were generally induced by different stressors (e.g. Sugen + hypoxia vs. PAB or monocrotaline vs. PAB or Sugen+hypoxia). Such comparisons are very interesting and have yielded considerable insight in the divergent responses of the RV to different physiological and chemical stressors. However, it remains unclear whether the differences found in these studies represent different stages of RVF or merely reflect the different stressors used. We aimed to solve this problem. To this end we compared two groups of rats that all underwent the same PAB banding, but either had or had not developed clinical symptoms of RVF.

METHODS

Animal model and study design

Wistar rats (n=21; all male; 160-180g; Charles River, the Netherlands) were randomized into 2 groups: sham (CON, n=7) or pulmonary artery banding (PAB, n=14, two of which died during surgery). PAB was performed through a left lateral thoracotomy as described before,[16] however, with a tighter constriction (1.1mm vs. 1.3mm before). Sham surgery was similar to the PAB surgery, with the exception of the actual banding of the pulmonary artery.

From the moment of PAB/sham surgery onward, the animals were daily checked for signs of clinical RV failure (see *2.2 Definition of clinical RV failure*).[18] When a rat was identified as developing clinical RV failure, echocardiography and pressure-volume analysis was performed: these rats are the PAB+Clinical Failure (PAB+CF) group (n=5). Four rats with a PAB that did not show signs of clinical RVF, yet also had decreased distance run during voluntary treadmill exercise_were analyzed and terminated at the same follow-up duration (PAB minus Clinical Failure: PAB- group, n=4). At 11 weeks the remaining rats (7 CON and 3 PAB) were terminated. See **figure 1a** for the experimental set-up. A detailed description of the methods is provided in the online-only Data Supplement.

Definition of clinical RV failure

Rats were examined daily for clinical signs of RV failure according to a predefined ABCDE-checklist,[6,18] which includes Appearance, Activity, Bodyweight, Circulation (peripheral), Cyanosis, Dyspnea/tachypnea and Edema, Effusions (see online-only Data Supplement). Clinical RV failure was defined as presence of at least: inactivity and ruffled fur and severe dyspnea and palpable ascites. The presence of ascites and pleural effusion was in all cases confirmed after termination.

Pressure-volume measurements, echocardiography, exercise

Functional analysis of the RV was performed before termination using invasive pressure-volume measurements in anesthetized (isoflurane/air mixture, 5% induction; 2-3% maintenance; analgesia with buprenorphine 0.01 mg/kg s.c.), ventilated rats following thoracotomy using a conductance catheter as described before[18] and in the online-only Data supplement. Stroke volume as measured by echocardiography (in mL) was used to calibrate the conductance-derived stroke volume (in arbitrary units) derived from the conductance signal. Steady-state pressure-volume loops were used for calculation of all parameters. End systolic and end diastolic elastance were determined using the single-beat method; vena cava

occlusion caused immediate fatal deterioration of cardiac function in the majority of PAB+CF rats precluding this method of determining elastance.

Echocardiography was performed at 5 weeks and at termination as described before.[18] Apical 3- and 4-chamber views and parasternal short- and long axis views were used to measure ventricular and atrial dimensions and tricuspid annular plane systolic excursion (TAPSE) and to assess tricuspid insufficiency. The gradient across the PAB was measured using continuous wave Doppler. Cardiac output was calculated as (aorta diameter)^2 * 3.14 * velocity time integral * heart rate, using systolic aorta diameter and pulsed wave Doppler measurements of aorta flow. Beat-to-beat variation was accounted for by averaging measurements from 6 to 12 consecutive beats.

Voluntary exercise was measured using running wheels mounted in the cages for 5 consecutive days at baseline and after 5 weeks as described previously[6,16,18] and in the online-only Data Supplement.

Histological analyses

Ventricular remodelling was studied using RV free wall tissue. We used using standard histological techniques for measurement of RV cardiomyocyte cross-sectional area, fibrosis, capillary density and macrophage infiltration, as described in the online-only Data Supplement.

Gene expression

Changes in gene expression in the RV myocardium were investigated using transcriptome-wide expression profiling and qRT-PCR for specific genes. Total RNA was extracted using TRIzol reagent (Invitrogen Corporation, Carlsbad, CA, USA); high quality was confirmed (RQI 9.3) using Experion (Bio-Rad, Veenendaal, the Netherlands). For the array-studies, RNA was purified for individual rats (n=7/4/5 CON/PAB-/PAB+CF) using the Qiagen RNeasy mini kit (Venlo, The Netherlands); RNA quality was verified (RIN >9) (Agilent, Amstelveen, the Netherlands). Biotin-labeling, hybridization, washing, scanning of GeneChip Rat Gene 1.1 ST arrays (Affymetrics) and processing in the MADMAX pipeline (Nutrigenomics Consortium, Wageningen, The Netherlands)[19] using Bioconductor software packages were all performed according to standard Affymetrix protocols at expert labs. Extensive quality control is described in the online-only Data supplement. Array data are deposited at the Gene Expression Omnibus (GEO) database (GSE46863).

Significantly regulated genes were related to biological processes using DAVID.[20] Gene set enrichment analysis,[21] which includes expression of all genes (not just

significantly regulated genes) was performed, allowing detection of significant regulation of gene sets, even if the expression of individual genes is not significantly different between groups.

Statistical analysis

Quantitative data are expressed as mean±standard error of the mean (SEM). Testing of differences between CON, PAB- and PAB+CF was performed using ANOVA with Bonferroni post hoc correction for multiple testing. The rats that survived 11 weeks of PAB (n=3) were not included in the PAB- group so that the time exposed to PAB was equal in the PAB- and PAB+CF groups and potential confounding of the results by time-differences was avoided.[22] Retrospective PAB- vs. PAB+CF comparisons at the 5 week time point were evaluated using t-tests. P<0.05 was considered significant (PASW Statistics 20 for Windows, SPSS, Chicago, Illinois). Statistical analysis of the transcriptome array is described separately in the online-only Data Supplement.

RESULTS

After a mean period of 52±5 days, 42% of the rats developed clinical RVF (5/12, **figure 1b**). Tightness of PAB was similar in rats with or without signs of clinical RVF, assessed by peak RV pressure that was equally increased in both groups at 5 weeks (echo-measured PAB gradient (**figure 1c**) as well as at termination (invasively measured RV pressure, **figure 1d**).

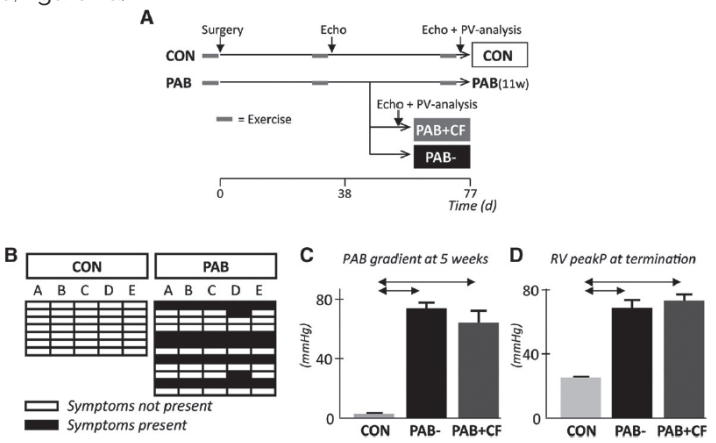

Figure 1. A Schematic overview of experimental set-up. B Clinical symptoms of RV failure. Solid box = symptoms present. Open box = symptoms absent. Each row represents 1 rat. ABCDE refer to: A activity and appearance, B bodyweight, C cyanosis and/or hampered peripheral circulation, D dyspnea and/or tachypnea, E effusions: pleural or ascites (see supplement for details). C PAB gradient measured by echocardiography at 5 weeks after surgery. D Invasively measured RV peak pressure measured before termination. Mean±SEM. Arrows indicate p<0.05 between respective groups.

Rats with or without clinical signs of failure showed distinct functional, morphological and pathological profiles

All rats with PAB showed functional and morphological RV-abnormalities, but these were significantly more pronounced in PAB+CF than in PAB-. At termination, PAB+CF rats had a lower cardiac index (both when cardiac output was indexed for bodyweight or tibialength) (**figure 2a**), RV stroke volume (**table 1**) and TAPSE (**figure 2b**). Furthermore, PAB+CF rats had a more enlarged right atrium (**figure 2c**) and pericardial effusion (3/5 of PAB+CF vs. 0/4 of PAB- rats; **figure 2d**). In PAB+CF, the right atrium was also more hypertrophic (**figure 2e**) and the liver wet/dry-weight ratio was increased signifying congestion (**figure 2f**). In line with this, postmortem examination revealed macroscopic liver congestion (so-called 'nutmeg liver') and ascites in PAB+CF, but not in PAB- (representative images in **figure 2g**).

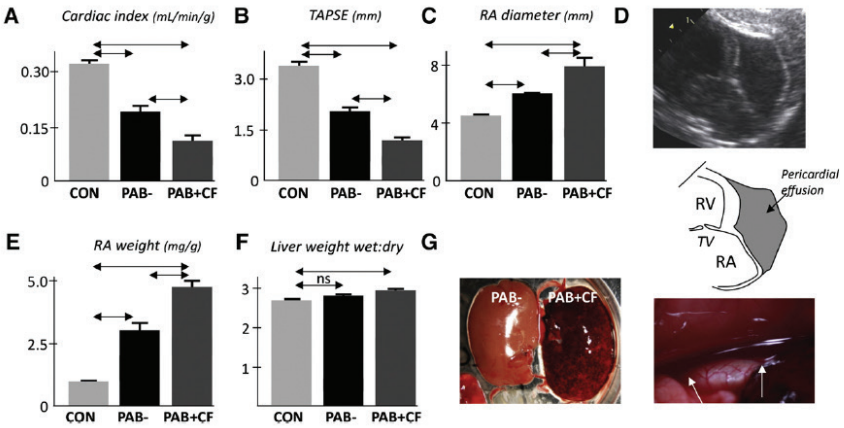

Figure 2. Echocardiographic and pathological confirmation of clinical RVF. PAB+CF was distinct from PAB- with regard to cardiac index (A), TAPSE (B), RA diameter (C), presence of pericardial effusion (example echo-image in D), RA weight (E) and liver wet-to-dry ratio (F). Representative images of liver congestion (left-hand panel in G) and ascites (right-hand panel in G). Mean±SEM. Arrows indicate $p<0.05$ between respective groups. TAPSE= tricuspid annular plane systolic excursion, RA= right atrium, TV= tricuspid valve.

PAB consistently induced RV dilatation and tricuspid insufficiency, but no differences were found between PAB- and PAB+CF (**table 1**).

Table 1. Additional heartcatheterization and echocardiographic data in CON, PAB- and PAB+CF.

	CON	PAB-	PAB+CF
Number of rats	7	4	5
Weights			
Bodyweight at termination (g)	488±23	431±28*	456±21*
RV free wall weight (mg)	272±18	624±47*	582±41*
LV+IVS weight (mg)	883±48	846±92	823±54
Heartcath parameters			
HR (/min)	308±5	258±24	264±15
dP/dtmax corr	49.8±2.2	32.3±3.7*	32.6±1.7*
dP/dtmin corr (*-1)	47.7±1.8	32.7±2.8*	23.9±4.0*
Tau (ms)	17.6±0.5	27.3±3.9*	23.1±2.5
Tau/cyclelength (ms/s)	90±2	114±9*	100±8
Echocardiographic parameters 5wk			
Tricuspid insufficiency (present)	0%	100%*	100%*
Pericardial effusion (present)	0%	0%	40%*†
RVEDD (mm)	3.0±0.2	5.3±0.4*	6.0±0.1*
PAB gradient (mmHg)	4±1	74±5*	64±9*
RA diameter (mm)	3.5±0.1	5.2±0.3*	7.2±1.0*
TAPSE (mm)	2.9±0.1	1.7±0.2*	1.3±0.2*
HR (/min)	368±8	315±18	279±20*
SV (uL)	295±13	205±20*	153±17*
Echocardiographic parameters endpoint			
Tricuspid insufficiency (present)	0%	100%*	100%*
Pericardial effusion (present)	0%	0%	60%*†
RVEDD (mm)	4.5±0.1	6.2±0.2*	6.5±0.5*
PAB gradient (mmHg)	3±1	72±11*	62±10*
RA diameter (mm)	4.5±0.1	6.0±0.1*	7.7±0.6*
TAPSE (mm)	3.4±0.2	2.0±0.2*	1.2±0.1*
HR (/min)	368±6	304±11*	301±13*
SV (uL)	426±30	271±24*	152±21*

LV= left ventricle, IVS= interventricular septum, HR= heart rate, dP/dt max corr= dP/dt max normalized for RV peak pressure, dP/dt min corr= dP/dt min normalized for RV end systolic pressure, RVEDD= right ventricular enddiastolic volume, PAB= pulmonary artery banding, RA= right atrium, TAPSE= tricuspid annular plane systolic excursion, SV= stroke volume. Values are mean ± SEM. *= p<0.05 vs. CON, † vs. PAB-

Pulmonary artery banding resulted in enhanced systolic function, while the occurrence of clinical symptoms is associated with worse diastolic function

Pressure-volume analysis revealed hemodynamic distinctions between PAB- and PAB+CF (representative pressure-volume loops in **figure 3a-c**). End systolic elastance (a measure of contractility) showed a trend to be higher in PAB+CF (**figure 3e**). However, the performed stroke work in PAB+CF was significantly lower than in PAB- (**figure 3f**), reflecting decreased stroke volume despite enhanced end systolic elastance.

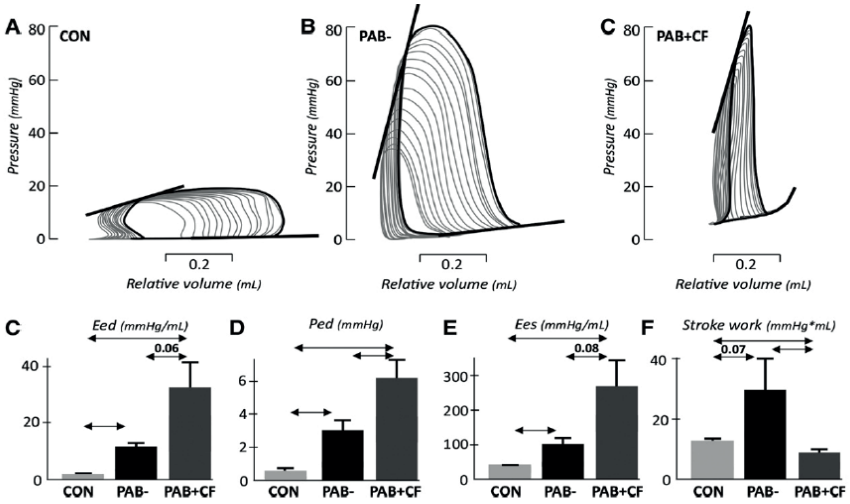

Figure 3. Pressure-volume analysis. Representative pressure-volume loops of CON, PAB- and PAB+CF (A-C), end systolic pressure volume relations indicated by solid lines, end diastolic pressure volume relations indicated by dashed lines. Indices of diastolic function; end diastolic elastance (C) and end diastolic pressure (D). The single-beat method was used to determine elastance in all groups because of the fatality of the procedure in the majority of animals in the PAB+CF group. However, in many animals (all in the CON- and PAB groups and some in the PAB+CF group) we were able to perform vena cava occlusion without problems. In this figure data during vena cave occlusion are shown to illustrate the hemodynamic changes in the different groups. End systolic elastance (E) and stroke work (F). Mean±SEM. Arrows indicate $p<0.05$ between respective groups. Eed= end diastolic elastance, Ped= end diastolic pressure, Ees = end systolic pressure

Clinical right ventricular failure in pressure overload is characterized by enhanced systolic function and diastolic dysfunction.

Advanced diastolic dysfunction hallmarked PAB+CF compared to PAB-: both end diastolic elastance (**figure 3c**, p=0.06) and end diastolic pressure (**figure 3d**) were higher in PAB+CF. This was due to increased stiffness rather than to incomplete active relaxation as tau did not differ between PAB- and PAB+CF (**table 1**).

Association of regulatory mechanisms of cardiomyocyte relaxation, fibrosis, hypertrophy and capillary growth to RVF with clinical symptoms

In PAB+CF, mRNA expression of the compliant isoform of titin, N2Ba, was significantly increased (**table 1**), indicating an adaptive response to counter passive ventricular stiffness. However, activities of protein kinase A and G, phosphorylation status of phospholamban and expression of SERCA ATPase, which regulate active cardiomyocyte relaxation were not significantly changed (**table 1**). Diastolic dysfunction has also been associated with increased stiffness due to interstitial fibrosis and/or hypertrophy. However, fibrosis was lower in PAB+CF than in PAB- (**figure 4a,e**).

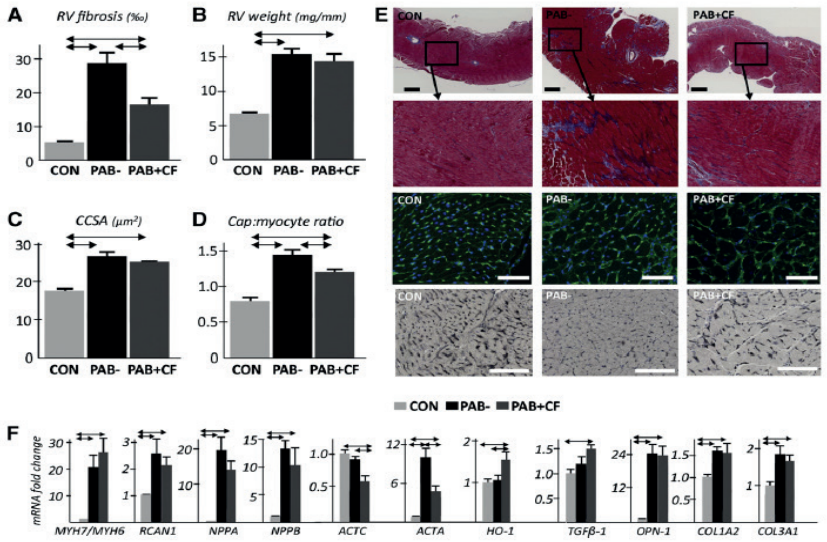

Figure 4. Histology and gene expression. RV fibrosis (A, E: two top rows are representative images of Masson-Trichrome stained RVs, ruler is 500μm, black box with 1mm). RV hypertrophy (RV free wall weight normalized for tibia length, B) and RV cardiomyocyte cross-sectional area (C, E third row are representative images of RV sections stained with a membrane marker (wheat germ agglutinin, green), ruler is 75μm. RV capillary density, expressed as capillary-to-cardiomyocyte ratio (D, E bottom row are representative images of RV sections stained with capillary-marker lectin, ruler is 130μm). mRNA expression of genes related to hypertrophy, fetal gene program, oxidative stress and fibrogenesis (CON =1, relative to 36B4 reference gene expression). Mean±SEM. Arrows indicate $p<0.05$ between respective groups. CCSA= cardiomyocyte cross-sectional area, cap= capillary, MYH7/6= /-myosin heavy chain, RCAN1= regulator of calcineurin 1, NPPA/B= natriuretic pro-peptides type A/B, ACTC= -cardiac actin, ACTA= -skeletal actin, HO-1= hemoxygenase-1, TGFβ-1= transforming growth factor- -1, OPN-1= osteopontin-1, COL1A2/3A1= collagen subunits 1A2 and 3A1.

This was not accompanied by blunted signaling in the pro-fibrotic pathways or attenuated expression of collagen-isoforms (**figure 4f**). Fibrosis has been suggested to result from deficient hemoxigenase-1 (HO-1) activation; one of the protective

mechanisms against oxidative stress7, and in line with this we found that HO-1 was specifically upregulated in PAB+CF (**figure 4f**). We could not demonstrate differences in NOX-4 activation or macrophage infiltration between PAB- and PAB+CF (*data not shown*).

The amount of RV hypertrophy was equal in PAB- and PAB+CF, whether expressed as (normalized) RV weight or cardiomyocyte cross sectional surface area (**figure 4b,c,e**). Also mRNA expression of genes involved in hypertrophy (myosin heavy chain-isoforms, regulator of calcineurin 1) and the natriuretic peptides type A and B were increased equally in PAB- and PAB+CF (**figure 4f**). However, mRNA expression of the two isoforms of actin was different in PAB- and PAB+CF. The predominant isoform (ACTC) was normal in PAB-, but downregulated in PAB+CF (**figure 4f**). The fetal isoform (ACTA) which is known to be upregulated in response to stress was indeed upregulated in pressure load, but ~50% less in PAB+CF than in PAB- (**figure 4f**).

Insufficient capillary growth to supply the hypertrophic myocardium is suggested to be a main cause of pressure-load induced heart failure7. In both groups capillary density was decreased (**figure 4e**), accompanied by a reduction in VEGF-A and VEGF receptor type 2 expression (*data not shown*). However, in PAB+CF the number of capillaries per cardiomyocyte was significantly less than in PAB- (**figure 4d**).

Cardiac index and voluntary exercise predict the onset of RVF with clinical symptoms

We performed echocardiography and voluntary exercise measurements at 35 days after PAB surgery, well before the onset of clinical RVF (52±5 days). Retrospectively comparing PAB- and PAB+CF rats, we found that voluntarily run distance, RV stroke volume, TAPSE and cardiac index (both when cardiac output was indexed for body weight or tibia length) were all significantly lower at 5 weeks in the rats that later developed clinical RVF as compared with those that did not develop symptoms of RVF (**figure 5a-d**). In contrast, there were no differences between PAB+CF and PAB- with regard to ventricular dilatation and tricuspid insufficiency at 5 weeks (**table 1**). While significantly different between PAB+CF and PAB-, cardiac index (**figure 5e**) and TAPSE (**table 1**) were stable from 5 weeks onward, also in rats that developed clinical RVF.

The hemodynamic data of the PAB- group (which was prematurely terminated concurrently with the PAB+CF group) and the PAB rats that survived 11 weeks were similar (**supplemental table 1**).

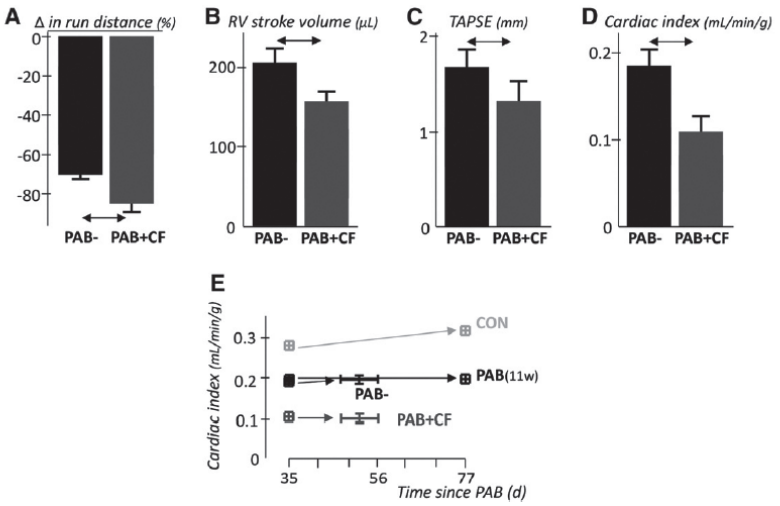

Figure 5 .Comparison of PAB- and PAB+CF at 5 weeks. PAB- and PAB+CF were significantly different at 5 weeks with regard to run distance (A, percentage change in run distance at 5 weeks vs. baseline), RV stroke volume (B), TAPSE (C) and cardiac index (D, in mL/min/g bodyweight). Cardiac index was stable in all groups at termination vs. 5 weeks (E). Mean±SEM. Arrows indicate $p<0.05$ between respective groups. PAB(11w)= PAB rats terminated at 11wks, TAPSE= tricuspid annular plane systolic excursion.

Changes in gene expression following PAB

Because no evident culprit has yet been found in RVF, and the etiology of RVF is likely multifactorial, we performed transcriptome-wide expression profiling, to study pathways involved in RVF. PAB induced significant changes in expression of >3000 genes. 1,437 of these and 263 of the significantly regulated gene sets were present in both PAB- and PAB+CF (**figure 6**, **supplemental table 1**). As expected, up regulation in the common gene pattern predominantly involved cardiac/cellular growth, and multiple interwoven and well known signaling pathways (MAPK-ERK1/2, PI3K-Akt-NFkappaBeta-mTOR, Integrins, TGF-beta, endothelin etc.). Down regulation was seen in specific gene sets related to metabolism, for example down regulation of PPAR alpha signaling, intermediary enzymes in fatty acid metabolism, PGC1 alpha signaling, mitochondrial gene expression and oxidative phosphorylation (**figure 6**, **supplemental table 1**).

Whereas genes involved in fatty acid metabolism were downregulated in rats subjected to pressure load, with and without clinical symptoms, genes involved in glycolysis and gluconeogenesis were specifically downregulated in rats with clinical right ventricular failure.

Changes in gene expression specifically associated with either PAB+CF or PAB-

1,666 genes and 104 gene sets were specifically regulated in PAB+CF, many of which related to cellular (energy) metabolism (**figure 6**, **supplemental table 1**, **table supplemental table 3**). Most prominently, there was a significant down regulation of glycolysis/gluconeogenesis related gene sets in PAB+CF, in contrast to PAB- (**figure 7**). In addition, while the changes in fatty acid metabolism and beta-oxidation were comparable between PAB- and PAB+CF, the down regulation of oxidative phosphorylation, the tricarboxylic acid cycle and amino acid metabolism appeared to be more pronounced in PAB-CF than in PAB- (**figure 7**).

In contrast to the PAB+CF group, only a few additional genes (215) and gene sets (20) were specifically regulated in PAB- (**figure 6**, **supplemental table 1**). The 215 genes were not significantly related to a specific biological process. Likewise, the found gene sets were aspecific. No gene sets were regulated in opposite directions in PAB- vs. PAB+CF.

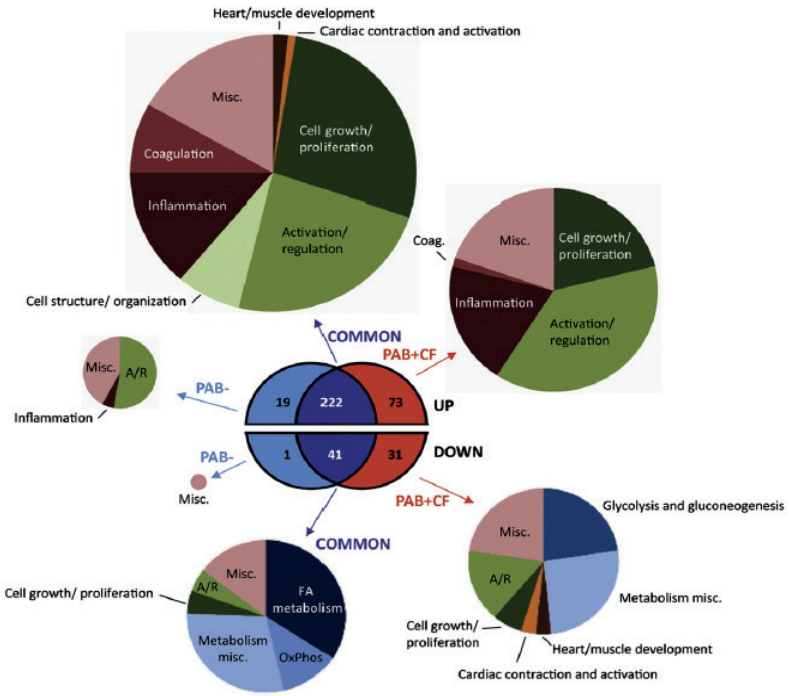

Figure 6. Significantly regulated gene sets in CON, PAB- and PAB+CF. Gene set enrichment analysis. Number of differentially enriched gene sets vs. CON in PAB-and PAB+CF is indicated in the circles, separately for positive/ negative enrichment (up regulation/down regulation). Commonly enriched gene sets are represented by the overlap. Pie-charts show distribution of the gene sets in categories for PAB-, PAB+CF and COMMON, again separately for positive/negative enrichment. N=7/4/5 for CON/PAB-/PAB+CF. False discovery rate (FDR) <15%, nominal P value <0.05 and normalized enrichment score >1.3 was considered significant.

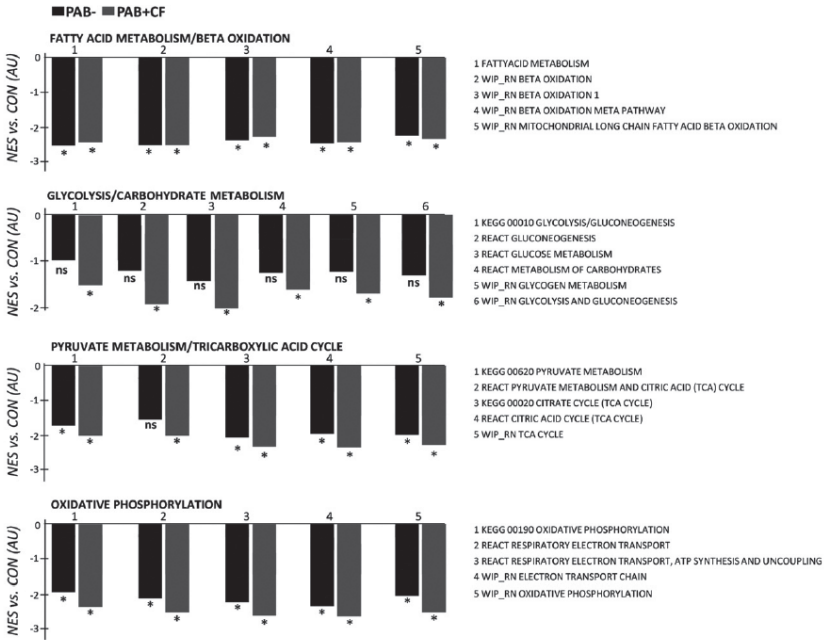

Figure 7. Enrichment of gene sets associated with energy metabolism. Normalized enrichment scores (NES) of PAB- and PAB+CF vs. CON. N=7/4/5 for CON/PAB-/PAB+CF. * indicates false discovery rate (FDR) <15%, nominal P value <0.05 and normalized enrichment score >1.3 for respective gene set vs. CON.

DISCUSSION

In this study, the rat model of chronic 'tight' pulmonary artery banding induced RV failure in all rats, and severe RV failure with clinical symptoms in half of the rats. Progressive RV failure was characterized hemodynamically by progressive diastolic dysfunction. Diastolic dysfunction occurred despite adaptive responses to maintain active relaxation, and was not due to increased fibrosis. RV failure with clinical symptoms is associated with a hypoxia-prone cellular environment in the RV myocardium, increased intrinsic protective response to oxidative stress and suppressed myocardial metabolism.

The here described approach to the PAB model gives insight in advanced (clinical) RVF due to increased pressure load and can be used to unravel the mechanisms involved in the progression from RV adaptation to RV failure and to assess the effect of interventions on these mechanisms.

PAB and the development of RVF

The tight PAB used in this study led to various degrees of RV failure, in which we made a distinction based on clinical symptoms. About half of the rats developed severe RVF with clinical symptoms that necessitated termination. This would be analogous to NYHA class IV. The other PAB rats did develop RVF (reduced voluntary exercise tolerance, RV dysfunction etc.) but displayed no overt clinical signs. This would be analogous to NYHA class II-III. This variability in phenotype may have different explanations. Firstly, it may represent variability in PAB tightness, as the rats with a tighter PAB would develop a more severe phenotype. However, in **figure 1** we showed that systolic RV pressures and PAB gradient were equal in both PAB- and PB+CF groups at both 5 weeks and at the endpoint, which excludes PAB variability as explanation. The fact that the 'stress' imposed on all RVs was equal, suggests that the differences in phenotype are explained by differences in adaptation. Indeed, the inherent ability to cope with pressure load appears to differ among rats. As shown in **figure 5**, functional parameters are already different between groups at 5 weeks; which is weeks before clinical symptoms occur. This inherent vulnerability for (or resilience against-) RV pressure load is not explained by major differences in genetic make-up as we used an inbred rat strain for all experiments. Rather, our data suggest that differences may exist in the mechanisms regulating diastolic function.

Clinical RVF is characterized by diastolic dysfunction with enhanced contractility

Recently, there is renewed debate about the involvement of diastolic versus systolic dysfunction in the progression of RV failure.[23] Whereas previously the role of systolic dysfunction has received most attention, the results of the present study stress the importance of diastolic dysfunction in the development of clinical RV failure. These findings are confirmed by recent studies in human ex-plant RV tissue.[24]

Surprisingly, no decrease in systolic function, rather increased contractility was observed. Enhanced contractility in RVF might seem paradoxical, but it is a consistent finding in the chronic pressure overloaded RV[14,16,25,26] and in PAH patients.[24] From previous experimental studies, as well as from a recent study in PAH patients[24] it is known that chronic RV pressure overload induces diastolic dysfunction.[14,16] This study now adds the observation that the occurrence of clinical RVF is associated with deteriorating diastolic function. Diastolic function is the resultant of both active relaxation, which depends on Ca^{2+} re-uptake by phospholamban-modulated SERCA2a and sodium-calcium exchanger NCX, and passive chamber properties. Active relaxation of the RV is thought to be disturbed in acute pressure overload.[27] In the current study in chronic pressure load however, active relaxation (tau) was only mildly prolonged and did not further increase with clinical RVF.

Also expression of SERCA2a, phospholamban and NCX was comparable between groups and not correlated to deterioration of diastolic function. In contrast, passive chamber properties (Eed, EDP) revealed progressive stiffening of the RV. Interstitial fibrosis contributes to myocardial stiffening in heart failure. However, we found interstitial fibrosis to be less increased in the PAB-rats with clinical RVF and deteriorated diastolic dysfunction, as compared to those without clinical RVF and less diastolic dysfunction. The pro-fibrotic signaling (TGFβ1, osteopontin) appeared similarly activated in both groups, suggesting a higher degradation of collagen in the PAB-rats with RVF. In other words, the increased myocardial stiffening in PAB-rats with clinical RVF cannot be explained by increased interstitial fibrosis. In other species (e.g. rabbits) fibrosis may play a more prominent role.[28,29] Stiffening of sarcomeres might be another explanation for the deterioration of diastolic function. We observed an increased expression of the more compliant N2Ba titin isoform in PAB+CF, which may be an adaptive response. However, titin compliance also depends on phosphorylation, which is mediated by PKG-1.[24] We did not measure titin phosphorylation, but PKG-1 activity was not increased in PAB+CF, which may (partly) explain the adverse change in ventricular stiffness.

The key to effective treatment of RVF may not be found in interventions preserving RV diastolic function, for instance by increasing titin phosphorylation status.

Clinical RVF is associated with a hypoxia-prone cellular environment

In this PAB model, the development of clinical signs of RVF was associated with a state of hypoxia-prone cellular environment and increased intrinsic protective response to oxidative stress. Pathological hypertrophy, characterized by activation of e.g. the calcineurin-NFAT signaling system[30] was similarly present in both PAB-groups. However, capillary-myocyte ratio was reduced in PAB-rats with clinical RVF. This finding is in line with previous studies suggesting that insufficient capillary formation to supply the hypertrophic myocardium contributes to the development clinical RVF.[8]

Myocyte hypoxia may also lead to RV failure via increased oxidative stress,[31] which has been linked to cardiac stiffness.[32] We found circumstantial evidence of increased oxidative stress (increased heme oxygenase-1 mRNA expression; a powerful anti-oxidant enzyme in heart failure,[33] in PAB-rats with clinical RVF, but not in those without clinical RVF. Obviously, besides HO-1, multiple pathways (both related and unrelated to oxidative stress) are contributing to the formation and degradation of fibrosis in RV failure, many of which show significantly changed expression in the transcriptome array. However, the upregulation of HO-1 is intriguing, especially because the direction of expression change is opposite to that in the Sugen-hypoxia model of RVF, in which the stress to induce the model itself may cause oxidative stress.[34]

Downregulation of energy metabolism in RVF

Relative hypoxia and altered states of oxidative stress of the hypertrophic myocardium have been suggested to cause metabolic changes in the RV.[35] RV pressure load leads to changes in fatty acid oxidation (FAO) and uncoupling of glycolysis from glucose-oxidation (GO), but so far it is unclear whether these changes are adaptive or, in contrast, contribute to failure.[31,36,37] In compensated PAB models FAO has been described to be enhanced and pharmacological inhibition of FAO improved cardiac output.[36,37] However, in our failing PAB model there was marked down regulation of the FAO related gene program which suggests that this therapeutic approach might be detrimental in advanced clinical RVF. Although downregulation of genes expressing FAO enzymes not necessarily implies reduced protein, Faber et al previously showed reduced levels of proteins involved in FAO in a model of PAB.[38] The concomitant down regulation of gene sets involved in carbohydrate metabolism, tricarboxylic acid cycle and oxidative phosphorylation in PAB+CF may reflect energy deprivation of the myocardium which is thought to be a final common pathway in heart failure.[39] Indeed, in models of compensated RV pressure load, transcriptome and protemic studies show upregulation of carbohydrate and oxidative phosphorylation pathways,[29,38] which may be a prelude to the transition to failure. Taken together, these findings substantiate hypotheses originating from studies in left ventricular failure and gene profiling studies in different models of RV overload, and suggest that multi-level disruption of the myocardial energy metabolism may be pivotal in the pathobiology of RV failure. Yet, despite the similarities with findings in LV failure, application of medical therapies successful in targeting LV failure did not show any benefit in patients or animal models of RVF.[18,34,40] Thus, the similarities in response do not explain the different phenotypes and further studies to the differences in response are warranted to explain the development of RV failure.

Predictability of clinical RVF facilitates future mechanistic and intervention studies

The here presented approach to the PAB model yields exciting opportunities for mechanistic and intervention studies to further explore the role of myocardial energy metabolism in RVF. As shown in **figure 5**, echocardiographic measurements at 5 weeks (when all rats are still asymptomatic) can be used to predict which rats will develop symptoms of RVF in a limited timeframe. This feature allows for detailed metabolic studies (answering the question whether the metabolic derangement is cause or effect in RVF). Moreover, it allows targeted interventions in either phenotype; at the 5 week time point rats could be randomized to receive pharmacological treatment targeted at either prevention or delay of symptoms (in the PAB+CF group) or improvement of function in the more compensated phenotype (PAB- group).

Limitations

This study comes with some limitations that should be discussed. 1) We studied a relatively small number of animals. The clear distinction in phenotype and major differences in function, morphology and biology however underline that our study had sufficient power. 2) The definition of RVF is a recurring subject of debate. The lack of a generally accepted definition for RVF is hampering studies addressing the progression from beneficial RV-adaptation to maladaptive RV-responses or RVF. We sought for a clinical relevant definition of RVF and used clinical signs of heart failure in the PAB rats. However, since RV failure is not a distinct entity but rather a continuum of progressive disease states, our clinical definition of RV failure, dichotomizing rats in a group with or without clinical RV failure in an effort to study differences throughout the process of RV failure, may be artificial. However, because of the analogy with the clinical presentation in patients, we considered this approach as a clinical relevant definition of RVF. 3) The observational approach of this study yielded several associations between clinical RVF and biological/genetic changes, but obviously, does not prove causal relationships. Nevertheless, the identification of these associations allows for focused studies to delineate the mechanistic role of these changes in RVF.

CONCLUSION

The rat model of chronic 'tight' pulmonary artery banding leads to various degrees of RVF, including severe RVF with clinical symptoms in about half of the animals, characterized by progressive deterioration of diastolic function, a hypoxia-prone cellular environment in the RV myocardium, increased intrinsic protective response to oxidative stress and suppressed myocardial metabolism. This model represents clinical RVF due to increased pressure load and allows for unraveling of the mechanisms involved in the progression from RV adaptation to RV failure and the effect of intervention on these mechanisms.

ACKNOWLEDGEMENTS

The authors are greatly indebted to Michel Weij, who performed the pulmonary artery banding surgeries. We would also like to thank Bibiche Boersma and Martin Dokter for excellent technical assistance and Andre Zandvoort and Annemieke Smit-van Oosten for valuable help with the animal experiments.

FINANCIAL SUPPORT

This study was supported by the Sebald foundation and the Netherlands Heart Foundation [grant#: 2007T068]

CONFLICTS OF INTEREST

None declared.

REFERENCES

1. Norozi K, Wessel A, Alpers V, Arnhold JO, Geyer S, Zoege M, Buchhorn R. Incidence and Risk Distribution of Heart Failure in Adolescents and Adults With Congenital Heart Disease After Cardiac Surgery. *Am J Cardiol* 2006;**97**:1238–1243.
2. Wolferen SA Van, Marcus JT, Boonstra A, Marques KMJ, Bronzwaer JGF, Spreeuwenberg MD, Postmus PE, Vonk-Noordegraaf A. Prognostic value of right ventricular mass, volume, and function in idiopathic pulmonary arterial hypertension. *Eur Heart J* 2007;**28**:1250–1257.
3. Meyer P, Filippatos GS, Ahmed MI, Iskandrian AE, Bittner V, Perry GJ, White M, Aban IB, Mujib M, Italia LJD, Ahmed A. Effects of Right Ventricular Ejection Fraction on Outcomes in Chronic Systolic Heart Failure. 2010;252–259.
4. Bartelds B, Borgdorff M a., Smit-Van Oosten A, Takens J, Boersma B, Nederhoff MG, Elzenga NJ, Gilst WH Van, Windt LJ De, Berger RMF. Differential responses of the right ventricle to abnormal loading conditions in mice: Pressure vs. volume load. *Eur J Heart Fail* 2011;13:1275–1282.
5. Voelkel NF, Quaife RA, Leinwand LA, Barst RJ, McGoon MD, Meldrum DR, Dupuis J, Long CS, Rubin LJ, Smart FW, Suzuki YJ, Gladwin M, Denholm EM, Gail DB. Right ventricular function and failure: Report of a National Heart, Lung, and Blood Institute working group on cellular and molecular mechanisms of right heart failure. *Circulation* 2006;114:1883–1891.
6. Borgdorff M a J, Bartelds B, Dickinson MG, Steendijk P, Vroomen M de, Berger RMF. Distinct loading conditions reveal various patterns of right ventricular adaptation. *Am J Physiol Heart Circ Physiol* 2013;305:H354-64.
7. Gomez-Arroyo JG, Farkas L, Alhussaini AA, Farkas D, Kraskauskas D, Voelkel NF, Bogaard HJ. The monocrotaline model of pulmonary hypertension in perspective. *Am J Physiol - Lung Cell Mol Physiol* 2012;302:363–369.
8. Bogaard HJ, Natarajan R, Henderson SC, Long CS, Kraskauskas D, Smithson L, Ockaili R, McCord JM, Voelkel NF. Chronic pulmonary artery pressure elevation is insufficient to explain right heart failure. *Circulation* 2009;120:1951–1960.
9. Faber MJ, Dalinghaus M, Lankhuizen IM, Steendijk P, Hop WC, Schoemaker RG, Duncker DJ, Lamers JM, Helbing WA. Right and left ventricular function after chronic pulmonary artery banding in rats assessed with biventricular pressure-volume loops. *Am J Physiol Hear Circ Physiol* 2006;291:H1580-6.
10. Schou UK, Peters CD, Wan Kim S, Frøkiær J, Nielsen S. Characterization of a rat model of right-sided heart failure induced by pulmonary trunk banding. *J Exp Anim Sci* 2007;43:237–254.
11. Bartelds B, Borgdorff M, Berger R. Right Ventricular Adaptation in Congenital Heart Diseases. *J Cardiovasc Dev Dis* 2014;1:83–97.
12. Haddad F, Doyle R, Murphy DJ, Hunt SA. Right ventricular function in cardiovascular disease, part II: Pathophysiology, clinical importance, and management of right ventricular failure. *Circulation* 2008;117:1717–1731.
13. Andersen A, Nielsen JM, Peters CD, Schou UK, Sloth E, Nielsen-Kudsk JE. Effects of phosphodiesterase-5 inhibition by sildenafil in the pressure overloaded right heart. *Eur J Heart Fail* European Society of Cardiology; 2008;10:1158–1165.
14. Gaynor SL, Maniar HS, Bloch JB, Steendijk P, Moon MR. Right atrial and ventricular adaptation to chronic right ventricular pressure overload. *Circulation* 2005;112:212–218.

15. Hessel MHM, Steendijk P, Adel B Den, Schutte CI, Laarse A Van Der. Characterization of right ventricular function after monocrotaline-induced pulmonary hypertension in the intact rat. *Am J Physiol - Hear Circ Physiol* 2006;291:2424–2430.
16. Borgdorff M a J, Bartelds B, Dickinson MG, Boersma B, Weij M, Zandvoort A, Silljé HHW, Steendijk P, Vroomen M De, Berger RMF. Sildenafil enhances systolic adaptation, but does not prevent diastolic dysfunction, in the pressure-loaded right ventricle. *Eur J Heart Fail* 2012;14:1067–1074.
17. Schäfer S, Ellinghaus P, Janssen W, Kramer F, Lustig K, Milting H, Kast R, Klein M. Chronic inhibition of phosphodiesterase 5 does not prevent pressure-overload-induced right-ventricular remodelling. *Cardiovasc Res* 2009;82:30–39.
18. Borgdorff MA, Bartelds B, Dickinson MG, Steendijk P, Berger RMF. A cornerstone of heart failure treatment is not effective in experimental right ventricular failure. *Int J Cardiol* Elsevier Ireland Ltd; 2013;169:183–189.
19. Lin K, Kools H, Groot PJ de, Gavai AK, Basnet RK, Cheng F, Wu J, Wang X, Lommen A, Hooiveld GJEJ, Bonnema G, Visser RGF, Muller MR, Leunissen JAM. MADMAX – Management and analysis database for multiple ~omics experiments. *J Integr Bioinform* 2011;8:160.
20. Huang DW, Sherman BT, Lempicki RA. Systematic and integrative analysis of large gene lists using DAVID bioinformatics resources. *Nat Prot*oc 2009;4:44–57.
21. Subramanian A, Tamayo P, Mootha VK, Mukherjee S, Ebert BL, Gillette MA, Paulovich A, Pomeroy SL, Golub TR, Lander ES, Mesirov JP. Gene set enrichment analysis: A knowledge-based approach for interpreting genome-wide expression profiles. *Proc Natl Acad Sci U S A* 2005;102:15545–15550.
22. Toischer K, Rokita AG, Unsöld B, Zhu W, Kararigas G, Sossalla S, Reuter SP, Becker A, Teucher N, Seidler T, Grebe C, Preu L, Gupta SN, Schmidt K, Lehnart SE, Krüger M, Linke WA, Backs J, Regitz-Zagrosek V, Schäfer K, Field LJ, Maier LS, Hasenfuss G. Differential cardiac remodeling in preload versus afterload. *Circulation* 2010;122:993–1003.
23. Vaidya A, Kawut SM. Relax or contract: What's right? *Circulation* 2013;128:1999–2001.
24. Rain S, Handoko ML, Trip P, Gan CT-J, Westerhof N, Stienen GJ, Paulus WJ, Ottenheijm CAC, Marcus JT, Dorfmüller P, Guignabert C, Humbert M, Macdonald P, Remedios C Dos, Postmus PE, Saripalli C, Hidalgo CG, Granzier HL, Vonk-Noordegraaf A, Velden J Van Der, Man FS De. Right ventricular diastolic impairment in patients with pulmonary arterial hypertension. *Circulation* F.S. De Man, Department of Pulmonology, VU University Medical Center, Institute for Cardiovascular Research, 1081 HV Amsterdam, Netherlands; 2013;128:2016–2025.
25. Borgdorff MA, Bartelds B, Dickinson MG, Wiechen MPH van, Steendijk P, Vroomen M de, Berger RMF. Sildenafil treatment in established right ventricular dysfunction improves diastolic function and attenuates interstitial fibrosis independent from afterload. *AJP Hear Circ Physiol* 2014;307:H361–H369.
26. Leeuwenburgh BPJ, Helbing WA, Steendijk P, Schoof PH, Baan JAN. Biventricular systolic function in young lambs subject to chronic systemic right ventricular pressure overload. *Am J Physiol - Hear Circ Phys*iol 2001;281:2697–2704.
27. Correia-Pinto J, Henriques-Coelho T, Roncon-Albuquerque R, Leite-Moreira AF. Differential right and left ventricular diastolic tolerance to acute afterload and NCX gene expression in

wistar rats. *Physiol Res* 2006;55:513–526.

28. Apitz C, Honjo O, Humpl T, Li J, Assad RS, Cho MY, Hong J, Friedberg MK, Redington AN. Biventricular structural and functional responses to aortic constriction in a rabbit model of chronic right ventricular pressure overload. *J Thorac Cardiovasc Surg* The American Association for Thoracic Surgery; 2012;144:1494–1501.
29. Friehs I, Cowan DB, Choi Y-H, Black KM, Barnett R, Bhasin MK, Daly C, Dillon SJ, Libermann TA, McGowan FX, Nido PJ del, Levitsky S, McCully JD. Pressure-overload hypertrophy of the developing heart reveals activation of divergent gene and protein pathways in the left and right ventricular myocardium. *AJP Hear Circ Physiol* 2013;304:H697-708.
30. Wilkins BJ, Dai YS, Bueno OF, Parsons SA, Xu J, Plank DM, Jones F, Kimball TR, Molkentin JD. Calcineurin/NFAT Coupling Participates in Pathological, but not Physiological, Cardiac Hypertrophy. *Circ* Res 2004;94:110–118.
31. Piao L, Marsboom G, Archer SL. Mitochondrial metabolic adaptation in right ventricular hypertrophy and failure. *J Mol Med* S. L. Archer, Harold Hines Jr. Department of Medicine, University of Chicago, Chicago, IL 60637, United States; 2010;88:1011–1020.
32. Steinberg SF. Oxidative stress and sarcomeric proteins. *Circ Res* 2013;112:393–405.
33. Wang G, Hamid T, Keith RJ, Zhou G, Partridge CR, Xiang X, Kingery JR, Lewis RK, Li Q, Rokosh DG, Ford R, Spinale FG, Riggs DW, Srivastava S, Bhatnagar A, Bolli R, Prabhu SD. Cardioprotective and antiapoptotic effects of heme oxygenase-1 in the failing heart. *Circulation* 2010;121:1912–1925.
34. Bogaard HJ, Mizuno S, Hussaini A a. Al, Toldo S, Abbate A, Kraskauskas D, Kasper M, Natarajan R, Voelkel NF. Suppression of histone deacetylases worsens right ventricular dysfunction after pulmonary artery banding in rats. *Am J Respir Crit Care Med* 2011;183: 1402–1410.
35. Bogaard HJ, Abe K, Noordegmaf A V, Voelkel NF. The right ventricle under pressure. *Chest* N. F. Voelkel, Department oj Pulmonary Medicine and Critical Care, Virginia Commonwealth University, Sanger Hall, Richmond, VA 23284; 2009;135:794–804.
36. Gomez-Arroyo J, Mizuno S, Szczepanek K, Tassell B Van, Natarajan R, Remedios CG Dos, Drake JI, Farkas L, Kraskauskas D, Wijesinghe DS, Chalfant CE, Bigbee J, Abbate A, Lesnefsky EJ, Bogaard HJ, Voelkel NF. Metabolic gene remodeling and mitochondrial dysfunction in failing right ventricular hypertrophy secondary to pulmonary arterial hypertension. *Circ Hear* Fail 2013;6:136–144.
37. Fang Y-H, Piao L, Hong Z, Toth PT, Marsboom G, Bache-Wiig P, Rehman J, Archer SL. Therapeutic inhibition of fatty acid oxidation in right ventricular hypertrophy: Exploiting Randle's cycle. *J Mol Med* S.L. Archer, Medicine/Cardiology, University of Chicago, Chicago, IL 60637, United States; 2012;90:31–43.
38. Faber MJ, Dalinghaus M, Lankhuizen IM, Bezstarosti K, Verhoeven AJM, Duncker DJ, Helbing WA, Lamers JMJ. Time dependent changes in cytoplasmic proteins of the right ventricle during prolonged pressure overload. *J Mol Cell Cardiol* M. Dalinghaus, Erasmus MC-Sophia, Department of Pediatrics, Division of Pediatric Cardiology, 3015 GJ Rotterdam, Netherlands; 2007;43:197–209.
39. Neubauer S. The Failing Heart — An Engine Out of Fuel. *N Engl J Med* 2007;356:1140–1151.
40. Roche SL, Redington AN. Right ventricle: Wrong targets? Another blow for pharmacotherapy in congenital heart diseases. *Circulation* 2013;127:314–316.

SUPPLEMENTARY MATERIAL

Animal care and experiments were conducted according to the Dutch Animal Experimental Act and conform to the *Guide for the Care and Use of Laboratory Animals* published by the US National Institutes of Health (NIH Publication No. 85-23, revised 1996). The Animal Experiments Committee of the University of Groningen, the Netherlands approved the experimental protocol.

Symptoms and signs of clinical RV failure (ABCDE system)

Rats were daily checked for symptoms of RV failure, as described before.[1,2] The A-symptoms were considered present when the animal had a ruffled fur, red discoloration of head and neck (due to decreased cleaning-behaviour) or was less active than previously, despite stimulation. Bodyweight in RVF can either decrease due to low intake or steeply increase due fluid retention in chest and abdomen. The bodyweight-symptom was therefore considered present if there was a change in bodyweight of more than 15 grams in <48 hours. Cyanosis was checked at exposed skin on head, paws and tail. Hampered peripheral circulation was considered present if both front paws and hind legs/tail were pale and markedly colder than normally. Dyspnea and tachypnea were defined as markedly increased breathing-effort and, -frequency, respectively. Edema and effusions were defined as fluid collection in thorax and/or abdomen, palpable (ascites) and confirmed at termination (pleural/ pericardial effusion and ascites).

Voluntary exercise

To measure voluntary exercise,[3,4] running wheels were mounted in the rat cages. Five days before PAB/sham surgery, 5 days before the 5-wks time point and 5 days before sacrifice (for those that reached the 11-wks time point; due to the sudden onset of clinical RVF (<48u), exercise testing could not be performed in PAB- and PAB+CF rats at end point), rats were allowed to run in the cage wheel. Running distance was recorded daily using a digital magnetic counter (Commodoor Cycle Odometer, Commodoor, the Netherlands) and used as a measure of voluntary exercise. Because of large inter-individual variation, the percentage change in run distance versus baseline was used as outcome.

Echocardiography

Echocardiography was performed at 5 weeks and at termination in all animals. Echocardiography was performed as described previously[4] using a Vivid Dimension

7 system and 10S-transducer (GE Healthcare, Waukesha, WI, USA). Rats were anesthetized with isoflurane (5% induction; 2-3% maintenance; a pulse-oxymeter (Nonin Medical, Plymouth, MN, USA) was used to monitor adequacy of anesthesia). We used apical 3- and 4- chamber views and parasternal short and long axis views to measure RV dimensions, tricuspid insufficiency, TAPSE, and gradient across the PAB. Cardiac output was calculated using systolic aorta diameter and pulsed wave Doppler of aorta flow as (aorta diameter)^2 × 3.14 × velocity time integral (VTI) x heart rate. The mean of measurements from 6-12 consecutive beats with a proper signal was taken to average out beat-to-beat variation.

Pressure-volume analysis

At termination, hemodynamic characterization of the RV was performed by pressure-volume analysis, obtained by RV catheterization according to a previously described protocol.[4]

Rats were anesthetized with isoflurane (5% induction; 2-3% maintenance; a pulse-oxymeter (Nonin Medical, Plymouth, MN, USA) was used to monitor adequacy of anesthesia), intubated and ventilated. Analgesia was applied using buprenorphine 0.01 mg/kg s.c. at the start of the procedure. Subsequently the rat was positioned supine under a stereomicroscope (Zeiss, Hamburg, Germany) and fixated on a temperature-controlled warming pad. The right jugular vein was dissected and cannulated facilitating hypertonic saline infusions. Following bilateral thoracotomy and pericardiotomy a combined pressure-conductance catheter (SPR-869, Millar Instruments Inc., Houston, TX, USA) was introduced via the apex into the RV and positioned in the RV outflow tract. RV pressures and conductance were recorded using a MPVS 400 processor at a sample rate of 1.000 Hz with Chart 5 (Millar Instruments Inc., Houston, TX, USA). Subsequently, via the dissection in the neck, the right carotid artery was exposed and the catheter was introduced via the right carotid artery and ascending aorta into the LV to measure LV pressures. Blood loss during the procedure was minimal (<0.5mL). Analyses were performed offline using custom-made software (CircLab 2012, P. Steendijk). Steady-state pressure-conductance data were obtained by averaging the values of 3 steady-state recordings (at least 7 loops each).

Parameters obtained from pressure-volume loops included heart rate, peak pressure, end diastolic pressure and maximal and minimal first time-derivative of pressure (dP/dtmax and dP/dtmin). The relaxation time constant (tau) was calculated as the time constant of monoexponential decay of RV pressure during isovolumic relaxation.

Stroke volume (in arbitrary units) derived from the conductance signal was calibrated, using stroke volume (in mL) measured by echocardiography. End systolic and end diastolic elastance were determined using the single-beat method;[5,6] vena cava

occlusion caused immediate fatal deterioration of cardiac function in the PAB+CF rats precluding this method to determine elastance.

Organ weights, staining

After heart catheterization, the rats were euthanized by removing the heart from the thorax. Heart, lungs and liver were dissected. RV, interventricular septum, LV and both atria were separated and weighed. The liver lobe and lung lobe were weighed, dried overnight at 65˚C and weighed again to determine wet weight/dry weight ratio. Midventricular RV sections were fixated (formalin) and stained to assess cardiomyocyte cross-sectional area (wheat germ agglutinin), fibrosis (Masson Tri-chrome), capillary density (lectin) and macrophages (CD68) as described previously.[3,4,7,8] Microscopy-imaging was performed at the UMCG Imaging Center (UMIC), which is supported by the Netherlands Organization for Health Research and Development (ZonMW grant 40-00506-98-9021).

Western blot

Protein was extracted using RIPA buffer; protein concentration was measured using Protein Assay (Bio-Rad Laboratories B.V., Veenendaal). Protein was put on a gel and after electrophoresis semi-dry blotting was performed. Protein transfer to the blot was confirmed with Ponceau S staining. After blotting, the membrane was blocked using 5% Elk in TBS/0,1% Tween for at least 30 min and incubated with antibodies specific to SERCA, PLN and phosphorylated PLN and standard secondary antibodies. Tubulin was used as a loading control. Protein detection and quantification was done with ImageQuant LAS 4000 (GE Healthcare Life Sciences).

Protein kinase activity assays

PKG activity was measured in RV (free wall) tissue using the cyclex cyclic GMP dependent protein kinase (cGK) assay kit (CycLex Co., Nagano, Japan). Samples were prepared in extraction buffer (50 mM potassium phosphate buffer, 1 mM EDTA, 1 mM EGTA, 5 mM DTT, 4 ul/mL phosphate inhibitor), potassium phosphate buffer and DE-buffer (20 mM Tris-HCl, 60 mM NaCl, 0,5 mM EDTA, 1 mM EGTA, 4 uL/mL phosphatase inhibitors) according to the assay protocol. 100uL of each sample was then added to the plate, which was precoated with recombinant G-kinase substrate. After incubation (30 min, 30˚C) and a washing step, incubation with 100uL of HRP conjugated anti-phopho-specific antibody for an hour at room temperature was performed. After another washing step, substrate reagent was added to incubate for 15 minutes; with stop solution the reaction was terminated. Absorbance was read in

at dual wavelengths of 450/540 nm. Data are presented as quantities of cGK activity expressed in units per ug protein, as measured with the BioRad DC Protein Assay.

PKA activity was measured using the MESACUP Protein Kinase Assay (MBL CO., Ltd, Nagoya, Japan). Sample preparation was done similarly to PKG sample preparation with the same extraction buffers. 100 uL of each prepared sample was added to each well (incubated for 10 min, 25˚C) followed by stop solution. After washing 100 uL biotinylated antibody 2B9 was added (incubated for 60 min, 25˚C) and again the plate was washed. The addition of POD-conjugated streptavidin (incubated for 60 minutes at 25˚C), substrate solution (incubated for 3 min at 25˚C) and stop solution was interspersed by washing steps. The absorbance was read at a wavelength of 492 nm. Data are presented as relative PKA activity.

qRT-PCR

To characterize the hypertrophy response and study the regulation fibrosis and capillary growth, expression of the fetal gene program (myosin heavy chain isoforms, natriuretic pro peptides type A and B) and markers of hypertrophy (ACTA, ACTC, RCAN1), fibrosis (TGFβ-1, OPN-1, Col1A2, Col3A1), capillary growth (VEGF-A, VEGF-R1, VEGF-R2), and oxidative stress (HO-1, NOX-4) were measured. We also specifically measured mRNA expression of genes involved in the regulation of systolic and diastolic function (SERCA-ATPase, phospholamban, sodium-calcium exchanger (NCX) and titin isoforms N2B and N2Ba. RV (free wall) tissue was snap-frozen in liquid nitrogen. Total RNA was extracted using TRIzol reagent (Invitrogen Corporation, Carlsbad, CA, USA); high quality was confirmed (RQI 9.3) using Experion (Bio-Rad, Veenendaal, the Netherlands), before conversion to cDNA by QuantiTect Reverse Transcription (Qiagen, Venlo, the Netherlands). Gene expression was measured with Absolute QPCR SYBR Green ROX mix (Abgene, Epsom, UK) in the presence of 7.5ng cDNA and 200nM forward and reverse primers. qRT-PCR was carried out on the Biorad CFX384 (Bio-Rad, Veenendaal, the Netherlands) using a standard protocol. Primer sequences are available upon request. mRNA levels are expressed in relative units based on a standard curve obtained by a calibrator cDNA mixture. All measured mRNA expression levels were corrected for 36B4 reference gene expression.

Transcriptome-wide expression profiling

Total RNA was isolated from the right ventricular free wall using TRI reagent (Sigma, St. Louis, MO) according to the manufacturer's protocol. RNA was purified for individual rats (n=7/4/5 CON/PAB-/PAB+CF) using the Qiagen RNeasy mini kit (Venlo, The Netherlands); RNA quality was verified (RIN >9) (Agilent, Amstelveen, the Netherlands). Biotin-labeling, hybridization, washing and scanning of GeneChip Rat

Gene 1.1 ST arrays (Affymetrics) were performed according to standard Affymetrix protocols.

Quality control and normalization

Scans of the Affymetrix arrays were processed in the MADMAX pipeline (Nutrigenomics Consortium, Wageningen, The Netherlands)[9] using Bioconductor software packages. Quality control was carried out by visual inspection of the heat map, Affymetrics Quality Control metrics, Relative Log Expression-plot, Normalized Unscaled Standard Error-plot and hierarchical clustering. Expression levels of probe sets were normalized using the robust multi-array average algorithm[10] with 19239 transcripts passing the filter. Probe sets were assigned to genes using the custom CDF library version 15.1.1. Array data are deposited at the Gene Expression Omnibus (GEO) database (GSE46863).

Differential expression of individual genes

Differentially expressed probe sets were identified using an IBMT regularized t-test.[11] P values were corrected for multiple testing using a false discovery rate method. Probe sets that satisfied the criterion of a false discovery rate <1% were considered significantly regulated.

Gene set enrichment analysis

Gene set enrichment analysis (GSEA, version 3.1)[12] was used to explore changes in the global gene expression pattern. Out of 899 predefined gene sets (gene set size set to min=50, max=500), those passing the criteria false discovery rate (FDR) <15%, nominal *P* value <0.05 and normalized enrichment score >1.3 were considered significant. All gene sets available were obtained from the C2-curated Molecular Signatures Database.

DAVID

Database for Annotation, Visualization and Integrated Discovery (DAVID) software was used to categorize genes into biological processes.[13,14] In DAVID, statistical significance of differential expression of a biological process was assessed using moderated *t*-tests; p-values were adjusted for multiple testing to control false discovery rate using the Benjamini method. P<0.01 was considered significant.

Comparisons in transcriptome array

Within the mentioned significance criteria, the PAB- vs. CON and PAB+CF vs. CON comparisons were sufficiently powered. The third comparison (PAB- vs. PAB+CF), however, only yielded significantly regulated genes with additional filtering (fold change>1.3). We therefore described the differences between PAB- and PAB+CF by contrasting the PAB-/CON and PAB+CF/CON comparisons.

SUPPLEMENTAL REFERENCES

1. Borgdorff MA, Bartelds B, Dickinson MG, Steendijk P, Berger RMF. A cornerstone of heart failure treatment is not effective in experimental right ventricular failure. *Int J Cardiol* Elsevier Ireland Ltd; 2013;169:183–189.
2. Borgdorff M a J, Bartelds B, Dickinson MG, Steendijk P, Vroomen M de, Berger RMF. Distinct loading conditions reveal various patterns of right ventricular adaptation. *Am J Physiol Heart Circ Physiol* 2013;305:H354-64.
3. Bartelds B, Borgdorff M a., Smit-Van Oosten A, Takens J, Boersma B, Nederhoff MG, Elzenga NJ, Gilst WH Van, Windt LJ De, Berger RMF. Differential responses of the right ventricle to abnormal loading conditions in mice: Pressure vs. volume load. *Eur J Heart Fail* 2011;13:1275–1282.
4. Borgdorff M a J, Bartelds B, Dickinson MG, Boersma B, Weij M, Zandvoort A, Silljé HHW, Steendijk P, Vroomen M De, Berger RMF. Sildenafil enhances systolic adaptation, but does not prevent diastolic dysfunction, in the pressure-loaded right ventricle. *Eur J Heart Fail* 2012;14:1067–1074.
5. Brimioulle S, Wauthy P, Ewalenko P, Rondelet B, Vermeulen F, Kerbaul F, Naeije R. Single-beat estimation of right ventricular end-systolic pressure-volume relationship. *Am J Physiol Heart Circ Physiol* 2003;284:H1625-30.
6. Rain S, Handoko ML, Trip P, Gan CT-J, Westerhof N, Stienen GJ, Paulus WJ, Ottenheijm CAC, Marcus JT, Dorfmüller P, Guignabert C, Humbert M, Macdonald P, Remedios C Dos, Postmus PE, Saripalli C, Hidalgo CG, Granzier HL, Vonk-Noordegraaf A, Velden J Van Der, Man FS De. Right ventricular diastolic impairment in patients with pulmonary arterial hypertension. *Circulation* F.S. De Man, Department of Pulmonology, VU University Medical Center, Institute for Cardiovascular Research, 1081 HV Amsterdam, Netherlands; 2013;128:2016–2025.
7. Albada ME Van, Marchie Sarvaas GJ Du, Koster J, Houwertjes MC, Berger RMF, Schoemaker RG. Effects of erythropoietin on advanced pulmonary vascular remodelling. *Eur Respir J* 2008;31:126–134.
8. Yu L, Ruifrok WPT, Meissner M, Bos EM, Goor H Van, Sanjabi B, Harst P Van Der, Pitt B, Goldstein IJ, Koerts JA, Veldhuisen DJ Van, Bank RA, Gilst WH Van, Silljé HHW, Boer RA De. Genetic and pharmacological inhibition of galectin-3 prevents cardiac remodeling by interfering with myocardial fibrogenesis. *Circ Hear Fail* 2013;6:107–117.
9. Lin K, Kools H, Groot PJ de, Gavai AK, Basnet RK, Cheng F, Wu J, Wang X, Lommen A, Hooiveld GJEJ, Bonnema G, Visser RGF, Muller MR, Leunissen JAM. MADMAX – Management and analysis database for multiple ~omics experiments. *J Integr Bioinform* 2011;8:160.
10. Allison DB, Cui X, Page GP, Sabripour M. Microarray data analysis: From disarray to consolidation and consensus. *Nat Rev Genet* 2006;7:55–65.
11. Sartor MA, Tomlinson CR, Wesselkamper SC, Sivaganesan S, Leikauf GD, Medvedovic M. Intensity-based hierarchical Bayes method improves testing for differentially expressed genes in microarray experiments. *BMC Bioinformatics* 2006;7:1–17.
12. Subramanian A, Tamayo P, Mootha VK, Mukherjee S, Ebert BL, Gillette MA, Paulovich A, Pomeroy SL, Golub TR, Lander ES, Mesirov JP. Gene set enrichment analysis: A knowledge-based approach for interpreting genome-wide expression profiles.

Proc Natl Acad Sci U S A 2005;**102**:15545–15550.

13. Huang DW, Sherman BT, Lempicki RA. Systematic and integrative analysis of large gene lists using DAVID bioinformatics resources. *Nat Protoc* 2009;4:44–57.
14. Huang DW, Sherman BT, Lempicki RA. Bioinformatics enrichment tools: Paths toward the comprehensive functional analysis of large gene lists. *Nucleic Acids Res* 2009;37:1–13.

SUPPLEMENTAL FIGURES

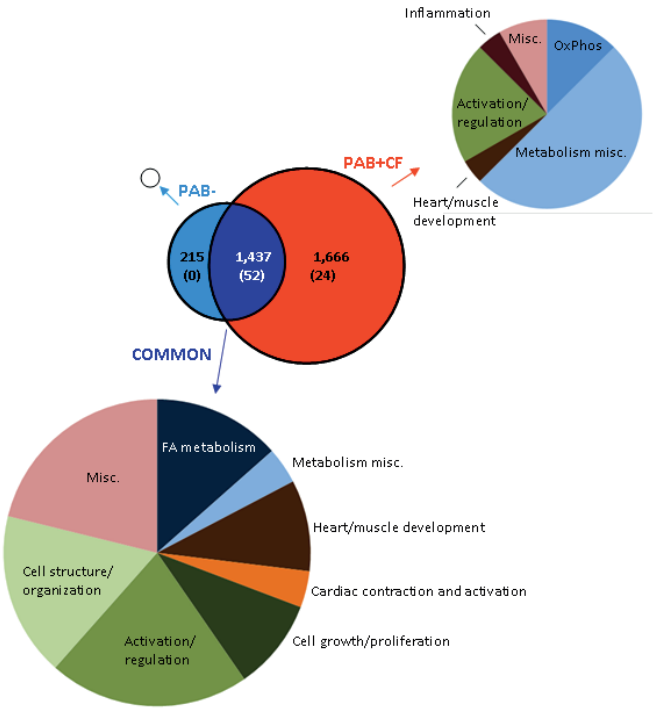

Supplemental figure 1 . Significantly regulated genes in PAB- and PAB+CF. Analysis of gene expression. Number of differentially expressed genes vs. CON in PAB- (blue) and PAB+CF (red) is indicated in the circles. Commonly regulated genes in purple. Number of significantly related biological processes (DAVID) between brackets. Pie-chart shows distribution of the related biological processes in categories for PAB+CF and COMMON. N=7/4/5 for CON/PAB-/PAB+CF. Individual genes: Limma P controlled with false discovery rate <1% was considered significant. DAVID: P<0.01 and Benjamini <0.01 was considered significant.

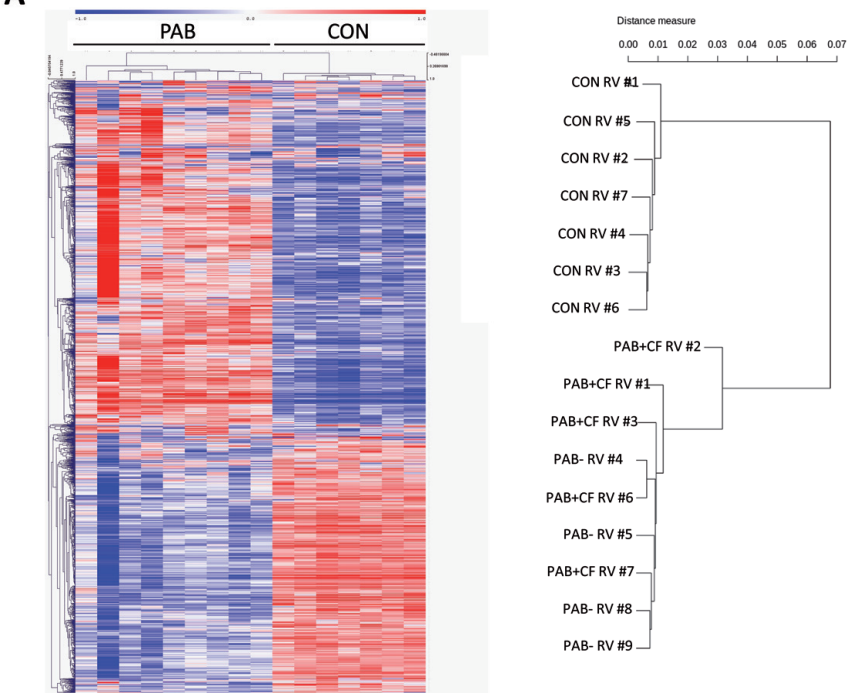

Supplemental figure 2. A Heat map display of mRNA expressed in CON, PAB- and PAB+CF. B Dendrogram using Ward hierarchical clustering on the Pearson distance measure (RMA).

SUPPLEMENTAL TABLES

Supplemental table 1. Heartcatherization and echocardiographic data in PAB- and PAB (11w).

	PAB-	PAB (11w)	*p-value*
Number of rats	4	3	
Heartcath parameters			
HR (/min)	258±24	272±6	*0.65*
dP/dtmax corr	32.3±3.7	32.7±2.0	*0.94*
dP/dtmin corr (*-1)	32.7±2.8	32.1±3.7	*0.89*
Tau (ms)	27.3±3.9	25.4±0.7	*0.70*
Tau/cyclelength (ms/s)	114±9	115±4	*0.91*
Echocardiographic parameters 5wk			
Tricuspid insufficiency (%)	100%	100%	*1.00*
Pericardial effusion (%)	0%	0%	*1.00*
RVEDD (mm)	5.3±0.4	5.8±0.3	*0.36*
PAB gradient (mmHg)	74±5	63±4	*0.17*
RA diameter (mm)	5.2±0.3	3.5±0.4	*0.19*
TAPSE (mm)	1.7±0.2	1.9±0.4	*0.52*
HR (/min)	315±18	329±9	*0.56*
SV (uL)	205±20	233±6	*0.29*
Echocardiographic parameters endpoint			
Tricuspid insufficiency (%)	100%	100%	*1.00*
Pericardial effusion (%)	0%	0%	*1.00*
RVEDD (mm)	6.2±0.2	7.0±0.4	*0.10*
PAB gradient (mmHg)	72±11	113±12	*0.06*
RA diameter (mm)	6.0±0.1	6.5±0.3	*0.13*
TAPSE (mm)	2.0±0.2	2.0±0.1	*0.96*
HR (/min)	304±11	328±14	*0.23*
SV (uL)	271±24	292±33	*0.63*

HR= heart rate, dP/dt max corr= dP/dt max normalized for RV peak pressure, dP/dt min corr= dP/dt min normalized for RV end systolic pressure, RVEDD= right ventricular enddiastolic volume, PAB= pulmonary artery banding, RA= right atrium, TAPSE= tricuspid annular plane systolic excursion, SV= stroke volume. Values are mean ± SEM. Significance indicated by p-values from t-test PAB- vs. PAB(11w).

Supplemental table 2. Genes up- or down regulated vs. CON in both PAB- and PAB+CF.
Due to excessive length not added to this version of the manuscript.

Supplemental table 3. Gene Sets specifically downregulated in PAB+CF

CATEGORY	GENE SET
Glycolysis and glyconeogenesis	REACT_GLUCOSE METABOLISM
Metabolism miscellaneous	REACT_PYRUVATE METABOLISM AND CITRIC ACID (TCA) CYCLE
Activation and regulation	REACT_PKB-MEDIATED EVENTS
Activation and regulation	REACT_MTOR SIGNALLING
Glycolysis and glyconeogenesis	REACT_GLUCONEOGENESIS
Growth, proliferation and cellcyle	WIP_RN_NUCLEAR_RECEPTORS
Miscellaneous	KEGG_05016_HUNTINGTON'S DISEASE
Glycolysis and glyconeogenesis	WIP_RN_GLYCOLYSIS_AND_GLUCONEOGENESIS
Miscellaneous	REACT_OLFACTORY SIGNALING PATHWAY
Metabolism miscellaneous	WIP_RN_TRYPTOPHAN_METABOLISM
Growth, proliferation and cellcyle	REACT_TRNA AMINOACYLATION
Glycolysis and glyconeogenesis	WIP_RN_GLYCOGEN_METABOLISM
Metabolism miscellaneous	KEGG_00380_TRYPTOPHAN METABOLISM
Contraction and activation	KEGG_04260_CARDIAC MUSCLE CONTRACTION
Metabolism miscellaneous	KEGG_00330_ARGININE AND PROLINE METABOLISM
Development heart and muscle	KEGG_05412_ARRHYTHMOGENIC RIGHT VENTRICULAR CARDIOMYOPATHY (ARVC)
Glycolysis and glyconeogenesis	REACT_METABOLISM OF CARBOHYDRATES
Miscellaneous	KEGG_04910_INSULIN SIGNALING PATHWAY
Miscellaneous	WIP_RN_HYPOTHETICAL_NETWORK_FOR_DRUG_ADDICTION
Activation and regulation	REACT_CALMODULIN INDUCED EVENTS
Activation and regulation	REACT_PLC-GAMMA1 SIGNALLING
Miscellaneous	REACT_CAM PATHWAY
Metabolism miscellaneous	KEGG_00592_ALPHA-LINOLENIC ACID METABOLISM
Metabolism miscellaneous	KEGG_00230_PURINE METABOLISM
Metabolism miscellaneous	NCI_RETINOIC_ACID_PATHWAY
Miscellaneous	WIP_RN_MONOAMINE_GPCRS
Glycolysis and glyconeogenesis	KEGG_00051_FRUCTOSE AND MANNOSE METABOLISM
Miscellaneous	BIOC_INSULINPATHWAY
Glycolysis and glyconeogenesis	KEGG_00010_GLYCOLYSIS / GLUCONEOGENESIS
Metabolism miscellaneous	REACT_PEROXISOMAL LIPID METABOLISM
Activation and regulation	NCI_MAPKTRKPATHWAY

SIZE= number of genes in respective GSEA set, NES= normalized enrichment score (analogous to fold change), NOM= nominal, FDR= false discovery rate.

SIZE	NES PAB+CF vs. CON	NOM p-value PAB+CF	FDR q-value PAB+CF
45	-2.01	0.000	0.001
27	-1.98	0.000	0.002
19	-1.91	0.002	0.005
19	-1.88	0.000	0.006
27	-1.85	0.002	0.008
34	-1.78	0.002	0.017
165	-1.76	0.000	0.021
36	-1.75	0.002	0.022
41	-1.74	0.000	0.023
41	-1.73	0.005	0.025
24	-1.73	0.009	0.025
33	-1.68	0.007	0.040
44	-1.67	0.004	0.043
68	-1.67	0.002	0.041
49	-1.65	0.000	0.049
68	-1.65	0.002	0.049
76	-1.64	0.003	0.050
126	-1.64	0.000	0.050
31	-1.64	0.010	0.051
17	-1.63	0.016	0.054
24	-1.62	0.011	0.058
17	-1.61	0.000	0.058
18	-1.57	0.029	0.080
151	-1.53	0.002	0.114
26	-1.53	0.035	0.114
31	-1.53	0.023	0.110
32	-1.52	0.042	0.115
18	-1.52	0.045	0.116
62	-1.51	0.012	0.123
15	-1.49	0.057	0.146
32	-1.48	0.034	0.146

3

CHAPTER 3

Metabolic remodelling in the pressure loaded right ventricle: shifts in glucose and fatty acid metabolism – a systematic review and meta-analysis

A.M.C. Koop, G.P.L. Bossers, M.J. Ploegstra, Q.A.J. Hagdorn, R.M.F. Berger, H.H.W. Silljé, B. Bartelds

- Journal of American Heart Association. 2019; 8

ABSTRACT

Background

Right ventricular (RV) failure due to chronic pressure load is an important determinant of outcome in pulmonary hypertension. Progression towards RV failure is characterized by diastolic dysfunction, fibrosis and metabolic dysregulation. Metabolic modulation has been suggested as therapeutic option, yet, metabolic dysregulation may have various faces in different experimental models and disease severity. In this systematic review and meta-analysis, we aimed to identify metabolic changes in the pressure loaded RV and formulate recommendations required to optimize translation between animal models and human disease.

Methods and results

Medline and EMBASE were searched to identify original studies describing cardiac metabolic variables in the pressure loaded RV. We identified mostly rat-models, inducing pressure load by hypoxia, sugen-hypoxia, monocrotaline, pulmonary artery banding (PAB) or strain (fawn hooded rats, FHR), and human studies. Meta-analysis revealed increased Hedges' g (effect size) of the gene expression of GLUT1 and HK1 and glycolytic flux. The expression of MCAD was uniformly decreased. Mitochondrial respiratory capacity and fatty acid uptake varied considerably between studies, yet there was a model effect in carbohydrate respiratory capacity in MCT-rats.

Conclusion

This systematic review and meta-analysis on metabolic remodelling in the pressure loaded RV showed a consistent increase in glucose uptake and glycolysis, strongly suggest a downregulation of beta-oxidation, and showed divergent and model specific changes regarding fatty acid uptake and oxidative metabolism. To translate metabolic results from animal models to human disease, more extensive characterization, including function, and uniformity in methodology and studied variables, will be required.

INTRODUCTION

Right ventricular (RV) function is an important predictor for clinical outcome in a variety of cardiac diseases.[1-4] In patients with pulmonary hypertension (PH), RV failure is the main cause of death[2]. Development of RV failure due to sustained pressure load is characterized by progressive diastolic dysfunction, changes in fibrotic content and metabolic remodelling.[5-9]

The healthy adult myocardium primarily uses long-chain fatty acids as substrates, in contrast to the fetal heart which uses primarily glucose and lactate.[10-13] Under stress, the heart switches to a so-called "fetal phenotype", which includes a change in substrate utilization from oxidative metabolism towards glycolysis.[12] While these changes may have advantages, i.e. better ratio ATP production vs. oxygen use, they may also have disadvantages, e.g. increase of stimulation of inflammatory cascades via intermediaries.

The right ventricle under pressure may be especially susceptible to changes in substrate utilization because of its unique physiological properties.[14] The RV is a thin-walled crescent shaped structure that under physiological conditions is coupled to low-resistance pulmonary circulation. Increased pressure load in the RV, prevalent in pulmonary hypertension, congenital heart disease, and also in LV failure, concerns a relatively high load for the RV. In addition, the RV may be more susceptible compared to the left ventricle (LV) because of the relatively higher disadvantageous changes in coronary perfusion with increased afterload.

Several studies have attempted to improve RV adaptation by metabolic modulation. Metabolic intervention tested whether direct or indirect stimulation of glucose oxidation by compounds as dichloroacetate (DCA), ranolazine (RAN), trimetazidine (TMZ) and 6-diazo-5-oxo-L-norleucine (DON), could be supportive in the pressure loaded RV.[15-21]

Indeed, these modulation seems to affect cardiac performance positively, but due to the limited number of studies, different models, different compounds and different study parameters, consensus has not been reached, complicating translation to clinical practice.[22,23]

To support the validated setup of clinical trials and to identify challenges and opportunities in evaluating metabolic findings in animal models for human disease, a comprehensive appreciation of all evidence collected in previous studies addressing metabolic adaptation of the RV to pressure load is necessary. The aim of this systematic review and meta-analysis is to provide an overview of the current knowledge about metabolic remodelling, focusing on carbohydrate and fatty acid metabolism in the pressure loaded RV. Both experimental and clinical studies

were included, taking into account the different models or type of disease, and the degree and duration of RV pressure load, and RV- and clinical function. In addition, we present an overview of the performed studies regarding interventions affecting metabolism in the right ventricle under pressure.

MATERIAL AND METHODS

Literature search

We performed a systematic literature search in Medline and EMBASE on 29 November 2017. The search strategy and global methodological approach using *Systematic Review Protocol for Animal Studies, version 2.0* formatted by SYRCLE[24,25] was published on the online platform of the working group Collaborative Approach to Meta-Analysis and Review of Animal Data form Experimental Studies (CAMARADES) at 13 December 2016. The search strategy was composed to capture overlapping parts of the following domains: (i) right ventricle, (ii) pressure load, and (iii) metabolism (see supplemental methods).

Study selection

Two researchers (A.M.C.K. and G.P.L.B.) independently screened the identified abstracts according to the following inclusion criteria: (i) English, (ii) original article, (iii) right ventricular pressure load, (iv) no reversible pressure load, (v) no mixed loading, and (vi) right ventricular metabolism. Full texts were screened for control group and sufficiency of the model by confirming increased pressure load by at least (a) increased right ventricular pressure load (i.e. right ventricular systolic pressure (RSVP) or mean pulmonary artery pressure (mPAP)), or (b) hypertrophy (i.e. RV weight, Fulton index (RV divided by LV + interventricular septum (IVS)) or RV to body weight ratio (RV/BW)). For inclusion of human studies, a control group for pressure load measurements was not required, since inclusion of individuals at study-level did meet the criteria of international guidelines for pulmonary hypertension.[26]

Data extraction

For the meta-analysis inclusion, the study had to report on metabolic variables, that were investigated in at least two or more other studies. Variable of metabolism was defined as: a) mRNA expression of genes involved in substrate uptake of metabolism, b) protein expression and/or activity of genes involved in substrate uptake of metabolism, or c) metabolism measured in vivo or in vitro using either oxygraphy in isolated mitochondria (e.g. Oroboros, Clark-type electrode), oxygraphy in whole cells (e.g. Seahorse) or in isolated hearts (e.g. Langendorf). General upstream regulators also involved in metabolism (e.g. mitogen-activated protein kinase and protein kinase B (AKT)) were not included. In addition, study characteristics as species, model/type of pressure load, degree and duration of pressure load of selected studies were extracted. We extracted the mean, standard deviation (SD) (if not presented, standard error (SE)) and number of subjects (n) of the selected variables

from all eligible studies. Universal Desktop Ruler (Avpsoft) was used to derive data from graphs. In case of missing information, authors were contacted. If response was lacking, we approached the data as follows: when the SD was unknown, the SD was calculated when mean difference, (corrected) p-value and number of used subjects were available; in case of unknown SD of the control groups, we used the SD of the experimental group;if the exact n was unknown, the greatest number given was used for the calculation of the SD.

Data synthesis

Effect sizes, defined as Hedges' g, with associated confidence interval of 95% were calculated, where after multiple separate random effects meta-analyses were performed using STATA 11. When the actual number of animals (n) used for a certain variable was unknown (i.e. not reported in the manuscript and not acquired after contacting the author), the smallest n mentioned by the authors was used to calculate the Hedges' g. Combined effect sizes of a particular variable were calculated for (1) the different models (shown by the grey squares) and (2) all studies describing the variable (shown by the black squares). Heterogeneity was assessed using Cochran's Q-test and the I^2 quantity. In order to explore the sources of heterogeneity, meta-regression analyses were performed for duration and degree of pressure load if information was available for more than two groups. To perform meta-regression analysis of a variable with duration, actual duration of pressure load had to be given (i.e. variables were excluded from meta-regression analysis if corresponding duration was defined as a time-interval (e.g. 2-6 weeks)). To be included for meta-regression analyses concerning the degree of pressure load, RV loading had to be measured as actual pressure rather than increase in hypertrophy. Unfortunately, meta-regression of cardiac or RV function was impossible due to lack of available data. In addition, differences between models were tested with unpaired t-test or one-way ANOVA with post-hoc Tukey's correction.

Since their different function in biological processes, gene expression (at mRNA level) and protein expression of studied variables were separately included in meta-analysis. In some studies, mitochondrial content was tested by different measurement techniques within the same animals. To avoid overrepresentation of included subjects, the results of only one (the superior) technique/definition was included for meta-analysis. We ranked the different definitions of mitochondrial content (which were used in the same animals) as follows: (1) ratio mitochondria to myofibrils, (2) mitochondrial yield, (3) citrate synthase activity, (4) citrate synthase at mRNA level, (5) whole tissue citrate synthase activity. However, all results (from all different techniques) are visually shown in the figures.

If the concerning study did not provide the exact number of animals used for the test of a particular variable, the mean of the range of the number of animals reported in the concerning study was presented in our figures. The number of included animals per model provided in the current figures, may give a slight overestimation in case of multiple groups using the same control group.

RESULTS

Identified studies

In total, 1393 unique citations were identified, as shown in **figure 1**. Based on title abstract screening, 1282 citations were excluded. Of the 111 articles selected for full text review, 86 articles concerned animal studies and 28 articles concerned human studies, three articles described both (see **supplemental table 1**). After full text review, 35 studies were excluded because no control group for the metabolic variables was included (n=22), no increase in RV pressure was measured (n=11), or full text was not available (n=2). The former involved mostly the human studies. We included 28 studies for meta-analysis (**supplemental table 1**), two of the studies described both human and animal data (Piao, 2013[16] and Gomez-Arroyo, 2013[27]).

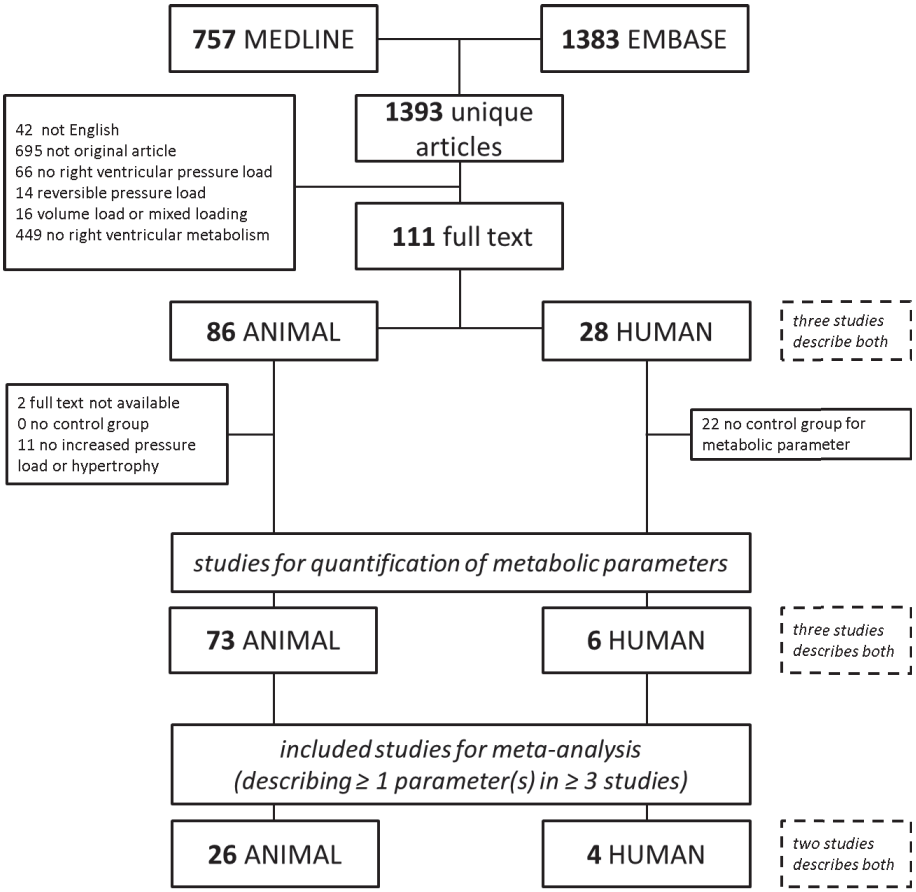

Figure 1. Flow chart systematic study selection and inclusion meta-analysis.

From three selected publications, three study groups were excluded (Balestra 2015, MCT30[28]; Rumsey 1999, 1 day[29]; and Zhang 2014, 2 weeks[30]), since pressure load and hypertrophy did not increase significantly or was not reported. All other groups had at least increased RVSP (**suppl. figure 1a**), RV weight, Fulton index (**suppl. figure 1b**) or RV/BW ratio.

Glucose transport and glycolysis

We identified three variables of glucose transport which were described in three or more studies: FDG uptake and expression of transporters GLUT1 and 4 (**figure 2**). The uptake of the glucose-analogue FDG was uniformly increased in animal models[19,31,32] as well as in patients with PH[33] (**figure 2a**). Numerous studies investigated the expression of the major glucose transporters, GLUT1 and GLUT4 and correlated this with FDG-uptake. Our meta-analysis revealed that GLUT1 mRNA as well as protein level was significantly increased in the pressure loaded RV (**figure 2b**).The increase in GLUT1 mRNA expression was universal in all models[15,18,21,27,34-37], but protein levels

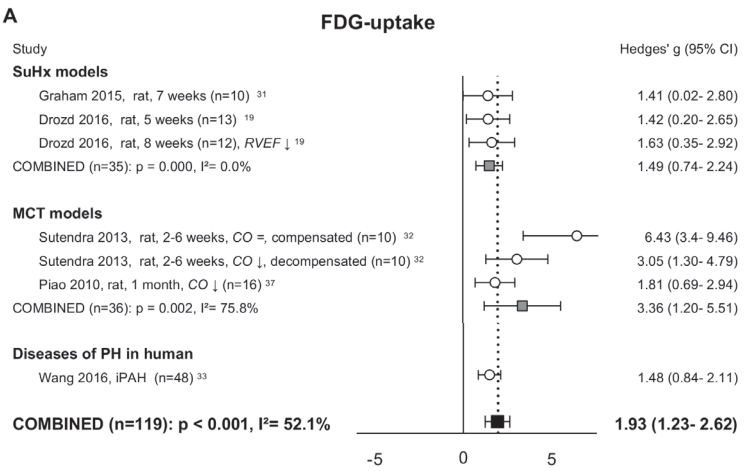

B-1 GLUT1 - mRNA

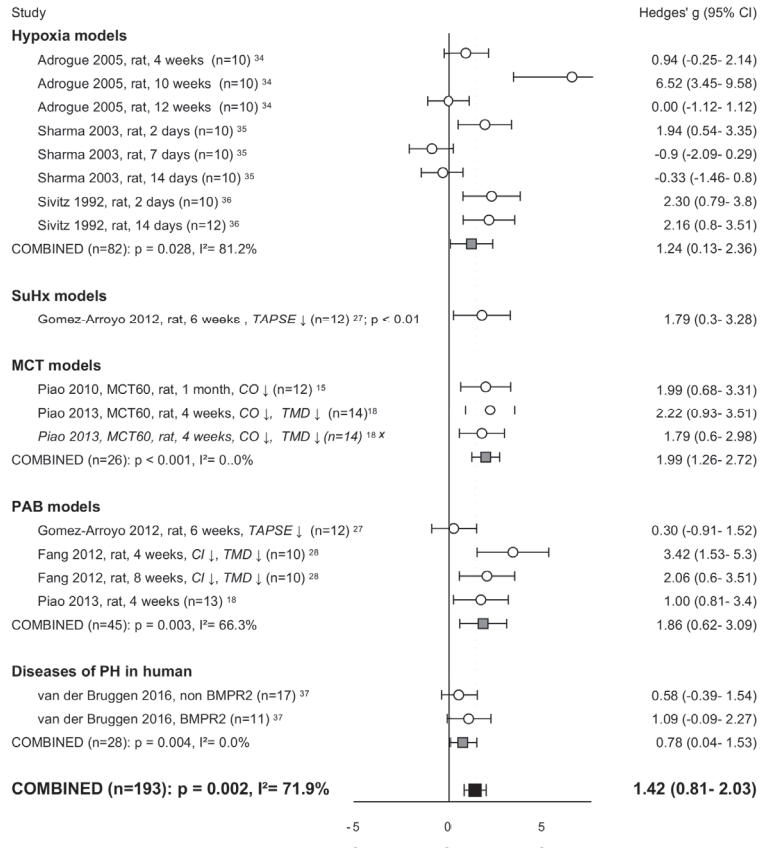

B-2 GLUT1 - protein

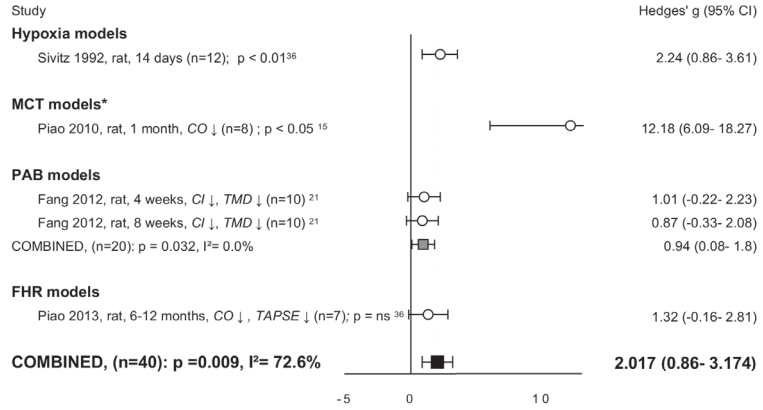

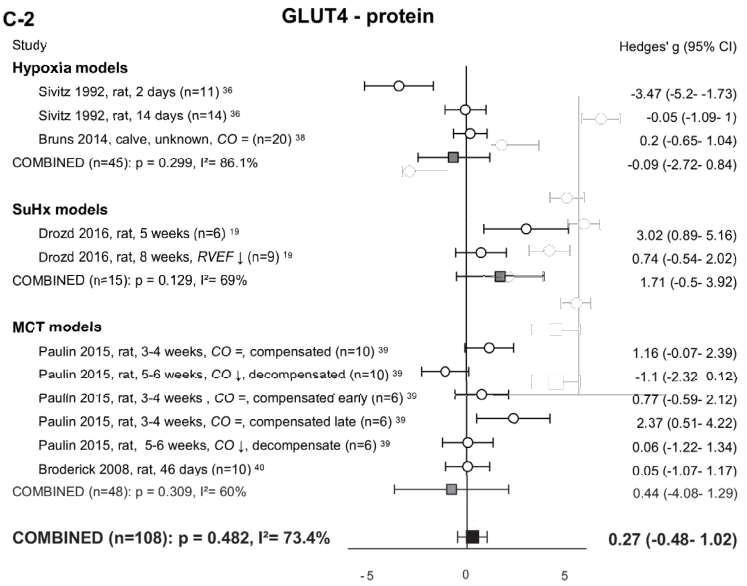

Figure 2. Right ventricular uptake of carbohydrates. Forrest plots of FDG-uptake (A), GLUT1 expression at mRNA (B-1) and protein (B-2) level, and GLUT4 expression at mRNA (C-1) and protein (C-2) level. Data are presented as Hedges' g. Combined Hedges' g are presented as squares: grey representing Hedges' g of a specific model, black representing Hedges' g of all included studies. Bars represent 95% confidence interval. SuHx = Sugen hypoxia, PAB = pulmonary artery banding, MCT = monocrotaline, FHR = fawn hooded rats, PH = pulmonary hypertension, FDG-uptake = fluorodeoxyglucose uptake , GLUT = glucose transporter. CO = cardiac output, CI = cardiac index, TAPSE = tricuspid annular plane systolic movement, RVEF = RV ejection fraction, ↓ = decreased, "=" = not statistically significant affected. 95% CI = 95% confidence interval, n = number of included animals, i^2 = level of heterogeneity, ^{X} = not included in meta-analysis, * = significantly ($p < 0.05$) increased compared to hypoxia, PAB- and FHR-models.

were higher in the monocrotaline (MCT)-model[15] as compared to the hypoxia, PAB and FHR models[15,16,21] ($p < 0.05$ for all groups). In contrast to GLUT1, the gene expression of GLUT[34-36] and the GLUT4 proteins levels[19,36,38-40] were not altered (**figure 2c**). Meta-regression analyses for FDG-uptake, GLUT1 and GLUT4, revealed no statistical significant correlations with duration or degree of RV pressure load (**suppl. table 2**). Meta-regression of GLUT1 at protein level and GLUT4 at gene level with degree of RV pressure load is not performed due to missing pressure measurements in the concerning studies.

Glucose transport is coupled with glucose –phosphorylation by hexokinases, driving glucose into glycolysis. The mRNA expression of HK1 (**figure 3a**) was significantly increased in all models[18,21,27,29,30]. In addition, meta-regression analysis showed a negative trend with the duration of RV pressure load (p=0.08) (**figure 3b**). HK2 expression was not altered [15,16,21,27,29,30,37] (**figure 3c**) and meta-regression analysis revealed no correlations with duration of degree of pressure load (**suppl. table 2** and

3). Unfortunately, protein levels of HK1 were only determined in one study[18] and HK2 protein levels were not determined at all, and therefore it is unclear how HK protein levels are affected by pressure overload. Glycolysis was studied on isolated hearts in a Langendorf perfusion system, of three RV pressure overload models: MCT[15], PAB[21] and FHR[16]. In addition, glycolysis was determined by Seahorse in RV preparations of the FHR-model[16]. Meta-analysis of the data revealed that glycolysis was significantly increased in cardiac tissue of these RV pressure loaded hearts (**figure 3d**).

Right ventricular glucose uptake and glycolysis are increased in conditions of increased pressure load.

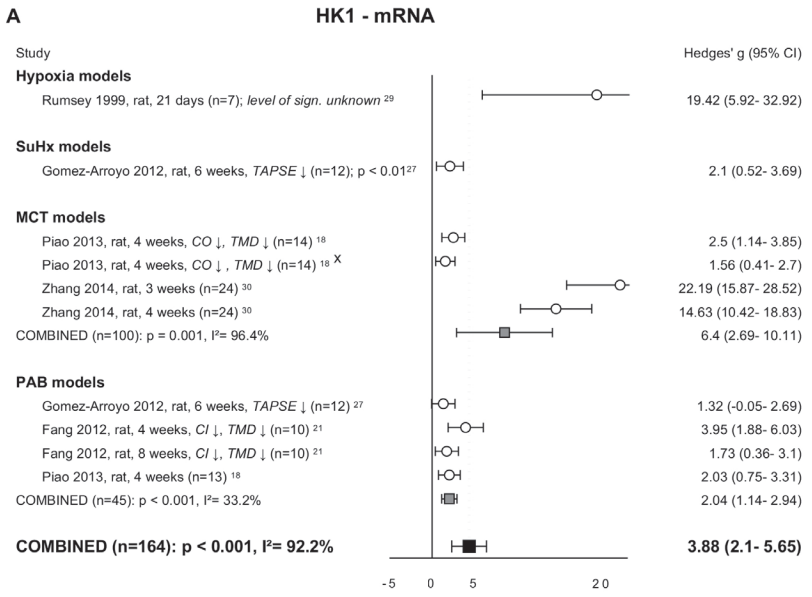

B **HK1 (mRNA) versus duration of RV pressure load**

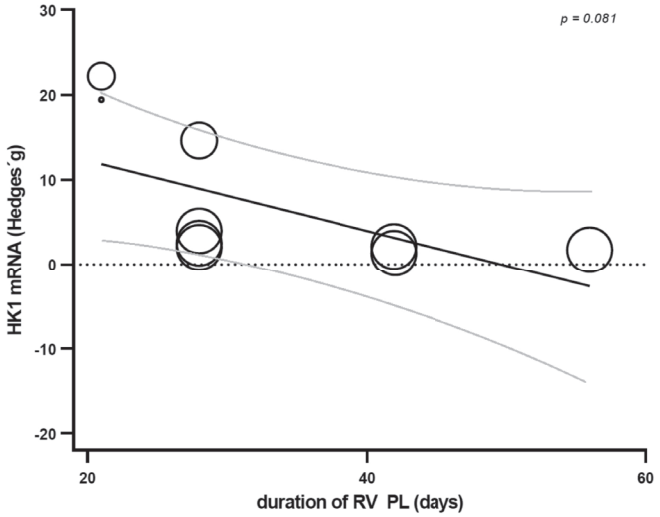

C **HK2 - mRNA**

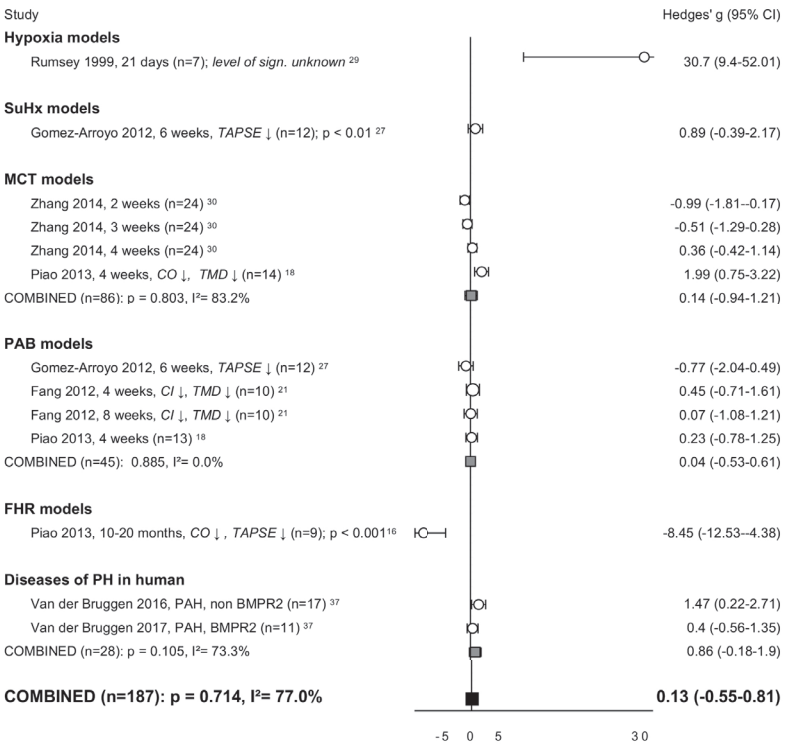

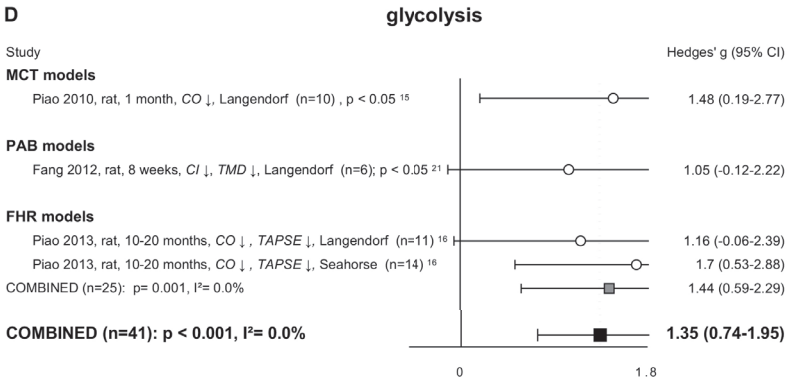

Figure 3. Glycolysis. Forrest plot of HK1 (A) and bubble plot showing meta-regression analysis of HK1 expression at mRNA level with the duration of RV pressure load (B). Forrest plots of HK2 (C) expression at mRNA level and glycolytic flux measured with Seahorse or Langendorf (D). Data are presented as Hedges' g. Combined Hedges' g are presented as squares: grey representing Hedges' g of a specific model, black representing Hedges' g of all included studies. Bars represent 95% confidence interval. Bubble size represents relative study precision, calculation based on standard deviation. Black line represents regression line, grey lines represents 95% confidence interval. SuHx = Sugen hypoxia, PAB = pulmonary artery banding, MCT = monocrotaline, FHR = fawn hooded rats, PH = pulmonary hypertension, HK = hexokinase. *CO* = cardiac output, *CI* = cardiac index, *TAPSE* = tricuspid annular plane systolic movement, ↓ = decreased, "=" = not statistically significant affected. 95% CI = 95% confidence interval, n = number of included animals, i^2 = level of heterogeneity, ^{X} = not included in meta-analysis.

Transport of fatty acids

Transporter cluster differentiation 36 (CD36), the main transporter of fatty acids across the plasma membrane, was only investigated in three studies (either RNA or protein)[27,37,41] and hence did not meet the criteria for meta-analysis. Transport of fatty acids over the mitochondrial membrane is highly regulated by carnitine palmitoyltransferases (CPT1 and CPT2) (outer and inner membrane, respectively). Only meta-analysis of subunit CPT1B was possible, but revealed ambivalent and non-significant results[16,27,34,37] (**figure 4a**). However, CPT1B mRNA negatively correlated with duration of pressure overload (**figure 4b**).

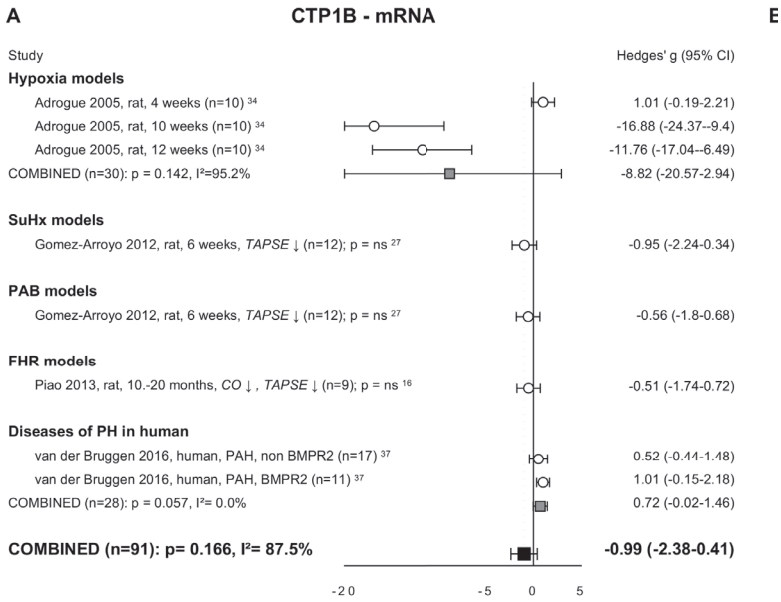

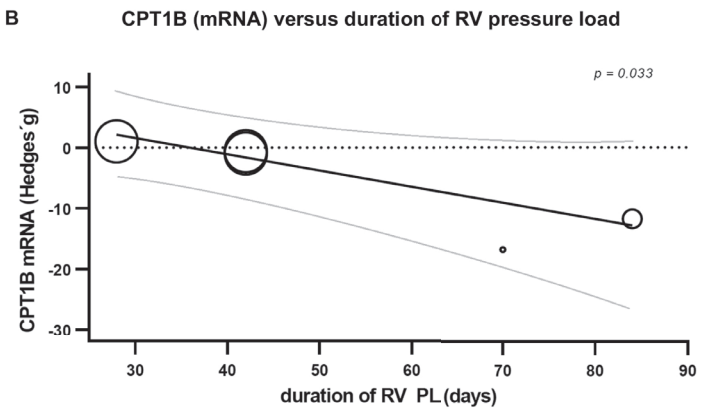

Figure 4. Right ventricular uptake of fatty acids. Forrest plot of CPT1B expression at mRNA level (A). Bubble plot showing the relation between CPT1B expression at mRNA level with duration of pressure load (B). Data are presented as Hedges' g. Combined Hedges' g are presented as squares: grey representing Hedges' g of a specific model, black representing Hedges' g of all included studies. Bars represent 95% confidence interval. Bubble size represents relative study precision, calculation based on standard deviation. Black line represents regression line, grey lines represents 95% confidence interval. SuHx = Sugen hypoxia, PAB = pulmonary artery banding, FHR = fawn hooded rats, PH = pulmonary hypertension, CPT1B = carnitine palmitoyltransferase. CO = cardiac output, CI = cardiac index, TAPSE = tricuspid annular plane systolic movement, ↓ = decreased, "=" = not statistically significant affected. 95% CI = 95% confidence interval, n = number of included animals, i^2 = level of heterogeneity.

Mitochondrial function

Mitochondrial content

Mitochondrial content was studied using different assays and subsequently expressed as: the ratio of mitochondrial DNA – nuclear (18S) DNA, the ratio of the number mitochondria to myofibrils, mitochondrial yield (mg mitochondrial protein per gram RV), citrate synthase activity or citrate synthase mRNA expression. Combining all the data from different models[27,28,42–45] and including all analyses, a significant decrease of mitochondrial content in the pressure loaded RV could be demonstrated ($g = -0.60$, $p = 0.016$). However, several studies used data form the same experiment. After exclusion of the possible duplicate measurements (choosing most optimal determination, ranked according order above), mitochondrial content tended to decrease, but lost its statistical significance ($g = -0.68$, $p = 0.054$)(**figure 5a**). Plotting duration against mitochondrial content suggests a curvilinear association, with a significant negative correlation in the first six weeks (**figure 5b**). In addition, mitochondrial content is negative correlated to the degree of RV pressure load (**suppl. figure 4**).

A **mitochondrial content**

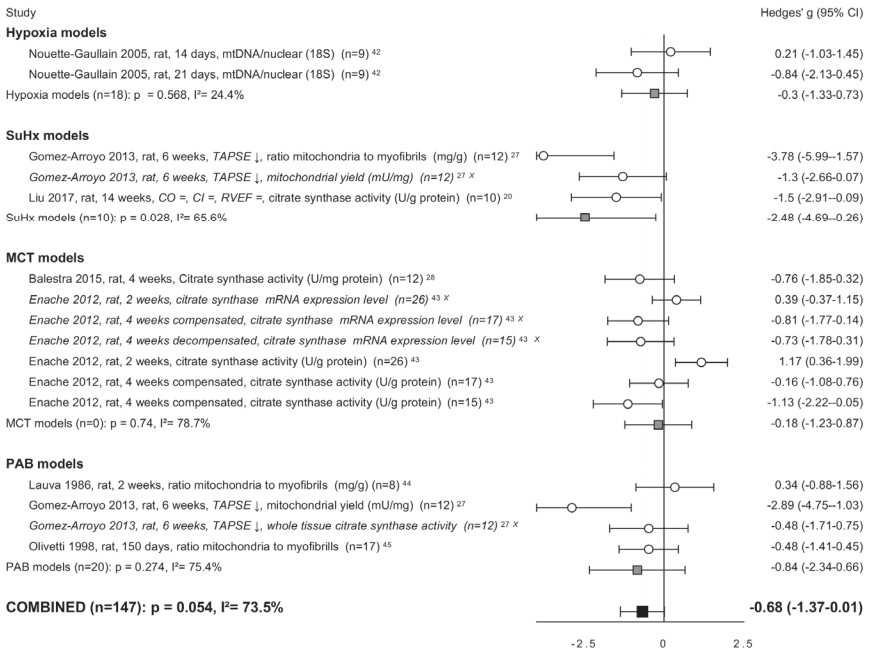

B **mitochondrial content versus duration of RV pressure load**

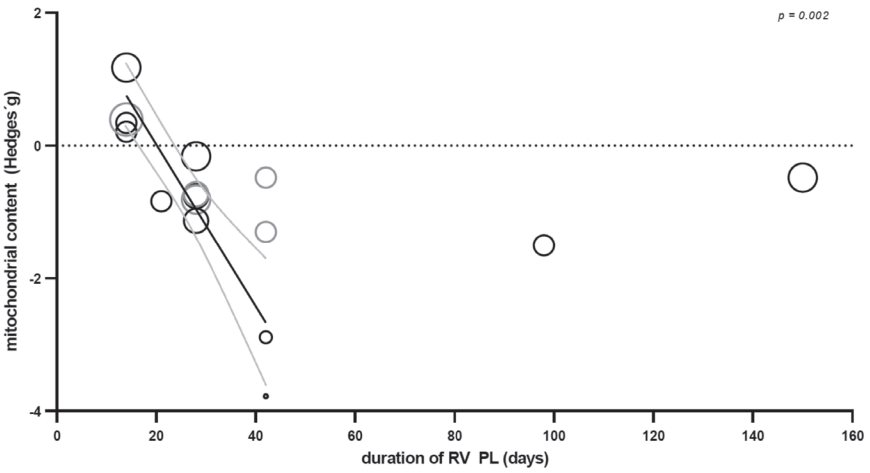

C **PDH activity**

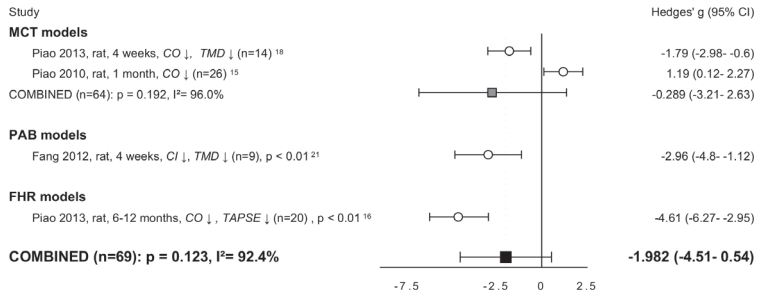

mitochondrial respiratory capacity for carbohydrates

D-1 **carbohydrates – isolated mitochondria (ADP-driven)**

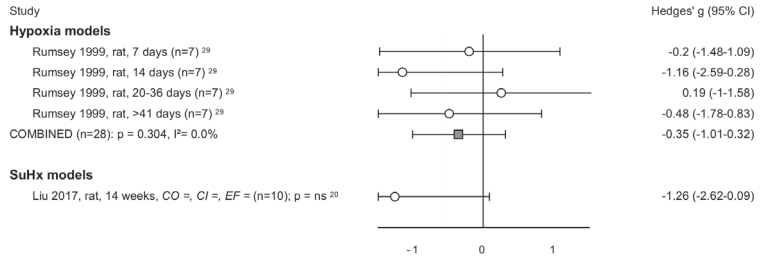

D-2 **carbohydrates – intact cardiomyocytes**

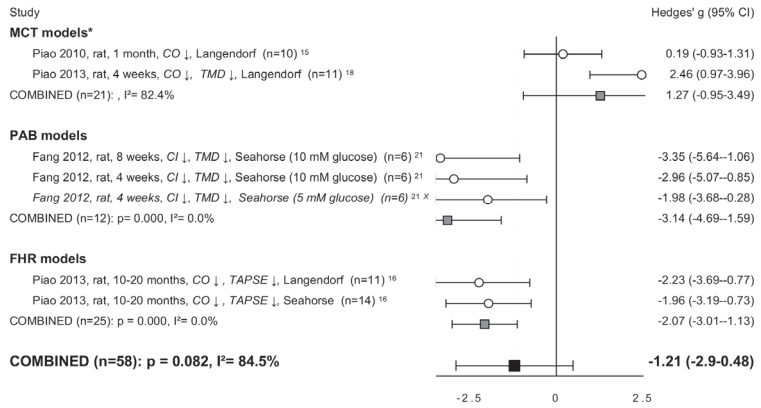

E **MCAD - mRNA**

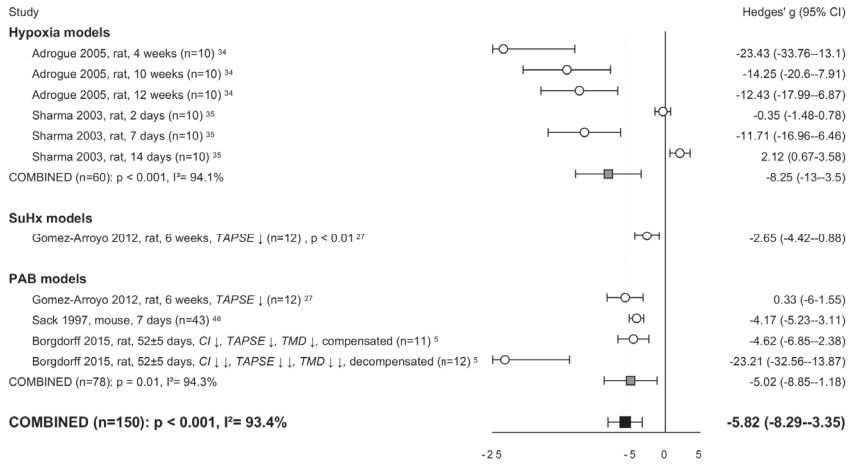

mitochondrial respiratory capacity for fatty acids

F-1 **fatty acids – isolated mitochondria (ADP-driven)**

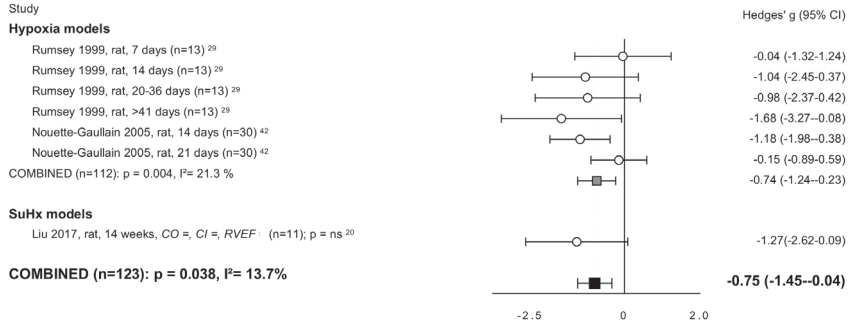

F-2 **fatty acids – intact cardiomyocytes**

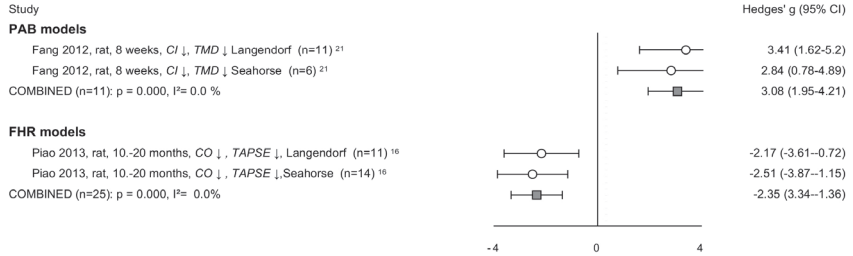

Figure 5. Mitochondrial function. Plots of mitochondrial content measured by mentioned methods (A). Bubble plot showing relation between mitochondrial content and duration of RV pressure load (B). Forrest plot of PDH activity as reflection of mitochondrial breakdown of pyruvate to acetyl-CoA (C). Forrest plots of mitochondrial respiratory capacity for carbohydrate metabolites measured in isolated mitochondria (ADP-driven) (D-1) or intact cardiomyocytes (D-2). Forrest plots of MCAD expression at mRNA level (E), as representative of the -oxidation. Forrest plots of mitochondrial respiratory capacity for fatty acids measured in isolated mitochondria (F-1) and intact cardiomyocytes (F-2). Data are presented as Hedges' g. Combined Hedges' g are presented as squares: grey representing Hedges' g of a specific model, black representing Hedges' g of all included studies. Bars represent 95% confidence interval. Bubble size represents relative study precision, calculation based on standard deviation. Grey bubbles are not included in meta-analysis. Black line represents regression line, grey lines represents 95% confidence interval. SuHx = Sugen hypoxia, PAB = pulmonary artery banding, MCT = monocrotaline, FHR = fawn hooded rats, CO = cardiac output, CI = cardiac index, TAPSE = tricuspid annular plane systolic movement, RVEF = RV ejection fraction, ↓ = decreased, ↓↓ = decreased compared to decompensated group, "=" = not statistically significant affected. 95% CI = 95% confidence interval, n = number of included animals, i^2 = level of heterogeneity, ^{x} = not included in meta-analysis. * = significantly ($p < 0.05$) increased compared to PAB.

Glucose oxidation

Activity of PDH, the enzyme converting pyruvate into acetyl-CoA in the mitochondria, tended to be decreased in RV pressure load but did not reach statistically significance (g = -1.982, p = 0.123)[15,16,18,21] (**figure 5c**). A similar result was observed for PDK4, a negative regulator of PDH, (resp. g = -1.91, p = 0.110), where meta-analysis of expression at both mRNA[16,34,35] and protein level[16,17,32] was unchanged (**suppl. figure 2a,b**). The same was true for PDK1 and PDK2 at protein level[16,17,32] (**suppl. figure 2c,d**). Heterogeneity was not explained by the duration or degree of pressure load (**suppl. tables 2 and 3**), or the different models.

Respiratory capacity of glucose or pyruvate was reported in seven articles. Analysis was divided in ADP-driven respiratory state measured in isolated mitochondria with oxygraphy (Oroboros or Clark-type) (n=2)[20,29] (**figure 5d-1**), and respiratory capacity measured in intact cardiomyocytes with Seahorse (n=2)[16,21] or isolated heart model (Langendorf) (n=3)[15,16,18] (**figure 5d-2**). Subsequently, measurements in isolated mitochondria did not met the inclusion criteria for meta-analysis. Respiratory capacity measured by all methods showed a negative trend, albeit meta-analysis of respiratory capacity for carbohydrates in intact cardiomyocytes did not reveal a significant decrease (g = -1.21 p = 0.082). Respiratory capacity did increase in the MCT-model compared to PAB ($p < 0.05$) (**figure 5d**). Meta-regression analyses did not reveal correlations between respiratory capacity and duration or degree of RV pressure load.

Oxidative fatty acid metabolism

β-oxidation involved genes including ACADVL (1), EHHADH (2), HADHA (1), ACAA2 (3), ACAT1 (1), MCAD (synonym ACADM) (6), ACADS (3), ACOT2 (1) were all described, but only MCAD did meet the criteria for inclusion in meta-analysis. MCAD at mRNA level decreased in all models of RV pressure load (hypoxia $p < 0.001$, SuHx $p < 0.01$, and PAB $p < 0.05$)[5,27,34,35,46] (**figure 5e**). No correlations with duration or degree of pressure load were observed (**suppl. table 2** and **3**). At protein level three studies[27,46,47] were included in meta-analysis, which tended to decrease, but did not reach statistically significance ($g = -2.02$, $p = 0.141$)(**suppl. figure 3**).

Oxidative metabolism in the pressure loaded right ventricle has been studied in various models, showing ambivalent results for both glucose and fatty acid metabolism.

Mitochondrial respiration regarding fatty acid oxidation measured in the ADP-driven state (n=4) decreased, when tested in models of hypoxia[29,42] and SuHx[20] (**figure 5f-1**). Respiratory capacity in intact cardiomyocytes was extracted from two publications showing contrary results in PAB[21] compared to FHR-model[16] (**figure 5f-2**).

Transcriptional regulators of metabolism

This systematic search identified several regulators of transcriptional regulators of metabolism, i.e. PGC1α (5), PPARα (4), PPARγ (1), FOXO1 (1), Mef2c (1), HIF1 (4) and cMyc (1) (numbers include both gene expression at mRNA level and protein expression). Meta-analysis was performed for PGC1α and PPARα. PGC1α is best known as the master regulator of mitochondrial biogenesis and interacts with PPARα which predominantly acts on lipids metabolism. Combined Hedges' g of PGC1α mRNA expression[27,43] decreased (**suppl. figure 4b**) and meta-regression revealed a negative correlation with duration of pressure load (**suppl. figure 4c**). Meta-analysis for PGC1α protein expression did not reveal significant change (**suppl. figure 4d**), but did show a model effect for MCT[43] vs. SuHx[20,27] ($p < 0.05$) (**suppl. figure 4b**). Combined Hedges' g of PPARα mRNA expression[27,34,35] during pressure load did not change significantly (**suppl. figure 4e**) and no correlations with duration, degree or model of RV pressure were observed. PPARα protein expression was studied once in SuHx-rats, demonstrating a decrease ($p < 0.001$).[27]

Results are summarized in **figure 6** and **supplemental table 4**.

Effect of interventions on metabolism in the pressure loaded RV

Twenty studies described the effect of an intervention on metabolic parameter(s). Overall, these intervention studies were aiming to decrease glycolysis by the increase of glucose oxidation. This could be established by re-coupling of glycolysis with glucose oxidation, by e.g. DCA or DON, or indirectly by inhibition of fatty acid metabolism, by e.g. TMZ or RAN. Seven studies, included metabolic variables which were included in meta-analyses above.[15-21] Of these metabolic variables, effect sizes derived from certain metabolic variable of intervention group treated with metabolic therapy compared to those of intervention group without treatment, are shown in **supplemental table 5**. The effect of dichloroacetate on PDH activity was studied in three studies showing a significant increase a FHR model[16], with contrary results regarding two MCT-models[15,17]. The effects of a therapeutic interventions on all other 21 reported variables were studied incidentally, precluding data synthesis and conclusions.

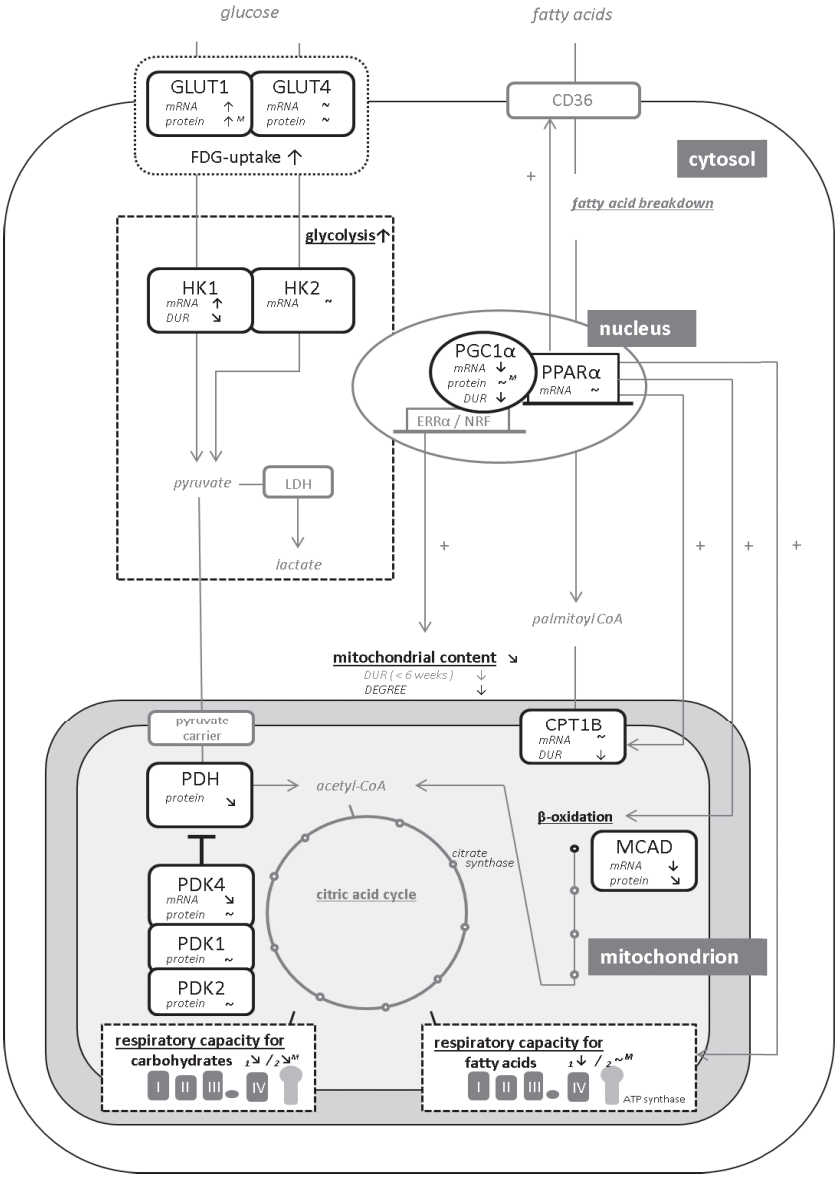

Figure 6. Metabolic changes in the pressure loaded right ventricle: summarizing results of multiple meta-analyses. FDG-uptake = fluorodeoxyglucose uptake, GLUT = glucose transporter, HK = hexokinase, LDH = lactate dehydrogenase, PDH = pyruvate dehydrogenase, PDK = pyruvate dehydrogenase kinase, CD36 = cluster differentiation 36 (cellular fat transporter), PPARα = peroxisome proliferator-activated receptor alpha; PGC1α = PPAR gamma complex 1 alpha, ERRα = oestrogen related receptor alpha, NRF = nuclear respiratory factor, CPT1B = carnitine palmitoyltransferase 1B, MCAD = medium chain acyl CoA dehydrogenase. Black components are included in meta-analysis. DUR = duration, significant increase or positive relation, significant decrease or negative relation, positive trend ($p<0.15$), negative trend ($p<0.15$), ~ unchanged, ^{M} model effect.

DISCUSSION

In this systematic review on metabolism in the pressure loaded RV, we identified 26 animal and four human studies eligible for meta-analysis. The systematic review combined with multiple separate meta-analyses yielded a uniform increase in glucose uptake and glycolysis, whereas fatty acid uptake and changes in oxidative metabolism were less consistent. The effect of therapeutic interventions could not be analyzed due to the large variety of used outcome variables and used compounds.

In the current study, there are strong indications that glycolysis is increased in the pressure overloaded RV. Both gene expression of HK1, an important enzyme controlling the first step of glycolysis, and the capacity for glycolysis measured by Seahorse and Langendorf were significantly increased. In contrast, HK2 was unchanged. Previous studies in the LV have identified HK2 as modulator of reactive oxygen species an described attenuating effects on cardiac hypertrophy.[48,49] HK2, involved in anabolic pathways by providing glucose-6-phosphate for glycogen synthesis, also fulfills a role in providing glucose-6-phosphate to the pentose phosphate pathway. Contrary to the many roles of HK2, HK1 primarily facilities glycolysis.[50,51] HK1 is primarily expressed in neonatal cardiomyocytes and is associated with the fetal gene program,[50,52,53] characterized by better resistance against an oxygen poor environment such as in the RV pressure load.[5,39,54-56] The activation of the fetal gene program is also reflected in an increased expression of GLUT1, supporting increased glucose uptake which increases the ability of increased glycolysis.[16,27,32] Remarkably, HK1 and GLUT1 both concern insulin-independent isoforms whereas HK2 and GLUT4 concern insulin-dependent isoforms.[57] The current meta-analysis reveals a clear pattern in the pressure-overloaded RV differentiating between the insulin-independent versus insulin-dependent profiles, directing to glycolysis by activation of insulin-insensitive mechanisms.

The increase of glycolysis in the pressure loaded RV is also supported by the increased glucose uptake measured by FDG by PET-CT. PET-CT has the ability to assess the actual uptake in vivo, whereas gene or protein expression of involved genes and respiratory capacity of isolated mitochondria, are an approximation of the actual situation in vivo. However, FDG-uptake represents glucose uptake rather than metabolic capacity itself. Studies describing FDG-uptake which were excluded from meta-analysis, endorse our findings.[58-62] In addition, increased RV FDG-uptake has been associated with increased pressure load[58,60,63,64] and altered dimensions,[60,62,64,65] and inverse correlations with RV-function,[62,63,65] cardiac function[60] and clinical outcome.[66,67]

Meta-analysis of substrate specific oxidative metabolism in the pressure loaded RV reflects an ambivalent character. Glucose oxidation is regulated via PDK which

inhibits breakdown of pyruvate. The expression of PDK in response to pressure load in the RV varied widely with different models used (**suppl. figure 4a-d**). In addition, the respiratory capacity for carbohydrates was also affected by the model used. Although in both MCT and PAB model cardiac performance was decreased to the same extent respiratory capacity increased in MCT models, but decreased in pressure load only via PAB. Similarly, with respect to respiratory capacity for fatty acids, PAB models behaved differently from FHR, while there are no data from MCT models. Taken together, these data suggest that the RV oxidative capacity changes in response to pressure load are dependent upon methodological differences, and may be subsequently dependent on model or disease, cardiac function and possibly on clinical severity. More cooperations between research groups and comparative studies between fixed RV-PA uncoupling (in PAB) vs. dynamic RV-PA uncoupling (e.g. in MCT) are needed to identify the systemic changes that may interfere with the cardiac response. Intriguingly, whereas there was variation in the respiratory capacity for fatty acids, the changes in one of genes oxidizing fatty acids (MCAD) were uniform. Downregulation of the -oxidation was supported in literature by decrease of other genes from the acyl-coenzyme A (CoA) dehydrogenases family at both mRNA[16,27] and protein level[27,46,68]. Downregulation of the oxidation phase has been suggested based on decreased expression of genes as HADH[5,69], HADHA, HADHB and EHHADH[5,68,70]. In addition, malonyl-coA decarboxylase (MCD) is described to be decreased in a model of hypoxia[34]. Oxidative metabolism in general in the pressure loaded RV was studied in two studies and therefore not included in meta-analysis. The clearance of ^{11}C-acetate was used as representative of tricarboxylic cycle. RV clearance rates correlated to the rate pressure product and oxygen consumption in idiopathic PAH (iPAH)[71], and appeared to higher PH (chronic thromboembolic PH (CTEPH), pulmonary arterial hypertension (PAH) and PH with unclear multifactorial mechanisms) compared to controls[72]. The current study stresses the need for further research in order to clarify changes due to pressure load itself and changes as results of the specific inducement of RV pressure load or a potential systemic disease.

The systematic literature search showed that processes involved in the transport of long-chain fatty acids varied in different models and different cohorts of patients with PH. Gene expression of CD36, the transporter of long-chain fatty acids across the cellular membrane, was decreased in SuHx rats, unaffected in PAB rats and increased at protein level in patients with a BMPR2 mutation[27,41]. Studies measuring gene expression of fatty acid binding proteins (FABP1-7) and fatty acids transporters (SLC7A1-6) in the pressure loaded RV are scarce and were ambivalent[16,31]. We excluded studies describing actual fatty acid uptake measured with PET-tracers in patient cohort without a control group. These studies also yielded various changes. Different cohorts representing different types of diseases, including precapillary PH and chronic obstructive lung disease, showed both pressure load dependent[73,74]

and independent[59,50,75] cellular uptake. Support of load dependent uptake was given by the reversibility of increased uptake after abolishing increased pressure load in patients with chronic thromboembolic pulmonary hypertension[74]. In addition, positive correlations between fatty acid uptake and markers of RV hypertrophy were observed[60,75] and, as shown for glucose uptake measured by PET-CT, uptake of free fatty acids has been inversely correlated with RV ejection fraction[59,75] as well. Although, no correlation was found with cardiac index[74], fatty acid uptake has been positively correlated with clinical outcome, expressed by six minute walking distance, NYHA class and mortality[74,75]. Mitochondrial uptake of long-chain fatty acids in the healthy heart is predominately facilitated by CPT1B. CPT1B at mRNA level negatively correlated with the duration of pressure load (**figure 4b**). However, CPT1B expression in human forms of PAH tended to increase[37]. Few studies described CPT1A, describing inconsistent results.[14,16,27,76] Although CPT1A was originally considered as an insignificant player in muscle (including heart) tissue, recent publications identified increased CPT1A as a key step in early metabolic remodelling which is linked to reduced fatty acid oxidation.[77] Besides the contradictive results regarding fatty acid uptake between the different animal models and between different patients cohorts, no structural consistency was found between a specific animal models with a specific human disease. Nevertheless, a disease specific pattern seems to apply for intramyocardial lipid deposition. Published results indicate lipid accumulation based on decreased fatty acid oxidation and increased fatty acid uptake by increased translation of CD36 to plasma membrane in heritable PAH specifically, [78,79] whereas RV ceramide content in chronic hypoxia decreased.[80] Unfortunately, only three studies reported intracardiac lipid deposition studying varied lipids which made meta-analysis impossible. Further research should aim better understanding of the translational possibilities from experimental studies to human disease.

PGC1α acts on transcriptions factors as the PPARs and is an important transcription factor of mitochondrial content. Co-activation of PGC1α with PPAR isoforms is known to induce activation of downstream genes regarding fatty acid handling including uptake and -oxidation, especially fat transporter genes CD36 and CPT1B, and -oxidation gene MCAD.[81-84] PPARα is the most studied PPAR in the heart and this also applies for the pressure loaded RV specifically.[27,34,85] Nevertheless, data of PPARα expression in the pressure loaded RV is still limited and mostly showing statistically insignificant results (**suppl. figure 4d**). This is in contrast to PGC1α, which is significantly negative affected in the pressure loaded RV and seems to be related to mitochondrial content in models of RV pressure load. It need to be said that the different studies identified mitochondrial content with different methods since standardized methods are lacking. Future studies should clarify if decreased mitochondrial content indeed is predominately established in models of SuHx and to what extend this mechanism is relevant for human PH disease. Remarkably, both

PGC1 and PPAR are not identified in studies with unbiased approach by performing microarray[5,55,86-88] or proteomics[87]. This could imply changes of PGC1α or PPARα are not causal for altered processes due to RV pressure load.

As shown in this review, metabolic modulation has been primarily focused on the reduction of glycolysis by activation of glucose oxidation. The most studied compound is DCA which inhibits PDK and hereby indirectly stimulates activation of PDH. Interestingly, in the pressure loaded RV, the different isoforms of PDK and PDH encompasses varied results (**suppl. figure 2 and figure 5**). However, studies specifically focusing on interfering on the activity of these enzymes in the pressure loaded RV by DCA, show positive effects on cell homeostasis, mitochondrial function and cardiac function,[15-17] with no effect on these functions in controls.[15] In MCT and FHR, at respectively six weeks and more than 10-20 months of treatment, DCA leads to normalized levels of the upregulated PDK2 and PDK4, with restoration of PDH activity.[16-17] This was accompanied by normalization of FOXO1 levels, which were upregulated in disease in FHR animals and patients with PAH.[16] This suits the concept of activation of the fetal gene program and insulin-independent mechanisms in the pressure loaded RV, since sustained FOXO1 activation in neonatal cardiomyocytes is known to diminish insulin signaling and impaired glucose metabolism.[89]

Limitations

This study comes with some limitations that should be discussed. To guarantee actual pressure load on the RV, meta-analysis includes both studies with proven increased pressure load by RSVP and mPAP, and by RVH. RVH was expressed as increased RV weight, Fulton index or RV to bodyweight ratio. Although hypertrophy is a plausible effect of pressure load, the degree of hypertrophy within studies from current literature search is independent of the actual degree of pressure load *(data not shown)*. This might be explained by a predominant use of models of severe pressure load. This together with the fact that RVH based on weight is a widely supported confirmation of RV pressure overload, resulted in RVH as inclusion criterion in addition to increased pressure load.

In line with the statement of the Systematic Review Center for Laboratory animal Experimentation (SYRCLE),[24] the aim of this meta-analysis was to assess the general direction and magnitude of RV pressure load of the specific variable (rather than to obtain a precise point estimate explicitly) with additional exploration of the sources of heterogeneity by using meta-regression analyses. We used effect size defined as Hedge's g. Hedge's g is the golden standard in small samples (<10 samples per group), which includes a correction factor for small sample size bias,[90,91] and therefore is considered as golden standard in meta-analysis of

systematic reviews in animal data form experimental studies. However, we feel that the use of Hedge's g encompasses a specific point that should be addressed. Since the use of effect sizes implies standardized mean differences, calculations are based on a pooled SD, although unequal variances may be present. This may induce type I errors. However, the small and unequal sample sizes will likely cancel out this effect. An alternative statistic method would be statistics by using Z-scores, but because we aimed to provide an overview of the results of the different studies, by the visualization by figures, this method was not preferred. The interpretation of meta-analysis results were challenged by substantial degrees of heterogeneity, which was partly explored by performing (1) meta-regression analysis for duration and degree of pressure load, and (2) t-tests or One Way ANOVA of the results of the different models. This resulted in three significant correlations with duration and various differences between models. Only one correlation was found with the degree of RV pressure load, which could be due to the fact included studies encompass significant loading conditions. Systematically test for the effect of used species was impossible due to the fact only one study concerned animal species other than rat. This, however, contributed to large homogeneity at this particular point. Further, we decided to use an almost similar approach for human as for animal studies in order to be able to apply the same methods regarding meta-analysis. Subsequently, a number of clinical studies were excluded from meta-analysis due to aspects regarding study-design. Nevertheless, most of excluded studies described FDG-uptake and supported the in the meta-analyses presented results. Other human studies that were excluded from the meta-analyses described uptake of fatty acids, as has been described above.

Considerations regarding future research

Due to use of differing designs of the included studies, power of the meta-analysis is limited. In contrast to clinical trials, replication is still scarce in experimental research. Current study emphasizes the need for replication and the use of more standardization in models, methods and outcome variables in studies studying metabolic derangements in RV pressure load. This could achieved in joint publications of between different research groups. Available data describes in certain extend the degree and duration of pressure load. In pursuing actual translation, absolute determination of pressure load will be necessary in both animals and human, aiming on differentiation between the actual component of pressure load and the etiology of disease including potential comorbidities.

Performing studies by means of replication and the use of standardized models is essential to draw robust conclusions about metabolic derangements in the pressure loaded right ventricle.

The etiology of disease, or the character of the model, is important since models of PAH, as hypoxia, SuHx, MCT and FHR, may differ in their systemic effects and are known for differences in disease severity and cardiovascular interaction. These differences are driven by involvement of endothelial damage, level of inflammation, cytokine migration and vasoconstriction. While isolated hypoxia with the absence of endothelial damage in the pulmonary vasculature induces mild PH only, FHR leads to more progressive PH, whereas SuHx and MCT will induce failure, with high rates of mortality in MCT. Exact mechanisms still need to be unraveled. The current meta-analysis directs to further exploration of the role of diseases which expose the RV to altered insulin sensitivity or oxygen tension in remodelling during RV pressure load. Current overview shows that determination of protein expression is limited compared to gene expression, and often shows divergent results. Also, measurements of substrate activities are relatively scarce. We suggest future studies in the pressure loaded RV should be more uniform and integral with respect to expression level (gene, protein , or activity level). The *to be studied variables of metabolism* should be uniform and most optimal chosen based on research using unbiased approaches (i.e. microarray, RNA sequences, proteomics or metabolomics). Given the above mentioned observations, the translational applicability between, and within, animal models and human diseases of PH should most critically and carefully be considered.

CONCLUSION

This systematic review and meta-analysis of metabolic variables in the pressure loaded RV showed uniform increase in glucose uptake and glycolysis. Results regarding fatty acid uptake and changes in oxidative metabolism were divergent and model specific. To actually use metabolism as therapeutic target in the RV exposed to increased pressure load in clinical practice, we need to learn more about model and disease specific mechanisms of fatty acid uptake and mitochondrial impairment.

SOURCE OF FUNDING

Not applicable.

DISCLOSURES

None.

REFERENCES

1. Norozi K, Wessel A, Alpers V, Arnhold JO, Geyer S, Zoege M, Buchhorn R. Incidence and Risk Distribution of Heart Failure in Adolescents and Adults With Congenital Heart Disease After Cardiac Surgery. *Am J Cardiol* 2006;97:1238–1243.
2. Wolferen SA Van, Marcus JT, Boonstra A, Marques KMJ, Bronzwaer JGF, Spreeuwenberg MD, Postmus PE, Vonk-Noordegraaf A. Prognostic value of right ventricular mass, volume, and function in idiopathic pulmonary arterial hypertension. *Eur Heart J* 2007;28:1250–1257.
3. Ghio S, Gavazzi A, Campana C, Inserra C, Klersy C, Sebastiani R, Arbustini E, Recusani F, Tavazzi L. Independent and Additive Prognostic Value of Right Ventricular Systolic Function and Pulmonary Artery Pressure in Patients With Chronic Heart Failure. *J Am Coll Cardiol* Elsevier Masson SAS; 2001;37:183–188.
4. Meyer P, Filippatos GS, Ahmed MI, Iskandrian AE, Bittner V, Perry GJ, White M, Aban IB, Mujib M, Italia LJD, Ahmed A. Effects of Right Ventricular Ejection Fraction on Outcomes in Chronic Systolic Heart Failure. 2010;252–259.
5. Borgdorff MAJ, Koop AMC, Bloks VW, Dickinson MG, Steendijk P, Sillje HHW, Wiechen MPH van, Berger RMF, Bartelds B. Clinical symptoms of right ventricular failure in experimental chronic pressure load are associated with progressive diastolic dysfunction. *J Mol Cell Cardiol* Elsevier Ltd; 2015;79:244–253.
6. Ryan JJ, Archer SL. The right ventricle in pulmonary arterial hypertension: Disorders of metabolism, angiogenesis and adrenergic signaling in right ventricular failure. *Circ Res* S.L. Archer, Department of Medicine, Queen's University, Kingston, ON K7L 3N6, Canada; 2014;115:176–188.
7. Borgdorff MAJ, Dickinson MG, Berger RMF, Bartelds B. Right ventricular failure due to chronic pressure load: What have we learned in animal models since the NIH working group statement? *Heart Fail Rev* M.A.J. Borgdorff, Department of Pediatric Cardiology, Center for Congenital Heart Diseases, Beatrix Children's Hospital, University Medical Center Groningen, Groningen, Netherlands; 2015;20:475–491.
8. Samson N, Paulin R. Epigenetics, inflammation and metabolism in right heart failure associated with pulmonary hypertension. *Pulm Circ* 2017;7:572–587.
9. Koop AMC, Hagdorn QAJ, Bossers GPL, Leusden T van, Gerding A, Weeghel M van, Vaz FM, Koonen DPY, Silljé HHW, Berger RMF, Bartelds B. Right ventricular pressure overload alters cardiac lipid composition. *Int J Cardiol* Elsevier B.V.; 2019;
10. Bartelds B, Knoester H, Smid GB, Takens J, Visser GH, Penninga L, Leij FR van der, Beaufort-Krol GC, Zijlstra WG, Heymans HS, Kuipers JR. Perinatal changes in myocardial metabolism in lambs. *Circulation* 2000;102:926–931.
11. Bartelds B, Knoester H, Beaufort-Krol GC, Smid GB, Takens J, Zijlstra WG, Heymans HSA, Kuipers JRG. Myocardial Lactate Metabolism in Fetal and Newborn Lambs. *Circulation* 1999;1892–1897.
12. Lopaschuk GD. Metabolic Modulators in Heart Disease – Past, Present and Future. *Can J Cardiol* Canadian Cardiovascular Society; 2017;33:838–849.
13. Neubauer S. The Failing Heart — An Engine Out of Fuel. *N Engl J* Med 2007;356:1140–1151.

14. Sanz J, Sánchez-Quintana D, Bossone E, Bogaard HJ, Naeije R. Anatomy, Function, and Dysfunction of the Right Ventricle: JACC State-of-the-Art Review. *J Am Coll Cardiol* 2019;73:1463–1482.

15. Piao L, Fang Y-H, Cadete VJJ, Wietholt C, Urboniene D, Toth PT, Marsboom G, Zhang HJ, Haber I, Rehman J, Lopaschuk GD, Archer SL. The inhibition of pyruvate dehydrogenase kinase improves impaired cardiac function and electrical remodeling in two models of right ventricular hypertrophy: Resuscitating the hibernating right ventricle. *J Mol Med* S. L. Archer, Section of Cardiology, Department of Medicine, University of Chicago, Chicago, IL 60637, United States; 2010;88:47–60.

16. Piao L, Sidhu VK, Fang Y-H, Ryan JJ, Parikh KS, Hong Z, Toth PT, Morrow E, Kutty S, Lopaschuk GD, Archer SL. FOXO1-mediated upregulation of pyruvate dehydrogenase kinase-4 (PDK4) decreases glucose oxidation and impairs right ventricular function in pulmonary hypertension: therapeutic benefits of dichloroacetate. *J Mol Med* S.L. Archer, Department of Medicine, Queen's University Kingston, Kingston, K7L 3N6, ON, Canada; 2013;91:333–346.

17. Sun X-Q, Zhang R, Zhang H-D, Yuan P, Wang X-J, Zhao Q-H, Wang L, Jiang R, Jan Bogaard H, Jing Z-C. Reversal of right ventricular remodeling by dichloroacetate is related to inhibition of mitochondria-dependent apoptosis. *Hypertens Res* Z.-C. Jing, State Key Laboratory of Cardiovascular Disease, Fu Wai Hospital, National Center for Cardiovascular Disease, Peking Union Medical College, Chinese Academy Medical Science, Beijing, China; 2016;39:302–311.

18. Piao L, Fang Y-H, Parikh K, Ryan JJ, Toth PT, Archer SL. Cardiac glutaminolysis: A maladaptive cancer metabolism pathway in the right ventricle in pulmonary hypertension. *J Mol Med* S.L. Archer, Department of Medicine, Queen's University, Etherington Hall, Kingston, ON K7L 3N6, Canada; 2013;91:1185–1197.

19. Drozd K, Ahmadi A, Deng Y, Jiang B, Petryk J, Thorn S, Stewart D, Beanlands R, DeKemp RA, DaSilva JN, Mielniczuk LM. Effects of an endothelin receptor antagonist, Macitentan, on right ventricular substrate utilization and function in a Sugen 5416/hypoxia rat model of severe pulmonary arterial hypertension. *J Nucl Cardiol* L.M. Mielniczuk, Division of Cardiology, Department of Medicine, University of Ottawa Heart Institute, Ottawa, Canada; 2016;1–11.

20. Liu A, Philip J, Vinnakota KC, Bergh F Van den, Tabima DM, Hacker T, Beard DA, Chesler NC. Estrogen maintains mitochondrial content and function in the right ventricle of rats with pulmonary hypertension. *Physiol Rep* 2017;5:1–12.

21. Fang Y-H, Piao L, Hong Z, Toth PT, Marsboom G, Bache-Wiig P, Rehman J, Archer SL. Therapeutic inhibition of fatty acid oxidation in right ventricular hypertrophy: Exploiting Randle's cycle. *J Mol Med* S.L. Archer, Medicine/Cardiology, University of Chicago, Chicago, IL 60637, United States; 2012;90:31–43.

22. Khan SS, Cuttica MJ, Beussink-Nelson L, Kozyleva A, Sanchez C, Mkrdichian H, Selvaraj S, Dematte JE, Lee DC, Shah SJ. Effects of ranolazine on exercise capacity, right ventricular indices, and hemodynamic characteristics in pulmonary arterial hypertension: a pilot study. *Pulm Circ* United States; 2015;5:547–556.

23. Michelakis ED, Gurtu V, Webster L, Barnes G, Watson G, Howard L, Cupitt J, Paterson I, Thompson RB, Chow K, Regan DPO, Zhao L, Wharton J, Kiely DG, Kinnaird A, Boukouris AE, White C, Nagendran J, Freed DH, Wort SJ, Gibbs JSR, Wilkins MR. Inhibition of

pyruvate dehydrogenase kinase improves pulmonary arterial hypertension in genetically susceptible patients. *Sci Transl Med* 2017;4583:1–13.

24. Vries RBM De, Hooijmans CR, Langendam MW, Luijk J Van, Leenaars M. A protocol format for the preparation , registration and publication of systematic reviews of animal intervention studies. *Evidenced-based Preclin Med* 2015;1.
25. Vries RBM De, Wever KE, Avey MT, Stephens ML, Sena ES, Leenaars M. The Usefulness of Systematic Reviews of Animal Experiments for the Design of Preclinical and Clinical Studies. *ILAR J* 2014;55:427–437.
26. Galiè N, Hoeper MM, Humbert M, Torbicki A, Vachiery JL, Barbera JA, Beghetti M, Corris P, Gaine S, Gibbs JS, Gomez-Sanchez MA, Jondeau G, Klepetko W, Opitz C, Peacock A, Rubin L, Zellweger M, Simonneau G. Guidelines for the diagnosis and treatment of pulmonary hypertension. *Eur Respir J* 2009;34:1219–1263.
27. Gomez-Arroyo J, Mizuno S, Szczepanek K, Tassell B Van, Natarajan R, Remedios CG Dos, Drake JI, Farkas L, Kraskauskas D, Wijesinghe DS, Chalfant CE, Bigbee J, Abbate A, Lesnefsky EJ, Bogaard HJ, Voelkel NF. Metabolic gene remodeling and mitochondrial dysfunction in failing right ventricular hypertrophy secondary to pulmonary arterial hypertension. *Circ Hear Fail* 2013;6:136–144.
28. Balestra GM, Mik EG, Eerbeek O, Specht PAC, Laarse WJ van der, Zuurbier CJ. Increased in vivo mitochondrial oxygenation with right ventricular failure induced by pulmonary arterial hypertension: Mitochondrial inhibition as driver of cardiac failure? *Respir Res* C.J. Zuurbier, Department of Anesthesiology, Laboratory of Experimental Intensive Care and Anesthesiology, AMC, Amsterdam, Netherlands; 2015;16.
29. Rumsey WL, Abbott B, Bertelsen D, Mallamaci M, Hagan K, Nelson D, Erecinska M. Adaptation to hypoxia alters energy metabolism in rat heart. *Am J Physiol - Hear Circ Physiol* W.L. Rumsey, Zeneca Pharmaceuticals, Wilmington, DE 19850-5437, United States; 1999;276:H71–H80.
30. Zhang W-H, Qiu M-H, Wang X-J, Sun K, Zheng Y, Jing Z-C. Up-regulation of hexokinase1 in the right ventricle of monocrotaline induced pulmonary hypertension. *Respir Res* Y. Zheng, First Hospital of Jilin University, Center of Cardiovascular Disease, Changchun, China; 2014;15.
31. Graham BB, Kumar R, Mickael C, Sanders L, Gebreab L, Huber KM, Perez M, Smith-Jones P, Serkova NJ, Tuder RM. Severe pulmonary hypertension is associated with altered right ventricle metabolic substrate uptake. *Am J Physiol - Lung Cell Mol Physiol* B.B. Graham, Division of Pulmonary Sciences and Critical Care Medicine, Univ. of Colorado Denver, Aurora, United States; 2015;309:L435–L440.
32. Sutendra G, Dromparis P, Paulin R, Zervopoulos S, Haromy A, Nagendran J, Michelakis ED. A metabolic remodeling in right ventricular hypertrophy is associated with decreased angiogenesis and a transition from a compensated to a decompensated state in pulmonary hypertension. *J Mol Med* E.D. Michelakis, Department of Medicine, University of Alberta, Edmonton, AB T6G 2B7, Canada; 2013;91:1315–1327.
33. Wang L, Li W, Yang Y, Wu W, Cai Q, Ma X, Xiong C, He J, Fang W. Quantitative assessment of right ventricular glucose metabolism in idiopathic pulmonary arterial hypertension patients: A longitudinal study. *Eur Heart J Cardiovasc Imaging* W. Fang, Department of Nuclear Medicine, Chinese Academy of Medical Sciences and Peking Union Medical College, FuWai Hospital, Beijing, China; 2016;17:1161–1168.

34. Adrogue J V, Sharma S, Ngumbela K, Essop MF, Taegtmeyer H. Acclimatization to chronic hypobaric hypoxia is associated with a differential transcriptional profile between the right and left ventricle. *Mol Cell Biochem* H. Taegtmeyer, Department of Internal Medicine, Division of Cardiology, University of Texas Houston - Medical School, Houston, TX 77030, United States; 2005;278:71–78.

35. Sharma S, Taegtmeyer H, Adrogue J, Razeghi P, Sen S, Ngumbela K, Essop MF. Dynamic changes of gene expression in hypoxia-induced right ventricular hypertrophy. *Am J Physiol - Hear Circ Physiol* H. Taegtmeyer, Dept. of Internal Medicine, Division of Cardiology, Univ. of Texas-Houston Med. School, Houston, TX 77030, United States; 2004;286:H1185–H1192.

36. Sivitz WI, Lund DD, Yorek B, Grover-McKay M, Schmid PG. Pretranslational regulation of two cardiac glucose transporters in rats exposed to hypobaric hypoxia. *Am J Physiol - Endocrinol Metab* W.I. Sivitz, Dept. of Internal Medicine, Univ. of Iowa Hospitals and Clinics, Iowa City, IA 52246, United States; 1992;263:E562–E569.

37. Bruggen CE van der, Happé CM, Dorfmüller P, Trip P, Spruijt OA, Rol N, Hoevenaars FP, Houweling AC, Girerd B, Marcus JT, Mercier O, Humbert M, Handoko ML, Velden J van der, Vonk Noordegraaf A, Bogaard HJ, Goumans M-J, Man FS de. Bone Morphogenetic Protein Receptor Type 2 Mutation in Pulmonary Arterial HypertensionCLINICAL PERSPECTIVE. *Circul*ation 2016;133:1747–1760.

38. Bruns DR, Dale Brown R, Stenmark KR, Buttrick PM, Walker LA. Mitochondrial integrity in a neonatal bovine model of right ventricular dysfunction. *Am J Physiol - Lung Cell Mol Physiol* L.A. Walker, Univ. of Colorado-Denver, Dept. of Medicine, Cardiology, Aurora, United States; 2015;308:L158–L167.

39. Paulin R, Sutendra G, Gurtu V, Dromparis P, Haromy A, Provencher S, Bonnet S, Michelakis ED. A miR-208-Mef2 axis drives the decompensation of right ventricular function in pulmonary hypertension. *Circ Res* E.D. Michelakis, Department of Medicine, Cardiology, University of Alberta, Edmonton, Canada; 2015;116:56–69.

40. Broderick TL, King TM. Upregulation of GLUT-4 in right ventricle of rats with monocrotaline-induced pulmonary hypertension. *Med Sci Monit* T. L. Broderick, Department of Physiology, Midwestern University, Glendale, AZ 85308, United States; 2008;14:BR261–BR264.

41. Talati MH, Brittain EL, Fessel JP, Penner N, Atkinson J, Funke M, Grueter C, Jerome WG, Freeman M, Newman JH, West J, Hemnes AR. Mechanisms of Lipid Accumulation in the Bone Morphogenetic Protein Receptor Type 2 Mutant Right Ventricle. *Am J Respir Crit Care Med* United States; 2016;194:719–728.

42. Nouette-Gaulain K, Malgat M, Rocher C, Savineau J-P, Marthan R, Mazat J-P, Sztark F. Time course of differential mitochondrial energy metabolism adaptation to chronic hypoxia in right and left ventricles. *Cardiovasc Res* F. Sztark, Laboratoire d'Anesthésiologie, E.A. Physiologie Mitochondriale, Universite Bordeaux 2, 33076 Bordordeaux, France; 2005;66:132–140.

43. Enache I, Charles A-L, Bouitbir J, Favret F, Zoll J, Metzger D, Oswald-Mammosser M, Geny B, Charloux A. Skeletal muscle mitochondrial dysfunction precedes right ventricular impairment in experimental pulmonary hypertension. *Mol Cell Biochem* I. Enache, Service de Physiologie et d'Explorations Fonctionnelles, Pôle de Pathologie Thoracique, Centre Hospitalier Universitaire Strasbourg, Nouvel Hôpital Civil, 67091 Strasbourg, France; 2013;373:161–170.

44. Lauva IK, Brody E, Tiger E, Kent RL, Copper G 4th, Marino TA. Control of myocardial tissue components and cardiocyte organelles in pressure-overload hypertrophy of the cat right ventricle. *Am J Anat* United States; 1986;177:71–80.

45. Olivetti G, Ricci R, Lagrasta C, Maniga E, Sonnenblick EH, Anversa P. Cellular basis of wall remodeling in long-term pressure overload-induced right ventricular hypertrophy in rats. *Circ Res* Department of Pathology, University of Parma, 43100 Parma; 1988;**63**:648–657.

46. Sack MN, Disch DL, Rockman HA, Kelly DP. A role for Sp and nuclear receptor transcription factors in a cardiac hypertrophic growth program. *Proc Natl Acad Sci U S A* D.P. Kelly, Center for Cardiovascular Research, Box 8086, Washington Univ. Sch. of Medicine, St. Louis, MO 63110, United States; 1997;94:6438–6443.

47. Sheikh AM, Barrett C, Villamizar N, Alzate O, Valente AM, Herlong JR, Craig D, Lodge A, Lawson J, Milano C, Jaggers J. Right ventricular hypertrophy with early dysfunction: A proteomics study in a neonatal model. *J Thorac Cardiovasc Surg* A.M. Sheikh, Department of Pediatric Cardiac Surgery, the Neuroproteomics Center, Durham, NC, United States; 2009;137:1146–1153.

48. Mccommis KS, Douglas DL, Krenz M, Baines CP. Cardiac-speci fi c Hexokinase 2 Overexpression Attenuates Hypertrophy by Increasing Pentose Phosphate Pathway Flux. 2013;2:1–14.

49. Wu R, Wyatt E, Chawla K, Tran M, Ghanefar M, Laakso M, Epting CL, Ardehali H. Hexokinase II knockdown results in exaggerated cardiac hypertrophy via increased ROS production. 2012;633–646.

50. Calmettes G, John SA, Weiss JN, Ribalet B. Hexokinase – mitochondrial interactions regulate glucose metabolism differentially in adult and neonatal cardiac myocytes. 2013;425–436.

51. Gottlob K, Majewski N, Kennedy S, Kandel E, Robey RB, Hay N. Inhibition of early apoptotic events by Akt / PKB is dependent on the first committed step of glycolysis and mitochondrial hexokinase. 2001;1406–1418.

52. Fritz HL, Smoak IW, Branch S. Hexokinase I expression and activity in embryonic mouse heart during early and late organogenesis. 1999;14:359–365.

53. John JC St., Ramalho-Santos J, Gray HL, Petrosko P, Rawe VY, Navara CS, Simerly CR, Schatten GP. The Expression of Mitochondrial DNA Transcription Factors during Early Cardiomyocyte *In Vitro* Differentiation from Human Embryonic Stem Cells. *Cloning Stem Cells* 2005;7:141–153.

54. Reddy S, Zhao M, Hu D-Q, Fajardo G, Katznelson E, Punn R, Spin JM, Chan FP, Bernstein D. Physiologic and molecular characterization of a murine model of right ventricular volume overload. *Am J Physiol Heart Circ Physi*ol 2013;304:H1314-27.

55. Reddy S, Zhao M, Hu D-Q, Fajardo G, Hu S, Ghosh Z, Rajagopalan V, Wu JC, Bernstein D. Dynamic microRNA expression during the transition from right ventricular hypertrophy to failure. *Physiol Genomic*s 2012;44:562–575.

56. Drake JI, Bogaard HJ, Mizuno S, Clifton B, Xie B, Gao Y, Dumur CI, Fawcett P, Voelkel NF, Natarajan R. Molecular signature of a right heart failure program in chronic severe pulmonary hypertension. *Am J Respir Cell Mol Bi*ol 2011;45:1239–1247.

57. Postic C, Leturque A, Printz RL, Maulard P, Loizeau M, Granner DK, Girard J. Development and regulation of glucose transporter and hexokinase expression in rat. *Am J Physiol* 1994;266:E548-59.

58. Frille A, Steinhoff KG, Hesse S, Grachtrup S, Wald A, Wirtz H, Sabri O, Seyfarth H-J. Thoracic [18F]fluorodeoxyglucose uptake measured by positron emission tomography/computed tomography in pulmonary hypertension. *Med (United States)* A. Frille, Department of Respiratory Medicine, University of Leipzig, Leipzig, Germany; 2016;95.

59. Ohira H, deKemp R, Pena E, Davies RA, Stewart DJ, Chandy G, Contreras-Dominguez V, Dennie C, Mc Ardle B, Mc Klein R, Renaud JM, DaSilva JN, Pugliese C, Dunne R, Beanlands R, Mielniczuk LM. Shifts in myocardial fatty acid and glucose metabolism in pulmonary arterial hypertension: a potential mechanism for a maladaptive right ventricular response. *Eur Heart J Cardiovasc Imaging* England; 2015;

60. Sakao S, Daimon M, Voelkel NF, Miyauchi H, Jujo T, Sugiura T, Ishida K, Tanabe N, Kobayashi Y, Tatsumi K. Right ventricular sugars and fats in chronic thromboembolic pulmonary hypertension. *Int J Cardiol* S. Sakao, Department of Respirology (B2), Graduate School of Medicine, Chiba University, Chuo-ku, Chiba, Japan; 2016;219:143–149.

61. Bokhari S, Raina A, Rosenweig EB, Schulze PC, Bokhari J, Einstein AJ, Barst RJ, Johnson LL. PET imaging may provide a novel biomarker and understanding of right ventricular dysfunction in patients with idiopathic pulmonary arterial hypertension. *Circ Cardiovasc Imaging* S. Bokhari, Department of Medicine, Division of Cardiology, New York Presbyterian Hospital at Columbia University Medical Center, New York, NY 10032, United States; 2011;4:641–647.

62. Saygin D, Highland KB, Farha S, Park M, Sharp J, Roach EC, Tang WHW, Thomas JD, Erzurum SC, Neumann DR, DiFilippo FP. Metabolic and functional evaluation of the heart and lungs in pulmonary hypertension by gated 2-[18F]-Fluoro-2-deoxy-D-glucose positron emission tomography. *Pul*m Circ 2017;7:428–438.

63. Nakaya T, Ohira H, Tsujino I. Right heart morphology, function and metabolism in pulmonary hypertension. *Respir Cir*c 2016;64:543–547.

64. Oikawa M, Kagaya Y, Otani H, Sakuma M, Demachi J, Suzuki J, Takahashi T, Nawata J, Ido T, Watanabe J, Shirato K. Increased [18F]fluorodeoxyglucose accumulation in right ventricular free wall in patients with pulmonary hypertension and the effect of epoprostenol. *J Am Coll Cardiol* Y. Kagaya, Department of Cardiovascular Medicine, Tohoku University, Graduate School of Medicine, Aoba-ku, Sendai 980-8574, Japan; 2005;45:1849–1855.

65. Lundgrin EL, Park MM, Sharp J, Tang WHW, Thomas JD, Asosingh K, Comhair SA, DiFilippo FP, Neumann DR, Davis L, Graham BB, Tuder RM, Dostanic I, Erzurum SC. Fasting 2-deoxy-2-[18F]fluoro-D-glucose positron emission tomography to detect metabolic changes in pulmonary arterial hypertension hearts over 1 year. *Ann Am Thorac Soc* S.C. Erzurum, Respiratory Institute, Cleveland Clinic, Cleveland, OH 44195, United States; 2013;10:1–9.

66. Li W, Wang L, Xiong C-M, Yang T, Zhang Y, Gu Q, Yang Y, Ni X-H, Liu Z-H, Fang W, He J-G. The Prognostic Value of 18F-FDG Uptake Ratio Between the Right and Left Ventricles in Idiopathic Pulmonary Arterial Hypertension. *Clin Nucl Med* 2015;40:859–863.

67. Tatebe S, Fukumoto Y, Oikawa-Wakayama M, Sugimura K, Satoh K, Miura Y, Aoki T, Nochioka K, Miura M, Yamamoto S, Tashiro M, Kagaya Y, Shimokawa H. Enhanced [18F] fluorodeoxyglucose accumulation in the right ventricular free wall predicts long-term prognosis of patients with pulmonary hypertension: a preliminary observational study.

Eur Heart J Cardiovasc Imaging England; 2014;15:666–672.

68. Faber MJ, Dalinghaus M, Lankhuizen IM, Bezstarosti K, Verhoeven AJM, Duncker DJ, Helbing WA, Lamers JMJ. Time dependent changes in cytoplasmic proteins of the right ventricle during prolonged pressure overload. *J Mol Cell Cardiol* M. Dalinghaus, Erasmus MC-Sophia, Department of Pediatrics, Division of Pediatric Cardiology, 3015 GJ Rotterdam, Netherlands; 2007;43:197–209.
69. Baandrup JD, Markvardsen LH, Peters CD, Schou UK, Jensen JL, Magnusson NE, Ørntoft TF, Kruhøffer M, Simonsen U. Pressure load: The main factor for altered gene expression in right ventricular hypertrophy in chronic hypoxic rats. *PLoS One* U. Simonsen, Department of Pharmacology, Aarhus University, Aarhus, Denmark; 2011;6.
70. Faber MJ, Dalinghaus M, Lankhuizen IM, Bezstarosti K, Dekkers DHW, Duncker DJ, Helbing WA, Lamers JMJ. Proteomic changes in the pressure overloaded right ventricle after 6 weeks in young rats: Correlations with the degree of hypertrophy. *Proteomics* J.M.J. Lamers, Department of Biochemistry, Cardiovascular Research School COEUR, Erasmus MC, 3000 DR Rotterdam, Netherlands; 2005;5:2519–2530.
71. Wong YY, Raijmakers P, Campen J Van, Laarse WJ Van Der, Knaapen P, Lubberink M, Ruiter G, Noordegraaf A V, Lammertsma AA. 11C-acetate clearance as an index of oxygen consumption of the right myocardium in idiopathic pulmonary arterial hypertension: A validation study using 15O-labeled tracers and PET. *J Nucl Med* A.A. Lammertsma, Department of Nuclear Medicine and PET Research, VU University Medical Center, 1081 BT Amsterdam, Netherlands; 2013;54:1258–1262.
72. Yoshinaga K, Ohira H, Tsujino I, Oyama-Manabe N, Mielniczuk L, Beanlands RSB, Katoh C, Kasai K, Manabe O, Sato T, Fujii S, Ito YM, Tomiyama Y, Nishimura M, Tamaki N. Attenuated right ventricular energetics evaluated using 11C-acetate PET in patients with pulmonary hypertension. *Eur J Nucl Med Mol Imaging* K. Yoshinaga, Department of Molecular Imaging, Hokkaido University, Graduate School of Medicine, Kita-Ku 060-8638m Sapporo Hokkaido, Japan; 2014;41:1240–1250.
73. Matsushita T, Ikeda S, Miyahara Y, Yakabe K, Yamaguchi K, Furukawa K, Iwasaki T, Shikuwa M, Fukui J, Kohno S. Use of [123I]-BMIPP myocardial scintigraphy for the clinical evaluation of a fatty-acid metabolism disorder of the right ventricle in chronic respiratory and pulmonary vascular disease. *J Int Med Res* T. Matsushita, Second Dept. of Internal Medicine, Nagasaki University School of Med., Nagasaki 852-8501, Japan; 2000;28:111–123.
74. Sakao S, Miyauchi H, Voelkel NF, Sugiura T, Tanabe N, Kobayashi Y, Tatsumi K. Increased right ventricular fatty acid accumulation in chronic thromboembolic pulmonary hypertension. *Ann Am Thorac Soc* S. Sakao, Department of Respirology (B2), Graduate School of Medicine, Chiba University, Chuo-ku, Chiba, Japan; 2015;12:1465–1472.
75. Nagaya N, Goto Y, Satoh T, Uematsu M, Hamada S, Kuribayashi S, Okano Y, Kyotani S, Shimotsu Y, Fukuchi K, Nakanishi N, Takamiya M, Ishida Y. Impaired regional fatty acid uptake and systolic dysfunction in hypertrophied right ventricle. *J Nucl Med* Y. Goto, Division of Cardiology, Department of Medicine, National Cardiovascular Center, Suita, Osaka 565, Japan; 1998;39:1676–1680.
76. Drake JI, Gomez-Arroyo J, Dumur CI, Kraskauskas D, Natarajan R, Bogaard HJ, Fawcett P, Voelkel NF. Chronic carvedilol treatment partially reverses the right ventricular failure transcriptional profile in experimental pulmonary hypertension. *Physiol Genomics* N. F. Voelkel, Richmond, VA 23298, United States; 2013;45:449–461.

77. Lewandowski ED, Fischer SK, Fasano M, Banke NH, Walker LA, Huqi A, Wang X, Lopaschuk GD, O'Donnell JM. Acute liver carnitine palmitoyltransferase I overexpression recapitulates reduced palmitate oxidation of cardiac hypertrophy. *Circ Res* 2013;112:57–65.

78. Talati M, Hemnes A. Fatty acid metabolism in pulmonary arterial hypertension : role in right ventricular dysfunction and hypertrophy. *Pulm Circ* 2015;**1**:269–278.

79. Brittain EL, Talati M, Fessel JP, Zhu H, Penner N, Calcutt MW, West JD, Funke M, Lewis GD, Gerszten RE, Hamid R, Pugh ME, Austin ED, Newman JH, Hemnes AR. Fatty acid metabolic defects and right ventricular lipotoxicity in human pulmonary arterial hypertension. *Circulation* E.L. Brittain, Division of Cardiovascular Medicine, Vanderbilt University Medical School, Nashville, United States; 2016;133:1936–1944.

80. Bitar FF, Bitar H, Sabban M El, Nasser M, Yunis KA, Tawil A, Dbaibo GS. Modulation of ceramide content and lack of apoptosis in the chronically hypoxic neonatal rat heart. *Pediatr Res* F.F. Bitar, Department of Pediatrics, American University of Beirut, Beirut, Lebanon; 2002;51:144–149.

81. Huss JM, Gigue V, Kelly DP. Estrogen-Related Receptor ␣ Directs Peroxisome Proliferator-Activated Receptor ␣ Signaling in the Transcriptional Control of Energy Metabolism in Cardiac and Skeletal Muscle. *Society* 2004;24:9079–9091.

82. Burkart EM, Welch MJ, Kelly DP, Burkart EM, Sambandam N, Han X. Nuclear receptors PPAR b / d and PPAR a direct distinct metabolic regulatory programs in the mouse heart Find the latest version : Nuclear receptors PPAR / and PPAR direct distinct metabolic regulatory programs in the mouse heart. 2007;117:3930–3939.

83. Yang J, Sambandam N, Han X, Gross RW, Courtois M, Kovacs A, Febbraio M, Finck BN, Kelly DP. CD36 deficiency rescues lipotoxic cardiomyopathy. *Circ Res* 2007;**100**:1208–1217.

84. Duncan JG, Bharadwaj KG, Fong JL, Mitra R, Sambandam N, Courtois MR, Lavine KJ, Goldberg IJ, Kelly DP. Rescue of Cardiomyopathy in Peroxisome Proliferator-Activated Receptor- ␣ Transgenic Mice by Deletion of Lipoprotein Lipase Identifies Sources of Cardiac Lipids and Peroxisome Proliferator-Activated Receptor-a Activators. *Circulation* 2010;121:426–435.

85. Sharma S, Adrogue J V., Golfman L, Uray I, Lemm J, Youker K, Noon GP, Frazier OH, Taegtmeyer H. Intramyocardial lipid accumulation in the failing human heart resembles the lipotoxic rat heart. *FASEB J* 2004;18:1692–1700.

86. Urashima T, Zhao M, Wagner R, Fajardo G, Farahani S, Quertermous T, Bernstein D, Quertermous T, Molecular BD. Molecular and physiological characterization of RV remodeling in a murine model of pulmonary stenosis. 2008;94304.

87. Friehs I, Cowan DB, Choi Y-H, Black KM, Barnett R, Bhasin MK, Daly C, Dillon SJ, Libermann TA, McGowan FX, Nido PJ del, Levitsky S, McCully JD. Pressure-overload hypertrophy of the developing heart reveals activation of divergent gene and protein pathways in the left and right ventricular myocardium. *AJP Hear Circ Physiol* 2013;304:H697-708.

88. Kreymborg K grosse, Uchida S, Gellert P, Schneider A, Boettger T, Voswinckel R, Wietelmann A, Szibor M, Weissmann N, Ghofrani AH, Schermuly R, Schranz D, Seeger W, Braun T. Identification of right heart-enriched genes in a murine model of chronic outflow tract obstruction. *J Mol Cell Cardiol* Elsevier Ltd; 2010;49:598–605.

89. Ni YG, Wang N, Cao DJ, Sachan N, Morris DJ, Gerard RD, Kuro-o M, Rothermel BA, Hill JA. FoxO transcription factors activate Akt and attenuate insulin signaling in heart by inhibiting protein phosphatases. *Proc Natl Acad Sci* 2007;104:20517–20522.

90. Hedges L, Olkin I. Statistical methods for meta-analysis. Orlando: Academic Press; 1985. Orlando: Academic Press; 1985;

91. Vesterinen HM, Sena ES, Egan KJ, Hirst TC, Churolov L, Currie GL, Antonic A, Howells DW, Macleod MR. Meta-analysis of data from animal studies: A practical guide. *J Neurosci Methods* Elsevier B.V.; 2014;221:92–102.

SUPPLEMENTARY MATERIAL

Search strategy

1. Component 'right ventricle'

"right ventricle"[tiab] OR "right ventricles"[tiab] OR "right ventricular"[tiab] OR "ventriculus

dexter"[tiab] OR "right heart"[tiab] OR "RV"[tiab]

2. Component 'pressure load'

"pressure load"[tiab] OR " pressure loading"[tiab] OR " pressure loaded"[tiab] OR " pressure loads"[tiab] OR " pressure overload"[tiab] OR " pressure overloading"[tiab] OR " pressure overloaded"[tiab] OR "pressure overloads"[tiab] OR "increased afterload"[tiab] OR "increased afterloading"[tiab] OR "afterloaded"[tiab] OR "increased afterloads"[tiab] OR "pulmonary artery banding"[tiab] OR " pulmonary hypertension"[tiab] OR "pulmonary arterial hypertension"[tiab] OR "pulmonary valve stenosis"[tiab] OR "pulmonary valve calcification"[tiab] OR "calcification pulmonary valve"[tiab] OR "pulmonary valve diseases"[tiab] OR "pulmonary valve disease"[tiab] OR "pulmonary stenosis"[tiab] OR "stenosis pulmonary valve"[tiab] OR "pulmonary outflow tract obstruction"[tiab] OR "obstruction pulmonary outflow tract"[tiab] OR "pulmonary artery obstruction"[tiab] OR "pulmonary artery stenosis"[tiab]

3. Component 'metabolism'

"metabolism"[tiab] OR "metabolic"[tiab] OR "energy metabolism"[tiab] OR "basal metabolism"[tiab] OR "carbohydrate metabolism"[tiab] OR "metabolic network"[tiab] OR "metabolic pathways"[tiab] OR "metabolic networks and pathways"[tiab] OR "biosynthetic pathways"[tiab] OR "metabolic activation"[tiab] OR "metabolic inactivation"[tiab] OR "secondary metabolism"[tiab] OR "metabolic remodeling"[tiab] OR "metabolic remodelling"[tiab] OR "metabolic"[tiab] OR "metabolic reprogramming"[tiab] OR "metabolite"[tiab] OR "metabolomic"[tiab] OR "metabolomics"[tiab] OR "metabolite profile"[tiab] OR "metabolites profiles"[tiab] OR "metabolite derangements"[tiab] OR "metabolomic signatures"[tiab] OR "substrate flux"[tiab] OR "mitochondria"[tiab] OR "mitochondrial"[tiab] OR "mitochondrion"[tiab] OR "mitochondrial energy transduction"[tiab] OR "glucose metabolism"[tiab] OR " glucose oxidation"[tiab] OR "gluconeogenesis"[tiab] OR "glycogenolysis"[tiab] OR "glycolysis"[tiab] OR "glycosylation"[tiab] OR "pyruvate"[tiab] OR "glucose"[tiab] OR "pentose phosphate pathway"[tiab] OR "fatty acid"[tiab] OR "fatty acids"[tiab] OR "long chain fatty acids"[tiab] OR "lipid metabolism"[tiab] OR "lipolysis"[tiab] OR "lipoylation"[tiab] OR "fatty acid oxidation"[tiab] OR "lipotoxicity"[tiab] OR "triglyceride"[tiab] OR "ceramide"[tiab] OR "lipid deposition"[tiab] OR "beta-oxidation"[tiab] OR "beta oxidation"[tiab] OR "fatty acid transport"[tiab] OR "-oxidation"[tiab] OR "branched chain amino acids"[tiab] OR "branched chain amino acid"[tiab] OR "amino acid"[tiab]

OR “amino acids”[tiab] OR “BCAA”[tiab] OR “branched chain aminotransferase”[tiab] OR “branched-chain aminotransferase”[tiab] OR “BCAT”[tiab] OR “brached chain keto acids”[tiab] OR “brached-chain keto acids”[tiab] OR “BCKA”[tiab] OR “BCKA dehydrogenase complex”[tiab] OR “BCKD”[tiab] OR “ketone”[tiab] OR “ketones”[tiab] OR “ketogenesis”[tiab] OR “ketosis”[tiab] OR “ketone body”[tiab] OR “citric acid cycle”[tiab] OR “tricarboxylic acid cycle”[tiab] OR “TCA cycle”[tiab] OR “Krebs cycle”[tiab] OR “ATP”[tiab] OR “ADP”[tiab] OR “adenosine diphosphate”[tiab] OR “adenosine triphosphate”[tiab] OR “respiratory transport”[tiab] OR “oxidation-reducation”[tiab] OR “oxidative phosphorylation”[tiab] OR “phosphorylation”[tiab] OR “electron transport”[tiab] OR “electron transport chain”[tiab] OR “metabolic targets”[tiab] OR “metabolic therapy”[tiab] OR “fatty acid oxidation inhibitor”[tiab] OR “glucose oxidation inhibitor”[tiab] OR “fatty acid uptake inhibitor”[tiab] OR “metabolic inhibitor”[tiab] OR “metabolic activator”[tiab] OR “inhibition of metabolic pathways”[tiab] OR “inhibition of metabolic pathway”[tiab] OR “metabolic inducers”[tiab] OR “metabolic inducer”[tiab] OR “metabolic inducement”[tiab] OR “metabolic activation”[tiab] OR “metabolic regulation”[tiab] OR “regulation of metabolism”[tiab] OR “regulation of fatty acid”[tiab] OR “regulation of fatty acids”[tiab] OR “stimulation of fatty acid metabolism”[tiab] OR “inhibition of fatty acid metabolism”[tiab] OR “regulation of glucose oxidation”[tiab] OR “regulation of glycolysis”[tiab] OR “stimulation of glucose oxidation”[tiab] OR “inhibition of glycolysis”[tiab] OR “inhibition of glucose oxidation”[tiab] OR “amino acid administration”[tiab] OR “amino acids administration”[tiab] OR “metabolic defect”[tiab] OR “catabolic defect”[tiab] OR “cell respiration”[tiab] OR “cell hypoxia”[tiab] OR “respiratory burst”[tiab] OR “anaerobiosis”[tiab] OR “oxidative stress”[tiab]

3

SUPPLEMENTAL TABLES

Supplemental table 1. List of studies studying metabolic parameters in the pressure loaded right ventricle included for full text review.

Author	Year	Title	PMID	Embase Accession ID
Cooper, et al.[1]	1974	Normal myocardial function and energetics after reversing pressure overload hypertrophy	4274811	1975096311
Cooper, et al.[2]	1981	Chronic progressive pressure overload of the cat right ventricle.	6450649	
Reibel, et al.[3]	1983	Altered coenzyme A and carnitine metabolism in pressure-overload hypertrophied hearts.	6222659	
Lauva, et al.[4]	1986	Control of myocardial tissue components and cardiocyte organelles in pressure-overload hypertrophy of the cat right ventricle.	2877565	
Schneider, et al.[5]	1987	Development and regression of right heart ventricular hypertrophy: biochemical and morphological aspects.	2963447	
Olivetti, et al.[6]	1988	Cellular basis of wall remodeling in long-term pressure overload-induced right ventricular hypertrophy in rats.	2970334	
Hung, et al.[7]	1988	Morphometry of right ventricular papillary muscle in rat during development and regression of hypoxia-induced hypertension.	3381706	
Saito, et al.[8]	1991	Oxygen metabolism of the hypertrophic right ventricle in open chest dogs.	1839241	
Morioka, et al.[9]	1992	Changes in contractile and non-contractile proteins, intracellular Ca2+ and ultrastructures during the development of right ventricular hypertrophy and failure in rats.	1534855	

Animal	Human	Specie	Model	Disease	Inclusion meta-analysis
x		cat	PAB		
x		cat	PAB		
x		cat			
x		cat	PAB		x
x					
x		rat	PAB		x
x					
x		dog	PAB		
x		rat	MCT60		

Author	Year	Title	PMID	Embase Accession ID
Sivitz, et al.[10]	1992	Pretranslational regulation of two cardiac glucose transporters in rats exposed to hypobaric hypoxia.	1415537	
Baudet, et al.[11]	1994	Biochemical, mechanical and energetic characterization of right ventricular hypertrophy in the ferret heart.	7731052	
Ishikawa, et al.[12]	1995	Enalapril improves heart failure induced by monocrotaline without reducing pulmonary hypertension in rats: roles of preserved myocardial creatine kinase and lactate dehydrogenase isoenzymes.	7721499	
Do, et al.[13]	1995	Intracellular pH during hypoxia in normal and hypertrophied right ventricle of ferret heart.	7602610	
Sack, et al.[14]	1997	A role for Sp and nuclear receptor transcription factors in a cardiac hypertrophic growth program.	9177236	
Nagaya, et al.[15]	1998	Impaired regional fatty acid uptake and systolic dysfunction in hypertrophied right ventricle.	9776267	
Rumsey, et al.[16]	1999	Adaptation to hypoxia alters energy metabolism in rat heart.	9887019	
O'Brien, et al.[17]	1999	F1-ATP synthase beta-subunit and cytochrome c transcriptional regulation in right ventricular hemodynamic overload and hypertrophically stimulated cardiocytes.	10072725	
Matsushita, et al.[18]	2000	Use of [123I]-BMIPP myocardial scintigraphy for the clinical evaluation of a fatty-acid metabolism disorder of the right ventricle in chronic respiratory and pulmonary vascular disease.	10983861	
Bitar, et al.[19]	2002	Modulation of ceramide content and lack of apoptosis in the chronically hypoxic neonatal rat heart.	11809907	

Animal	Human	Specie	Model	Disease	Inclusion meta-analysis
x		rat	hypoxia		x
x		ferret	PAC		
x		rat	MCT50		
x		ferret	PAB		
x		mouse	PAB		x
	x			PH (mPAP > 20)	
x		rat	hypoxia		x
x		feline (cat)	PAB		
	x			RVPO	
x		rat	hypoxia		

Author	Year	Title	PMID	Embase Accession ID
Ecarnot-Laubreit, et al.[20]	2003	The activation pattern of the antioxidant enzymes in the right ventricle of rat in response to pressure overload is of heart failure type.	14503927	
Farahmand, et al.[21]	2004	Antioxidant and oxidative stress changes in experimental cor pulmonale.	15228082	
Cisar, et al.[22]	2004	Differential expression of mitochondrial electron transport chain proteins in cardiac tissues of broilers from pulmonary hypertension syndrome-resistant and -susceptible lines.	15339019	
Sharma, et al.[23]	2004	Dynamic changes of gene expression in hypoxia-induced right ventricular hypertrophy.	14630626	
Nouette-Gaulain, et al.[24]	2004	Time course of differential mitochondrial energy metabolism adaptation to chronic hypoxia in right and left ventricles.	15769456	
Adrogue, et al.[25]	2005	Acclimatization to chronic hypobaric hypoxia is associated with a differential transcriptional profile between the right and left ventricle.	16180091	
van Beek-Harmsen and van der Laarse[26]	2005	Immunohistochemical determination of cytosolic cytochrome C concentration in cardiomyocytes.	15995138	
Schott, et al.[27]	2005	Pressure overload and neurohumoral activation differentially affect the myocardial proteome.	15732135	
Faber, et al.[28]	2005	Proteomic changes in the pressure overloaded right ventricle after 6 weeks in young rats: correlations with the degree of hypertrophy.	15912512	
Kluge, et al.[29]	2005	Different mechanisms for changes in glucose uptake of the right and left ventricular myocardium in pulmonary hypertension.	15632029	

Animal	Human	Specie	Model	Disease	Inclusion meta-analysis
x		rat	MCT60		
x		rat	MCT60		
x		broiler	hypoxia		
x		rat	hypoxia		x
x		rat	hypoxia		x
x		rat	hypoxia		x
x		rat	MCT40		
x		rat	MCT50		
x		rat	PAB		
	x			PH	

Author	Year	Title	PMID	Embase Accession ID
Oikawa, et al.[30]	2005	Increased [18F]fluorodeoxyglucose accumulation in right ventricular free wall in patients with pulmonary hypertension and the effect of epoprostenol.	15936618	
Redout, et al.[31]	2007	Right-ventricular failure is associated with increased mitochondrial complex II activity and production of reactive oxygen species.	17582388	
Faber, et al.[32]	2007	Time dependent changes in cytoplasmic proteins of the right ventricle during prolonged pressure overload.	17603072	
Basu, et al.[33]	2007	Etiopathologies associated with intercostal muscle hypermetabolism and prominent right ventricle visualization on 2-deoxy-2[F-18]fluoro-D-glucose-positron emission tomography: significance of an incidental finding and in the setting of a known pulmonary disease.	17610018	
Nagendran, et al.[34]	2008	A dynamic and chamber-specific mitochondrial remodeling in right ventricular hypertrophy can be therapeutically targeted.	18603070	
Broderick and King.[35]	2008	Upregulation of GLUT-4 in right ventricle of rats with monocrotaline-induced pulmonary hypertension.	19043358	
Mouchaers, et al.[36]	2009	Endothelin receptor blockade combined with phosphodiesterase-5 inhibition increases right ventricular mitochondrial capacity in pulmonary arterial hypertension.	19395550	
Sheikh, et al.[37]	2009	Right ventricular hypertrophy with early dysfunction: A proteomics study in a neonatal model.	19379982	
Redout, et al.[38]	2010	Antioxidant treatment attenuates pulmonary arterial hypertension-induced heart failure.	20061549	

Animal	Human	Specie	Model	Disease	Inclusion meta-analysis
	x			PH	
x		rat	MCT80		
x		rat	PAB		
	x			Various diseases	
x		rat	MCT		
x		rat	MCT60		x
x		rat	MCT40		
x		piglet	PAB		x
x		rat	MCT80		

Author	Year	Title	PMID	Embase Accession ID
Yen, et al.[39]	2010	Sildenafil limits monocrotaline-induced pulmonary hypertension in rats through suppression of pulmonary vascular remodeling.	20224427	x
Piao, et al.[40]	2010	The inhibition of pyruvate dehydrogenase kinase improves impaired cardiac function and electrical remodeling in two models of right ventricular hypertrophy: resuscitating the hibernating right ventricle.	19949938	x
Drake, et al.[41]	2011	Molecular signature of a right heart failure program in chronic severe pulmonary hypertension.	21719795	x
Saini-Chohan, et al.[42]	2011	Persistent pulmonary hypertension results in reduced tetralinoleoyl-cardiolipin and mitochondrial complex II + III during the development of right ventricular hypertrophy in the neonatal pig heart.	21841017	x
Baandrup, et al.[43]	2011	Pressure load: the main factor for altered gene expression in right ventricular hypertrophy in chronic hypoxic rats.	21246034	x
Bokhari, et al.[44]	2011	PET imaging may provide a novel biomarker and understanding of right ventricular dysfunction in patients with idiopathic pulmonary arterial hypertension.	21926260	
Wong, et al.[45]	2011	Right ventricular failure in idiopathic pulmonary arterial hypertension is associated with inefficient myocardial oxygen utilization.	21900188	
Wong, et al.[46]	2011	Systolic pulmonary artery pressure and heart rate are main determinants of oxygen consumption in the right ventricular myocardium of patients with idiopathic pulmonary arterial hypertension.	22016028	

Animal	Human	Specie	Model	Disease	Inclusion meta-analysis
		rat	MCT60		
		rat	MCT60 & PAB		x
		rat	PAB + Suhx +Cu2diet		
		piglet	hypoxia		
		rat	hypoxia + PAB		
x				iPAH	
x				iPAH	
x				iPAH	

Author	Year	Title	PMID	Embase Accession ID
Qipshidze, et al.[47]	2012	Autophagy mechanism of right ventricular remodeling in murine model of pulmonary artery constriction.	22101525	x
Mosele, et al.[48]	2012	Effects of purple grape juice in the redox-sensitive modulation of right ventricular remodeling in a pulmonary arterial hypertension model.	22441302	x
Khoo, et al.[49]	2012	Obesity-induced tissue free radical generation: an in vivo immuno-spin trapping study.	22564528	x
Fang, et al.[50]	2012	Therapeutic inhibition of fatty acid oxidation in right ventricular hypertrophy: exploiting Randle's cycle.	21874543	x
Fang, et al.[51]	2012	Comparison of 18F-FDG uptake by right ventricular myocardium in idiopathic pulmonary arterial hypertension and pulmonary arterial hypertension associated with congenital heart disease.	23130105	
Wong, et al.[52]	2013	11C-Acetate clearance as an index of oxygen consumption of the right myocardium in idiopathic pulmonary arterial hypertension: a validation study using 15O-labeled tracers and PET.	23735834	
Sutendra, et al.[53]	2013	A metabolic remodeling in right ventricular hypertrophy is associated with decreased angiogenesis and a transition from a compensated to a decompensated state in pulmonary hypertension.	23846254	x
Piao, et al.[54]	2013	Cardiac glutaminolysis: a maladaptive cancer metabolism pathway in the right ventricle in pulmonary hypertension.	23794090	x
Drake, et al.[55]	2013	Chronic carvedilol treatment partially reverses the right ventricular failure transcriptional profile in experimental pulmonary hypertension.	23632417	2013387359
Alzoubi, et al.[56]	2013	Dehydroepiandrosterone restores right ventricular structure and function in rats with severe pulmonary arterial hypertension.	23585128	x

	Animal	Human	Specie	Model	Disease	Inclusion meta-analysis
			mouse	PAB		
			rat	MCT60		
			mouse	Diet + DMPO + MCT60		
			rat	PAB		x
	x				iPAH vs. CHD-PAH	
	x				iPAH	
			rat	MCT		x
			rat	PAB & MCT60		x
x			rat	SuHx		
			rat	SuHx		

Author	Year	Title	PMID	Embase Accession ID
Piao, et al.[57]	2013	FOXO1-mediated upregulation of pyruvate dehydrogenase kinase-4 (PDK4) decreases glucose oxidation and impairs right ventricular function in pulmonary hypertension: therapeutic benefits of dichloroacetate.	23247844	x
Gomez-Arroyo, et al.[58]	2013	Metabolic gene remodeling and mitochondrial dysfunction in failing right ventricular hypertrophy secondary to pulmonary arterial hypertension.	23152488	x
Friehs, et al.[59]	2013	Pressure-overload hypertrophy of the developing heart reveals activation of divergent gene and protein pathways in the left and right ventricular myocardium.	23262132	x
Enache, et al.[60]	2013	Skeletal muscle mitochondrial dysfunction precedes right ventricular impairment in experimental pulmonary hypertension.	23099843	x
Kojonazarov, et al.[61]	2013	The peroxisome proliferator-activated receptor Î²/Î´ agonist GW0742 has direct protective effects on right heart hypertrophy.	25006409	x
Yoshinaga, et al.[62]	2013	Attenuated right ventricular energetics evaluated using Â¹Â¹C-acetate PET in patients with pulmonary hypertension.	24615469	
Wang, et al.[63]	2013	Evaluation of right ventricular volume and ejection fraction by gated (18)F-FDG PET in patients with pulmonary hypertension: comparison with cardiac MRI and CT.	23354658	
Lundgrin, et al.[64]	2013	Fasting 2-deoxy-2-[18F]fluoro-D-glucose positron emission tomography to detect metabolic changes in pulmonary arterial hypertension hearts over 1 year.	23509326	
Ikeda, et al.[65]	2014	Crucial role of rho-kinase in pressure overload-induced right ventricular hypertrophy and dysfunction in mice.	24675663	2014358537

	Animal	Human	Specie	Model	Disease	Inclusion meta-analysis
	x		rat	FHR	PAH	x
	x		rat	SuHx & PAB	PAH	x
			rabit	PAB		
			rat	MCT60		x
			mice	PAB		
	x				PH	
	x				PH	
	x				PAH	
x			mouse	PAB		

Author	Year	Title	PMID	Embase Accession ID
Hemnes, et al.[66]	2014	Evidence for right ventricular lipotoxicity in heritable pulmonary arterial hypertension.	24274756	
Rawat, et al.[67]	2014	Increased reactive oxygen species, metabolic maladaptation, and autophagy contribute to pulmonary arterial hypertension-induced ventricular hypertrophy and diastolic heart failure.	25267798	
Liu, et al.[68]	2014	Inhibition of NOX/VPO1 pathway and inflammatory reaction by trimethoxystilbene in prevention of cardiovascular remodeling in hypoxia-induced pulmonary hypertensive rats.	24492474	
Ahmed, et al.[69]	2014	Naringenin adds to the protective effect of L-arginine in monocrotaline-induced pulmonary hypertension in rats: favorable modulation of oxidative stress, inflammation and nitric oxide.	24878387	
Frazziano, et al.[70]	2014	Nox-derived ROS are acutely activated in pressure overload pulmonary hypertension: indications for a seminal role for mitochondrial Nox4.	24213612	
Nergui, et al.[71]	2014	Role of endothelial nitric oxide synthase and collagen metabolism in right ventricular remodeling due to pulmonary hypertension.	24705390	
Ahmed, et al.[72]	2014	Role of oxidative stress, inflammation, nitric oxide and transforming growth factor-beta in the protective effect of diosgenin in monocrotaline-induced pulmonary hypertension in rats.	25062790	
Zhang, et al.[73]	2014	Up-regulation of hexokinase1 in the right ventricle of monocrotaline induced pulmonary hypertension.	25287584	
Tatebe, et al.[74]	2014	Enhanced [18F]fluorodeoxyglucose accumulation in the right ventricular free wall predicts long-term prognosis of patients with pulmonary hypertension: a preliminary observational study.	24408936	

Animal	Human	Specie	Model	Disease	Inclusion meta-analysis
x		mouse	BMPR2 & PAB		
x		rat	SuHx		
x		rat	hypoxia		
x		rat	MCT60		
x		mouse	PAC + Nox2-/-, p47phox-/-		
x		mice	hypoxia + eNOS-/-		
x		rat	MCT60		
x		rat	MCT50		x
	x			PAH	

Author	Year	Title	PMID	Embase Accession ID
Yang, et al.[75]	2014	The ratio of (18)F-FDG activity uptake between the right and left ventricle in patients with pulmonary hypertension correlates with the right ventricular function.	24662662	
Paulin, et al.[76]	2015	A miR-208-Mef2 axis drives the decompensation of right ventricular function in pulmonary hypertension.	25287062	
Moreira-Goncalyes, et al. [77]	2015	Cardioprotective effects of early and late aerobic exercise training in experimental pulmonary arterial hypertension.	26463598	2015442750
Borgdorff, et al.[78]	2015	Clinical symptoms of right ventricular failure in experimental chronic pressure load are associated with progressive diastolic dysfunction	25486580	2014633325
Balestra, et al.[79]	2015	Increased in vivo mitochondrial oxygenation with right ventricular failure induced by pulmonary arterial hypertension: mitochondrial inhibition as driver of cardiac failure?	25645252	
Bruns, et al.[80]	2015	Mitochondrial integrity in a neonatal bovine model of right ventricular dysfunction.	25416385	
Kaur, et al.[81]	2015	Poly (ADP-ribose) polymerase-1: an emerging target in right ventricle dysfunction associated with pulmonary hypertension.	25481773	
Aziz, et al.[82]	2015	Proteomic Profiling of Early Chronic Pulmonary Hypertension: Evidence for Both Adaptive and Maladaptive Pathology.	26246959	
Graham, et al.[83]	2015	Severe pulmonary hypertension is associated with altered right ventricle metabolic substrate uptake.	26115672	

Animal	Human	Specie	Model	Disease	Inclusion meta-analysis
	x			PH	
x		rat	MCT		x
x		rat	MCT60		
x		rat	PAB		x
x		rat	MCT30 & 60		x
x		calve	hypoxia		x
x		rat	MCT60		
x		dog	DMCT		
x		rat	SuHx		x

Author	Year	Title	PMID	Embase Accession ID
Khan, et al.[84]	2015	Effects of ranolazine on exercise capacity, right ventricular indices, and hemodynamic characteristics in pulmonary arterial hypertension: a pilot study.	26401256	
Sakao, et al.[85]	2015	Increased Right Ventricular Fatty Acid Accumulation in Chronic Thromboembolic Pulmonary Hypertension.	26356218	
Li, et al.[86]	2015	The Prognostic Value of 18F-FDG Uptake Ratio Between the Right and Left Ventricles in Idiopathic Pulmonary Arterial Hypertension.	26359560	2015437729
Drozd, et al.[87]	2016	Effects of an endothelin receptor antagonist, Macitentan, on right ventricular substrate utilization and function in a Sugen 5416/hypoxia rat model of severe pulmonary arterial hypertension.	27688036	20160703317
Brittain, et al.[88]	2016	Fatty Acid Metabolic Defects and Right Ventricular Lipotoxicity in Human Pulmonary Arterial Hypertension.	27006481	20160241851
Talati, et al.[89]	2016	Mechanisms of Lipid Accumulation in the Bone Morphogenetic Protein Receptor Type 2 Mutant Right Ventricle.	27077479	
Joshi, et al.[90]	2016	MicroRNA-140 is elevated and mitofusin-1 is downregulated in the right ventricle of the Sugen5416/hypoxia/normoxia model of pulmonary arterial hypertension.	27422986	
Peters, et al.[91]	2016	Regulation of myoglobin in hypertrophied rat cardiomyocytes in experimental pulmonary hypertension.	27572699	
Sun, et al.[92]	2016	Reversal of right ventricular remodeling by dichloroacetate is related to inhibition of mitochondria-dependent apoptosis.	26763846	20160371500
Van der Bruggen, et al.[93]	2016	Bone Morphogenetic Protein Receptor Type 2 Mutation in Pulmonary Arterial Hypertension: A View on the Right Ventricle.	26984938	

Animal	Human	Specie	Model	Disease	Inclusion meta-analysis
	x			PAH	
	x			CTEPH	
	x			iPAH	
x		rat	SuHx		x
x	x	mouse	BMPR2 R899X	PAH	
x		mouse	BMPR2		
x		rat	SuHx		
x		rat	MCT60		
x		rat	MCT60		x
	x			BMPR2	x

Author	Year	Title	PMID	Embase Accession ID
Gupte, et al.[94]	2016	Differential Mitochondrial Function in Remodeled Right and Nonremodeled Left Ventricles in Pulmonary Hypertension.	26370778	
Wang, et al.[95]	2016	Quantitative assessment of right ventricular glucose metabolism in idiopathic pulmonary arterial hypertension patients: a longitudinal study.	26588985	20160851284
Sakao, et al.[96]	2016	Right ventricular sugars and fats in chronic thromboembolic pulmonary hypertension.	27323340	20160461412
Ohira, et al.[97]	2016	Shifts in myocardial fatty acid and glucose metabolism in pulmonary arterial hypertension: a potential mechanism for a maladaptive right ventricular response.	26060207	
Frille, et al.[98]	2016	Thoracic [18F]fluorodeoxyglucose uptake measured by positron emission tomography/computed tomography in pulmonary hypertension.	27336898	20160485669
Campos, et al.[99]	2017	Effect of free and nanoencapsulated copaiba oil on monocrotaline-induced pulmonary arterial hypertension.	27798416	20160790386
Liu, et al.[100]	2017	Estrogen maintains mitochondrial content and function in the right ventricle of rats with pulmonary hypertension	28320896	20170235187
He, et al.[101]	2017	Galectin-3 mediates the pulmonary arterial hypertension–induced right ventricular remodeling through interacting with NADPH oxidase 4	28431936	20170283180
Cowley, et al.[102]	2017	Î±1A-Subtype Adrenergic Agonist Therapy for Failing Right Ventricle.	28822963	
Tian, et al.[103]	2017	Ischemia-induced Drp1 and Fis1-mediated mitochondrial fission and right ventricular dysfunction in pulmonary hypertension	28265681	20170177715
Nagy, et al.[104]	2017	Lack of ABCG2 leads to biventricular dysfunction and remodeling in response to hypoxia	28270772	20170166980

Animal	Human	Specie	Model	Disease	Inclusion meta-analysis
	x			PH	
	x			iPAH	x
	x			CTEPH	
	x			PAH	
	x			PH	
x		rat	MCT60		
x		rat	SuHx		x
x		rat	MCT60		
x		mice	bleomycin		
x		rat	MCT60		
x		mice	PAB / hypoxia		

Author	Year	Title	PMID	Embase Accession ID
Zhu, et al.[105]	2017	LOX-1 promotes right ventricular hypertrophy in hypoxia-exposed rats	28259654	20170244516
Wang, et al.[106]	2017	Oxidative profiling of the failing right heart in rats with pulmonary hypertension.	28472095	20170340497
Xu, et al.[107]	2017	PPAR Alleviates Right Ventricular Failure Secondary to Pulmonary Arterial Hypertension in Rats.	29151490	
Dos Santos Lacerda, et al.[108]	2017	Pterostilbene reduces oxidative stress, prevents hypertrophy and preserves systolic function of right ventricle in cor pulmonale model	28703274	20170659486
Puukila, et al.[109]	2017	Secoisolariciresinol diglucoside attenuates cardiac hypertrophy and oxidative stress in monocrotaline-induced right heart dysfunction	28321539	20170209991
Saygin, et al.[110]	2017	Metabolic and functional evaluation of the heart and lungs in pulmonary hypertension by gated 2-[18F]-Fluoro-2-deoxy-D-glucose positron emission tomography	28597761	20170459867
Siqueira, et al.[111]	2018	Effects of ovariectomy in antioxidant defence systems in right ventricle of female rats with pulmonary arterial hypertension induced by monocrotaline.	28854338	

Animal	Human	Specie	Model	Disease	Inclusion meta-analysis
x		rat	hypoxia		
x		rat	OVA/SuHx		
x		rat	MCT60		
x		rat	MCT60		
x		rat	MCT		
	x			PH	
x		rat	MCT		

Supplemental table 2.Meta-regression analyses: variables versus duration of RV pressure load.

	coefficient	constant	std.error	t	P > |t|	[95% conf.	interval]
FDG-uptake	-0.006	1.831118	0.028237	-0.21	0.851	-0.12751	0.115473
GLUT1 mRNA	0.007318	1.338181	0.017441	0.42	0.681	-0.03009	0.044725
GLUT1 protein	-0.06177	5.544784	0.193256	-0.32	0.780	-0.89329	0.769742
GLUT4 mRNA	-0.08868	-0.1779	0.094733	-0.94	0.385	-0.32048	0.143124
GLUT4 protein	0.062796	-1.92728	0.044244	1.42	0.251	-0.07801	0.2036
HK1 mRNA	-0.41346	20.52151	0.203145	-2.04	0.081	-0.89382	0.066904
HK2 mRNA	0.013838	-0.26506	0.035005	0.4	0.703	-0.06688	0.09456
CTP1B mRNA	-0.26705	9.571756	0.071064	-3.76	**0.033**	-0.49321	-0.0409
mitochondrial content	-0.0066	-0.41463	0.009553	-0.69	0.507	-0.02821	0.015005
mitochondrial content (first 6 weeks only)	*-0.12221*	*2.461455*	*0.025414*	*-4.81*	*0.002*	*-0.1823*	*-0.06211*
PDH mRNA	-0.0066	-0.26024	0.071658	-0.09	0.935	-0.31492	0.301721
PDK4 mRNA	-0.20665	0.005799	0.178042	-1.16	0.310	-0.70097	0.287676
PGC1a mRNA	-0.06271	0.634076	0.021666	-2.89	**0.044**	-0.12287	-0.00256
PGC1a protein	-0.04477	0.977281	0.03338	-1.34	0.272	-0.151	0.061461
PPAR mRNA	-0.03096	0.785598	0.023265	-1.33	0.232	-.0878866	0.025968
MCAD mRNA	-0.10478	-3.09365	0.096481	-1.09	0.313	-0.33292	0.123366
MCAD protein	0.120205	-5.58791	0.080062	1.5	0.272	-0.22427	0.464684
resp. cap. Glucose - ADP driven	-0.00781	-0.53042	0.009609	-0.81	0.566	-0.1299	0.114282
resp. cap. Glucose - whole cells	-0.11876	3.300385	0.114537	-1.04	0.409	-0.61157	0.374057
resp. cap. FA - ADP driven	-0.00753	-0.49098	0.010332	-0.73	0.519	-0.04041	0.025351

Significant p-values shown in **bold**.

Supplemental table 3.Meta-regression analyses: variables versus degree of RV pressure load.

	coefficient	constant	std. error	t	P > |t|	[95% conf.	interval]
FDG-uptake	-0.605857	3.8261	1.127987	-0.54	0.628	-4.19562	2.983902
GLUT1 mRNA	-0.097231	1.875722	0.258773	-0.38	0.771	-3.38525	3.19079
GLUT4 protein	0.6982679	-0.7738904	0.884316	0.79	0.460	-1.46558	2.86211
HK1 mRNA	2.672385	-14.20094	1.530079	1.75	0.223	-3.91101	9.255784
HK2 mRNA	0.2727004	-2.639479	0.392468	0.69	0.518	-0.73617	1.281572
mitochondrial content	-0.490853	0.6067835	0.163592	-3	**0.040**	-0.94506	-0.03665
PDH mRNA	-0.19941	1.375868	0.195707	-1.02	0.415	-1.04147	0.642648
PDK4 protein	-5.779816	6.268431	8.17396	-0.71	0.608	-109.64	98.0802
PDK1 mRNA	0.2356872	-2.020017	0.125199	1.88	0.311	-1.35512	1.826494
PDK1 protein	1.077672	-0.6647883	2.190228	0.49	0.709	-26.7518	28.90716
MCAD mRNA	1.856523	-19.68273	5.871176	0.32	0.782	-23.4051	27.11816
MCAD protein	-0.287837	0.7897496	0.113183	-2.54	0.239	-1.72596	1.150285
resp. cap. Glucose - ADP driven	0.2589947	-1.225371	0.286097	0.91	0.432	-0.65149	1.169482
resp. cap. FA - ADP driven	-0.257863	0.0167995	0.519064	-0.5	0.669	-2.49122	1.975488

Significant p-values shown in **bold**.

Supplemental table 4. Level of significance of meta-analysis and meta-regression.

	mRNA expression level				*protein expression level*			
parameter	meta-analysis	model effect *(increased compared)*	duration effect	effect of degree of pressure load	meta-analysis	model effect *(increased compared)*	duration effect	effect of degree of pressure load
GLUT1	(0.000)	~	~	~	(0.009)	MCT vs. hypoxia, PAB and FHR	~	~
GLUT4	~	~	~	~	~	~	~	~
CTP1B	~	~	(0.033)	N/A	N/A	N/A	N/A	N/A
HK1	(0.000)	~	(0.081)	~	N/A	N/A	N/A	N/A
HK2	~	~	~	~	N/A	N/A	N/A	N/A
PDH	~	~	~	~	(0.123)	~	~	N/A
PDK4	(0.110)	~	~	~	~	~	N/A	-
PDK1	N/A	N/A	N/A	~	~	~	N/A	~
PDK2	N/A	N/A	N/A	N/A	~	~	N/A	N/A
MCAD	(0.000)	~	~	~	(0.141)	~	~	~
PGC1	(0.008)	~	(0.044)	~	~	MCT vs. SuHx	~	N/A
PPAR	~	~	~	N/A	N/A	N/A	N/A	N/A

in vivo measurements

parameter	meta-analysis	model effect *(increased compared)*	duration effect	effect of degree of pressure load
FDG-uptake	(0.000)	~	~	~
Glycolysis – whole cells (i.e. Langendorf, Seahorse)	(0.000)	~	N/A	N/A
Respiratory capacity, carbohydrates – isolated mitochondria (i.e. Oroboros, Clark-type)	(0.085)	~	~	~
Respiratory capacity, carbohydrates – whole cells (i.e. Langendorf, Seahorse)	(0.082)	MCT vs. PAB and FHR	~	N/A
Respiratory capacity, fatty acids – isolated mitochondria (i.e. Oroboros, Clark-type)	(0.001)	~	(0.130)	~
Respiratory capacity, fatty acids – whole cells (i.e. Langendorf, Seahorse)	~	PAB vs. SuHx.	N/A	N/A

combined measurements

parameter	meta-analysis	model effect	duration effect	effect of degree of pressure load
Mitochondrial content	~	~	~ *(≤6 days* (0.002))	~

↑ *significant increase or positive relation;* ↓ *significant decrease or negative relation;* ↗ *positive trend (p<0.15);* ↘ *negative trend (p<0.15);* ~ *unchanged.*

Supplemental table 5. Overview of Hedges' g for metabolic parameters in models of RV pressure load subjected to therapeutic interventions.

animal	#	Year	Author	Hit duration	Model	Therapie	GLUT1 - mRNA	GLUT1 - protein	GLUT4 - protein	FDG-uptake	CPT1B - mRNA
Rat	19949938	2010	Piao[40]	1 month	MCT60	DCA	-1.68	-2.58		-0.41	
Rat	23247844	2012	Piao[57]	10-20 months	FHR	DCA, acute treatment					
Rat	23247844	2012	Piao[57]	10-20 months	FHR	DCA, chronic treatment (6 months)	-1.44				0.01
Rat	26763846	2016	Sun[92]	6 weeks	MCT	DCA 50mg/kg					
Rat	26763846	2016	Sun[92]	6 weeks	MCT	DCA 150mg/kg					
Rat	26763846	2016	Sun[92]	6 weeks	MCT	DCA 200 mg/kg					
Rat	23794090	2013	Piao[54]	4 weeks	MCT	DON	-2.19				
Rat	27688036	2016	Drozd[87]	9 weeks	SuHx	ERA			-2.67*	-1.20	
Rat	28320896	2017	Liu[100]	14 weeks	SuHx	oestrogen					
Rat	21874543	2012	Fang[50]	4 weeks	PAB	RAN	-1.46*	-0.45604			
Rat	21874543	2012	Fang[50]	4 weeks	PAB	RAN, in vitro					
Rat	21874543	2012	Fang[50]	8 weeks	PAB	TMZ	-1.30*	-1.33*			
Rat	21874543	2012	Fang[50]	8 weeks	PAB	TMZ, in vitro					

** p mentioned in study < 0.05*

Hedges' g

CPT1A - protein	HK1 - mRNA	HK1 - protein	HK2 - mRNA	PDH - activity	PDHa1 - protein	PDK4 - mRNA	PDK4 - protein	PDK1 - mRNA	PDK1 - protein	PDK2 - mRNA	PDK2 - protein	PGC1alpha - protein
				-0.99								
			-2.74*	4.13*		-1.51*	0.58	0.36	0.48	0.60	-0.95	
					1.62*		-6.14*		0.47		-1.78*	
					3.27*		-0.86*		0.40		-2.6*	
					3.38*		-6.89*		0.33		-3.20*	
	-1.10			1.14*								
												3.36*
-1.83*	-2.55*	-0.46	-0.08	2.01*								
-1.41*	-1.18*	-0.18	-0.18	1.36*								

animal	#	Year	Author	Hit duration	Model	Therapie	
Rat	19949938	2010	Piao[40]	1 month	MCT60	DCA	0.65
Rat	23247844	2012	Piao[57]	10-20 months	FHR	DCA, acute treatment	-0.79
Rat	23247844	2012	Piao[57]	10-20 months	FHR	DCA, chronic treatment (6 months)	-0.71
Rat	26763846	2016	Sun[92]	6 weeks	MCT	DCA 50mg/kg	
Rat	26763846	2016	Sun[92]	6 weeks	MCT	DCA 150mg/kg	
Rat	26763846	2016	Sun[92]	6 weeks	MCT	DCA 200 mg/kg	
Rat	23794090	2013	Piao[54]	4 weeks	MCT	DON	
Rat	27688036	2016	Drozd[87]	9 weeks	SuHx	ERA	
Rat	28320896	2017	Liu[100]	14 weeks	SuHx	oestrogen	
Rat	21874543	2012	Fang[50]	4 weeks	PAB	RAN	-0.99
Rat	21874543	2012	Fang[50]	4 weeks	PAB	RAN, in vitro	
Rat	21874543	2012	Fang[50]	8 weeks	PAB	TMZ	-1.47*
Rat	21874543	2012	Fang[50]	8 weeks	PAB	TMZ, in vitro	

** p mentioned in study < 0.05*

Hedges'g

Mitochondrial resp. capacity Glucose, isolated mitochondria	Mitochondrial resp. capacity Glucose, Langendorf	Mitochondrial resp. capacity Glucose, Seahorse	Mitochondrial resp. capacity fatty acids, isolated mitochondria	Mitochondrial resp. capacity FA, Langendorf	Mitochondrial resp. capacity FA, Seahorse	Mitochondrial content	Fulton
	3.20*						-1.59*
	3.51*			-1.22*			
		0.35			0.40		
							-2.72*
							-5.83*
							-5.97*
							-0.92
0.38			0.36			-0.01	-1.01*
		2.98*		-1.34*			-2.16*
				-14.63*			
		2.43 * (10 mM gluc), 1.99* (5mM gluc).		-1.28*	-7.29*		-1.79*
				-4.18*			

SUPPLEMENTAL FIGURES

A **right ventricular systolic pressure**

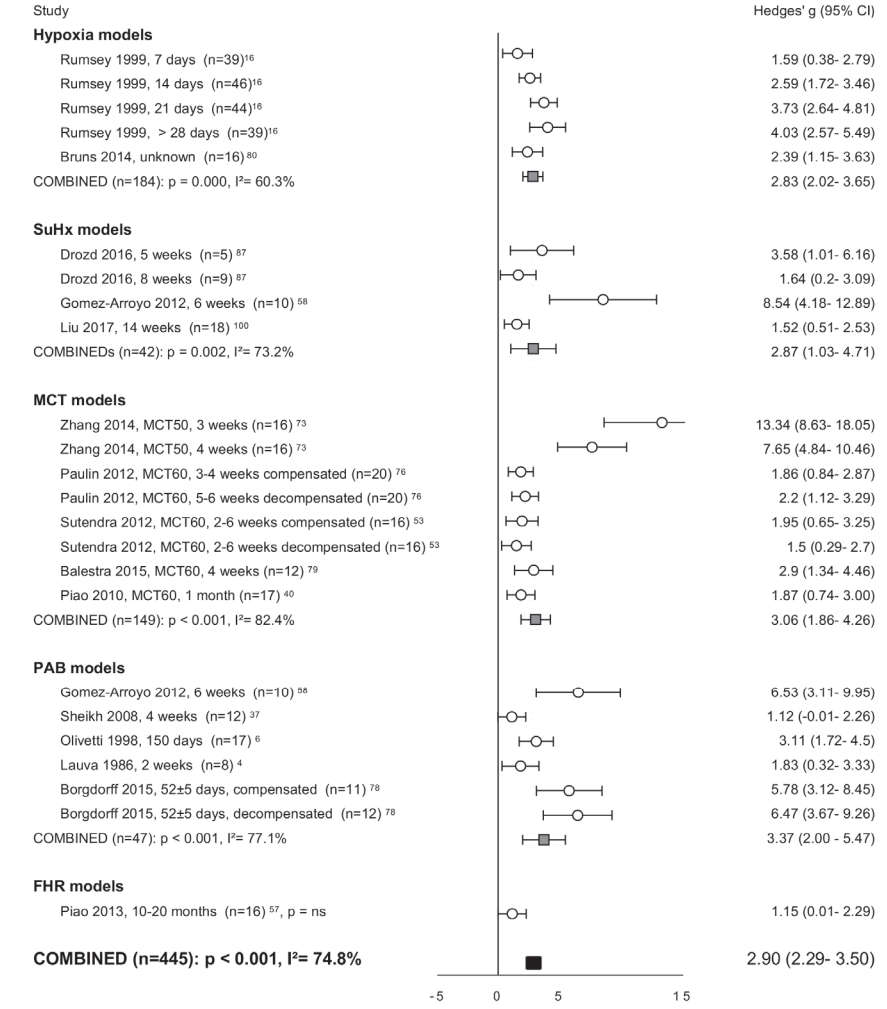

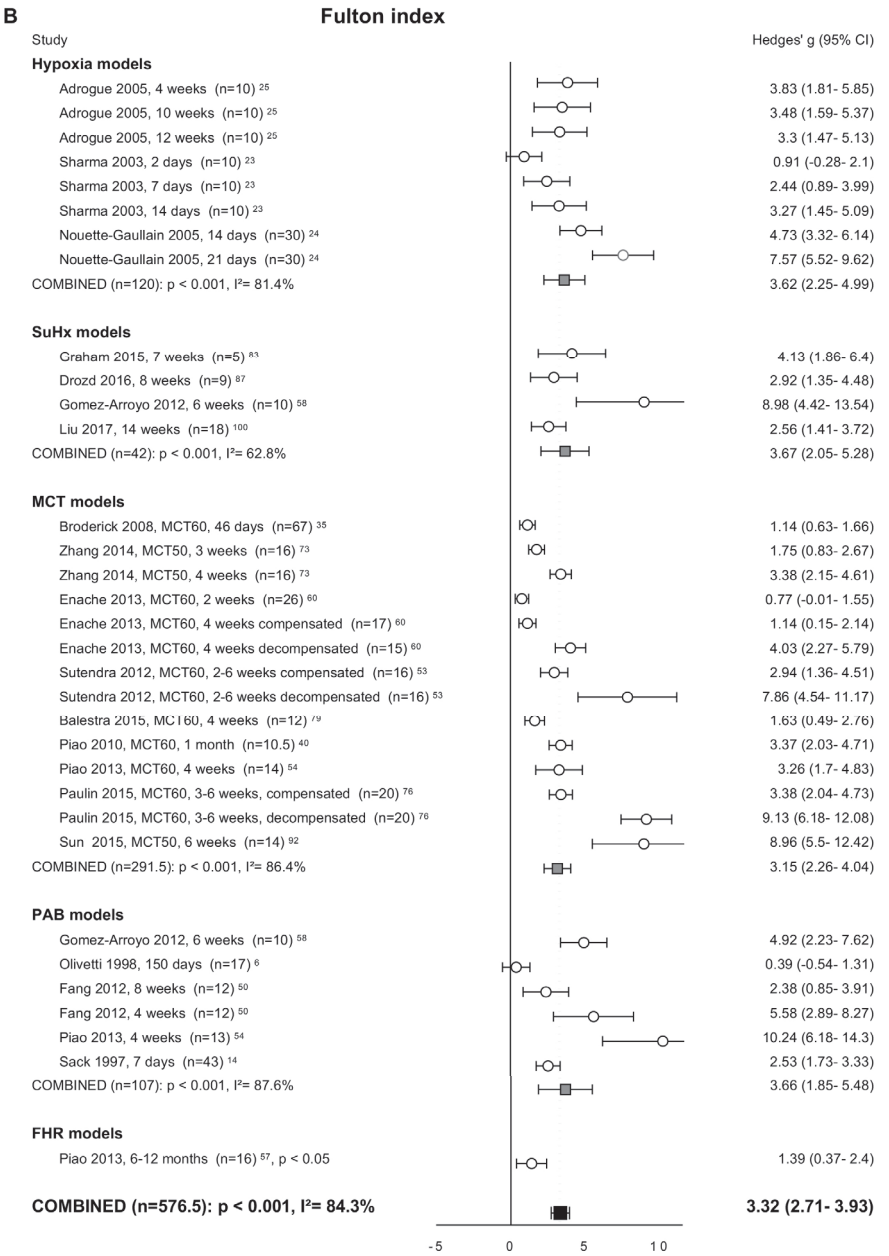

Supplemental figure 1. Models of increased pressure load. Forest plots of right ventricular systolic pressure (A) and Fulton index (B). Data are presented as Hedges' g (95% confidence interval). Combined Hedges' g are presented as squares: grey representing Hedges' g of a specific model, black representing Hedges' g of all included studies. Bars represent 95% confidence interval. *CI = confidence interval. n =*

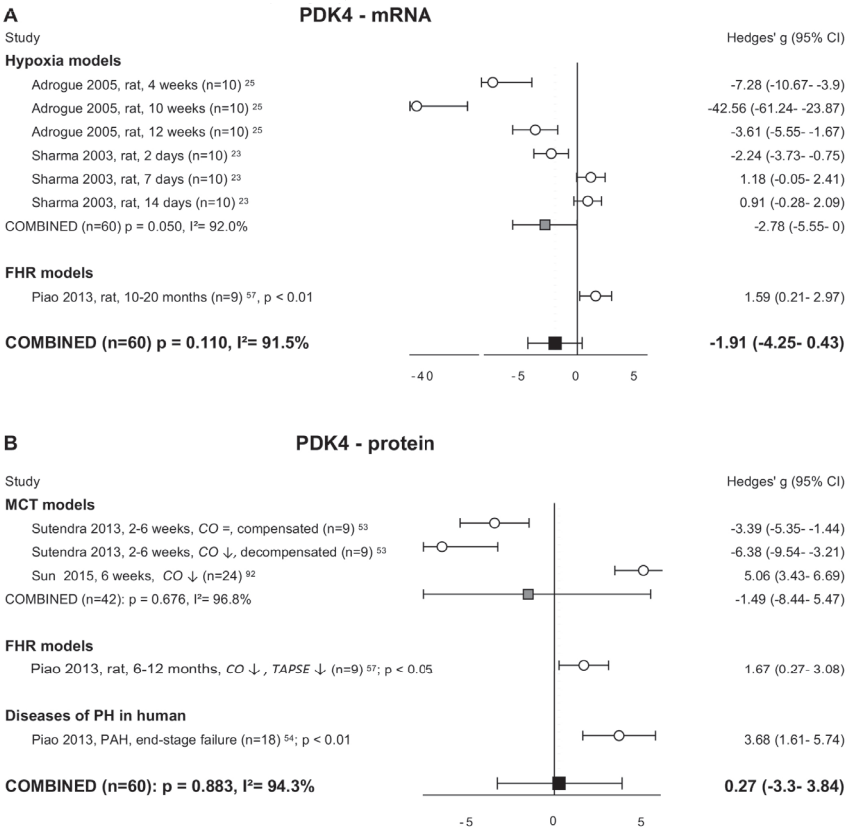
A
PDK4 - mRNA
Study
Hedges' g (95% CI)
Hypoxia models
Adrogue 2005, rat, 4 weeks (n=10) 25
-7.28 (-10.67- -3.9)
Adrogue 2005, rat, 10 weeks (n=10) 25
-42.56 (-61.24- -23.87)
Adrogue 2005, rat, 12 weeks (n=10) 25
-3.61 (-5.55- -1.67)
Sharma 2003, rat, 2 days (n=10) 23
-2.24 (-3.73- -0.75)
Sharma 2003, rat, 7 days (n=10) 23
1.18 (-0.05- 2.41)
Sharma 2003, rat, 14 days (n=10) 23
0.91 (-0.28- 2.09)
COMBINED (n=60) p = 0.050, I²= 92.0%
-2.78 (-5.55- 0)
FHR models
Piao 2013, rat, 10-20 months (n=9) 57, p < 0.01
1.59 (0.21- 2.97)
COMBINED (n=60) p = 0.110, I²= 91.5%
-1.91 (-4.25- 0.43)
-40
-5
0
5
B
PDK4 - protein
Study
Hedges' g (95% CI)
MCT models
Sutendra 2013, 2-6 weeks, CO =, compensated (n=9) 53
-3.39 (-5.35- -1.44)
Sutendra 2013, 2-6 weeks, CO ↓, decompensated (n=9) 53
-6.38 (-9.54- -3.21)
Sun 2015, 6 weeks, CO ↓ (n=24) 92
5.06 (3.43- 6.69)
COMBINED (n=42): p = 0.676, I²= 96.8%
-1.49 (-8.44- 5.47)
FHR models
Piao 2013, rat, 6-12 months, CO ↓, TAPSE ↓ (n=9) 57; p < 0.05
1.67 (0.27- 3.08)
Diseases of PH in human
Piao 2013, PAH, end-stage failure (n=18) 54; p < 0.01
3.68 (1.61- 5.74)
COMBINED (n=60): p = 0.883, I²= 94.3%
0.27 (-3.3- 3.84)
-5
0
5
C
PDK1 - protein
Study
Hedges' g (95% CI)
MCT models
Sutendra 2013, 2-6 weeks, CO =, compensated (n=9) 53
1.91 (0.45- 3.38)
Sutendra 2013, 2-6 weeks, CO ↓, decompensated (n=9) 53
0 (-1.17- 1.17)
Sun 2015, 6 weeks, CO ↓ (n=24) 92
-0.86 (-1.68- -0.04)
COMBINED (n=42): , I²= 81.0%
0.25 (-1.25- 1.75)
FHR models
Piao 2013, 6-12 months, CO ↓, TAPSE ↓ (n=9) 57, p = ns
1.14 (-0.15- 2.42)
COMBINED (n=51): p = 0.469, I²= 78.1%
0.46 (-0.78- 1.69)
-2
0
2

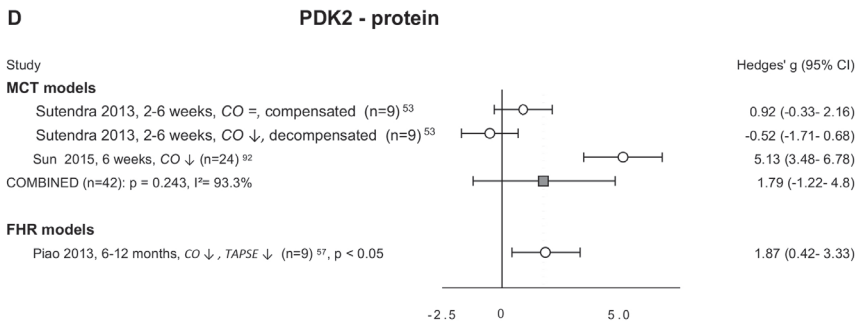

Supplemental figure 2. Forest plots of expression of PDK isoenzymes. PDK4 at both mRNA (A) and protein level (B), and PDK1 (C) and PDK2 (D) at protein level. Bars represent 95% confidence interval. PDK = pyruvate dehydrogenase kinase. *CO* = cardiac output, *CI* = cardiac index, *TAPSE* = tricuspid annular plane systolic movement, *RVEF* = RV ejection fraction, = decreased, "=" = not statistically significant affected. 95% CI = 95% confidence interval, n = number of included animals, i2 = level of heterogeneity, X = not included in meta-analysis.

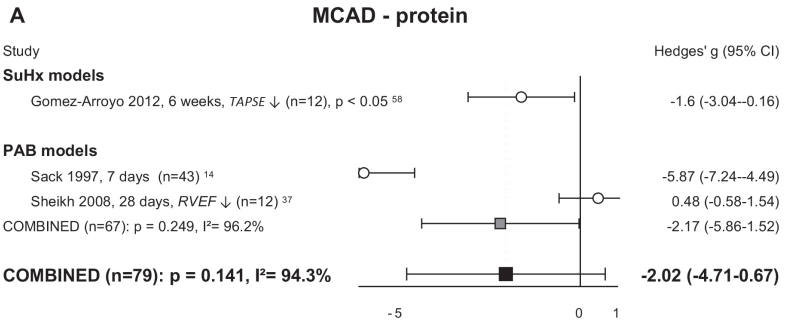

Supplemental figure 3. Forest plot MCAD at protein level. Bars represent 95% confidence interval. MCAD = medium chain acyl CoA dehydrogenase. *CO* = cardiac output, *CI* = cardiac index, *TAPSE* = tricuspid annular plane systolic movement, *RVEF* = RV ejection fraction, = decreased, "=" = not statistically significant affected. 95% CI = 95% confidence interval, n = number of included animals, i2 = level of heterogeneity, X = not included in meta-analysis.

A **mitochondrial content versus degree of pressure load**

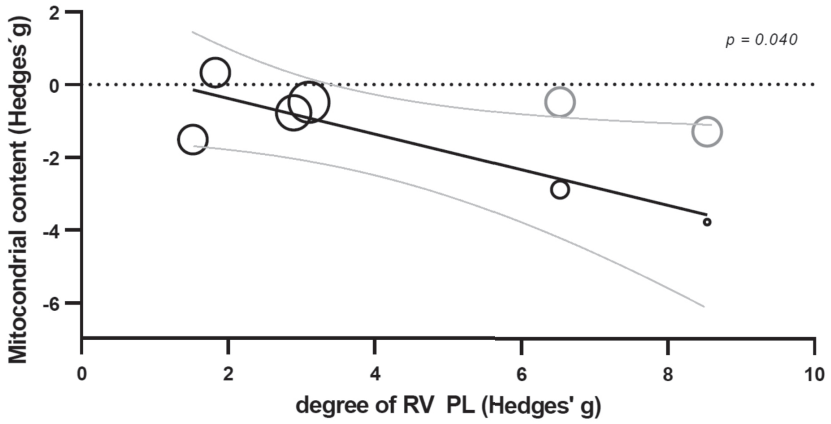

B **PGC1α - mRNA**

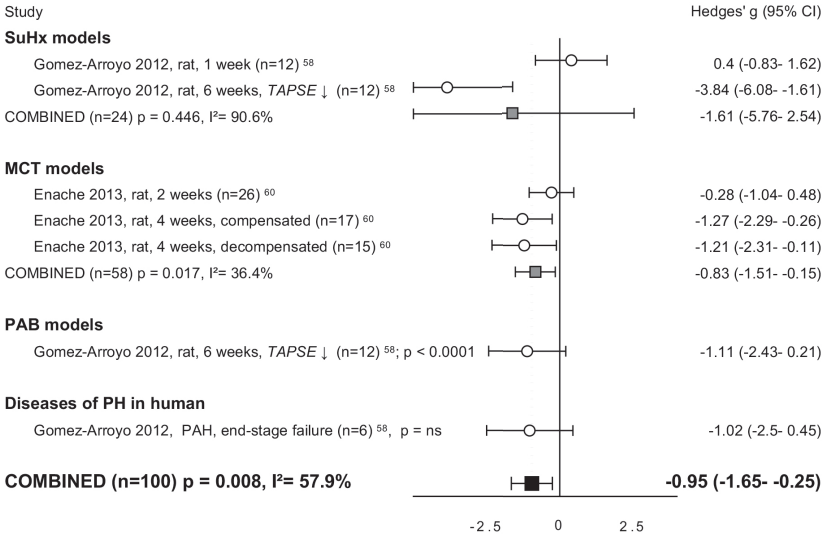

C **PGC1α (mRNA) versus duration of pressure load**

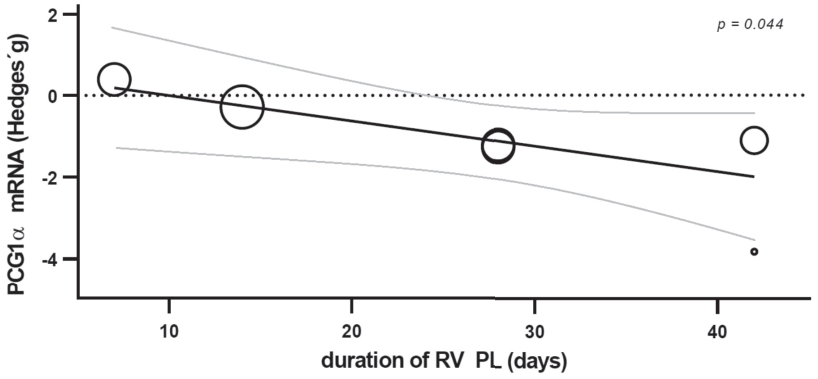

D **PGC1α - protein**

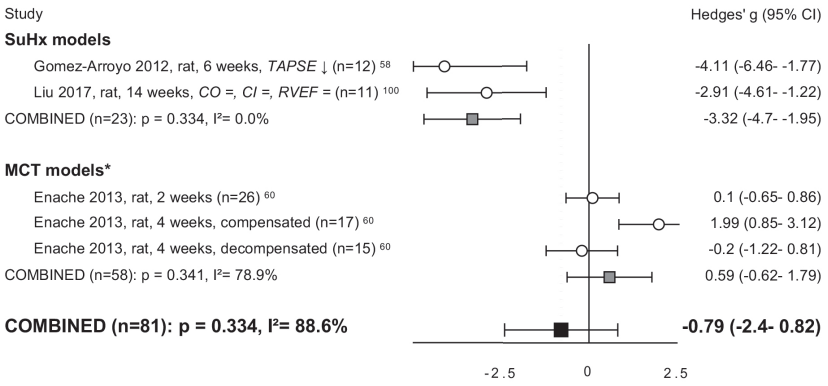

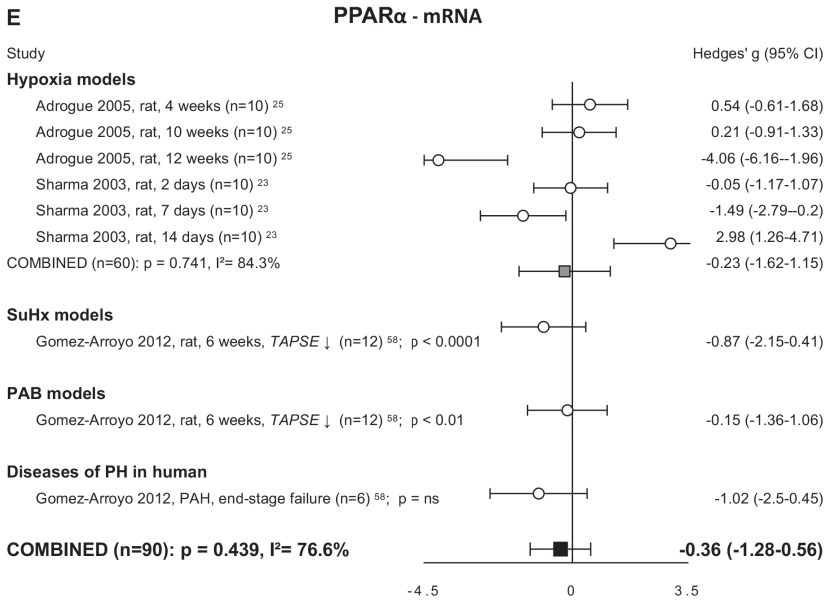

Supplemental figure 4. Regulators of metabolism. Meta-regression of mitochondrial content with degree of RV pressure load (A). PGC1 gene expression(B) and its relation with duration of pressure load shown by meta-regression in a bubble plot (C). Forrest plot of PGC1 protein expression (D). Forrest plot of PPAR gene expression (E). Data are presented as Hedges' g. Combined Hedges' g are presented as squares: grey representing Hedges' g of a specific model, black representing Hedges' g of all included studies. Bars represent 95% confidence interval. Bubble size represents relative study precision, calculation based on standard deviation. Black line represents regression line, grey lines represents 95% confidence interval. CO = cardiac output, CI = cardiac index, TAPSE = tricuspid annular plane systolic movement, RVEF = RV ejection fraction, = decreased, "=" = not statistically significant affected. 95% CI = 95% confidence interval, n = number of included animals, i^2 = level of heterogeneity. * = significantly ($p < 0.05$) increased compared to SuHx-model.

SUPPLEMENTAL REFERENCES

1. Cooper G, Satava RM, Harrison CE, Coleman HN. Normal myocardial function and energetics after reversing pressure overload hypertrophy. *Am J Physiol* Dept. Physiol. Biophys., Mayo Found., Rochester, Minn. 55901; 1974;226:1158–1165.
2. Cooper G 4th, Tomanek RJ, Ehrhardt JC, Marcus ML. Chronic progressive pressure overload of the cat right ventricle. *Circ Res* United States; 1981;48:488–497.
3. Reibel DK, Uboh CE, Kent RL. Altered coenzyme A and carnitine metabolism in pressure-overload hypertrophied hearts. *Am J Physiol - Hear Circ Physiol* Dep. Physiol., Thomas Jefferson Univ., Philadelphia, PA 19107; 1983;13:H839–H843.
4. Lauva IK, Brody E, Tiger E, Kent RL, Copper G 4th, Marino TA. Control of myocardial tissue components and cardiocyte organelles in pressure-overload hypertrophy of the cat right ventricle. *Am J Anat* United States; 1986;177:71–80.
5. Schneider M, Wiese S, Kunkel B, Hauk H, Pfeiffer B. Development and regression of right heart ventricular hypertrophy: Biochemical and morphological aspects. *Z Kardiol* Zentrum der Pathologie, Universitatsklinik, D-6000 Frankfurt/M; 1987;76:1–8.
6. Olivetti G, Ricci R, Lagrasta C, Maniga E, Sonnenblick EH, Anversa P. Cellular basis of wall remodeling in long-term pressure overload-induced right ventricular hypertrophy in rats. *Circ Res* Department of Pathology, University of Parma, 43100 Parma; 1988;63:648–657.
7. Hung KS, Pacheco H, Lessin D, Jordan K, Mattioli L. Morphometry of right ventricular papillary muscle in rat during development and regression of hypoxia-induced hypertension. *Adv Exp Med Biol* K.S. Hung, Department of Anatomy, University of Kansas Medical Center, Kansas City 66103.; 1988;227:337–346.
8. Saito D, Tani H, Kusachi S, Uchida S, Ohbayashi N, Marutani M, Maekawa K, Tsuji T, Haraoka S. Oxygen metabolism of the hypertrophic right ventricle in open chest dogs. *Cardiovasc Res* D. Saito, Department Cardiovascular Med., Okayama University Med. Sch., Okayama 700, Japan; 1991;25:731–736.
9. Morioka S, Honda M, Ishikawa S, Ishinaga Y, Yano S, Tanaka K, Moriyama K. Changes in contractile and non-contractile proteins, intracellular Ca^{2+} and ultrastructures during the development of right ventricular hypertrophy and failure in rats. *Jpn Circ J* S. Morioka, 4th Dept. of Internal Medicine, Shimane Medical University, Izumo, Japan; 1992;56:469–474.
10. Sivitz WI, Lund DD, Yorek B, Grover-McKay M, Schmid PG. Pretranslational regulation of two cardiac glucose transporters in rats exposed to hypobaric hypoxia. *Am J Physiol - Endocrinol Metab* W.I. Sivitz, Dept. of Internal Medicine, Univ. of Iowa Hospitals and Clinics, Iowa City, IA 52246, United States; 1992;263:E562–E569.
11. Baudet S, Kuznetsov A, Merciai N, Gorza L, Ventura-Clapier R. Biochemical, mechanical and energetic characterization of right ventricular hypertrophy in the ferret heart. *J Mol Cell Cardiol* S. Baudet, URA CNRS 1340, Lab. de Cardiologie Experimentale, Hopital Laennec, 44035 Nantes Cedex 01, France; 1994;26:1573–1586.
12. Ishikawa K, Hashimoto H, Mitani S, Toki Y, Okumura K, Ito T. Enalapril improves heart failure induced by monocrotaline without reducing pulmonary hypertension in rats: Roles of preserved myocardial creatine kinase and lactate dehydrogenase isoenzymes. *Int J Cardiol* H. Hashimoto, Department of Internal Medicine, Moriyama Citizen's Hospital, Nagoya 463, Japan; 1995;47:225–233.

13. Do E, Baudet S, Gow IF, Ellis D, Noireaud J. Intracellular pH during hypoxia in normal and hypertrophied right ventricle of ferret heart. *J Mol Cell Cardiol* J. Noireaud, Laboratoire Cardiol. Experimentale, Hopital G and R Laennec, BP 1005, 44035 Nantes Cedex 01, France; 1995;27:927–939.
14. Sack MN, Disch DL, Rockman HA, Kelly DP. A role for Sp and nuclear receptor transcription factors in a cardiac hypertrophic growth program. *Proc Natl Acad Sci U S A* D.P. Kelly, Center for Cardiovascular Research, Box 8086, Washington Univ. Sch. of Medicine, St. Louis, MO 63110, United States; 1997;94:6438–6443.
15. Nagaya N, Goto Y, Satoh T, Uematsu M, Hamada S, Kuribayashi S, Okano Y, Kyotani S, Shimotsu Y, Fukuchi K, Nakanishi N, Takamiya M, Ishida Y. Impaired regional fatty acid uptake and systolic dysfunction in hypertrophied right ventricle. *J Nucl Med* Y. Goto, Division of Cardiology, Department of Medicine, National Cardiovascular Center, Suita, Osaka 565, Japan; 1998;39:1676–1680.
16. Rumsey WL, Abbott B, Bertelsen D, Mallamaci M, Hagan K, Nelson D, Erecinska M. Adaptation to hypoxia alters energy metabolism in rat heart. *Am J Physiol - Hear Circ Physiol* W.L. Rumsey, Zeneca Pharmaceuticals, Wilmington, DE 19850-5437, United States; 1999;276:H71–H80.
17. O'Brien TX, Schuyler GT, Rackley MS, Thompson JT. F1 ATP synthase -subunit and cytochrome c transcriptional regulation in right ventricular hemodynamic overload and hypertrophically stimulated cardiocytes. *J Mol Cell Cardiol* T.X. O'Brien, Cardiology Division, 816 CSB, Medical University of South Carolina, Charleston, SC 29425-2221, United States; 1999;31:167–178.
18. Matsushita T, Ikeda S, Miyahara Y, Yakabe K, Yamaguchi K, Furukawa K, Iwasaki T, Shikuwa M, Fukui J, Kohno S. Use of [123I]-BMIPP myocardial scintigraphy for the clinical evaluation of a fatty-acid metabolism disorder of the right ventricle in chronic respiratory and pulmonary vascular disease. *J Int Med Res* T. Matsushita, Second Dept. of Internal Medicine, Nagasaki University School of Med., Nagasaki 852-8501, Japan; 2000;28:111–123.
19. Bitar FF, Bitar H, Sabban M El, Nasser M, Yunis KA, Tawil A, Dbaibo GS. Modulation of ceramide content and lack of apoptosis in the chronically hypoxic neonatal rat heart. *Pediatr Res* F.F. Bitar, Department of Pediatrics, American University of Beirut, Beirut, Lebanon; 2002;51:144–149.
20. Ecarnot-Laubriet A, Rochette L, Vergely C, Sicard P, Teyssier J-R. The Activation Pattern of the Antioxidant Enzymes in the Right Ventricle of Rat in Response to Pressure Overload is of Heart Failure Type. *Hear Dis* L. Rochette, Faculties of Medicine and Pharmacy, 21079, Dijon, Cedex, France; 2003;5:308–312.
21. Farahmand F, Hill MF, Singal PK. Antioxidant and oxidative stress changes in experimental cor pulmonale. *Mol Cell Biochem* P.K. Singal, Institute of Cardiovascular Sciences, St. Boniface Gen. Hosp. Res. Centre, Winnipeg, Man. R2H 2A6, Canada; 2004;260:21–29.
22. Cisar CR, Balog JM, Anthony NB, Iqbal M, Bottje WG, Donoghue AM. Differential expression of mitochondrial electron transport chain proteins in cardiac tissues of broilers from pulmonary hypertension syndrome-resistant and -susceptible lines. *Poult Sci* J.M. Balog, Poultry Prod. Prod. Safety Res. U., Ctr. of Excellence for Poultry Sci., University of Arkansas, Fayetteville, AR 72701, United States; 2004;83:1420–1426.

23. Sharma S, Taegtmeyer H, Adrogue J, Razeghi P, Sen S, Ngumbela K, Essop MF. Dynamic changes of gene expression in hypoxia-induced right ventricular hypertrophy. *Am J Physiol - Hear Circ Physiol* H. Taegtmeyer, Dept. of Internal Medicine, Division of Cardiology, Univ. of Texas-Houston Med. School, Houston, TX 77030, United States; 2004;**286**:H1185–H1192.

24. Nouette-Gaulain K, Malgat M, Rocher C, Savineau J-P, Marthan R, Mazat J-P, Sztark F. Time course of differential mitochondrial energy metabolism adaptation to chronic hypoxia in right and left ventricles. *Cardiovasc Res* F. Sztark, Laboratoire d'Anesthésiologie, E.A. Physiologie Mitochondriale, Universite Bordeaux 2, 33076 Bordordeaux, France; 2005;**66**:132–140.

25. Adrogue J V, Sharma S, Ngumbela K, Essop MF, Taegtmeyer H. Acclimatization to chronic hypobaric hypoxia is associated with a differential transcriptional profile between the right and left ventricle. *Mol Cell Biochem* H. Taegtmeyer, Department of Internal Medicine, Division of Cardiology, University of Texas Houston - Medical School, Houston, TX 77030, United States; 2005;278:71–78.

26. Beek-Harmsen BJ Van, Laarse WJ Van Der. Immunohistochemical determination of cytosolic cytochrome c concentration in cardiomyocytes. *J Histochem Cytochem* W.J. Van Der Laarse, Department of Physiology, Institute for Cardiovascular Research, VU University Medical Center, 1081 BT Amsterdam, Netherlands; 2005;53:803–807.

27. Schott P, Singer SS, Kögler H, Neddermeier D, Leineweber K, Brodde O-E, Regitz-Zagrosek V, Schmidt B, Dihazi H, Hasenfuss G. Pressure overload and neurohumoral activation differentially affect the myocardial proteome. *Proteomics* P. Schott, Georg-August-Universitat Gottingen, Abt. fur Kardiologie und Pneumologie, D-37075 Göttingen, Germany; 2005;5:1372–1381.

28. Faber MJ, Dalinghaus M, Lankhuizen IM, Bezstarosti K, Dekkers DHW, Duncker DJ, Helbing WA, Lamers JMJ. Proteomic changes in the pressure overloaded right ventricle after 6 weeks in young rats: Correlations with the degree of hypertrophy. *Proteomics* J.M.J. Lamers, Department of Biochemistry, Cardiovascular Research School COEUR, Erasmus MC, 3000 DR Rotterdam, Netherlands; 2005;**5**:2519–2530.

29. Kluge R, Barthel H, Pankau H, Seese A, Schauer J, Wirtz H, Seyfarth H-J, Steinbach J, Sabri O, Winkler J. Different mechanisms for changes in glucose uptake of the right and left ventricular myocardium in pulmonary hypertension. *J Nucl Med* R. Kluge, Department of Nuclear Medicine, University of Leipzig, D-04103 Leipzig, Germany; 2005;46:25–31.

30. Oikawa M, Kagaya Y, Otani H, Sakuma M, Demachi J, Suzuki J, Takahashi T, Nawata J, Ido T, Watanabe J, Shirato K. Increased [18F]fluorodeoxyglucose accumulation in right ventricular free wall in patients with pulmonary hypertension and the effect of epoprostenol. *J Am Coll Cardiol* Y. Kagaya, Department of Cardiovascular Medicine, Tohoku University, Graduate School of Medicine, Aoba-ku, Sendai 980-8574, Japan; 2005;45:1849–1855.

31. Redout EM, Wagner MJ, Zuidwijk MJ, Boer C, Musters RJP, Hardeveld C van, Paulus WJ, Simonides WS. Right-ventricular failure is associated with increased mitochondrial complex II activity and production of reactive oxygen species. *Cardiovasc Res* 2007;75:770–781.

32. Faber MJ, Dalinghaus M, Lankhuizen IM, Bezstarosti K, Verhoeven AJM, Duncker DJ, Helbing WA, Lamers JMJ. Time dependent changes in cytoplasmic proteins of the right ventricle during prolonged pressure overload. *J Mol Cell Cardiol* M. Dalinghaus, Erasmus MC-Sophia, Department of Pediatrics, Division of Pediatric Cardiology, 3015 GJ Rotterdam, Netherlands; 2007;43:197–209.

33. Basu S, Alzeair S, Li G, Dadparvar S, Alavi A. Etiopathologies associated with intercostal muscle hypermetabolism and prominent right ventricle visualization on 2-deoxy-2[F-18] fluoro-D-glucose-positron emission tomography: significance of an incidental finding and in the setting of a known pulmonary d. *Mol Imaging Biol* S. Basu, Division of Nuclear Medicine, Hospital of University of Pennsylvania, 3400 Spruce Street, Philadelphia, Pennsylvania 19104, USA.; 2007;9:333–339.

34. Nagendran J, Gurtu V, Fu DZ, Dyck JRB, Haromy A, Ross DB, Rebeyka IM, Michelakis ED. A dynamic and chamber-specific mitochondrial remodeling in right ventricular hypertrophy can be therapeutically targeted. *J Thorac Cardiovasc Surg* E.D. Michelakis, Pulmonary Hypertension Program, Department of Medicine, University of Alberta, Edmonton, Alta., Canada; 2008;136:168-178.e3.

35. Broderick TL, King TM. Upregulation of GLUT-4 in right ventricle of rats with monocrotaline-induced pulmonary hypertension. *Med Sci Monit* T. L. Broderick, Department of Physiology, Midwestern University, Glendale, AZ 85308, United States; 2008;14:BR261–BR264.

36. Mouchaers KTB, Schalij I, Versteilen AMG, Hadi AM, Nieuw Amerongen GP Van, Hinsbergh VWM Van, Postmus PE, Laarse WJ Van Der, Vonk-Noordegraaf A. Endothelin receptor blockade combined with phosphodiesterase-5 inhibition increases right ventricular mitochondrial capacity in pulmonary arterial hypertension. *Am J Physiol - Hear Circ Physiol* A. Vonk-Noordegraaf, Department of Pulmonary Diseases, Institute for Cardiovascular Research, Vrije Universiteit University Medical Center, Amsterdam, Netherlands; 2009;**297**:H200–H207.

37. Sheikh AM, Barrett C, Villamizar N, Alzate O, Valente AM, Herlong JR, Craig D, Lodge A, Lawson J, Milano C, Jaggers J. Right ventricular hypertrophy with early dysfunction: A proteomics study in a neonatal model. *J Thorac Cardiovasc Surg* A.M. Sheikh, Department of Pediatric Cardiac Surgery, the Neuroproteomics Center, Durham, NC, United States; 2009;137:1146–1153.

38. Redout EM, Toorn A Van Der, Zuidwijk MJ, Kolk CWA Van De, Echteld CJA Van, Musters RJP, Hardeveld C Van, Paulus WJ, Simonides WS. Antioxidant treatment attenuates pulmonary arterial hypertension-induced heart failure. *Am J Physiol - Hear Circ Physiol* W. S. Simonides, Laboratory for Physiology, Institute for Cardiovascular Research, VU University Medical Center Amsterdam, Amsterdam 1081 BT, Netherlands; 2010;298:H1038–H1047.

39. Yen C-H, Leu S, Lin Y-C, Kao Y-H, Chang L-T, Chua S, Fu M, Wu C-J, Sun C-K, Yip H-K. Sildenafil limits monocrotaline-induced pulmonary hypertension in rats through suppression of pulmonary vascular remodeling. *J Cardiovasc Pharmacol* H.-K. Yip, Division of Cardiology, Department of Internal Medicine, Chang Gung Memorial Hospital, Niao Sung Hsiang, Kaohsiung Hsien 83301, Taiwan; 2010;55:574–584.

40. Piao L, Fang YH, Cadete VJJ, Wietholt C, Urboniene D, Toth PT, Marsboom G, Zhang HJ, Haber I, Rehman J, Lopaschuk GD, Archer SL. The inhibition of pyruvate dehydrogenase kinase improves impaired cardiac function and electrical remodeling in two models of right ventricular hypertrophy: Resuscitating the hibernating right ventricle. *J Mol Med* 2010;88:47–60.

41. Drake JI, Bogaard HJ, Mizuno S, Clifton B, Xie B, Gao Y, Dumur CI, Fawcett P, Voelkel NF, Natarajan R. Molecular signature of a right heart failure program in chronic severe pulmonary hypertension. *Am J Respir Cell Mol Bio*l 2011;45:1239–1247.

42. Saini-Chohan HK, Dakshinamurti S, Taylor WA, Shen GX, Murphy R, Sparagna GC, Hatch GM. Persistent pulmonary hypertension results in reduced tetralinoleoyl-cardiolipin and mitochondrial complex II + III during the development of right ventricular hypertrophy in the neonatal pig heart. *Am J Physiol - Hear Circ Physiol* G. M. Hatch, Departments of Pharmacology and Therapeutics, Faculty of Medicine, Univ. of Manitoba, Winnepeg, MB R3E OT6, Canada; 2011;301:H1415–H1424.

43. Baandrup JD, Markvardsen LH, Peters CD, Schou UK, Jensen JL, Magnusson NE, Ørntoft TF, Kruhøffer M, Simonsen U. Pressure load: The main factor for altered gene expression in right ventricular hypertrophy in chronic hypoxic rats. *PLoS One* U. Simonsen, Department of Pharmacology, Aarhus University, Aarhus, Denmark; 2011;6.

44. Bokhari S, Raina A, Rosenweig EB, Schulze PC, Bokhari J, Einstein AJ, Barst RJ, Johnson LL. PET imaging may provide a novel biomarker and understanding of right ventricular dysfunction in patients with idiopathic pulmonary arterial hypertension. *Circ Cardiovasc Imaging* S. Bokhari, Department of Medicine, Division of Cardiology, New York Presbyterian Hospital at Columbia University Medical Center, New York, NY 10032, United States; 2011;4:641–647.

45. Wong YY, Ruiter G, Lubberink M, Raijmakers PG, Knaapen P, Marcus JT, Boonstra A, Lammertsma AA, Westerhof N, Laarse WJ Van Der, Vonk-Noordegraaf A. Right ventricular failure in idiopathic pulmonary arterial hypertension is associated with inefficient myocardial oxygen utilization. *Circ Hear Fail* A. Vonk-Noordegraaf, Department of Pulmonology, Institute for Cardiovascular Research, VU University Medical Center, 1081 HV Amsterdam, Netherlands; 2011;4:700–706.

46. Wong YY, Westerhof N, Ruiter G, Lubberink M, Raijmakers P, Knaapen P, Marcus JT, Boonstra A, Lammertsma AA, Laarse WJ Van Der, Vonk-Noordegraaf A. Systolic pulmonary artery pressure and heart rate are main determinants of oxygen consumption in the right ventricular myocardium of patients with idiopathic pulmonary arterial hypertension. *Eur J Heart Fail* A. Vonk-Noordegraaf, Department of Pulmonology, VU University Medical Center, 1081 HV Amsterdam, Netherlands; 2011;13:1290–1295.

47. Qipshidze N, Tyagi N, Metreveli N, Lominadze D, Tyagi SC. Autophagy mechanism of right ventricular remodeling in murine model of pulmonary artery constriction. *Am J Physiol - Hear Circ Physiol* N. Qipshidze, Department of Physiology and Biophysics, School of Medicine, University of Louisville, Louisville, Kentucky, United States; 2012;302:H688–H696.

48. Mosele F, Tavares AM V, Colombo R, Caron-Lienert R, Araujo ASR, Ribeiro MF, Belló-Klein A. Effects of purple grape juice in the redox-sensitive modulation of right ventricular remodeling in a pulmonary arterial hypertension model. *J Cardiovasc Pharmacol* A. Belló-Klein, Programa de Pós-Graduação em Fisiologia, Instituto de Ciências Básicas da Saúde, Universidade Federal Do Rio Grande Do sul, Porto Alegre, Rio Grande do Sul, Brazil; 2012;60:15–22.

49. Khoo NKH, Cantu-Medellin N, Devlin JE, Croix CM St., Watkins SC, Fleming AM, Champion HC, Mason RP, Freeman BA, Kelley EE. Obesity-induced tissue free radical generation: An in vivo immuno-spin trapping study. *Free Radic Biol Med* E.E. Kelley, Departments of Anesthesiology and Pharmacology, School of Medicine, University of Pittsburgh, Pittsburgh, PA 15213, United States; 2012;52:2312–2319.

50. Fang Y-H, Piao L, Hong Z, Toth PT, Marsboom G, Bache-Wiig P, Rehman J, Archer SL. Therapeutic inhibition of fatty acid oxidation in right ventricular hypertrophy: Exploiting Randle's cycle. *J Mol Med* S.L. Archer, Medicine/Cardiology, University of Chicago, Chicago, IL 60637, United States; 2012;90:31–43.

51. Fang W, Zhao L, Xiong C-M, Ni X-H, He Z-X, He J-G, Wilkins MR. Comparison of 18F-FDG uptake by right ventricular myocardium in idiopathic pulmonary arterial hypertension and pulmonary arterial hypertension associated with congenital heart disease. *Pulm Circ* United States; 2012;2:365–372.

52. Wong YY, Raijmakers P, Campen J Van, Laarse WJ Van Der, Knaapen P, Lubberink M, Ruiter G, Noordegraaf A V, Lammertsma AA. 11C-acetate clearance as an index of oxygen consumption of the right myocardium in idiopathic pulmonary arterial hypertension: A validation study using 15O-labeled tracers and PET. *J Nucl Med* A.A. Lammertsma, Department of Nuclear Medicine and PET Research, VU University Medical Center, 1081 BT Amsterdam, Netherlands; 2013;54:1258–1262.

53. Sutendra G, Dromparis P, Paulin R, Zervopoulos S, Haromy A, Nagendran J, Michelakis ED. A metabolic remodeling in right ventricular hypertrophy is associated with decreased angiogenesis and a transition from a compensated to a decompensated state in pulmonary hypertension. *J Mol Med* E.D. Michelakis, Department of Medicine, University of Alberta, Edmonton, AB T6G 2B7, Canada; 2013;91:1315–1327.

54. Piao L, Fang Y-H, Parikh K, Ryan JJ, Toth PT, Archer SL. Cardiac glutaminolysis: A maladaptive cancer metabolism pathway in the right ventricle in pulmonary hypertension. *J Mol Med* S.L. Archer, Department of Medicine, Queen's University, Etherington Hall, Kingston, ON K7L 3N6, Canada; 2013;91:1185–1197.

55. Drake JI, Gomez-Arroyo J, Dumur CI, Kraskauskas D, Natarajan R, Bogaard HJ, Fawcett P, Voelkel NF. Chronic carvedilol treatment partially reverses the right ventricular failure transcriptional profile in experimental pulmonary hypertension. *Physiol Genomics* N. F. Voelkel, Richmond, VA 23298, United States; 2013;45:449–461.

56. Alzoubi A, Toba M, Abe K, O'Neill KD, Rocic P, Fagan KA, McMurtry IF, Oka M. Dehydroepiandrosterone restores right ventricular structure and function in rats with severe pulmonary arterial hypertension. *Am J Physiol - Hear Circ Physiol* M. Oka, Depts. of Medicine and Pharmacology, Center for Lung Biology, Univ. of South Alabama, 3158 MSB Mobile, AL 36688-0002, United States; 2013;304:H1708–H1718.

57. Piao L, Sidhu VK, Fang YH, Ryan JJ, Parikh KS, Hong Z, Toth PT, Morrow E, Kutty S, Lopaschuk GD, Archer SL. FOXO1-mediated upregulation of pyruvate dehydrogenase kinase-4 (PDK4) decreases glucose oxidation and impairs right ventricular function in pulmonary hypertension: therapeutic benefits of dichloroacetate. *J Mol Med* 2012;**29**:1–14.

58. Gomez-Arroyo J, Mizuno S, Szczepanek K, Tassell B Van, Natarajan R, Remedios CG Dos, Drake JI, Farkas L, Kraskauskas D, Wijesinghe DS, Chalfant CE, Bigbee J, Abbate A, Lesnefsky EJ, Bogaard HJ, Voelkel NF. Metabolic gene remodeling and mitochondrial dysfunction in failing right ventricular hypertrophy secondary to pulmonary arterial hypertension. *Circ Hear Fail* 2013;6:136–144.

59. Friehs I, Cowan DB, Choi Y-H, Black KM, Barnett R, Nido PJ Del, Levitsky S, McCully JD. Pressure-overload hypertrophy of the developing heart reveals activation of divergent gene and protein pathways in the left and right ventricular myocardium. *FASEB J* I. Friehs, Cardiothoracic Surgery, Boston Children's Hospital, Boston, United States; 2013;27.

60. Enache I, Charles A-L, Bouitbir J, Favret F, Zoll J, Metzger D, Oswald-Mammosser M, Geny B, Charloux A. Skeletal muscle mitochondrial dysfunction precedes right ventricular impairment in experimental pulmonary hypertension. *Mol Cell Biochem* I. Enache, Service de Physiologie et d'Explorations Fonctionnelles, Pôle de Pathologie Thoracique, Centre Hospitalier Universitaire Strasbourg, Nouvel Hôpital Civil, 67091 Strasbourg, France; 2013;373:161–170.

61. Kojonazarov B, Luitel H, Sydykov A, Dahal BK, Paul-Clark MJ, Bonvini S, Reed A, Schermuly RT, Mitchell JA. The peroxisome proliferator-activated receptor beta/delta agonist GW0742 has direct protective effects on right heart hypertrophy. *Pulm Circ* United States; 2013;**3**:926–935.

62. Yoshinaga K, Ohira H, Tsujino I, Oyama-Manabe N, Mielniczuk L, Beanlands RSB, Katoh C, Kasai K, Manabe O, Sato T, Fujii S, Ito YM, Tomiyama Y, Nishimura M, Tamaki N. Attenuated right ventricular energetics evaluated using 11C-acetate PET in patients with pulmonary hypertension. *Eur J Nucl Med Mol Imaging* K. Yoshinaga, Department of Molecular Imaging, Hokkaido University, Graduate School of Medicine, Kita-Ku 060-8638m Sapporo Hokkaido, Japan; 2014;41:1240–1250.

63. Wang L, Zhang Y, Yan C, He J, Xiong C, Zhao S, Fang W. Evaluation of right ventricular volume and ejection fraction by gated 18F-FDG PET in patients with pulmonary hypertension: Comparison with cardiac MRI and CT. *J Nucl Cardiol* W. Fang, Department of Nuclear Medicine, Cardiovascular Institute, Fu Wai Hospital, Beijing 100037, China; 2013;20:242–252.

64. Lundgrin EL, Park MM, Sharp J, Tang WHW, Thomas JD, Asosingh K, Comhair SA, DiFilippo FP, Neumann DR, Davis L, Graham BB, Tuder RM, Dostanic I, Erzurum SC. Fasting 2-deoxy-2-[18F]fluoro-D-glucose positron emission tomography to detect metabolic changes in pulmonary arterial hypertension hearts over 1 year. *Ann Am Thorac Soc* S.C. Erzurum, Respiratory Institute, Cleveland Clinic, Cleveland, OH 44195, United States; 2013;10:1–9.

65. Ikeda S, Satoh K, Kikuchi N, Miyata S, Suzuki K, Omura J, Shimizu T, Fukumoto Y, Sakata Y, Shimokawa H. Crucial role of rho-kinase in pressure-overload-induced right ventricular hypertrophy and dysfunction in mice. *J Card Fail* S. Ikeda, Department of Cardiovascular Medicine, Tohoku University, Graduate School of Medicine, Sendai, Japan; 2014;**20**:S144.

66. Hemnes AR, Brittain EL, Trammell AW, Fessel JP, Austin ED, Penner N, Maynard KB, Gleaves L, Talati M, Absi T, Disalvo T, West J. Evidence for right ventricular lipotoxicity in heritable pulmonary arterial hypertension. *Am J Respir Crit Care* Med 2014;189:325–334.

67. Rawat DK, Alzoubi A, Gupte R, Chettimada S, Watanabe M, Kahn AG, Okada T, McMurtry IF, Gupte SA. Increased reactive oxygen species, metabolic maladaptation, and autophagy contribute to pulmonary arterial hypertension-induced ventricular hypertrophy and diastolic heart failure. *Hypertension* S.A. Gupte, Department of Pharmacology, Center for Pulmonary Hypertension, BSB 546, New York Medical College, Valhalla, United States; 2014;64:1266–1274.

68. Liu B, Luo X-J, Yang Z-B, Zhang J-J, Li T-B, Zhang X-J, Ma Q-L, Zhang G-G, Hu C-P, Peng J. Inhibition of NOX/VPO1 pathway and inflammatory reaction by trimethoxystilbene in prevention of cardiovascular remodeling in hypoxia-induced pulmonary hypertensive rats. *J Cardiovasc Pharmacol* J. Peng, Department of Pharmacology, School of Pharmaceutical Sciences, Central South University, Changsha 410078, China; 2014;63:567–576.

69. Ahmed LA, Obaid AAZ, Zaki HF, Agha AM. Naringenin adds to the protective effect of l-arginine in monocrotaline-induced pulmonary hypertension in rats: Favorable modulation

of oxidative stress, inflammation and nitric oxide. *Eur J Pharm Sci* L.A. Ahmed, Department of Pharmacology and Toxicology, Faculty of Pharmacy, Cairo University, Egypt; 2014;**62**:161–170.

70. Frazziano G, Ghouleh I Al, Baust J, Shiva S, Champion HC, Pagano PJ. Nox-derived ROS are acutely activated in pressure overload pulmonary hypertension: Indications for a seminal role for mitochondrial Nox4. *Am J Physiol - Hear Circ Physiol* P. J. Pagano, Dept. of Pharmacology and Chemical Biology, Vascular Medicine Institute, Univ. of Pittsburgh School of Medicine, Thomas E. Starzl Biomedical Science Tower, Pittsburgh, PA 15261, United States; 2014;306:H197–H205.
71. Nergui S, Fukumoto Y, Do.e Z, Nakajima S, Shimizu T, Ikeda S, Elias-Al-Mamun M, Shimokawa H. Role of endothelial nitric oxide synthase and collagen metabolism in right ventricular remodeling due to pulmonary hypertension. *Circ J* Y. Fukumoto, Department of Cardiovascular Medicine, Tohoku University Graduate School of Medicine, Aoba-ku, Sendai 980-8574, Japan; 2014;78:1465–1474.
72. Ahmed LA, Obaid AA, Zaki HF, Agha AM. Role of oxidative stress, inflammation, nitric oxide and transforming growth factor-beta in the protective effect of diosgenin in monocrotaline-induced pulmonary hypertension in rats. *Eur J Pharmacol* 2014;740:379–387.
73. Zhang W-H, Qiu M-H, Wang X-J, Sun K, Zheng Y, Jing Z-C. Up-regulation of hexokinase1 in the right ventricle of monocrotaline induced pulmonary hypertension. *Respir Res* Y. Zheng, First Hospital of Jilin University, Center of Cardiovascular Disease, Changchun, China; 2014;15.
74. Tatebe S, Fukumoto Y, Oikawa-Wakayama M, Sugimura K, Satoh K, Miura Y, Aoki T, Nochioka K, Miura M, Yamamoto S, Tashiro M, Kagaya Y, Shimokawa H. Enhanced [18F] fluorodeoxyglucose accumulation in the right ventricular free wall predicts long-term prognosis of patients with pulmonary hypertension: a preliminary observational study. *Eur Heart J Cardiovasc Imaging* England; 2014;15:666–672.
75. Yang T, Wang L, Xiong C-M, He J-G, Zhang Y, Gu Q, Zhao Z-H, Ni X-H, Fang W, Liu Z-H. The ratio of 18F-FDG activity uptake between the right and left ventricle in patients with pulmonary hypertension correlates with the right ventricular function. *Clin Nucl Med* C.-M. Xiong, State Key Laboratory of Cardiovascular Disease, Fuwai Hospital, Chinese Academy of Medical Sciences, Xicheng Direct, Beijing, 100037, China; 2014;39:426–430.
76. Paulin R, Sutendra G, Gurtu V, Dromparis P, Haromy A, Provencher S, Bonnet S, Michelakis ED. A miR-208-Mef2 axis drives the decompensation of right ventricular function in pulmonary hypertension. *Circ Res* E.D. Michelakis, Department of Medicine, Cardiology, University of Alberta, Edmonton, Canada; 2015;116:56–69.
77. Moreira-Gonçalves D, Ferreira R, Fonseca H, Padrão AI, Moreno N, Silva AF, Vasques-Nóvoa F, Gonçalves N, Vieira S, Santos M, Amado F, Duarte JA, Leite-Moreira AF, Henriques-Coelho T. Cardioprotective effects of early and late aerobic exercise training in experimental pulmonary arterial hypertension. *Basic Res Cardio*l 2015;110:57.
78. Borgdorff MAJ, Koop AMC, Bloks VW, Dickinson MG, Steendijk P, Sillje HHW, Wiechen MPH van, Berger RMF, Bartelds B. Clinical symptoms of right ventricular failure in experimental chronic pressure load are associated with progressive diastolic dysfunction. *J Mol Cell Cardiol* Elsevier Ltd; 2015;79:244–253.
79. Balestra GM, Mik EG, Eerbeek O, Specht PAC, Laarse WJ van der, Zuurbier CJ. Increased in vivo mitochondrial oxygenation with right ventricular failure induced by pulmonary arterial hypertension: Mitochondrial inhibition as driver of cardiac failure? *Respir Res* C.J.

Zuurbier, Department of Anesthesiology, Laboratory of Experimental Intensive Care and Anesthesiology, AMC, Amsterdam, Netherlands; 2015;16.

80. Bruns DR, Dale Brown R, Stenmark KR, Buttrick PM, Walker LA. Mitochondrial integrity in a neonatal bovine model of right ventricular dysfunction. *Am J Physiol - Lung Cell Mol Physiol* L.A. Walker, Univ. of Colorado-Denver, Dept. of Medicine, Cardiology, Aurora, United States; 2015;308:L158–L167.
81. Kaur G, Singh N, Lingeshwar P, Siddiqui HH, Hanif K. Poly (ADP-ribose) polymerase-1: An emerging target in right ventricle dysfunction associated with pulmonary hypertension. *Pulm Pharmacol Ther* K. Hanif, Division of Pharmacology, CSIR-Central Drug Research Institute, Lucknow, India; 2015;30:66–79.
82. Aziz A, Lee AM, Ufere NN, Damiano RJ, Townsend RR, Moon MR. Proteomic Profiling of Early Chronic Pulmonary Hypertension: Evidence for Both Adaptive and Maladaptive Pathology. *J Pulm Respir Med* United States; 2015;5.
83. Graham BB, Kumar R, Mickael C, Sanders L, Gebreab L, Huber KM, Perez M, Smith-Jones P, Serkova NJ, Tuder RM. Severe pulmonary hypertension is associated with altered right ventricle metabolic substrate uptake. *Am J Physiol - Lung Cell Mol Physiol* B.B. Graham, Division of Pulmonary Sciences and Critical Care Medicine, Univ. of Colorado Denver, Aurora, United States; 2015;309:L435–L440.
84. Khan SS, Cuttica MJ, Beussink-Nelson L, Kozyleva A, Sanchez C, Mkrdichian H, Selvaraj S, Dematte JE, Lee DC, Shah SJ. Effects of ranolazine on exercise capacity, right ventricular indices, and hemodynamic characteristics in pulmonary arterial hypertension: a pilot study. *Pulm Circ* United States; 2015;5:547–556.
85. Sakao S, Miyauchi H, Voelkel NF, Sugiura T, Tanabe N, Kobayashi Y, Tatsumi K. Increased right ventricular fatty acid accumulation in chronic thromboembolic pulmonary hypertension. *Ann Am Thorac Soc* S. Sakao, Department of Respirology (B2), Graduate School of Medicine, Chiba University, Chuo-ku, Chiba, Japan; 2015;12:1465–1472.
86. Li W, Wang L, Xiong C-M, Yang T, Zhang Y, Gu Q, Yang Y, Ni X-H, Liu Z-H, Fang W, He J-G. The Prognostic Value of 18F-FDG Uptake Ratio Between the Right and Left Ventricles in Idiopathic Pulmonary Arterial Hypertension. *Clin Nucl Med* 2015;40:859–863.
87. Drozd K, Ahmadi A, Deng Y, Jiang B, Petryk J, Thorn S, Stewart D, Beanlands R, DeKemp RA, DaSilva JN, Mielniczuk LM. Effects of an endothelin receptor antagonist, Macitentan, on right ventricular substrate utilization and function in a Sugen 5416/hypoxia rat model of severe pulmonary arterial hypertension. *J Nucl Cardiol* L.M. Mielniczuk, Division of Cardiology, Department of Medicine, University of Ottawa Heart Institute, Ottawa, Canada; 2016;1–11.
88. Brittain EL, Talati M, Fessel JP, Zhu H, Penner N, Calcutt MW, West JD, Funke M, Lewis GD, Gerszten RE, Hamid R, Pugh ME, Austin ED, Newman JH, Hemnes AR. Fatty acid metabolic defects and right ventricular lipotoxicity in human pulmonary arterial hypertension. *Circulation* E.L. Brittain, Division of Cardiovascular Medicine, Vanderbilt University Medical School, Nashville, United States; 2016;133:1936–1944.
89. Talati MH, Brittain EL, Fessel JP, Penner N, Atkinson J, Funke M, Grueter C, Jerome WG, Freeman M, Newman JH, West J, Hemnes AR. Mechanisms of Lipid Accumulation in the Bone Morphogenetic Protein Receptor Type 2 Mutant Right Ventricle. *Am J Respir Crit Care Med* United States; 2016;194:719–728.

90. Joshi SR, Dhagia V, Gairhe S, Edwards JG, McMurtry IF, Gupte SA. Microrna-140 is elevated and mitofusin-1 is downregulated in the right ventricle of the sugen5416/hypoxia/normoxia model of pulmonary arterial hypertension. *Am J Physiol - Hear Circ Physiol* S.A. Gupte, Department of Pharmacology, New York Medical College, Valhalla, United States; 2016;311:H689–H698.

91. Peters EL, Offringa C, Kos D, Laarse WJ Van der, Jaspers RT. Regulation of myoglobin in hypertrophied rat cardiomyocytes in experimental pulmonary hypertension. *Pflugers Arch* Germany; 2016;468:1697–1707.

92. Sun X-Q, Zhang R, Zhang H-D, Yuan P, Wang X-J, Zhao Q-H, Wang L, Jiang R, Jan Bogaard H, Jing Z-C. Reversal of right ventricular remodeling by dichloroacetate is related to inhibition of mitochondria-dependent apoptosis. *Hypertens Res* Z.-C. Jing, State Key Laboratory of Cardiovascular Disease, Fu Wai Hospital, National Center for Cardiovascular Disease, Peking Union Medical College, Chinese Academy Medical Science, Beijing, China; 2016;39:302–311.

93. Bruggen CE Van Der, Happé CM, Dorfmüller P, Trip P, Spruijt OA, Rol N, Hoevenaars FP, Houweling AC, Girerd B, Marcus JT, Mercier O, Humbert M, Handoko ML, Velden J Van Der, Vonk Noordegraaf A, Bogaard HJ, Goumans M-J, Man FS De. Bone morphogenetic protein receptor type 2 mutation in pulmonary arterial hypertension: A view on the right ventricle. *Circulation* F.S. De Man, Department of Pulmonary Diseases, Institute for Cardiovascular Research, VU University Medical Center, Amsterdam, Netherlands; 2016;133:1747–1760.

94. Gupte AA, Cordero-Reyes AM, Youker KA, Matsunami RK, Engler DA, Li S, Loebe M, Ashrith G, Torre-Amione G, Hamilton DJ. Differential Mitochondrial Function in Remodeled Right and Nonremodeled Left Ventricles in Pulmonary Hypertension. *J Card Fail* D.J. Hamilton, Houston Methodist Hospital and Research Institute, Houston, United States; 2016;**22**:73–81.

95. Wang L, Li W, Yang Y, Wu W, Cai Q, Ma X, Xiong C, He J, Fang W. Quantitative assessment of right ventricular glucose metabolism in idiopathic pulmonary arterial hypertension patients: A longitudinal study. *Eur Heart J Cardiovasc Imaging* W. Fang, Department of Nuclear Medicine, Chinese Academy of Medical Sciences and Peking Union Medical College, FuWai Hospital, Beijing, China; 2016;17:1161–1168.

96. Sakao S, Daimon M, Voelkel NF, Miyauchi H, Jujo T, Sugiura T, Ishida K, Tanabe N, Kobayashi Y, Tatsumi K. Right ventricular sugars and fats in chronic thromboembolic pulmonary hypertension. *Int J Cardiol* S. Sakao, Department of Respirology (B2), Graduate School of Medicine, Chiba University, Chuo-ku, Chiba, Japan; 2016;219:143–149.

97. Ohira H, deKemp R, Pena E, Davies RA, Stewart DJ, Chandy G, Contreras-Dominguez V, Dennie C, Mc Ardle B, Mc Klein R, Renaud JM, DaSilva JN, Pugliese C, Dunne R, Beanlands R, Mielniczuk LM. Shifts in myocardial fatty acid and glucose metabolism in pulmonary arterial hypertension: a potential mechanism for a maladaptive right ventricular response. *Eur Heart J Cardiovasc Imaging* England; 2015;

98. Frille A, Steinhoff KG, Hesse S, Grachtrup S, Wald A, Wirtz H, Sabri O, Seyfarth H-J. Thoracic [18F]fluorodeoxyglucose uptake measured by positron emission tomography/computed tomography in pulmonary hypertension. *Med (United States)* A. Frille, Department of Respiratory Medicine, University of Leipzig, Leipzig, Germany; 2016;95.

99. Campos C, Luz de Castro A, Vicente Tavares AM, Fernandes RO, Ortiz VD, Barboza TE, Pereira C, Apel M, Santos da Silva O, Llesuy S, Sander da Rosa Araujo A, Belló-Klein A. Effect of free and nanoencapsulated copaiba oil on monocrotaline-induced pulmonary arterial

hypertension. *J Cardiovasc Pharmacol* C. Campos, aUniversidade Federal Do Rio Grande Do Sul, Porto Alegre - RS - Brasil, bCentro Universitário UniRitter, Porto Alegre - RS - Brasil, cTecnano, Porto Alegre - RS - Brasil, dUniversidad de Buenos Aires – Argentina.; 2016;

100. Liu A, Philip J, Vinnakota KC, Bergh F Van den, Tabima DM, Hacker T, Beard DA, Chesler NC. Estrogen maintains mitochondrial content and function in the right ventricle of rats with pulmonary hypertension. *Physiol Re*p 2017;5:1–12.
101. He J, Li X, Luo H, Li T, Zhao L, Qi Q, Liu Y, Yu Z. Galectin-3 mediates the pulmonary arterial hypertension–induced right ventricular remodeling through interacting with NADPH oxidase 4. *J Am Soc Hypertens* Elsevier Inc; 2017;11:275-289.e2.
102. Cowley PM, Wang G, Chang AN, Makwana O, Swigart PM, Lovett DH, Stull JT, Simpson PC, Baker AJ. The alpha1A-adrenergic receptor subtype mediates increased contraction of failing right ventricular myocardium. *Am J Physiol Heart Circ Physiol* United States; 2015;**309**:H888-96.
103. Tian L, Neuber-Hess M, Mewburn J, Dasgupta A, Dunham-Snary K, Wu D, Chen KH, Hong Z, Sharp WW, Kutty S, Archer SL. Ischemia-induced Drp1 and Fis1-mediated mitochondrial fission and right ventricular dysfunction in pulmonary hypertension. *J Mol Med* Journal of Molecular Medicine; 2017;95:381–393.
104. Nagy BM, Nagaraj C, Egemnazarov B, Kwapiszewska G, Stauber RE, Avian A, Olschewski H, Olschewski A. Lack of ABCG2 leads to biventricular dysfunction and remodeling in response to hypoxia. *Front Physiol* 2017;8:1–14.
105. Zhu TT, Zhang WF, Luo P, Qian ZX, Li F, Zhang Z, Hu CP. LOX-1 promotes right ventricular hypertrophy in hypoxia-exposed rats. *Life Sci* Elsevier Inc.; 2017;174:35–42.
106. Wang X, Shults N V., Suzuki YJ. Oxidative profiling of the failing right heart in rats with pulmonary hypertension. *PLoS One* 2017;12:e0176887.
107. Xu Y, Gu Q, Liu N, Yan Y, Yang X, Hao Y, Qu C. PPAR alleviates right ventricular failure secondary to pulmonary arterial hypertension in rats. *Int Heart J* 2017;58:948–956.
108. Santos Lacerda D dos, Türck P, Gazzi de Lima-Seolin B, Colombo R, Duarte Ortiz V, Poletto Bonetto JH, Campos-Carraro C, Bianchi SE, Belló-Klein A, Linck Bassani V, Sander da Rosa Araujo A. Pterostilbene reduces oxidative stress, prevents hypertrophy and preserves systolic function of right ventricle in cor pulmonale model. *Br J Pharmacol* 2017;174:3302–3314.
109. Puukila S, Fernandes RO, Türck P, Carraro CC, Bonetto JHP, Lima-Seolin BG de, Rosa Araujo AS da, Belló-Klein A, Boreham D, Khaper N. Secoisolariciresinol diglucoside attenuates cardiac hypertrophy and oxidative stress in monocrotaline-induced right heart dysfunction. *Mol Cell Biochem* Springer US; 2017;432:33–39.
110. Saygin D, Highland KB, Farha S, Park M, Sharp J, Roach EC, Tang WHW, Thomas JD, Erzurum SC, Neumann DR, DiFilippo FP. Metabolic and functional evaluation of the heart and lungs in pulmonary hypertension by gated 2-[18F]-Fluoro-2-deoxy-D-glucose positron emission tomography. *Pulm Cir*c 2017;7:428–438.
111. Siqueira R, Colombo R, Conzatti A, Luz de Castro A, Campos Carraro C, Tavares AMV, Gattelli Fernandes TR, Rosa Araujo AS da, Bello-Klein A. Effects of ovariectomy on antioxidant defence systems in the right ventricle of female rats with pulmonary arterial hypertension induced by monocrotoline. *Can J Physiol Pharmacol* 2018;96:295–303.

4

CHAPTER 4

Right ventricular pressure overload alters cardiac lipid composition

A.M.C. Koop, Q.A.J. Hagdorn, G.P.L. Bossers, T. van Leusden, A. Gerding, M. van Weeghel, F.M. Vaz, D.P.Y. Koonen, H.H.W. Silljé, R.M.F. Berger, B. Bartelds
- International Journal of Cardiology. 2019; 287:96-105.

ABSTRACT

Introduction

Right ventricular (RV) failure due to pressure load is an important determinant of clinical outcome in pulmonary hypertension, congenital heart disease and left ventricular failure. The last decades it has become clear that metabolic dysregulation is associated with the development of RV-failure. However, underlying mechanisms remain to be unraveled. Recently, disruption of intracardiac lipid content has been suggested as potential inducer of RV failure.

In the present study, we used a rat model of RV-dysfunction and aimed to obtain insight in temporal changes in RV-function, -remodelling and -metabolism and relate this to RV lipid content.

Methods and results

Male Wistar WU rats were subjected to pulmonary artery banding (n=25) or sham surgery (n=14) and cellular, hemodynamic and metabolic assessments took place after 2, 5 and 12 weeks. In this model RV dysfunction and remodelling occurred, including early upregulation of oxidative stress markers. After 12 weeks of pressure load, lipidomics revealed significant decreases of myocardial diglycerides and cardiolipins, driven by (poly-)unsaturated forms. The decrease of cardiolipins was driven by its most abundant form, tetralinoleoylcardiolipin. Mitochondrial capacity for fatty acid oxidation preserved, while the capacity for glucose oxidation increased.

Conclusion

RV dysfunction due to pressure load, is associated with decreased intracardiac unsaturated lipids, especially tetralinoleoylcardiolipin. This was accompanied with preserved mitochondrial capacity regarding fatty acids oxidation, with increased capacity for glucose oxidation, and early activation of oxidative stress. We suggest that early interventions should be directed towards preservation of lipid availability as possible mean in order to prevent RV failure.

INTRODUCTION

Right ventricular (RV) failure is a main determinant for mortality and morbidity in patients with pulmonary hypertension and in patients with congenital heart diseases.[1,2] RV failure due to progressive pressure load is characterized by diastolic dysfunction and uncoupling of the RV and pulmonary vasculature. The last decade, experimental studies have identified that RV dysfunction due to pressure load is associated with RV hypertrophy, fibrosis, and metabolic derangements.[4-6] Unfortunately, the increased knowledge of the cellular signature of RV dysfunction has not yet evolved into a RV specific therapy.[7] Also, the use of therapeutic strategies developed for left heart failure, e.g. ischemic heart diseases or hypertension, has not led to significant clinical improvements in patients with RV disease yet.[7-9]

Derangements of RV metabolism associated with RV dysfunction due to pressure load is a recognized feature in various experimental studies[4,10-18] and is confirmed in several studies in patients with pulmonary arterial hypertension (PAH)[5,19,20]. The RV under pressure has been shown to be vulnerable to changes in coronary perfusion pressure[1] and several experimental studies have described a state of so-called capillary rarefaction,[4,21,22] both of which may add to the metabolic derangements. The metabolic changes described involve suppression of genes involved in fatty acid metabolism[4,10,12-15,18,23,24], as well as deviation away from the glucose oxidation pathway[4,10,11,13,14,18,23]. More recently, studies are focusing on alterations in cardiac lipid content and it's potential harmful effect. Up to now only lipotoxicity has been recognized in the pressure loaded RV in a model of bone morphogenetic receptor type 2 (BMPR2)-mutation.[12] However, also myocardial shortage of lipids has been suggested to have negative reflections on cardiac remodelling and function.[25] Together these observations emphasizes the relevance of a deeper understanding of RV dysfunction induced by different types of disease and the therapeutic potential of lipid modulation therapies.

Hereby, it is necessary to expand our knowledge on early and temporal changes in RV metabolic derangements during disease progression and its relation with functional cardiac performance. This will help to understand whether metabolic modulation is a potential therapeutic candidate in RV pressure load as has been suggested in left heart failure.[26-30]

Here, we aimed to characterize the alterations in RV lipid content during chronic pressure load and to assess its correlation with RV-function, -remodelling and –metabolism over time.

METHODS

Animal experiments

Animal care and experiments were conducted according to the Dutch Animal Experimental Act and conform to the Guide for the Care and Use of Laboratory Animals published by the US National Institutes of Health (NIH Publication No. 85-23, revised 1996). The Animal Experiments Committee of the University of Groningen, in the Netherlands approved the experimental protocol (permit number: AVD1050020151342-2). Male Wistar WU rats (160-180 gram) were randomly subjected to pressure load by means of pulmonary artery banding (PAB, n=25) or sham surgery (control, n=13), and were checked daily for clinical signs of RV failure according to ABCDE criteria, as previously described.[31] Animals were terminated at 2 (n= 5 vs. 4), 5 (n= 11 vs. 4), and 12 weeks (n= 9 vs. 5) following surgery.

Hemodynamic measurements

Echocardiographic assessment of PAB-gradient, LV cardiac output (LV CO), stroke volume (SV) eccentricity index end diastolic (EI ED), eccentricity index end systolic (EI ES), and tricuspid annular plan systolic excursion (TAPSE) was performed at 2, 5 and 12 weeks according to previous described protocol.[31] Invasive pressure measurements performed by heart catheterization including end diastolic pressure (EDP), RV contractility (dP/dt_{max}), RV stifness (dP/dt_{min}) and cardiac power were performed before termination, whereafter blood and organs were taken out and preserved. For detailed description of hemodynamic measurements, see supplemental methods.

Histology

Ventricular remodelling was characterized by cardiomyocyte cross-sectional area (wheat germ agglutinin), fibrosis (Masson Trichrome) and capillary density (Lectin) in the RV free wall, as described previously.[4] Perivascular fibrosis greater than 200 μm was excluded for analysis of the section.

Gene expression

Gene expression of markers of cardiomyocyte stress, hypertrophy, fibrosis, metabolic regulators, substrate transporters, inflammation, oxidative stress, and cardiolipin synthesis and remodelling were assessed at mRNA level measured with standard qPCR as described in detail in the supplemental methods.

Mitochondrial measurements

Mitochondria were isolated from fresh RV tissue subjected to 12 weeks of pressure load by PAB, as dscribed in the supplemental methods. Mitochondrial respiration was measured by the oxygen consumption rate with either pyruvate and malate, or palmitoyl CoA and malate as substrate, in the presence of ADP in a stirred, 2-channel high-resolution respirometry (Oroboros, Innsbruck, Austra). The different states, including the ADP-driven state 3 (State 3) as well uncoupled state 3 (State 3u), representing mitochondrial conditions (ADP or respectively ATP-rich environment, and intact respectively absence of membrane gradient), were analysed as described in the supplemental methods. Oxygen consumption rate was corrected for protein content. Citrate synthase activity kit (Sigma Aldrich, USA) was used as a marker of mitochondrial density.

Assessment triglyceride level plasma

Triglyceride (TG) levels in plasma were measured by enzymatic methods using commercial kits according to the manufacturer's instruction (Roche Diagnostics, Mannheim, Germany).

Assessment of cardiac lipid content

Lipidomics as performed on snap frozen RV tissue subjected to 12 weeks of pressure load by PAB. Sample work up and semi-quantitive analysis of the lipodome was perfomed as previously described.[32,33]

Bioinformatics and statistical analysis

Quantative data (except the lipidomic data, see below) are expressed as mean±standard error of the mean (SEM). GraphPad Prism 5.04 was used for data analysis. Comparisons between control and PAB-groups were tested with unpaired Students t-test, whereas comparisons over time (2 versus 5 weeks, 5 versus 12 weeks and 2 versus 12 weeks) within groups (control or PAB) were tested with one-way ANOVA. Bonferroni post hoc correction was used for multiple testing. The p-value of <0.05 was considered as statistical significant. Control groups were pooled, since no differences were observed in time. With respect to the measurements of the mitochondrial respiration, control groups were presented individually. Bioinformatics and statistical analyses of the lipidomics data were performed as described before [32]. Totals for the major classes were defined as the summation of the relative abundance of all identified lipids within the same class normalized to the corresponding internal standard. Statistical analysis of the lipid classes were performed using the statistical programming language R (https://www.r-project.org/) together with the "MixOmics" package (https://doi.org/10.1371/journal.pcbi.1005752). A q-value of 0.01 was assumed to be significant. Partial least squares-discriminant analysis (PLS-DA) was used to assess the variable importance in the projection (VIP)-score of individual lipids. Lipids were assumed to be significant if $p < 0.05$, false discovery rate (FDR) < 0.1 and VIP > 1. Boxplots displays the full range (minimum, first quartile, median, third quartile, and maximum), including statistical outliers.

Assessment of inflammatory status and oxidative stress

RV gene expression of different inflammatory and oxidative stress markers were assessed at mRNA level by standard qPCR. Macrophage infiltatrion in the RV was assessed by cluster of differentiation 68 (CD68) staining, as decribed previously.[34] Advanced oxidation protein products (AOPP) (ab242295, Abcam, Cambridge, United Kingdom) and anti-oxidant capacity assay (ab65329, Abcam, Cambridge, United Kingdom) were performed in RV tissue to the manufacturer's instruction.

Plasma levels of growth differentiation factor 15 (GDF-15) were measured by ELISA (MGD150, R&D, USA). AOPP were assessed in plasma as well (ab242295, Abcam, Cambridge, United Kingdom).

RESULTS

RV pressure load induced RV dysfunction

PAB induced a pressure load of the RV that increased over time (**figure 1a**) and echocardiographic markers of relevant pressure load were present (**suppl. table 1**). In PAB-rats, TAPSE (**figure 1b**), RV dP/dt_{max} (**figure 1c**) and RV dP/dt_{min} (**figure 1d**) were reduced. RV end diastolic pressure (**figure 1e**) tended to increase at 2 weeks after PAB, but gradually decreased again over time. Cardiac index was maintained over 12 weeks in rats with PAB (**figure 1f**) and in line with that, these rats did not develop clinical signs of RV failure using the ABCDE-criteria.[8] Finally, RV workload (**suppl. table 1**) and power (**figure 1g**) increased significantly in the PAB-groups, without changes over time.

Pressure load induced RV remodelling

PAB induced hypertrophy after 2 weeks, expressed by RV weight normalized for tibia length (**figure 1h**). RV cardiomyocyte cross sectional area (**figure 1i,j**) and capillary myocyte ratio (**figure 1k**) increased in PAB-rats compared to control and over time (5 and 12 weeks, vs. 2 weeks after PAB). The capillary density, irrespectively of the number of cardiomyocytes, decreased at all time points compared to control (21, 20 and 23, vs. 31.05 vessels per square millimeter) (**figure 1j**). RV fibrosis increased significantly compared to control only after 5 weeks of PAB (**figure 1j,l**), whereas gene expression of the fibrotic markers collagen subunits 1A2 (COL1A2) and 3A1 (COL3A1) and transforming growth factor 1 (TGFβ1) and 2 (TGFβ2) were all increased already 2 weeks after PAB and gradually decreased at 5 and 12 weeks (**figure 1m**). Gene expression of both natriuretic pro-peptide A (NPPA), as marker of myocardial stress, and the ratio of myosin heavy chain isoforms and (**suppl. table 2**), as marker of the switch to fetal gene programme, were increased at all time points (**figure 1m**). Finally, gene expression of regulator of calcineurin 1 (RCAN1) involved in activation of hypertrophy was increased at 5 and 12 weeks (**figure 1m**).

12 weeks of RV pressure load induced a discrete shift towards carbohydrate metabolism

Next we assessed mitochondrial respiratory capacity and expression of metabolic regulatory and transporter genes. In rats with PAB, the mitochondrial respiratory capacity using palmitoyl CoA as substrate was not significantly decreased, in both State 3 (**suppl. figure 1a**) and State 3u (**figure 2a, first graph**). The respiratory capacity using pyruvate as substrate was unchanged for State 3 (**suppl. figure 1b**). However, State 3u, representing the maximal respiratory capacity, did increase after 12 weeks of PAB as compared with control (**figure 2a, second graph**).

Mitochondrial respiratory capacity in the pressure loaded right ventricle was preserved for fatty acid metabolism. However, at five and twelve weeks of pressure load a relative increase of mitochondrial respiratory capacity was found in favour of the use of carbohydrates over fatty acids.

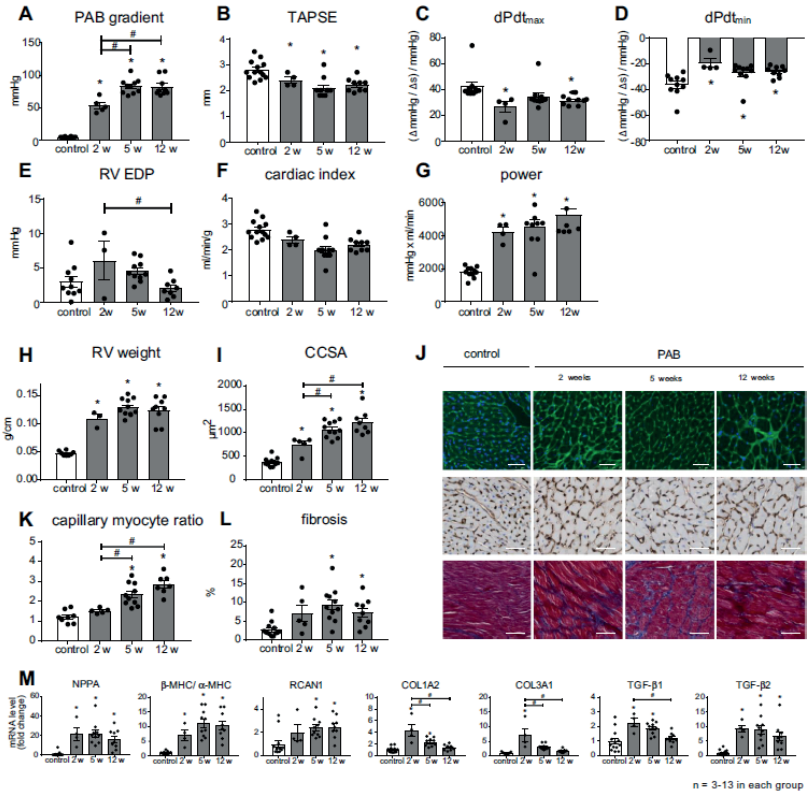

Figure 1. Hemodynamic and molecular changes over time in RV pressure load. PAB-gradient measured by Doppler echocardiography (A). Right ventricular systolic and diastolic function expressed by TAPSE (B) and dP/dt Max corrected for RVpeakpressure (C), and dP/dt Min corrected for RV peakpressure (D) and RV EDP (E). Cardiac index (cardiac output corrected for bodyweight) (F). Power (RV peakpressure multiplied by stroke volume) (G). RV weight correct for bodyweight (H), RV cross sectional area (I), RV capillary myocyte ratio (K) and RV fibrosis (L). Representative images of histological analyses: wheat germ agglutinin, lectin and masson-trichrome staining respectively (ruler is 50 μm) (J). mRNA expression of genes involved in cardiomyocyte stress, hypertrophy, fetal gene program, and fibrosis (M). Data presented as mean±SEM. * = $p < 0.05$ compared to control, # = $p < 0.05$ compared to indicated time point. ● = individual animal, white = control group, grey = pulmonary artery banding groups. PAB = pulmonary artery banding. 2w, 5w and 12w = 2, 5 and 12 weeks after PAB. TAPSE = tricuspid annular plane systolic excursion, dPdt = delta pressure delta time, EDP = end diastolic pressure. . CCSA = cross cardiomyocyte sectional area. NPPA = natriuretic propeptide type A, RCAN1 = regulator of calcineurin 1, MHC = myocyte heavy chain, COL1A2 = collagen subunit 1A2, COL3A1 = collagen subunit 3A1, TGF-β = transforming growth factor β.

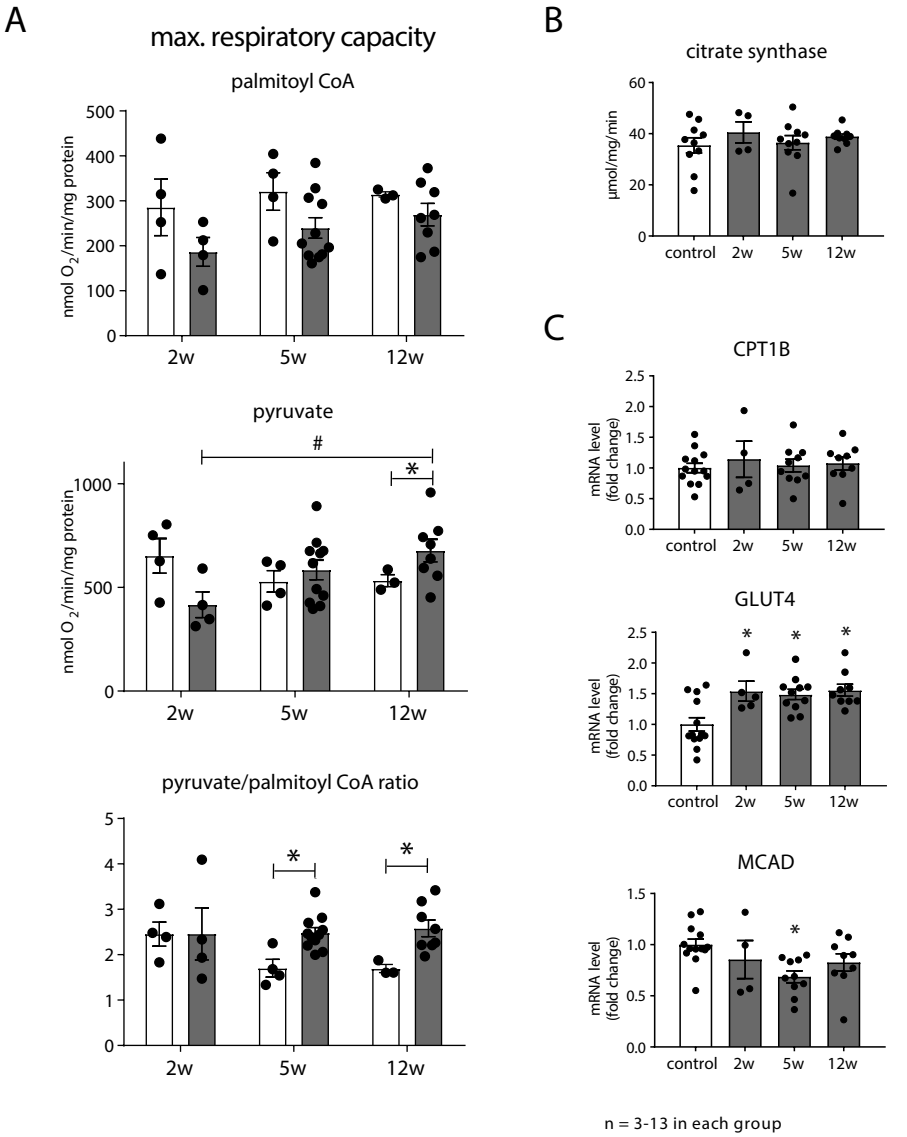

Figure 2. Right ventricular fatty acid and glucose metabolism during pressure load over time. Maximal mitochondrial respiratory capacity (state 3 uncoupled) measured by oxygen consumption rates in isolated mitochondria from RV tissue in the presence of palmitoyl coA or pyruvate, and the ratio of these two (A). Citrate synthase as marker of mitochondrial content (B). mRNA level of regulatory genes in metabolic transport and regulation (C). Data presented as mean ± SEM. * = $p < 0.05$ compared to control, # = $p < 0.05$ compared to indicated time point. = individual animal, white = control group, grey = pulmonary artery banding groups, 2w, 5w and 12 w = 2, 5, and 12 weeks. O2 = oxygen. MCAD = medium-chain acyl coA, PPAR = peroxisome proliferator-activated receptor a, PGC1 = PPAR gamma coactivator gene 1, CPT1B = carnitine palmitoyltarnsferase isoform 1B, GLUT4 = glucose transporter 4.

The ratio of both State 3 at 5 weeks (**suppl. figure 1c**), and State 3u at 5 and 12 weeks (**figure 2a, third graph**) shifted in favour of the use of carbohydrates over fatty acids. To test whether these changes correlated with changed mitochondrial content, citrate synthase was assessed, which was not different (**figure 2b**). The expression of carnitine palmitoyltransferase 1b (CPT1B), fatty acid transporter on the mitochondrial membrane, did not change in rats with PAB as compared with control, whereas expression of glucose transporter 4 (GLUT4) was increased at all time points (**figure 2c**). At this stage of disease, metabolic regulators peroxisome proliferator-activated receptor alpha (PPAR) and peroxisome proliferator-activated receptor gamma coactivator 1-alpha (PGC1) remained unchanged (**suppl. table 2**). Medium chain acyl CoA dehydrogenase (MCAD) mRNA levels decreased at 5 weeks (**figure 2c**).

RV pressure load induced changes in intra-cardiac lipid content

The RV lipid content was determined at the 12 weeks time point by semi-quantitative measurements of lipids such as TG, DG, Cer, cardiolipin (CL), phosphaphatidylcholine (PC), phosphatidylethanolamine (PE), phosphatidylinositol (PI), phosphatidylglycerol (PG) and phosphatidic acid (PA) (**suppl. table 3** and **4**). These were also assessed per major class (e.g. all TG), per cluster (e.g. TG within cluster 62) and as individual lipid species (e.g. TG(42:4), representing the *lipid (number of carbon atoms : number of double bonds)*). PAB induced several changes in RV lipid content (**figure 3**). In the major class analyses, RV content of DG, one of the non-phospholipids, was decreased 12 weeks after PAB as compared with RVs from control rats (**figure 3a**). TG and Cer showed a negative trend (**figure 3a**). Less uniform were the changes in lipid content for the phospholipids (**figure 3b**). RV cardiolipin content was decreased at 12 weeks after PAB compared to controls, whereas PC and PE were not decreased. RV content of precursor phospholipids PI, PG and PA did not show any differences between the PAB and control groups (**figure 3c**). Zooming in at the individual level, the heat map of significantly changed non-phospholipids showed a uniform decrease with exception of Cer(d34:0) and Cer(d36:0) (**figure 3d**). The heat map of individual cardiolipins showed lower levels of CL(72:8) and CL(72:9)(**figure 3e**). CL(72:8), tetralinoleoylcardiolipin, dominated the decrease of cardiolipins, whereas the sum of other, less abundant, cardiolipin species appeared to be increased (**figure 3f**). Within TG and DG species, PAB induced a shift from (poly-)unsaturated fatty acids (PUFA's) to more saturated fatty acids (see data supplement for additional boxplots and complete heat maps), e.g. TG 62 cluster and DG 42 (**figure 3g**). Plasma total TG levels were unchanged

Tetralinoleoylcardiolipin, an essential lipid in theinner mitochondrial membrane and essential for mitochondrial energy production, decreasesdin right ventricular pressure overload.

(control vs. PAB after 12 weeks: 1.7 vs. 1.6 mmol/L).

Since cardiolipin content was decreased, we further investigated enzymes of cardiolipin synthesis and remodelling at the mRNA level. Cytidinediphosphate-diacylglycerol synthase (CDS), an enzyme involved in cardiolipin synthesis did not change after PAB. Also, cardiolipin remodelling enzymes phospholipase A_2 (PLA_2) and tafazzin (TAZ) were unaffected at the mRNA level (**suppl. table 2**).

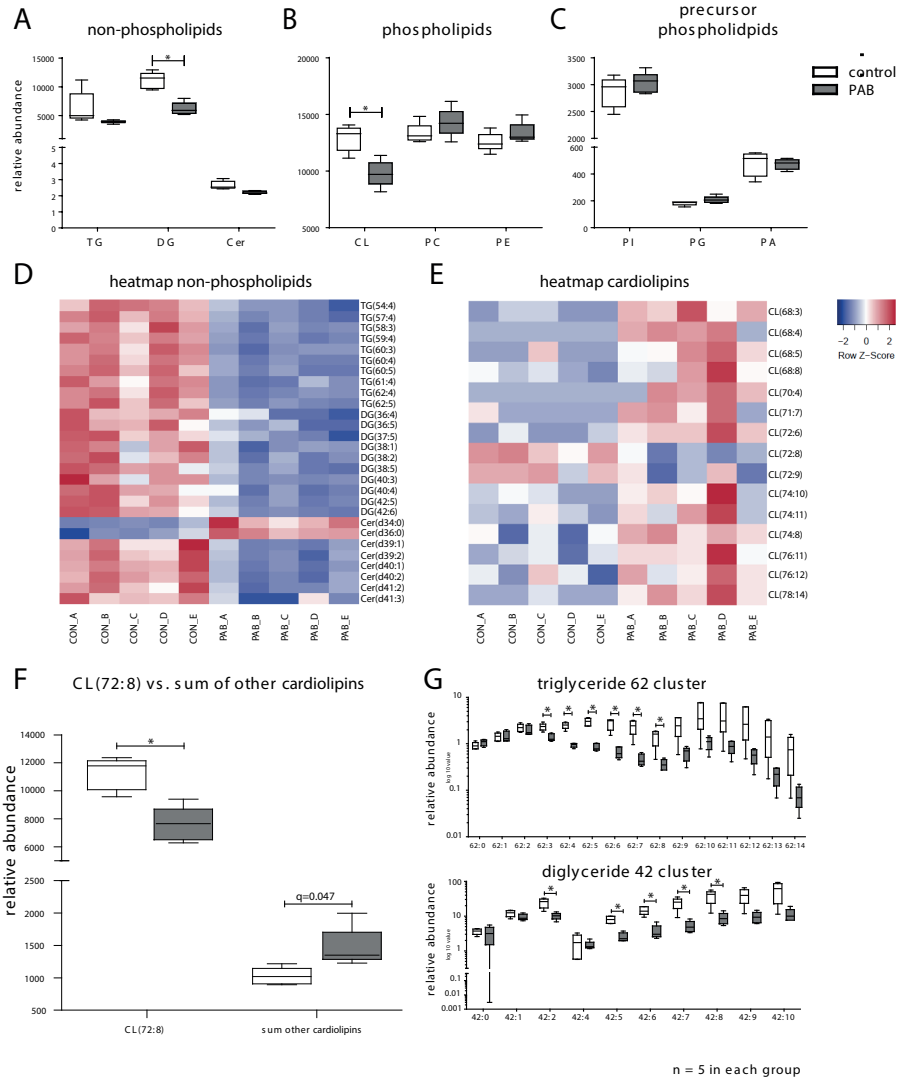

Figure 3. Right ventricular lipid content. Class totals of non-phosholipids (A), phospholipids (B), and precursor phospholipids (C). Heatmap of individual significantly changed non-phospholipids selected on top ten VIP-score within class (D). Heatmap of individual cardiolipins VIP > 1 (E). CL(72:8) versus sum of other cardiolipin (F). Representive examples of progressieve decrease of poly-unsaturated fatty acids within lipid clusters of TG and DG (G). TG = triglyceride, DG = diglyceride, Cer = ceramide, PC = phosphatidylcholine, PE = phosphatidylethanolamine, PI = phosphatidylinositol, PG = phosphatidylglycerol, PA = phosphatidic acid, CL = cardiolipin

RV pressure load effects on inflammation and oxidative stress

To assess the effects of pressure load on inflammation and oxidative stress in the RV, we analyzed recruitment of cytokines (interleukines) and macrophages (CD68), activation of oxidative stress (NAPDH oxidases), oxidation protein products and anti-oxidative markers in RV tissue. Cardiac gene expression of inflammatory markers CD68.

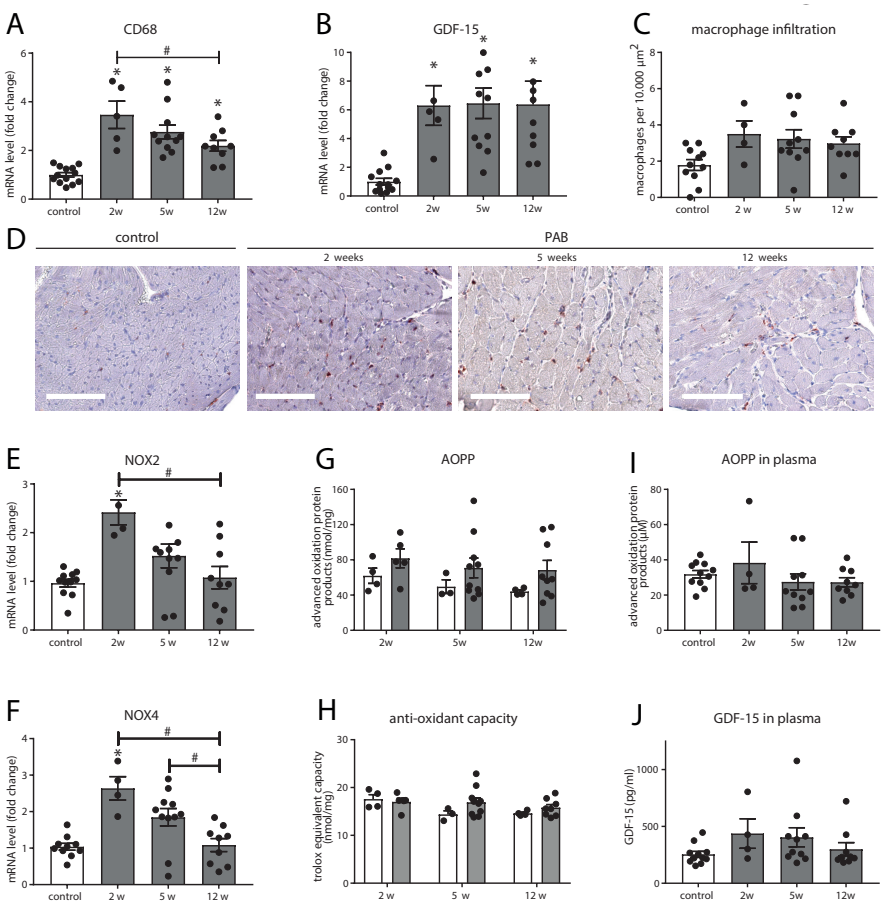

Figure 4. Inflammation and oxidative stress over time in RV pressure load. mRNA expression of macrophage marker CD68 (A), and GDF-15 (B) in RV tissue. Macrophage infiltration measured by CD68-staining (C), with representative images of histological analysis (ruler is 100 µm) (D). mRNA expression of NOX2 and NOX4 as activators of oxidative stress (E-F). AOPP as marker of actual oxidative stress (G) and anti-oxidant capacity assay (H) in RV tissue. Levels of AOPP and GDF-15 in blood-plasma (I-J). Data presented as mean±SEM. * = $p < 0.05$ compared to control, # = $p < 0.05$ compared to indicated time point. = individual animal, white = control group, grey = pulmonary artery banding groups. PAB = pulmonary artery banding. 2w, 5w and 12w = 2, 5 and 12 weeks after PAB. CD68 = cluster differation 68, GDF-15 = growth differation factor 15, NOX = NAPDH oxidase, AOPP = advanced oxidation protein products.

(**figure 4a**) and GDF-15 (**figure 4b**) increased after 2 weeks. IL-6 was increased at two weeks only, albeit with a large interindividual variation (**suppl. table 2**). Expression of other cytokines (IL-1 (with fold changes in control versus PAB of 1:0.94, 0.33:0.47 and 0.55:0.38 at two, five, and twelve weeks respectively) and IL-33 (**suppl. table 2**) did not change in response to pressure load. To assess whether the upregulated gene expression of CD68 resulted in increased macrophage infiltration, CD68 staining was performed. CD68 staining revealed positive trend of increased infiltration of macrophages in the pressure loaded RV at all time points, yet the increase was not statistically significant (**figure 4c,d**). RV pressue load did induce a transient increase in cardiac expression of NADPH oxidases 2 and 4 (**figure 4e,f resp.**), both of which are known to induce oxidative stress. Actual measurement of oxidative stress, by using advanced oxidation protein products (AOPP) assay, showed a positieve trend at all time points compared to controls, however, statistical significance was not met (**figure 4g**). No decreases in anti-oxidative capacity were observed, possibly due to the relatively low levels of oxidative stress (**figure 4h**). Expression of superoxide dismutase was unaffected (**suppl. table 2**).

Levels of AOPP and GDF-15 in blood plasma, showed no differences when compared to controls at all time points (**figure 4i,j resp.**).

DISCUSSION

With this study in chronic experimental RV pressure load, we aimed to characterize the alterations in RV lipid content during chronic pressure load and to assess its correlation with RV-function, -remodelling and -metabolism over time. The main finding of this study is that chronic pressure load of the RV induces a decrease of myocardial lipid content, that is associated with the development of RV dysfunction. The decrease of intracardiac lipids was mostly expressed in the lipid major classes diglycerides and cardiolipins, driven by (poly)unsaturated forms. This included tetralinoleoyl-cardiolipin, the most abundant form of cardiolipin. The decrease in fatty acids was not accompanied by an impairment of mitochondrial fatty acid oxidation, whereas the mitochondrial respiratory capacity for glucose oxidation increased. RV pressure overload induced early expression of inflammatory and oxidative stress markers, that gradually faded again in the following weeks. This pattern corresponds to the pattern of the expression of pro-fibrotic genes, that preceded the occurrence of fibrosis in the RV.

Decrease of cardiolipin levels, predominantly tetralinoleoyl-cardiolipin, has been described in different forms of heart failure, including pediatric heart failure.[35-39] Cardiolipin in the tetralinoleoyl-form (noted as CL18:2_4, L_4 or more generally CL(72:8)) is the most abundant cardiolipin in the mitochondrial membrane of most tissues and

is essential for optimal mitochondrial energy production.[39-41] Defects in cardiolipin content affect complexes I, II, III and IV of the electron transport chain,[42-46] leading to reduced oxidative capacity and increased production of reactive oxygen species.[45-48] Nevertheless, we did not find evidence of impaired mitochondrial function and one may speculate that the reductions in RV cardiolipin content precede a decrease in respiratory capacity due to a dysfunctional mitochondrial inner membrane leading to progressive oxidative stress.

In addition to a decreased cardiolipin content, the reduction of (P)UFA's also affected other lipid major classes. Since in this study mitochondria were not affected in number and their respiratory capacity for fatty acids, these reductions may be caused by oxidative stress or by reduced levels of common precursor lipids due to decreased uptake of long-chain fatty acids (LCFA). PUFA's are known to be vulnerable to oxidative stress because of their hydrogen atoms close to multiple double bounds, which are easily taken by hydroxyl radicals. The current study did show initial increases of inducers of oxidative stress, which faded over time. The pattern was also recognized at the level of actual oxidative stress and inflammation, however, these results did not reach statistical significance. We speculate that PUFA's serve as primary preventive response and enables preservation of anti-oxidant capacity in the pressure overloaded RV. Another explanation may be inadequate uptake of essential lipids in the stressed RV. Diminished levels of CD36, a prominent LCFA transport protein in contracting cardiomyocytes,[49] have previously been observed in LV hyperthrophy and heart failure.[50] In addition, in the LV, adequate lipid turnover mediated by TG-pools has been shown to protect the heart against ceramides, known as inducer of mitochondrial dysfunction and apoptosis, making sufficient lipid availability even more relevant. All this toghether suggests that limited availability of PUFA's, including cardiolipin, precedes deterioration of RV hemeostasis and function.

In the LV, upregulation of NADPH oxidase is known to induce fibrosis by the expression of TGFβ1,[51,52] which is accompanied with diastolic dysfunction.[51] A similar pattern is observed in the current model of RV pressure overload. NADPH oxidase is recognized as activator of oxidative stress.[53,54] In the current study we show upregulation of NAPDH oxidase 2 and 4, without significant upregulation of actual oxidative stress. Although this might be due to lack of sufficient statistical power, this might also imply that in the state of compensated RV dysfunction, activation of oxidative stress is mild and might be balanced by protective mechanisms other than anti-oxidants and proteins. How exactly upregulation of NADPH oxidase is triggered, is yet still unknown. In the diabetic mice heart, growing evidence suggest that NADPH oxidase is stimulated by hyperglyceamia,[55,56] whereas in hypertensive rats NADPH oxidase seems to be indirectly stimulated by systemic and local effects of angiotensin II.[52,57] In pressure overload ventricles, both left[57,58] and right, the exact

mechanism still needs to be unraveled. In this respect, it is of specific interest that the current study shows early upregulation of GLUT4, which might contribute to higher levels of glucose in cardiomyocytes. In diabetic disease, hyperglyceamia leads to fibrosis by inflammation.[59] These observations suggest that similar mechansims, including oxidative stress, inflammation and pro-fibrotic activity, may be involved in the early adaptation of the RV to increased pressure load and preceding RV failure. Further research should clarify the initial cause of NADPH oxidase activation in the pressure loaded RV.

Levels of oxidative stress and inflammation, measured by AOPP assay and GDF-15 ELISA, appeared to be not increased in blood plasma. This is in line with the relatively low activation of oxidative stress and inflammation in RV tissue, but also with the fact plasma pools are rarely influenced by dynamic changes in cardiac expression only.[60] Furthermore, blood derived biomarkers, other than cardiac specific markers, predominantly reflect systemic offects of heart failure,[60] while the animals in the current study developed RV dysfunction, but no clinical overt heart failure.

Our findings are opposed to those in experimental PH due to BMPR2-deficiency, where intracardiac accumulation of fatty acid intermediaries has been associated to progressive RV dysfunction.[12] The results of the present study suggest a difference between chronic pressure load in the presence or absence of PH, or more specificly involvement of the BMPR2-mutation. The ambivalent character of these findings are in line with different changes in metabolic capacity reported in the different models of RV pressure load,[13,61-64] and need to be considered in developing therapeutic strategies in RV dysfunction due to different types of disease. The present study suggests that therapies aiming at maintenance of mitochondrial integrity via restoration of cardiolipin content may be more appropriate than targeting fatty acid oxidation itself. Recent studies showed that preservation of cardiolipin by diet or therapeutics led to preservation of normal mitochondrial function and preservation of left venticular function. Dietary measures, such as high-linoleate safflower oil, were able to preserve tetralinoleoylcardiolipin content and mitochondrial function, and improved left ventricular function in spontaneously hypertensive heart failure rats.[65,66] Resveratrol is known to improve fatty acid oxidation, to reduce ROS production, to be cardiac protective and to improve survival in experimental models of diabetic cardiomyopathy, myocardial infarction induced tachycardia, exercise training and high-fat diet induced cardiac myopathy,[67-70] and has been described as therapeutic option for up regulation of cardiolipin content.[71] In Barth syndrome, a cardiomyopathy due to disruption of the TAZ gene leading to reduced mature cardiolipin levels, substitution of cardiolipin itself via nanoparticles is currently being tested as a new therapeutic strategy. Preservation of substrates availability is a potential candidate for prevention or early interception in the development of RV dysfunction, whereas

therapeutics inhibiting oxidative stress and stimulating antioxidants are likely to be more relevant in established heart failure than in early adaptation.

In the current study we did not test the effect of metabolic modulation, used in previous studies in RV-failure. This study aimed at identification of changes in metabolic regulation over time, early in the process of RV adaptation towards RV dysfunction, preceding clinically overt RV failure. The results of this comprehensive study do challenge the widely assumed concept that altered metabolism in RV failure represents "an engine out of fuel". Rather we speculate that early activation of oxidative stress affects intracardiac lipid content and thereby might contribute to acceleration of oxidative stress in the progression towards RV failure. Indeed, now we have identified early lipid alteration, including cardiolipins, in the development towards RV failure, the mechanism by which increased pressure load leads to this metabolic changes warrants further exploration. The results of this study reveal that both functional (**figure 1**) and histopathological (**figure 2**) changes of the pressure loaded RV precede significant changes in oxidative capacity (**figure 3**). Furthermore, there are no indications that the decrease of specific lipids was preceded by increased fatty acid metabolism. In addition, the initial increase in markers of oxidative stress preceded progressive functional deterioration. Based upon these findings we suggest to design intervention strategies based upon restoration of intracardiac fatty acid pool. To derive insights in metabolic changes, we studied several components of metabolism. By adding functional measurements of mitochondrial respiratory capacity using Oroboros, we attempted to create a better picture of the metabolic capacity in the pressure loaded RV. These data showed that the immediate increase in cardiac power (**figure 1g**), was associated with a slow increase in metabolic capacity of carbohydrates only. Combing these results with the altered lipid profile, indicates a role for preserving intracardiac lipid status in the initial response to pressure overload, rather than a change in fatty acid metabolic capacity itself.

CONCLUSION

In this study we showed that RV dysfunction, preceding RV failure due to chronic pressure load, is associated with decreased intracardiac unsaturated lipids, especially in the most abundant form of cardiolipin. These changes were accompanied by preserved mitochondrial capacity for fatty acid oxidation, with an increased mitochondrial capacity for glucose oxidation, and early expression of oxidative stress markers. We suggest that early interventions to prevent RV failure may be directed towards preservation of intracardiac lipid composition.

ACKNOWLEDGEMENTS

The authors thank Michel Weij and Annemieke van Oosten for performing pulmonary artery bandings, and, together with Bianca Schepers-Meijeringh, their assistance in the central animal facility. We would also like to thank Niels Kloosterhuis and Daphne Dekker for their excellent technical assistance. Lipidomics was performed by the AMC Core Facility Metabolomics, specifically by Martin Vervaart (Lab GMD), Angela Luyf (Bioinformatics Laboratory) and Mia Pras-Raves (Lab GMD).

REFERENCES

1. Wolferen SA Van, Marcus JT, Boonstra A, Marques KMJ, Bronzwaer JGF, Spreeuwenberg MD, Postmus PE, Vonk-Noordegraaf A. Prognostic value of right ventricular mass, volume, and function in idiopathic pulmonary arterial hypertension. *Eur Heart J* 2007;28:1250–1257.
2. Norozi K, Wessel A, Alpers V, Arnhold JO, Geyer S, Zoege M, Buchhorn R. Incidence and Risk Distribution of Heart Failure in Adolescents and Adults With Congenital Heart Disease After Cardiac Surgery. *Am J Cardiol* 2006;97:1238–1243.
3. Vonk Noordegraaf A, Westerhof BE, Westerhof N. The Relationship Between the Right Ventricle and its Load in Pulmonary Hypertension. *J Am Coll Cardiol* 2017;**69**:236–243.
4. Borgdorff MAJ, Koop AMC, Bloks VW, Dickinson MG, Steendijk P, Sillje HHW, Wiechen MPH van, Berger RMF, Bartelds B. Clinical symptoms of right ventricular failure in experimental chronic pressure load are associated with progressive diastolic dysfunction. *J Mol Cell Cardiol* Elsevier Ltd; 2015;79:244–253.
5. Ryan JJ, Archer SL. The right ventricle in pulmonary arterial hypertension: Disorders of metabolism, angiogenesis and adrenergic signaling in right ventricular failure. *Circ Res* S.L. Archer, Department of Medicine, Queen's University, Kingston, ON K7L 3N6, Canada; 2014;115:176–188.
6. Borgdorff MAJ, Dickinson MG, Berger RMF, Bartelds B. Right ventricular failure due to chronic pressure load: What have we learned in animal models since the NIH working group statement? *Heart Fail Rev* M.A.J. Borgdorff, Department of Pediatric Cardiology, Center for Congenital Heart Diseases, Beatrix Children's Hospital, University Medical Center Groningen, Groningen, Netherlands; 2015;20:475–491.
7. Roche SL, Redington AN. Right ventricle: Wrong targets? Another blow for pharmacotherapy in congenital heart diseases. *Circulatio*n 2013;127:314–316.
8. Borgdorff MA, Bartelds B, Dickinson MG, Steendijk P, Berger RMF. A cornerstone of heart failure treatment is not effective in experimental right ventricular failure. *Int J Cardiol* Elsevier Ireland Ltd; 2013;169:183–189.
9. Bom T Van Der, Winter MM, Bouma BJ, Groenink M, Vliegen HW, Pieper PG, Dijk APJ Van, Sieswerda GT, Roos-Hesselink JW, Zwinderman AH, Mulder BJM. Effect of valsartan on systemic right ventricular function: A double-blind, randomized, placebo-controlled pilot trial. *Circulation* 2013;127:322–330.
10. Piao L, Fang YH, Cadete VJJ, Wietholt C, Urboniene D, Toth PT, Marsboom G, Zhang HJ, Haber I, Rehman J, Lopaschuk GD, Archer SL. The inhibition of pyruvate dehydrogenase kinase improves impaired cardiac function and electrical remodeling in two models of right ventricular hypertrophy: Resuscitating the hibernating right ventricle. *J Mol Med* 2010;88:47–60.
11. Piao L, Fang Y-H, Parikh K, Ryan JJ, Toth PT, Archer SL. Cardiac glutaminolysis: A maladaptive cancer metabolism pathway in the right ventricle in pulmonary hypertension. *J Mol Med* S.L. Archer, Department of Medicine, Queen's University, Etherington Hall, Kingston, ON K7L 3N6, Canada; 2013;91:1185–1197.
12. Talati MH, Brittain EL, Fessel JP, Penner N, Atkinson J, Funke M, Grueter C, Jerome WG, Freeman M, Newman JH, West J, Hemnes AR. Mechanisms of Lipid Accumulation in the Bone Morphogenetic Protein Receptor Type 2 Mutant Right Ventricle. *Am J Respir Crit Care Med* United States; 2016;194:719–728.

13. Liu A, Philip J, Vinnakota KC, Bergh F Van den, Tabima DM, Hacker T, Beard DA, Chesler NC. Estrogen maintains mitochondrial content and function in the right ventricle of rats with pulmonary hypertension. *Physiol Rep* 2017;5:1–12.

14. Redout EM, Wagner MJ, Zuidwijk MJ, Boer C, Musters RJP, Hardeveld C van, Paulus WJ, Simonides WS. Right-ventricular failure is associated with increased mitochondrial complex II activity and production of reactive oxygen species. *Cardiovasc Res* W.S. Simonides, Laboratory for Physiology, Institute for Cardiovascular Research, VU University Medical Center, Amsterdam, Netherlands; 2007;75:770–781.

15. Faber MJ, Dalinghaus M, Lankhuizen IM, Bezstarosti K, Dekkers DHW, Duncker DJ, Helbing WA, Lamers JMJ. Proteomic changes in the pressure overloaded right ventricle after 6 weeks in young rats: Correlations with the degree of hypertrophy. *Proteomics* J.M.J. Lamers, Department of Biochemistry, Cardiovascular Research School COEUR, Erasmus MC, 3000 DR Rotterdam, Netherlands; 2005;5:2519–2530.

16. Sutendra G, Dromparis P, Paulin R, Zervopoulos S, Haromy A, Nagendran J, Michelakis ED. A metabolic remodeling in right ventricular hypertrophy is associated with decreased angiogenesis and a transition from a compensated to a decompensated state in pulmonary hypertension. *J Mol Med* E.D. Michelakis, Department of Medicine, University of Alberta, Edmonton, AB T6G 2B7, Canada; 2013;91:1315–1327.

17. Nagendran J, Gurtu V, Fu DZ, Dyck JRB, Haromy A, Ross DB, Rebeyka IM, Michelakis ED. A dynamic and chamber-specific mitochondrial remodeling in right ventricular hypertrophy can be therapeutically targeted. *J Thorac Cardiovasc Surg* E.D. Michelakis, Pulmonary Hypertension Program, Department of Medicine, University of Alberta, Edmonton, Alta., Canada; 2008;136:168-178.e3.

18. Gomez-Arroyo J, Mizuno S, Szczepanek K, Tassell B Van, Natarajan R, Remedios CG Dos, Drake JI, Farkas L, Kraskauskas D, Wijesinghe DS, Chalfant CE, Bigbee J, Abbate A, Lesnefsky EJ, Bogaard HJ, Voelkel NF. Metabolic gene remodeling and mitochondrial dysfunction in failing right ventricular hypertrophy secondary to pulmonary arterial hypertension. *Circ Hear Fail* 2013;6:136–144.

19. Hemnes AR, Brittain EL, Trammell AW, Fessel JP, Austin ED, Penner N, Maynard KB, Gleaves L, Talati M, Absi T, Disalvo T, West J. Evidence for right ventricular lipotoxicity in heritable pulmonary arterial hypertension. *Am J Respir Crit Care Me*d 2014;189:325–334.

20. Bruggen CE van der, Happé CM, Dorfmüller P, Trip P, Spruijt OA, Rol N, Hoevenaars FP, Houweling AC, Girerd B, Marcus JT, Mercier O, Humbert M, Handoko ML, Velden J van der, Vonk Noordegraaf A, Bogaard HJ, Goumans M-J, Man FS de. Bone Morphogenetic Protein Receptor Type 2 Mutation in Pulmonary Arterial HypertensionCLINICAL PERSPECTIVE. *Circulation* 2016;133:1747–1760.

21. Veerdonk MC van de, Bogaard HJ, Voelkel NF. The right ventricle and pulmonary hypertension. *Heart Fail Rev* 2016;

22. Albada ME van, Berger RMF, Niggebrugge M, Veghel R van, Cromme-Dijkhuis AH, Schoemaker RG. Prostacyclin therapy increases right ventricular capillarisation in a model for flow-associated pulmonary hypertension. *Eur J Pharmacol* M.E. van Albada, Department of Pediatrics, Division of Pediatric Cardiology, Beatrix Children's Hospital, Groningen, Netherlands; 2006;549:107–116.

23. Gupte AA, Cordero-Reyes AM, Youker KA, Matsunami RK, Engler DA, Li S, Loebe M, Ashrith G, Torre-Amione G, Hamilton DJ. Differential Mitochondrial Function in Remodeled Right and Nonremodeled Left Ventricles in Pulmonary Hypertension. *J Card Fail* D.J. Hamilton, Houston Methodist Hospital and Research Institute, Houston, United States; 2016;22:73–81.

24. Buermans HPJ, Redout EM, Schiel AE, Musters RJP, Zuidwijk M, Eijk PP, Hardeveld C Van, Kasanmoentalib S, Visser FC, Ylstra B, Simonides WS. Microarray analysis reveals pivotal divergent mRNA expression profiles early in the development of either compensated ventricular hypertrophy or heart failure. *Physiol Genomics* W.S. Simonides, Laboratory for Physiology, Institute for Cardiovascular Research (ICaR-VU), VU Univ. Medical Center, 1081 BT Amsterdam, Netherlands; 2005;21:314–323.

25. Nagaya N, Goto Y, Satoh T, Uematsu M, Hamada S, Kuribayashi S, Okano Y, Kyotani S, Shimotsu Y, Fukuchi K, Nakanishi N, Takamiya M, Ishida Y. Impaired regional fatty acid uptake and systolic dysfunction in hypertrophied right ventricle. *J Nucl Med* Y. Goto, Division of Cardiology, Department of Medicine, National Cardiovascular Center, Suita, Osaka 565, Japan; 1998;39:1676–1680.

26. Jaswal JS, Keung W, Wang W, Ussher JR, Lopaschuk GD. Targeting fatty acid and carbohydrate oxidation - A novel therapeutic intervention in the ischemic and failing heart. *Biochim Biophys Acta - Mol Cell Res* Elsevier B.V.; 2011;1813:1333–1350.

27. Fillmore N, Lopaschuk GD. Targeting mitochondrial oxidative metabolism as an approach to treat heart failure. *Biochim Biophys Acta - Mol Cell Res* Elsevier B.V.; 2013;1833:857–865.

28. Ashrafian H, Neubauer S. Metabolic modulation in heart failure: High time for a definitive clinical trial. *Heart* 2011;97:267–268.

29. Lee L, Campbell R, Scheuermann-Freestone M, Taylor R, Gunaruwan P, Williams L, Ashrafian H, Horowitz J, Fraser AG, Clarke K, Frenneaux M. Metabolic modulation with perhexiline in chronic heart failure: A randomized, controlled trial of short-term use of a novel treatment. *Circulation* 2005;112:3280–3288.

30. Revenco D, Morgan JP. Metabolic modulation and cellular therapy of cardiac dysfunction and failure. *J Cell Mol Med* 2009;13:811–825.

31. Borgdorff MA, Koop AM, Bloks VW, Dickinson MG, Steendijk P, Sillje HH, Wiechen MP van, Berger RM, Bartelds B. Clinical symptoms of right ventricular failure in experimental chronic pressure load are associated with progressive diastolic dysfunction. *J Mol Cell Cardiol* 2015;79:244–253.

32. Herzog K, Pras-Raves ML, Vervaart MAT, Luyf ACM, Kampen AHC van, Wanders RJA, Waterham HR, Vaz FM. Lipidomic analysis of fibroblasts from Zellweger spectrum disorder patients identifies disease-specific phospholipid ratios. *J Lipid Res* 2016;57:1447–1454.

33. Houtkooper RH, Rodenburg RJ, Thiels C, Lenthe H van, Stet F, Poll-The BT, Stone JE, Steward CG, Wanders RJ, Smeitink J, Kulik W, Vaz FM. Cardiolipin and monolysocardiolipin analysis in fibroblasts, lymphocytes, and tissues using high-performance liquid chromatography-mass spectrometry as a diagnostic test for Barth syndrome. *Anal Biochem* Elsevier Inc.; 2009;387:230–237.

34. Yu L, Ruifrok WPT, Meissner M, Bos EM, Goor H Van, Sanjabi B, Harst P Van Der, Pitt B, Goldstein IJ, Koerts JA, Veldhuisen DJ Van, Bank RA, Gilst WH Van, Silljé HHW, Boer RA De. Genetic and pharmacological inhibition of galectin-3 prevents cardiac remodeling by interfering with myocardial fibrogenesis. Circ Hear Fail 2013;6:107–117.

35. Saini-Chohan HK, Holmes MG, Chicco AJ, Taylor WA, Moore RL, McCune SA, Hickson-Bick DL, Hatch GM, Sparagna GC. Cardiolipin biosynthesis and remodeling enzymes are altered during development of heart failure. *J Lipid Res* 2009;50:1600–1608.

36. Chatfield KC, Sparagna GC, Sucharov CC, Miyamoto SD, Grudis JE, Sobus RD, Hijmans J, Stauffer BL. Dysregulation of cardiolipin biosynthesis in pediatric heart failure. *J Mol Cell Cardiol* 2014;74:251–259.

37. Schlame M, Towbin JA, Heerdt PM, Jehle R, DiMauro S, Blanck TJJ. Deficiency of Tetralinoleoyl-Cardiolipin in Barth Syndrome. *Ann Neurol* 2002;51:634–637.

38. Han X, Yang J, Yang K, Zhongdan Z, Abendschein DR, Gross RW. Alterations in myocardial cardiolipin content and composition occur at the very earliest stages of diabetes: A shotgun lipidomics study. *Biochemis*try 2007;46:6417–6428.

39. Sparagna GC, Chicco AJ, Murphy RC, Bristow MR, Johnson CA, Rees ML, Maxey ML, McCune SA, Moore RL. Loss of cardiac tetralinoleoyl cardiolipin in human and experimental heart failure. *J Lipid Res* 2007;48:1559–1570.

40. Schlame M, Otten D. Analysis of cardiolipin molecular species by high-performance liquid chromatography of its derivative 1,3-bisphosphatidyl-2-benzoyl-sn-glycerol dimethyl ester. *Anal Bioch*em 1991;195:290–295.

41. Schlame M, Ren M, Xu Y, Greenberg ML, Haller I. Molecular symmetry in mitochondrial cardiolipins. *Chem Phys Lipi*ds 2005;138:38–49.

42. Houtkooper RH, Vaz FM. Cardiolipin, the heart of mitochondrial metabolism. *Cell Mol Life Sci* 2008;65:2493–2506.

43. W??st RCI, Vries HJ De, Wintjes LT, Rodenburg RJ, Niessen HWM, Stienen GJM. Mitochondrial complex I dysfunction and altered NAD(P)H kinetics in rat myocardium in cardiac right ventricular hypertrophy and failure. *Cardiovasc Res* 2016;111:362–372.

44. Saini-Chohan HK, Dakshinamurti S, Taylor WA, Shen GX, Murphy R, Sparagna GC, Hatch GM. Persistent pulmonary hypertension results in reduced tetralinoleoyl-cardiolipin and mitochondrial complex II + III during the development of right ventricular hypertrophy in the neonatal pig heart. *Am J Physiol - Hear Circ Physiol* G. M. Hatch, Departments of Pharmacology and Therapeutics, Faculty of Medicine, Univ. of Manitoba, Winnepeg, MB R3E OT6, Canada; 2011;301:H1415–H1424.

45. Petrosillo G, Matera M, Moro N, Ruggiero FM, Paradies G. Mitochondrial complex I dysfunction in rat heart with aging: critical role of reactive oxygen species and cardiolipin. *Free Radic Biol Med* Elsevier Inc.; 2009;46:88–94.

46. Petrosillo G, Ruggiero FM, Venosa NDI, Paradies G. Decreased complex III activity in mitochondria isolated from rat heart subjected to ischemia and reperfusion : role of reactive oxygen species and cardiolipin 1. 2003;714–716.

47. Paradies G, Petrosillo G, Pistolese M, Ruggiero FM. The effect of reactive oxygen species generated from the mitochondrial electron transport chain on the cytochrome c oxidase activity and on the cardiolipin content in bovine heart submitochondrial particles. 2000;466:323–326.

48. Lesnefsky EJ, Hoppel CL. Cardiolipin as an oxidative target in cardiac mitochondria in the aged rat. *Biochim Biophys Acta - Bioenerg* 2008;1777:1020–1027.

49. Luiken JJJJ, Willems JJ, Vusse GJGJ van der, Glatz JFJF. Electrostimulation enhances FAT/CD36-mediated long-chain fatty acid uptake by isolated rat cardiac myocytes. *Am J*

Physiol - Endocrinol Metab 2001;281:E704–E712.

50. Kim TT, Dyck JRB. The Role of CD36 in the Regulation of Myocardial Lipid Metabolism. *BBA - Mol Cell Biol Lipids* Elsevier B.V.; 2016;
51. Li C, Zhang J, Xue M, Li X, Han F, Liu X, Xu L, Lu Y, Cheng Y, Li T, Yu X, Sun B, Chen L. SGLT2 inhibition with empagliflozin attenuates myocardial oxidative stress and fibrosis in diabetic mice heart. *Cardiovasc Diabetol* BioMed Central; 2019;18:1–13.
52. Zhao W, Zhao T, Chen Y, Ahokas RA, Sun Y. Oxidative stress mediates cardiac fibrosis by enhancing transforming growth factor-beta1 in hypertensive rats. *Mol Cell Biochem* 2008;317:43–50.
53. Murdoch CE, Zhang M, Cave AC, Shah AM. NADPH oxidase-dependent redox signalling in cardiac hypertrophy, remodelling and failure. *Cardiovasc Res* 2006;71:208–215.
54. Münzel T, Gori T, Keaney JF, Maack C, Daiber A. Pathophysiological role of oxidative stress in systolic and diastolic heart failure and its therapeutic implications. *Eur Heart J* 2015;36: 2555–2564.
55. Natali A, Nesti L, Fabiani I, Calogero E, Bello V Di. Impact of empagliflozin on subclinical left ventricular dysfunctions and on the mechanisms involved in myocardial disease progression in type 2 diabetes: Rationale and design of the EMPA-HEART trial. *Cardiovasc Diabetol* BioMed Central; 2017;16:1–12.
56. Yang Z, Laubach VE, French BA, Kron IL. Acute Hyperglycaemia enhances oxidative stress and exacerbates myocardial infarction by activating NADPH oxidase during reperfusion. *J Thorac Cardiovasc Surg* 2010;137:723–729.
57. Byrne,* JA, Grieve DJ, Bendall JK, Li J-M, Gove C, Lambeth JD, Cave AC, Shah AM. Contrasting Roles of NADPH Oxidase Isoforms in Pressure-Overload Versus Angiotensin II–Induced Cardiac Hypertrophy. *Circ Res* 2003;93:802–805.
58. Kobara M, Furumori-Yukiya A, Kitamura M, Matsumura M, Ohigashi M, Toba H, Nakata T. Short-Term Caloric Restriction Suppresses Cardiac Oxidative Stress and Hypertrophy Caused by Chronic Pressure Overload. *J Card Fail* Elsevier Inc; 2015;21:656–666.
59. Rutschow S, Unger T, Anker S, Westermann D, Linderer A, Schultheiss H-P, Jager S, Pauschinger M, Tschope C, Riad A. Contributions of Inflammation and Cardiac Matrix Metalloproteinase Activity to Cardiac Failure in Diabetic Cardiomyopathy: The Role of Angiotensin Type 1 Receptor Antagonism. *Diabetes* 2007;56:641–646.
60. Du W, Schouten EM, Silljé HHW, A.Voors A, Boer RA de, Kolk CWA van de, Piek A, Mueller C, Mebazaa A. Plasma levels of heart failure biomarkers are primarily a reflection of extracardiac production. *Theranostic*s 2018;8:4155–4169.
61. Rumsey WL, Abbott B, Bertelsen D, Mallamaci M, Hagan K, Nelson D, Erecinska M. Adaptation to hypoxia alters energy metabolism in rat heart. *Am J Physiol - Hear Circ Physiol* W.L. Rumsey, Zeneca Pharmaceuticals, Wilmington, DE 19850-5437, United States; 1999;276:H71–H80.
62. Nouette-Gaulain K, Malgat M, Rocher C, Savineau J-P, Marthan R, Mazat J-P, Sztark F. Time course of differential mitochondrial energy metabolism adaptation to chronic hypoxia in right and left ventricles. *Cardiovasc Res* F. Sztark, Laboratoire d'Anesthésiologie, E.A. Physiologie Mitochondriale, Universite Bordeaux 2, 33076 Bordordeaux, France; 2005;66:132–140.

63. Fang Y-H, Piao L, Hong Z, Toth PT, Marsboom G, Bache-Wiig P, Rehman J, Archer SL. Therapeutic inhibition of fatty acid oxidation in right ventricular hypertrophy: Exploiting Randle's cycle. *J Mol Med* S.L. Archer, Medicine/Cardiology, University of Chicago, Chicago, IL 60637, United States; 2012;90:31–43.

64. Piao L, Sidhu VK, Fang YH, Ryan JJ, Parikh KS, Hong Z, Toth PT, Morrow E, Kutty S, Lopaschuk GD, Archer SL. FOXO1-mediated upregulation of pyruvate dehydrogenase kinase-4 (PDK4) decreases glucose oxidation and impairs right ventricular function in pulmonary hypertension: therapeutic benefits of dichloroacetate. *J Mol Med (Berl)* L. Piao, Section of Cardiology, Department of Medicine, University of Chicago, Chicago, IL, USA.; 2013;91:333–346.

65. Mulligan CM, Sparagna GC, Le CH, Mooy AB De, Routh MA, Holmes MG, Hickson-Bick DL, Zarini S, Murphy RC, Xu FY, Hatch GM, McCune SA, Moore RL, Chicco AJ. Dietary linoleate preserves cardiolipin and attenuates mitochondrial dysfunction in the failing rat heart. *Cardiovasc Res* 2012;94:460–468.

66. Chicco AJ, Sparagna GC, McCune SA, Johnson CA, Murphy RC, Bolden DA, Rees ML, Gardner RT, Moore RL. Linoleate-rich high-fat diet decreases mortality in hypertensive heart failure rats compared with lard and low-fat diets. *Hypertension* 2008;**52**:549–555.

67. Dolinsky VW, Jones KE, Sidhu RS, Haykowsky M, Czubryt MP, Gordon T, Dyck JRB. Improvements in skeletal muscle strength and cardiac function induced by resveratrol during exercise training contribute to enhanced exercise performance in rats. *J Physiol* 2012;590:2783–2799.

68. Qin F, Siwik DA, Luptak I, Hou X, Wang L, Higuchi A, Weisbrod RM, Ouchi N, Tu VH, Calamaras TD, Miller EJ, Verbeuren TJ, Walsh K, Cohen RA, Colucci WS. The polyphenols resveratrol and S17834 prevent the structural and functional sequelae of diet-induced metabolic heart disease in mice. *Circulation* 2012;125:1757–1764.

69. Beaudoin MS, Perry CGR, Arkell AM, Chabowski A, Simpson JA, Wright DC, Holloway GP. Impairments in mitochondrial palmitoyl-CoA respiratory kinetics that precede development of diabetic cardiomyopathy are prevented by resveratrol in ZDF rats. *J Physiol* 2014;592:2519–2533.

70. Chen YR, Yi FF, Li XY, Wang CY, Chen L, Yang XC, Su PX, Cai J. Resveratrol attenuates ventricular arrhythmias and improves the long-term survival in rats with myocardial infarction. *Cardiovasc Drugs Ther* 2008;22:479–485.

71. Dolinsky VW, Cole LK, Sparagna GC, Hatch GM. Cardiac mitochondrial energy metabolism in heart failure: Role of cardiolipin and sirtuins. *Biochim Biophys Acta - Mol Cell Biol Lipids* Elsevier B.V.; 2016;1861:1544–1554.

SUPPLEMENTAL MATERIAL

Pulmonary artery banding

Pulmonary artery banding was performed with a 19-gauge needle by approaching through left thoracotomy, as described previously[6]. Sham surgery was identical to PAB surgery with exception of the banding itself. Surgery took place under anaesthesia (isoflurane/air mixture, 5% induction; 2–3% maintenance; analgesia with buprenorphine 0.01mg/kg s.c.) and ventilation through intubation.

Echocardiography

Echocardiography was performed at 2, 5 and 12 weeks in all animals according to previous described protocol using a Vivid Dimension 7 and 10S-transducer (GE Healthcare, Waukesha, WI, USA.).[5] Rats were anesthetized with isoflurane (induction 5%; 2-3% maintenance) and warmed at 37˚C. Parasternal long axis (PLAX), short axis (at aortic and midpapillary level), apical four chamber and 5 chamber view were derived to measure PAB-gradient, LV cardiac output (LV CO), stroke volume (SV) eccentricity index end diastolic (EI ED), eccentricity index end systolic (EI ES), and tricuspid annular plan systolic excursion (TAPSE). Cardiac output was calculated by systolic aortic diameter ^{2} · 3.14 · velocity time integral x heart rate. Heart rate was determined over ten heart beats.

Heart catheterization

Invasive pressure measurements were performed in anesthetized and intubated rats at 2, 5 or 12 weeks, using a pressure-admittance catheter (1.9F, 6mm spacing) (Transonic, Ithaca, NY, USA), where after termination took place. The catheter was warmed at 37˚C and, after bilateral thoracotomy and percarditomy, introduced in the RV at the apex towards the outflow tract. Pressure, phase and magnitude were recorded by ADVantage PV System (ADV500) processor (Transonic, Ithaca, NY, USA) with Chartlab 5. Analyses were performed with custom made software (Circlab 2012, P. Steendijk). In this study we selectively used volume independent derived parameters. Derived from RV peak pressure ($RV_{peak}P$) mean pulmonary artery pressure (mPAP) was calculated ($RV_{peak}P/1.61$) and used to determine the RV workload (mPAP · SV) and power (mPAP · CO). Both maximum and minimum delta pressure/delta time (RV dP/dt_{max} respectively RV dP/dt_{min}) were corrected for $RV_{peak}P$.

Organs and weights

After catheterization, blood and organs were taken out. The heart was prepared and divided into the right atrium, left atrium, left ventricle (LV) plus septum, and RV and individually weighted. The liver lobe was weighted as well before and after overnight at 65 °C. The liver wet/dry weight ratio was determined. The heart was snap-frozen and stored at -80 °C for further analyses. One third of the RV and LV including septum, lung and liver were fixated in formalin and paraffin sections were made.

Real-time polymerase chain reaction (qPCR)

RNA was extracted from nitrogen snap-frozen RV's using TRIzol reagent (Invitrogen Corporation, Carlsbad, CA, USA). RNA concentration and purity was assessed using Nanodrop spectrophotometer (Nanodrop 1000, Thermo Scientific, Breda, The Netherlands), where after cCNA was derived. Gene expression was measured with Absolute qPCR SYBR Green ROX mix (abgene, Epsom, UK) in the present of 7.5ng cDNA and 200 nM forward and reverse primers. Real time quantitative reverse transcription (qRT-PCR) was performed by the Biorad CFX384 (Bio-Rad, Veenendaal, the Netherlands) according standard protocol. Measured mRNA expression was corrected for expression of housekeeping gene GAPDH.

Supplemental table. Sequence of primers used for quantitative real-time PCR

	sequence forward primer	sequence reverse primer
GAPDH	TCTCTGCTCCTCCCTGTTCTA	TACGGCCAAATCCGTTCACA
αMHC	GACAACTCCTCCCGCTTTGG	AAGATCACCCGGGACTTCTC
βMHC	GTCAAGCTCCTAAGTAATCTGTT	GAAAGGATGAGCCTTTCTTTGC
RCAN1	TTAAGCGTCTGCCCGTTGAA	CCTGGTCTCACTTTCGCTGA
NPPA	ATGGGCTCCTTCTCCATCAC	TCTACCGGCATCTTCTCCTC
COL1A2	ATGGTGGCAGCCAGTTTG	GCTGTTCTTGCAGTGGTAGG
COL3A1	AGAGGATGGCTGCACTAAAC	CTTGATCAGGACCACCAATG
TGFβ1	AAGAAGTCACCCGCGTGCTA	TGTGTGATGTCTTTGGTTTTGTCA
TGFβ2	AAATCGACATGCCGTCCCAC	GGATGGCATCAAGGTACCCAC
MCAD	CCGTTCCCTCTCATCAAAAG	ACACCCATACGCCAACTCTT
PPARα	ATGAGTCCCCTGGCAATG	GGCATTCTTCCAAAACGG
PGC1α	ACCGTAAATCTGCGGGATGATG	CATTCTCAAGAGCAGCGAAAGC
CD36	TGCAAAGAAGGAAAGCCTGTG	GCTCATCTTCGTTAGGATTCAAGC
CPT1b	TTCCTGGACGAGGTGCTTTC	TTGGGGTACTGCTTTGGGTC
GLUT1	GCTGTGGCTGGCTTCTCTAA	CCGGAAGCGATCTCATCGAA
GLUT4	CCGTGGCCTCCTATGAGATACT	AGGCACCCCGAAGATGAGT
IL1β	TGTGATGAAAGACGGCACACC	GGGAACTGTGCAGACTCAAC
IL6	CCCACCAGGAACGAAAGTCA	TCTTGCGGAGAGAAACTT
IL33	CCCGCCTTGCAAAATCACAA	CCCTTCATGCTTGCTACCTGAT
MPO	CCACGGCCTTTCAATGTCAC	TCTCGGTATGTGATGATCTGGA
GDF15	TGACCCAGCTGTCCGGATAC	GTGCACGCGGTAGGCTTC
TAZ	CGGGCAGAAAACAAGTCAGC	AGCTGTTCTGCCTGCATCTT
SOD	TGGCTTGGCTTCAATAAGA	AAGGTAGTAAGCGTGCTCC
PLA2	ACCATCCCATCCAAGAGAGC	CAAACTCCAGAAGGCTCCCC
CDS2	ATTGGGGGCTTCTTTGCTAC	TCAGATGGCTCACAGTCCAC
CD68	CTCTCATCATTGGCCTGGTC	GGGCTGGTAGGTTGATTGTC

Mitochondrial isolation

Fresh RV tissue, transported in 0.9% KCl, was minced in 5 ml of ice cold isolation medium A (220mM mannitol, 70 mM sucrose, 5 mM TES, 0.1 mM EGTA, pH 7.3) supplemented with proteinase (0.2 mg/ml) and left for 5 minutes. 20 ml of ice cold isolation medium A supplemented with bovine serum albumin (1mg/ml) and homogenize with Potter-Elvehjem homogenizer with 10 up-and-down at 750 rpm. Homogenate was centrifuged at 800 g for ten minutes at 4˚C, where after the supernatant in a clean tube was centrifuged at 7200 g for ten minutes at 4˚C. After discarding the supernant, the pellet was suspend in 2 ml ice cold medium A and

again centrifuged at 7200 g for ten minutes at 4˚C. The pellet was suspended in 200 µl of ice cold medium A and transferred into an eppendorf and kept on ice during the experiment.

Mitochondrial respiration

Mitochondrial respiration was measured in a stirred, 2-channel high-resolution respirometry (Oroboros, Innsbruck, Austra) in the isolated mitochondria. The oxygen consumption rate was measured using two both in the presence of ADP. First pyruvate respiration was assessed by 2 mM pyruvate, the second protocol contained 25 mM Palmitoyl-CoA and 2 mM L-carnitine. 2 mM malate was added to the medium (MIR05) as well. State 3 was reached by adding 10 mM glucose, 1.5 U/ml hexokinase and 1 mM ATP, state 4 by adding 1.25 µM carboxyatractyloside (CAT) and state 3 uncoupled by added 1.5 µM carbonyl cyanide-4-(trifluoromethoxy)phenylhydrazone (FCCP). Oxygen consumption rate was corrected for protein content. Citrate synthase activity kit (Sigma Aldrich, USA) was used as a marker of mitochondrial density.

Internal standards used for lipidomic analysis

A defined amount of internal standards (0.5 nmol of DG(14:0)2, 0.5 nmol of TG(14:0)2, 0.5 nmol of CE(14:0), 1.0 nmol of CL(14:0)4, 0.02 nmol of BMP(14:0)2, 2.0 nmol of PC(14:0)2, 0.5 nmol of PG(14:0)2, 1.0 nmol of PS(14:0)2, 1.0 nmol of PE(14:0)2, 0.2 nmol of PA(14:0)2, 0.5 nmol of PI(8:0)2, 0.2 nmol of SM(14:0)2, 0.02 nmol of LPG(14:0), 0.1 nmol of LPE(14:0), 0.5 nmol of LPC(14:0), 0.05 nmol of LPA(14:0) (purchased from Avanti Polar Lipids, Alabaster, AL, USA)) was used.

Supplemental table. Numbers of used animals per studied parameter

	figure / table	control group(s) *(number of used animals)*			PAB groups *(number of used animals)*		
time point		pooled time points			2 weeks	5 weeks	12 weeks
PAB gradient	1A	10			5	10	9
TAPSE	1B	13			4	10	9
dP/dt_{max}	1C	10			4	10	9
dP/dt_{min}	1D	10			4	10	9
RV EDP	1E	10			3	10	8
cardiac index	1F	13			4	11	9
power	1G	11			4	10	9
heart rate	Table 1	13			4	10	9
left ventricular stroke volume	Table 1	13			4	11	9
eccentricity index end systolic	Table 1	13			5	11	9
eccentricity index end diastolic	Table 1	13			5	11	9
right ventricle / left ventricle ratio	Table 1	10			4	11	9
right atrium width	Table 1	10			4	11	9
right atrium length	Table 1	10			4	11	9
workload	Table 1	11			4	10	9
RV weight	2A	8			3	11	9
CCSA	2B	12			5	11	8
capillary myocyte ratio	2D	8			5	10	7
fibrosis	2E	13			5	11	9
NPPA	2F, 1st graph	13			4	10	9
bMHC/aMHC	2F, 2nd graph	13			4	10	9
RCAN1	2F, 3rd graph	13			4	10	9
COL1A2	2F, 4th graph	13			4	10	9
COL3A1	2F, 5th graph	9			4	10	9
TGFβ1	2F, 6th graph	13			4	10	9
TGFβ2	2F, 7th graph	13			4	10	9
time point		2 weeks	5weeks	12 weeks	2 weeks	5 weeks	12 weeks
max. respiratory capacity palmitoyl CoA State 3	S1A	4	4	3	4	11	8

max. respiratory capacity palmitoyl CoA State 3u	3A	4	4	3	4	11	8
max. respiratory capacity pyruvate State 3	S1B	4	4	3	4	11	8
max. respiratory capacity pyruvate State 3u	3B	4	4	3	4	11	8
pyruvate/palmitoyl CoA State 3	S1C	4	4	3	4	11	8
pyruvate/palmitoyl CoA State 3u	3C	4	4	3	4	11	8
AOPP	5G	4	3	4	5	10	9
anti-oxidant capacity	5H	4	3	4	5	10	9

time point		pooled time points	2 weeks	5 weeks	12 weeks
citrate synthase	3D	10	4	10	9
CD36	3E, 1st graph	13	5	11	9
CPT1B	3E, 2nd graph	13	4	11	9
GLUT4	3E, 3rd graph	13	5	11	9
PPAR	Table 2	13	4	11	9
PGC1	Table 2	13	4	11	9
MCAD	3E, 4th graph	13	4	11	9
CDS	Table 2	13	5	11	9
PLA_2	Table 2	13	5	11	9
TAZ	Table 2	13	5	11	9
GLUT1	Table 2	13	4	11	9
IL-6	Table 2	13	5	11	9
IL-33	Table 2	13	5	11	9
SOD	Table 2	13	5	11	9
CD68	5A	13	5	11	9
GDF-15	5B	13	5	11	9
macrophage infiltration	5C	11	4	10	9
NOX2	5E	11	4	11	9
NOX4	5F	10	4	11	9
AOPP in plasma	5I	11	4	10	9
GDF-15 in plasma	5J	11	4	10	9

SUPPLEMENTAL TABLES

Supplemental table 1. Hemodynamic data measured with echocardiography or cardiac catheterization.

	control pooled time points	PAB 2 weeks	5 weeks	12 weeks
heart rate (bpm)	398±9	364±21	308±9*	350±12
left ventricular stroke volume (mL)	0.336±0.009	0.358±0.031	0.397±0.020*#	0.420±0.032*†
eccentricity index end systolic	1.108±0.049	0.628±0.084*	0.560±0.038*	0.696±0.057*
eccentricity index end diastolic	1.061±0.034	0.743±0.103*	0.693±0.045*	0.726±0.031*
right ventricle / left ventricle ratio	0.687±0.019	1.548±0.171*	1.642±0.090*	1.562±0.191*
right atrium width (mm)	4.520±0.260	5.825±0.899	6.718±0.273*	6.344±0.295*
right atrium length (mm)	2.520±0.154	3.650±0.851	4.755± 0.230*	4.989±0.371*
workload (mmHg x mm)	4.549±0.233	11.789±1.227*	14.846±1.295*	14.048±0.862*

Values are mean±SEM. * = significant difference compared to control (p-value < 0.05). # = significant difference compared to PAB two weeks (p-value < 0.05). † Significant difference compared to PAB five weeks (p-value < 0.05). PAB = pulmonary artery banding.

Supplemental table 2. Gene expression at mRNA level compared to pooled control.

	fold change PAB versus control		
	2 weeks	5 weeks	12 weeks
GAPDH	1.095±0.133	0.899±0.055	0.933±0.069
α-MHC	0.726±0.098	0.622±0.046*	0.668±0.081*
β-MHC	3.353±0.653*	3.929±0.445*	3.871±0.405*
PPARα	0.940±0.351	0.885±0.065	0.914±0.125
PGC1α	0.908±0.236	0.694±0.062	0.716±0.085
CDS	1.061±0.120	1.048±0.092	0.936±0.091
PLA_2	0.832±0.103	0.912±0.161	0.676±0.060
TAZ	0.991±0.042	0.981±0.042	0.907±0.048
GLUT1	1.449±0.319	1.193±0.150	1.015±0.166
IL-6	7.389±4.097*	2.225±0.897	1.230±0.375#
IL-33	0.957±0.150	1.164±0.182	0.830±0.069
SOD	1.152±0.127	1.211±0.061	1.184±0.075

Values are mean±SEM. * = significant difference compared to sham (p < 0.05), # = significant difference compared to PAB two weeks (p < 0.05). PAB = pulmonary artery banding. PPAR = peroxisome proliferator-activated receptor alpha, PGC1 = peroxisome proliferator-activated receptor gamma coactivator 1-alpha, CDS = cytidinediphosphate-diacylglycerol synthase, PLA2 = phospholipase A2, TAZ = tafazzin, GLUT1= glucose transporter 1, CD68 = cluster differentiation 68, GDF-15 = growth differentiation factor 15, IL-6 = interleukin 6, IL-33 = interleukin 33, SOD = super oxide dismutase.

Supplemental table 3. Datasheet lipodomics.

Due to excessive length, table not added to the manuscript.

Supplemental table 4. Datasheet quantification ceramides.

Due to excessive length, table not added to the manuscript.

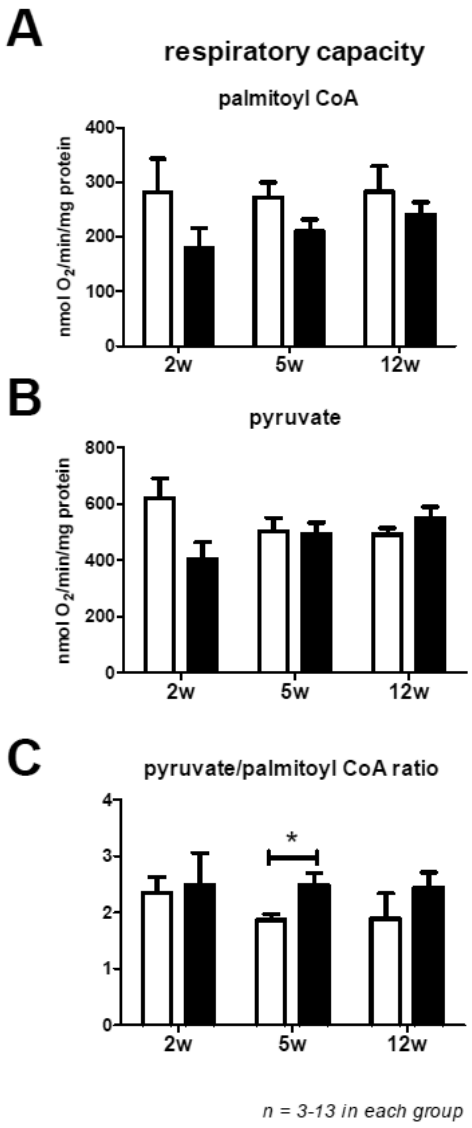

Supplemental figure 1. RV fatty acid and glucose metabolism during pressure load over time. Mitochondrial respiratory capicity (state 3) measured by oxygen consumption rates in isolated mitochondria from RV tissue in the presence of palmitoyl coA (A) or pyruvate (B), and the ratio of these two (C). Data presented as mean±SEM. * = $p < 0.05$ compared to control. white = control, black = pulmonary artery banding, 2w, 5w and 12 w = 2, 5, and 12 weeks. O2 = oxygen.

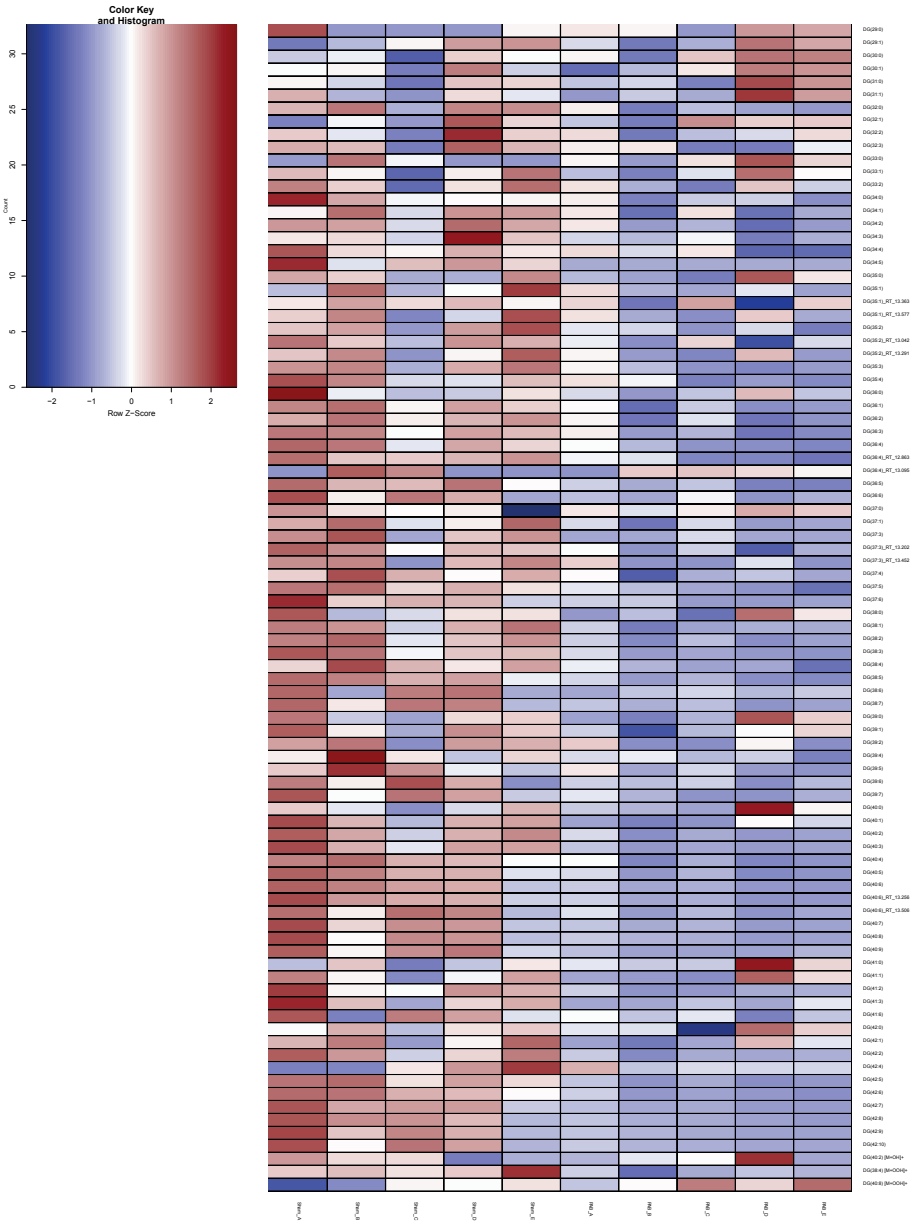

Supplemental figure 2. Diglyceride – complete heat map. DG = diglyceride. PAB = pulmonary artery banding.

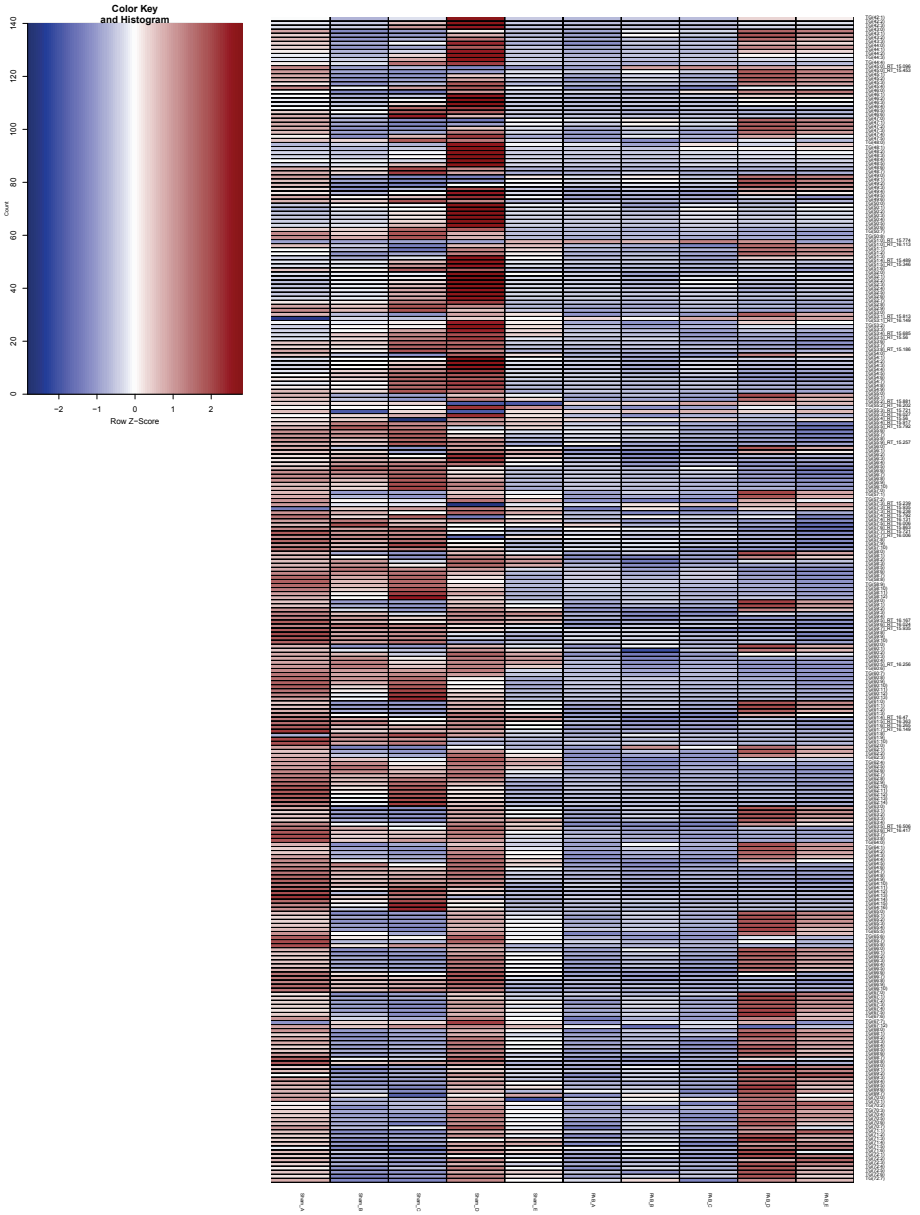

Supplemental figure 3. Triglycerides – complete heat map. TG = triglyceride. PAB = pulmonary artery banding.

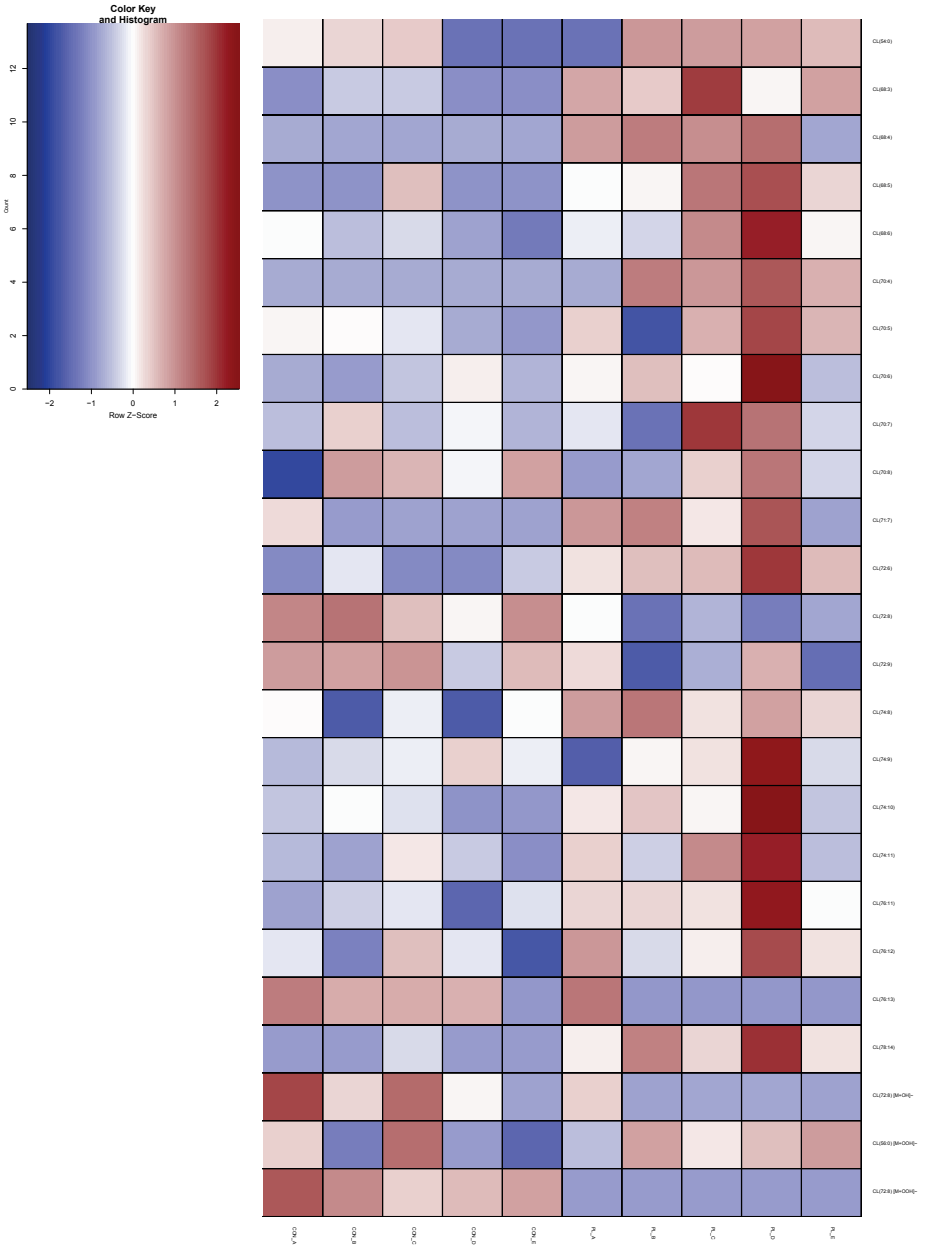

Supplemental figure 4. Cardiolipins – complete heat map. CL = cardiolipin. PAB = pulmonary artery banding.

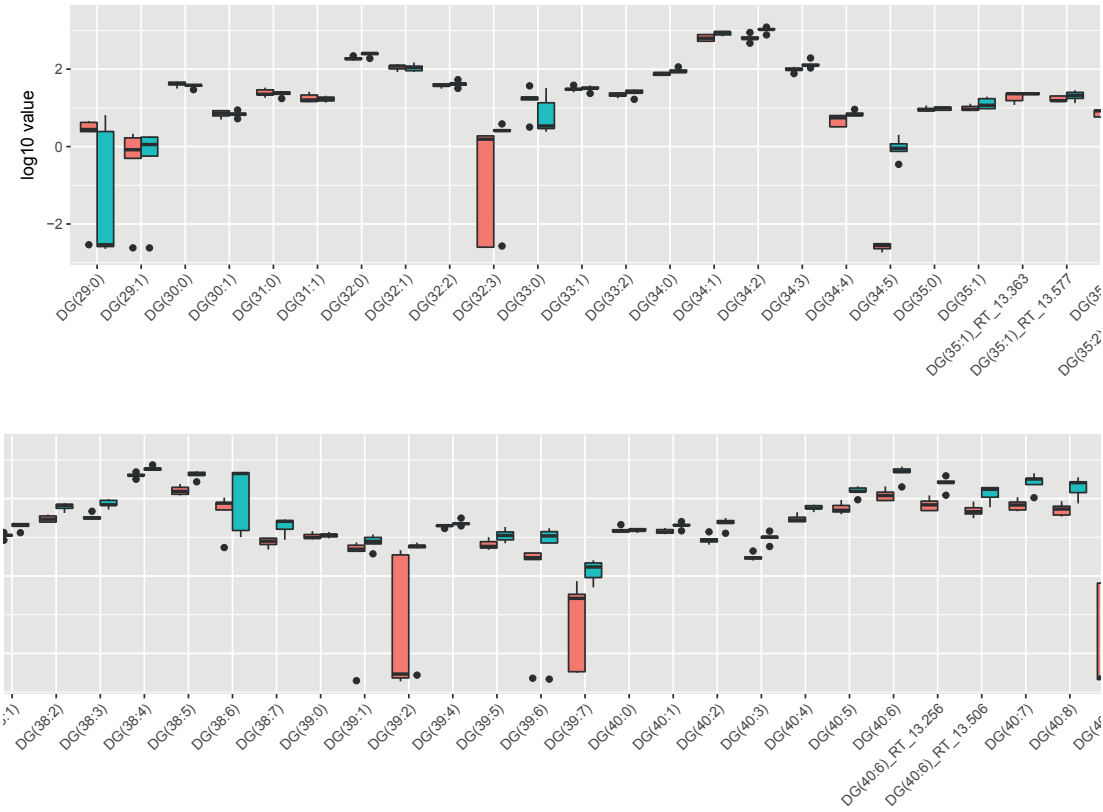

Supplemental figure 5. Diglyceride – all boxplots. Dots represent outliers, although included in statistical analysis. DG = diglyceride. PAB = pulmonary artery banding.

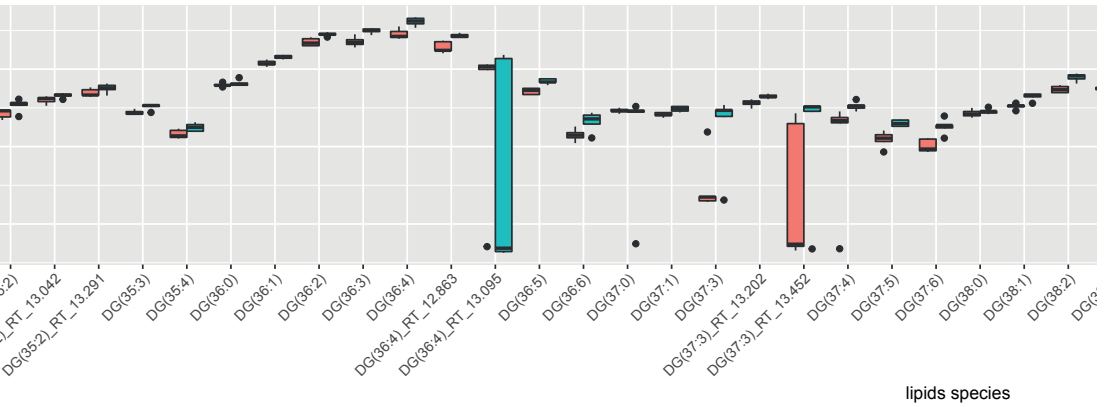
DG(35:2)_RT_13.042
DG(35:2)_RT_13.291
DG(35:3)
DG(35:4)
DG(36:0)
DG(36:1)
DG(36:2)
DG(36:3)
DG(36:4)
DG(36:4)_RT_12.863
DG(36:4)_RT_13.095
DG(36:5)
DG(36:6)
DG(37:0)
DG(37:1)
DG(37:3)
DG(37:3)_RT_13.202
DG(37:3)_RT_13.452
DG(37:4)
DG(37:5)
DG(37:6)
DG(38:0)
DG(38:1)
DG(38:2)
lipids species

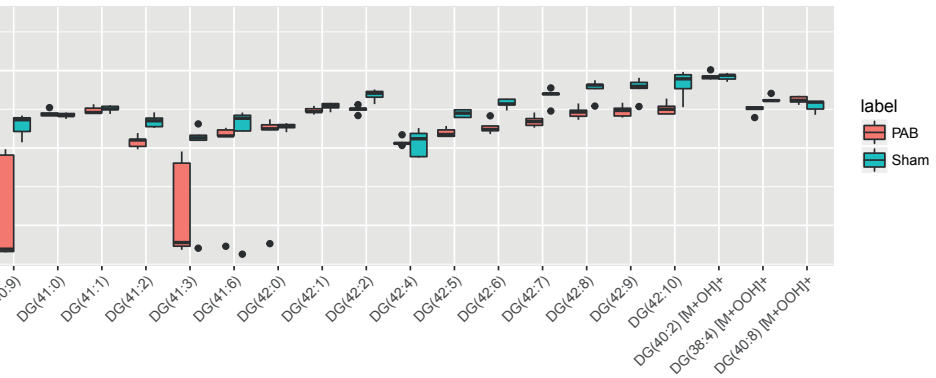
DG(41:0)
DG(41:1)
DG(41:2)
DG(41:3)
DG(41:6)
DG(42:0)
DG(42:1)
DG(42:2)
DG(42:4)
DG(42:5)
DG(42:6)
DG(42:7)
DG(42:8)
DG(42:9)
DG(42:10)
DG(40:2) [M+OH]+
DG(38:4) [M+OOH]+
DG(40:5) [M+OOH]+
label
PAB
Sham

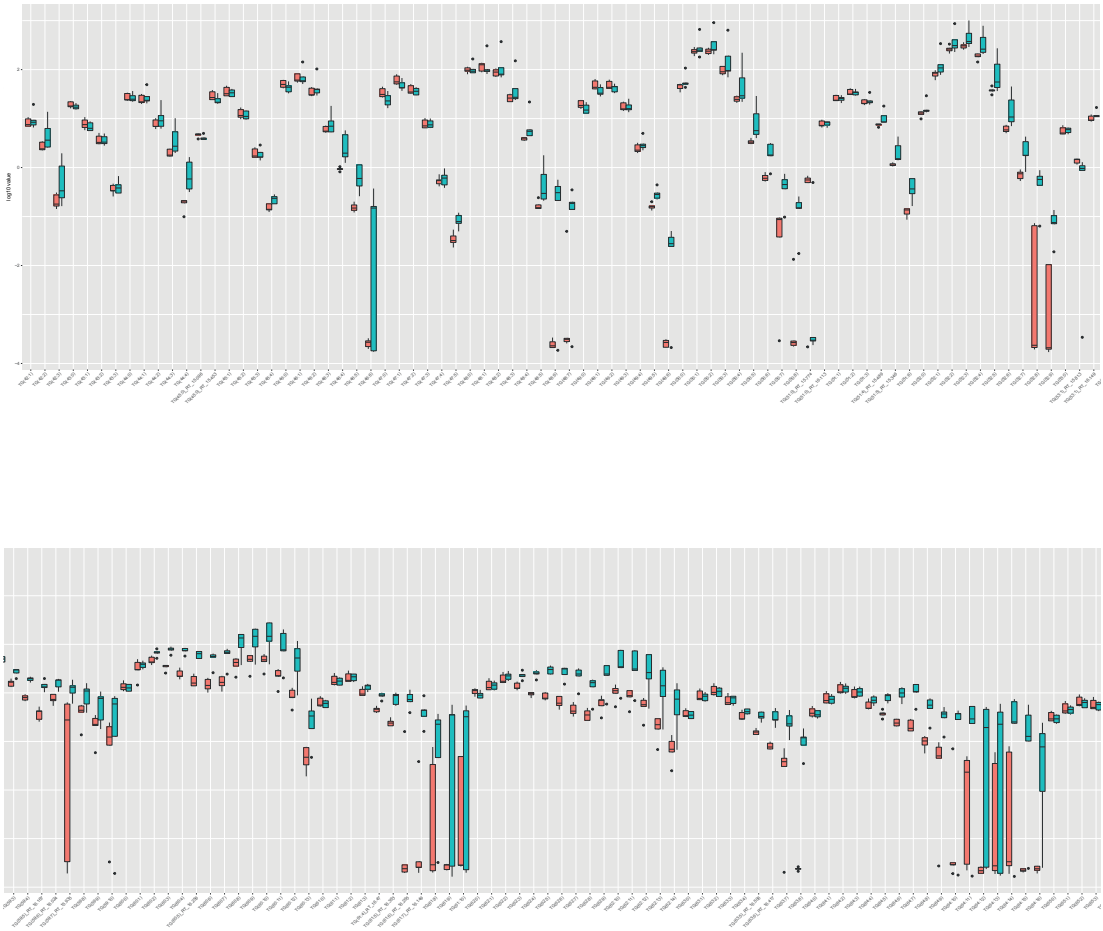

Supplemental figure 6. Triglyceride – all boxplots. Dots represent outliers, although included in statistical analysis. TG = triglyceride. PAB = pulmonary artery banding.

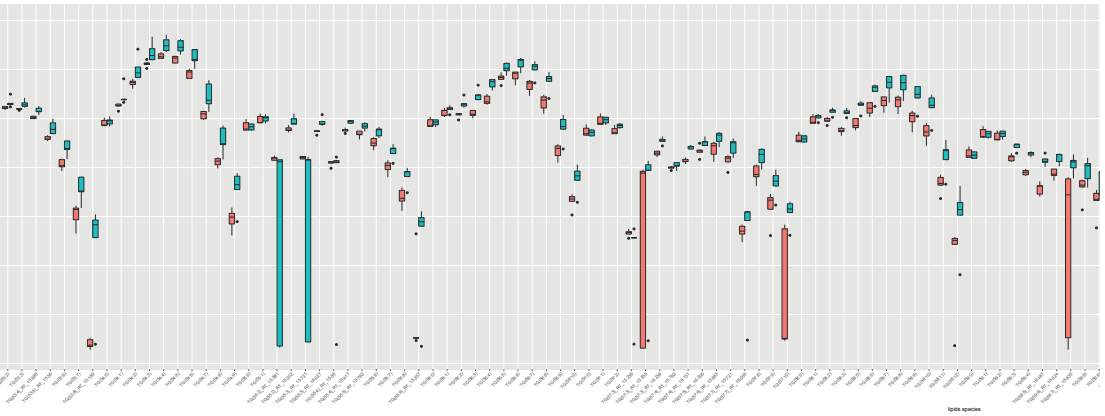

4

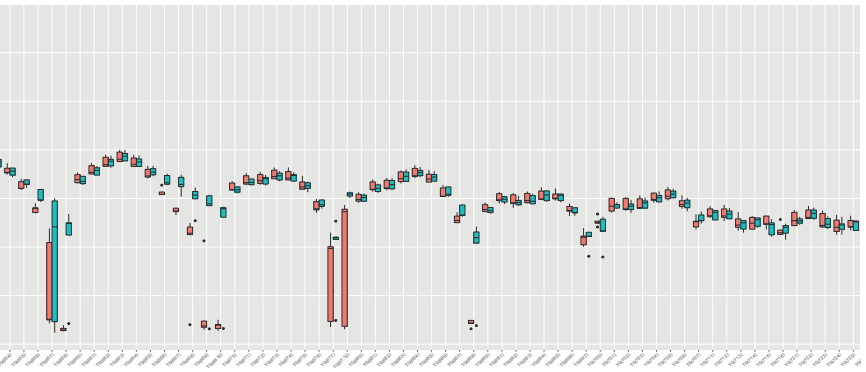

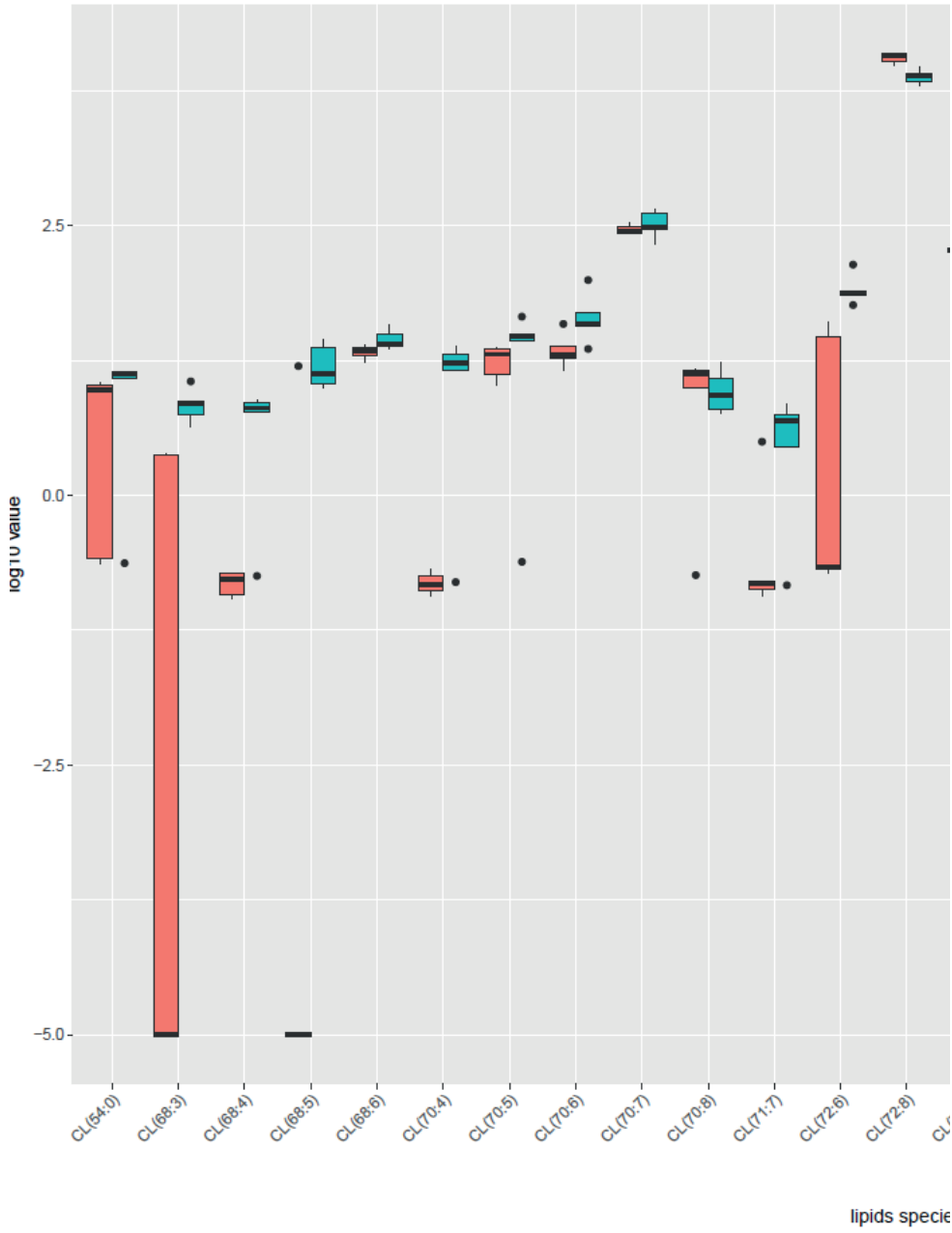

Supplemental figure 7. Cardiolipins – all boxplots. Dots represent outliers, although included in statistical analysis. CL = cardiolipin. PAB = pulmonary artery banding.


label
CON
PL
CL(74:8)
CL(74:9)
CL(74:10)
CL(74:11)
CL(76:11)
CL(76:12)
CL(76:13)
CL(78:14)
CL(72:8) [M+OH]-
CL(56:0) [M+OOH]-
CL(72:8) [M+OOH]-

Suppl. Fig. 6

5

CHAPTER 5

Quantification of biventricular function and morphology by cardiac magnetic resonance imaging in mice with pulmonary artery banding

A.M.C. Koop*, Q.A.J. Hagdorn*, C.W.A. van de Kolk, A. van Oosten, M. Weij, H.H.W. Silljé, T.P. Willems, R.M.F. Berger
- Journal of Visualized Experiments. 2020.

* These authors contributed equally to the manuscript.

SUMMARY

To understand the pathophysiology of right ventricular (RV) adaptation to abnormal loading, experimental models are crucial. However, assessment of RV dimensions and function is complex and challenging. This protocol provides a method to perform cardiac magnetic resonance imaging (CMR) as a noninvasive benchmark procedure in mice subjected to RV pressure load.

ABSTRACT

Right ventricular (RV) function and failure are major determinants of outcome in acquired and congenital heart diseases, including pulmonary hypertension. Assessment of RV function and morphology is complex, partly due to the complex shape of the RV. Currently, cardiac magnetic resonance (CMR) imaging is the golden standard for noninvasive assessment of RV function and morphology. The current protocol describes CMR imaging in a mouse model of RV pressure load induced by pulmonary artery banding (PAB). PAB is performed by placing a 6-0 suture around the pulmonary artery over a 23 G needle. The PAB gradient is determined using echocardiography at 2 and 6 weeks. At 6 weeks, the right and left ventricular morphology and function is assessed by measuring both end-systolic and end-diastolic volumes and mass by ten to eleven cine slices 1 mm thick using a 9.4 T magnetic resonance imaging scanner equipped with a 1,500 mT/m gradient. Representative results show that PAB induces a significant increase in RV pressure load, with significant effects on biventricular morphology and RV function. It is also shown that at 6 weeks of RV pressure load, cardiac output is maintained. Presented here is a reproducible protocol for the quantification of biventricular morphology and function in a mouse model of RV pressure load and may serve as a method for experiments exploring determinants of RV remodelling and dysfunction.

INTRODUCTION

Patients with acquired and congenital cardiovascular diseases, including pulmonary hypertension (PH), are at risk of right ventricular (RV) dysfunction and failure.[1] RV adaptation as a result of increased pressure load is characterized by concentric hypertrophy in early stages and progressive dilatation in end-stage disease. Furthermore, it is associated with disorders in metabolism and the extracellular matrix, processes of inflammation and, eventually, RV failure.[2-6] Animal models have been developed to explore the underlying processes of the progression towards RV failure. However, optimization of models and adequate assessment of RV function and dimensions has been challenging. For noninvasive assessment of RV function and dimensions, cardiac magnetic resonance (CMR) imaging is the golden standard. This technique creates images of the beating heart by using a strong magnetic field and radiofrequency waves. CMR is available for humans, and for animals such as laboratory rodents. As the latter require higher spatial resolution due to the smaller size of the heart, the magnetic field required to provide adequate images must be higher, compared to humans.

Multiple models mimicking RV pressure overload are available, including models of PH[7–17] a potent stimulus for pulmonary hypertension and right ventricular hypertrophy. When anesthetized rats adapted to chronic hypoxia spontaneously respired room air, their mean right intraventricular peak systolic pressure (RVSP and models of proximal RV pressure load.[2,3,10,18-23] The choice of either a model of PH or a model of proximal RV pressure load depends on the research question: the effect of an intervention on the pulmonary vasculature and therefore possibly RV afterload modulation (i.e., PH models), or the direct effect on the RV (i.e., proximal RV pressure load models). Several methods for experimental induction of PH are available, including use of monocrotaline (MCT),[12-14,16,22,24-26] MCT combined with an aortocaval shunt[9], chronic hypoxia,[7,27-29] and the combination of a vascular endothelial growth factor receptor antagonist, Sugen 5416, with chronic hypoxia.[8,10,30,31] Such models represent progressive pulmonary models of proximal RV pressure load and are not targeted at the pulmonary vasculature but induce a constant afterload by constriction of the pulmonary artery, with an accompanying increase of RV afterload.[2,3] This can be performed by a suture-banding (pulmonary artery banding, PAB) or a vascular clip around the pulmonary artery. PAB has been performed in several animal species, and cardiac dimensions and function have been studied in various ways, such as histology, transthoracic echocardiography (including speckle tracking), and heart catheterization.[2,32-40] PAB in small rodents, such as mice, is challenging. This is because subtle differences between the tightness of artery constriction have marked results on the degree of RV pressure load and subsequent functional status and survival. When the constriction is very tight, the animal will die during or shortly

after operation, whereas the desired phenotype will not be achieved when the constriction is not tight enough. However, the use of mice has advantages compared to other animals, because of the excellent genetic modification possibilities (i.e., transgenic or knockout models) and fast breeding. This is of added value in the study of diseases and in exploring the contribution of molecular and (epi-) genetic factors.

Animal study designs are shifting towards the investigation of temporal changes during disease.[2,3,8,13,21] For such studies, noninvasive modalities are necessary, because serial assessments can be performed. Alternatives to CMR in the assessment of cardiac remodelling could be (1) tissue characterization using histopathology, with multiple animals being sacrificed at different time points, (2) invasive functional assessment by pressure-volume analysis, or (3) echocardiography, which allows the researcher to identify cardiac hypertrophy or dilatation noninvasively within the same animal serially. CMR has two major advantages in assessment of the RV: (1) CMR is a noninvasive modality, enabling serial measurements in one animal, hereby contributing to reducing animal numbers needed for studies, and (2) CMR does not rely on a particular geometric shape and visualizes three-dimensionally. CMR-derived RV volumes and function measurements have been shown to be accurate and are considered to be the noninvasive golden standard in different cardiac entities in humans,[42-45] but had not yet been translated to a CMR protocol for mice with RV pressure overload.

Many models of PAB are described in the literature, but with high heterogeneity in methods of assessing hemodynamic effects and RV function and adaptation. This protocol outlines the procedure of PAB in mice with validation of the model by measuring the PAB gradient by echocardiography and evaluating cardiac dimensions and function with CMR. While a protocol of CMR in animals subjected to PAB has been published for rats, this combination has not been described for mice until now. While rats are most commonly used for PH models,[8,12-16,22,24-31,46] mice are most often used for transgenic or knock-out studies and thereby contribute to our understanding of mechanisms in pressure-loaded RV failure. This protocol could form the basis for future studies to unravel signaling pathways involved in the transition towards RV failure.

PROTOCOL

All experiments and animal care are conducted according to the Dutch Animal Experimental Act and conform to the Guide for the Care and Use of Laboratory Animals published by the US National Institutes of Health. The Animal Experiments Committee of the University of Groningen, the Netherlands, approved the current experimental protocol (permit number: 2014-041/3005).

1. Housing and acclimatization

1.1.1. Use 20–30 g wild type C57 black 6 (C57BL/6) mice (institutional breeding line described previously[47]), male and female, all more than 8 weeks old. House the mice in groups with a maximum of five per cage. In order to get used to human handling, let the mice acclimatize for at least 7 days. Do not perform any procedures during this period.

2. Pulmonary artery banding surgery

2.1. Preparation

2.1.1. Place the mouse in the induction chamber filled with 5% isoflurane/100% oxygen. Check for the lack of reflexes by giving a pain stimulus (i.e., toe pinch).

2.1.2. Shave the left hemithorax of the mouse using an electric shaver.

2.1.3. Gently pull out the tongue and hold with mild tension.

2.1.4. Illuminate the inner throat by placing a light source on the exterior throat at the level of the glottis.

2.1.5. Intubate the mouse endotracheally with a 20 G flexible cannula.

2.1.6. Place the animal on its right side on a heat mat (set temperature at 37 ˚C).

2.1.7. Connect the cannula to the miniventilator and start ventilation with 1.5%–2.5% isoflurane/oxygen (180 breaths/min, tidal 250 µL).

2.1.8. Inject 0.1 mg/kg buprenorphine subcutaneously for postoperative analgesia.

2.1.9. Prevent dehydration of the eye using eye ointment.

2.2. Pulmonary artery banding surgery by left lateral thoracotomy

2.2.1. Place the mouse on its right side by placing the right foreleg in a neutral position, the right hind leg extended, and the left foreleg bent back.

2.2.2. Disinfect the skin on the thorax with chloride-hexidine, swab two times.

2.2.3. Use sterile instruments for surgery. Open the skin with small scissors (round handle, 12 mm blades) from the left armpit parallel to the second and third rib.

2.2.4. Identify the m. pectoralis superficialis (oblique, superficial muscle) and the m. pectoralis profundus (oblique, underlying muscle).

2.2.5. Using suture loops, pull the m. pectoralis superficialis towards the ventral side and the m. pectoralis profundus towards the dorsal side of the mouse.

2.2.6. Open the second intercostal space and spread the ribs by using adapted paper clips, allowing the left heart ear, left lung, and the pulmonary artery to become visible.

2.2.7. Separate the arteria pulmonalis from the aorta. Place a suture loop around the pulmonary artery with a blunt 25 G needle that contains a 6-0 suture and place a lose 2-1-1 ligature around the arteria pulmonalis.

2.2.8. Place a 23 G needle parallel to the arteria pulmonalis within the 6-0 suture and first fix the most proximal suture knot and then distal knot of the 2-1-1 suture. Remove the 23 G needle. Make sure the knot is adequate.

2.2.9. Close the thorax with two or three separate sutures with a monofilament polypropylene 5-0 suture. Release the m. pectoralis superficalis and m. pectoralis profundus.

2.2.10. Suture the skin with a pure polyglycolic acid 5-0 suture. Use a continuous suture technique to minimize scar formation in the tissue; scar tissue will influence the image quality of the echocardiography.

2.2.11. Turn off the isoflurane while continuing ventilation with oxygen during recovery from anesthesia until the mouse regains its own, spontaneous respiration as can be observed from movement of the abdomen.

2.2.12. Uncouple the endotracheal tube from the ventilator. Check for spontaneous respiration, extubate only when spontaneous respiratory action is visible. When spontaneous respiration is not seen, connect the tube to the ventilator again and return to step 2.2.12.

2.2.13. Observe the mouse until it regains consciousness.

2.3 Sham surgery

2.3.1. Perform the above procedure with the exception of the banding (steps 2.2.2–2.2.6).

2.4. Postsurgical period

2.4.1. House the mouse individually in an incubator (37 ˚C) for 24 h.

2.4.2. Observe the mouse daily during the first 3 postoperative days. In case of any signs of discomfort, inject 0.1 mg/kg buprenorphine subcutaneously 2x daily for postoperative analgesia.

3. Echocardiography

3.1. Preparation

3.1.1. Perform PAB gradient analysis by means of echocardiography 14 days after PAB surgery.

3.1.2. Start the echocardiography device. Choose the cardiac package and a 14.0 MHz transducer.

3.2. Anesthesia

3.2.1. Place the mouse in the induction chamber filled with a mixture of 5% isoflurane and 100% oxygen.

3.2.2. Shave the thorax of the mouse.

3.2.3. Place the mouse on its back on the heat mat (temperature 37 ˚C) and place the snout in the ventilation mask.

3.2.4. Ventilate with a mixture of 1.5%–2.5% isoflurane and 100% oxygen (0.15 L/min) and room air (0.3 L/min).

3.2.5. Check the depth of the anesthesia by performing a toe pinch and adjust the anesthesia accordingly.

3.2.6. Prevent dehydration of the eye by using eye ointment.

3.3. Determination of PAB gradient by echocardiography

3.3.1. Place pediatric electrocardiogram-stickers on each foreleg and one on both hind legs. Use the stickers to hold the animal.

3.3.2. Apply ultrasound gel to the shaved part of the mouse's thorax.

3.3.3. To obtain the images of the pulmonary artery, two views can be used: the parasternal long axis (PLAX) or the parasternal short axis (PSAX) view. Obtain both and use the view that gives the best quality measurements and highest velocities for analysis.

3.3.4. Obtain PLAX and PSAX views.

3.3.5. Press the **color-Doppler button** to visualize blood flow.

3.3.6. Place the ultrasound probe at a 30˚ angle to the parasternal line to obtain PLAX (for detailed description see Cheng, et al.[48]the RV is significantly affected in pulmonary diseases such as pulmonary artery hypertension (PAH), visualizing the ascending aorta.

3.3.7. Sweep the probe minimally towards the left so the ascending aorta disappears behind the pulmonary artery. The appropriate PLAX is identified when the pulmonary artery is visualized, with blood flowing vertically.

3.3.8. Place the cursor in line with the pulmonary artery. Press the **continuous wave** (CW) **Doppler button** to derive velocity time integral measurements during three cardiac cycles. Press **Save**.

3.3.9. Rotate the probe 90˚ clockwise from the PLAX to obtain PSAX, then tilt the probe slightly towards the cranial/ventral direction to derive the PSAX at the aortic level. The appropriate PSAX view is identified if the RV outflow tract is situated between the aorta and the probe. This continues in the pulmonary artery, with blood flowing vertically. For a detailed description see Cheng et al.[48]

3.3.10. Place the cursor in line with the pulmonary artery. Press the **continuous wave** (CW) **Doppler button** to derive velocity time integral measurements during three cardiac cycles. Press **Save**.

3.3.11. Measure the three maximum velocities of the best view (PSAX or PLAX) and calculate the mean. Use the simplified Bernoulli's principle $delta\text{-}P = 4 \cdot V^2$ to derive the PAB gradient in millimeters mercury (mmHg).

4. Cardiac magnetic resonance imaging

4.1. Preparation

4.1.1. Perform CMR analysis 6 weeks (i.e., 42 days) after PAB surgery.

NOTE: Additionally, earlier timepoints after PAB surgery may be chosen when multiple timepoints are to be included, depending on the research question. Later timepoints could be considered; however, RV failure and death may increasingly occur.

4.1.2. Use a sufficiently powerful magnet (typically, >7 T is used for rodent CMR scanning). For the current protocol, a 9.4 T vertical system, with 1,500 mT/m gradient set and 89 mm bore size is used.

4.1.3. Install CMR postprocessing software for analyzing volumes and masses in the derived images. The software is deemed appropriate if it allows manual segmentation to determine end-diastolic (ED) and end-systolic (ES) volumes (EDV and ESV, respectively) and ventricular mass (measured both ED and ES).

4.2. Anesthesia and fixation

4.2.1. Place the mouse in the induction chamber filled with a mixture of 5% isoflurane and 100% oxygen. Verify the effect of the anesthesia by giving a pain stimulus by a toe pinch.

4.2.2. Put eye ointment on the eyes of the mouse to keep them moist during scanning.

4.2.3. Place the mouse in the scanner's animal bed with integrated air supply, a warmed (37 °C) mixture of 1.5%–2.5% isoflurane, 100% oxygen (0.15 L/min), and room air (0.3 L/min), and a pressure pad that enables observation of heart rate (aim for 400–500 bpm) and respiratory rate (aim for ~35 breaths per min) during scanning. Regulate the anesthesia based those two parameters. Make sure the bed is made of plastic, without any magnetic material.

4.2.4. Place the animal bed with the mouse into the scanner.

4.3. Performing cardiac magnetic resonance imaging

4.3.1. Make preacquisition adjustments by tuning the radiofrequency (RF) birdcage coil on 1 Hydrogen (1 H) resonance frequency.

4.3.2. Then set the magnetic field as homogeneous as possible using the automatic shimming procedure.

NOTE: The computerized shimming is done by the so-called Tuning method, which uses the area under the 1 H FID as a quality parameter. In this Tuning procedure a user-defined group of shims (Z, Z2, X, Y, XZ, and YZ) is examined in an iterative cycle. Each shim in succession is adjusted individually to maximize the area under the FID. This is essentially a linear procedure that works well quickly.

4.3.3. Optimize the RF pulse by maximizing the one-dimensional image profile with adjustment of RF pulse power.

4.3.4. Assign the exact position of the heart in the scanner by making scout scans using a tripilot sequence. Use a fast gradient echo sequence to acquire the scout images through the thorax: a transversal, coronal, and sagittal slice. (**figure 1a,b,c**)

4.3.5. Adjust the axes to the actual axes of the axial, two-chamber, and four-chamber view (**figure 1d,e**).

4.3.6. Subsequently, position the cine slices perpendicular to an imaginary axis between the RV outflow tract and the utmost apical part of the RV.

4.3.7. Derive ten to eleven 1 mm-thick cine slices without a slice gap to cover the entire top to base imaging of the RV (**figure 1f**) by means of the Self-gated IntraGate-fast

low-angle shot (FLASH) method, which obviates the need for an electrocardiogram (ECG) and respiratory gating. The acquisition parameters are displayed in **table 1**. Save the images in DICOM format.

4.4. Performing analyses on acquired images

4.4.1. Double click on the software to open the program.

4.4.2. Open images in the CMR postprocessing software by using the import button.

4.4.3. Identify the end-systolic phase (defined as the phase with the visually smallest RV cavity) and the end-diastolic phase (defined as the phase with the visually largest RV cavity).

4.4.4. According to guidelines from the Society for Cardiovascular Magnetic Resonance[49]cardiovascular magnetic resonance (CMR, draw the epicardial contours manually in end-diastole and end-systole from apex to base, by marking several points at the epicardial border of each image. At the last point, double click to complete the epicardial contour.

4.4.5. Do the same for the endocardial contours. (**figure 2**). The left ventricular and right ventricular EDV, ESV, ED mass, and ES mass are now automatically calculated by the software.

NOTE: Mass is defined as myocardial volume times myocardial density (i.e., 1.05).

4.4.6. Depending on the research question and population under study, index these variables for subject size by means of tibia length or body weight, according to previously published formulas[50].

4.4.7. Calculate the eccentricity index (EI) both in end-diastole and end-systole, by dividing the diameter of the LV cavity parallel to the intraventricular septum (IVS) by the diameter of the LV cavity perpendicular to the IVS, derived from the short axis at midpapillary level.

4.4.8. The software calculates the stroke volume (SV) in mL as *SV=EDV-ESV,* and ejection fraction (EF, %) as . $\mathrm{EF} = 100 * \frac{EDV - ESV}{EDV}$

4.4.9. Calculate the cardiac output (CO) in ml/min as . The heart rate is measured manually by the pressure pad embedded in the animal bed as described above, because the scanner is not able to register the high frequent heart rate adequately.

4.4.10. Depending on the research question and population under study, index the CO and SV for subject size by means of tibia length or body weight, according to

previously published formulas[50].

5. Statistical analyses

5.1. Open the software used for data visualization and statistical analyses.

5.2. Sort the data per group (PAB and sham) with every group in a separate column.

5.3. Use the Mann-Whitney test to compare PAB versus sham for every variable.

REPRESENTATIVE RESULTS

Mortality rate of the PAB surgical procedure is around 10%. The presented results show characteristics of mice in the sham (n = 5) and PAB (n = 8) groups. As shown in **figure 3**, PAB gradient values significantly increased compared to sham animals at 2 and 6 weeks after PAB. This increase of loading caused RV dilatation expressed as increased RV, EDV, and RV ESV (**figure 4a,b**). RV dysfunction occurred as RV EF decreased (**figure 4c**). RV SV remained unaffected (**figure 4d**). RV ED and RV ES mass increased, indicating right ventricular hypertrophy (**figure 4e,f**). LV EDV and LV ESV decreased (**figure 4g,h**). LV function in terms of LV EF and LV SV was unaffected (**Figure 4i,j**). Neither LV ED or LV ES mass changed (**Figure 4k,l**). Septal flattening at both end-diastole and end-systole occurred, reflected by significant decreases of both eccentricity indexes (**figure 4m,n**). Heart rate and SV were not different between PAB and sham animals and thus CO was unaffected (**figure 4p,q**). **Figure 4o** shows representative CMR images at midpapillary level, in end-diastole (top) and end-systole (below) in sham (left) and PAB (right).

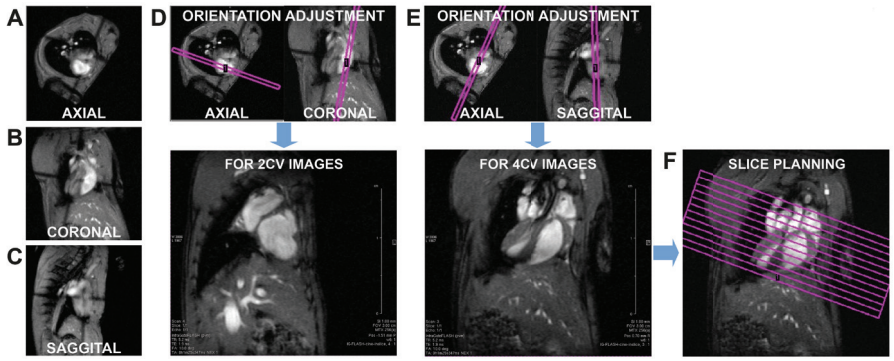

Figure 1. Slice orientation and planning. (A) Axial scout image, (B) coronal scout image, and (C) sagittal scout image. (D) Adjustment of the orientation slice for a two-chamber view (2CV) image. (E) Adjustment of the orientation slice for a four-chamber view (4CV) image. (F) Slice planning for cardiac cine imaging.

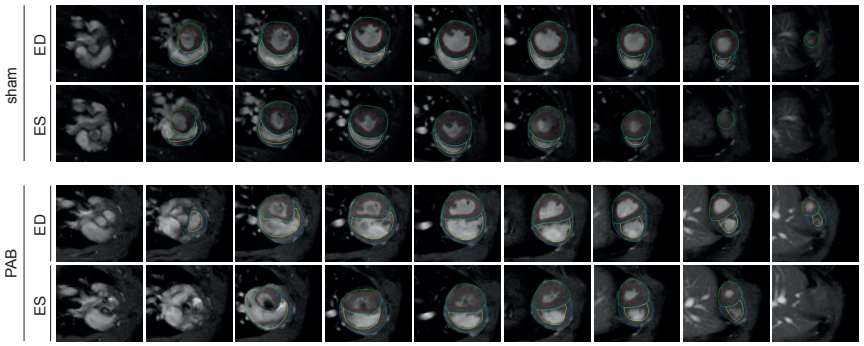

Figure 2. CMR quantification. For quantification, the endocardial (red for LV, yellow for RV) and epicardial (green for LV, blue for RV) contours were delineated in end-diastole (ED, top) and end-systole (ES, bottom) in a stack of short axis slices that covered both ventricles. These are shown in a sham and a pulmonary artery banding (PAB) mouse.

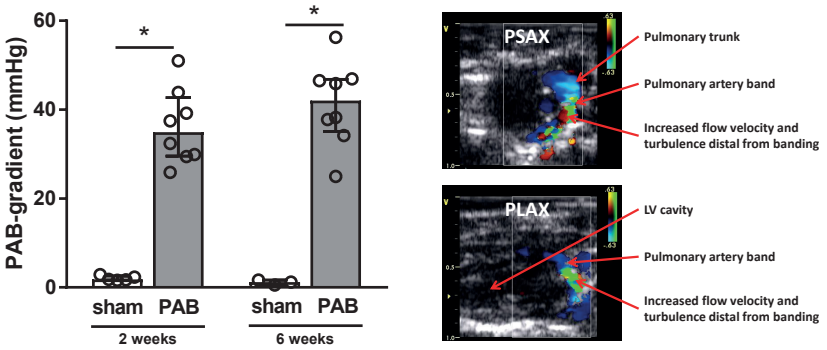

Figure 3. PAB gradient measured by Doppler echocardiography. Measurements were performed at 2 and 6 weeks respectively in the sham (n = 5) and pulmonary artery banding (PAB, n = 8) groups. The statistical analyses were performed using the Mann-Whitney test. Values are presented as median and interquartile range. * = $p < 0.05$ compared to sham. = individual animal. PSAX = parasternal short axis. PLAX = parasternal long axis. LV = left ventricle.

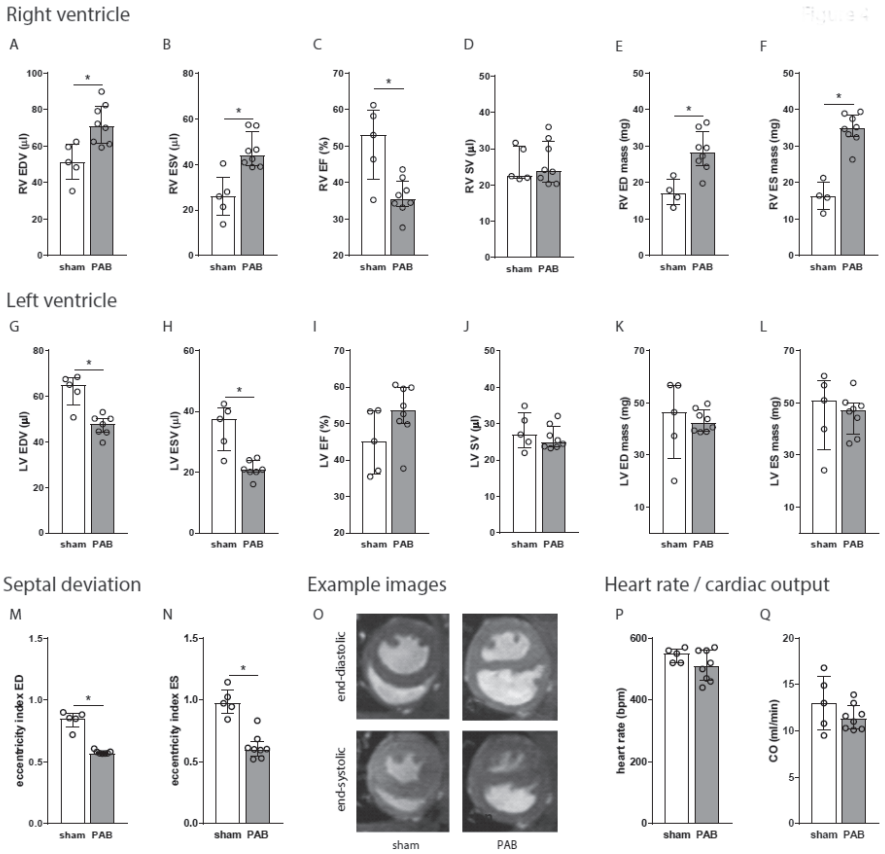

Figure 4. Representative results of morphological and functional changes. The first panel shows RV parameters: RV EDV (A), RV ESV (B), RV EF (C), RV ED mass (E), and RV ES mass (F). The LV parameters are shown in the second panel: LV EDV (G), LV ESV (H), LV EF (I), LV SV (J), LV ED mass (K), and LV ES mass (L). Septal deviation is represented by the eccentricity index ED (M) and ES (N). Cardiac dimensions are shown in representative images (O). Heart rate (P) and cardiac output (Q) are also shown. The changes were observed due to 6 weeks of PAB measured by CMR in the sham (n = 5) and pulmonary artery banding (PAB, n = 8) groups. The statistical analyses were performed using the Mann-Whitney test. Values are presented as median and interquartile range. * = $p < 0.05$ compared to sham. = individual animal. RV = right ventricle. LV = left ventricle. ED = end diastolic. ES = end systolic. EDV = ED volume. ESV = ES volume. SV = stroke volume. CO = cardiac output. EF = ejection fraction.

Table 1. Acquisition parameters of the CMR protocol.

Echo time (ms)	1.286
Repetition time (ms)	9.226
Radiofrequency pulse (ms)	0.300
Flip angle (degrees)	10
Spectral width (Hz)	75,757
Echo position (%)	20
Acquisition matrix	256 x 128
Reconstructed matrix	256 x 256
In-plane resolution (μm)	117x117
Averages	8
Frames per heart beat	15
Slice thickness (mm)	1
Navigator points	256
Acquisition time per slice (s)	120

DISCUSSION

This protocol provides a reproducible method for PAB in mice and the subsequent assessment of cardiac remodelling and functional adaptation using CMR.

PAB differs from other models of increased RV pressure load because it involves absolute and static increase of afterload without the presence of other triggers. RV pressure load in models of hypoxia, monocrotaline, shunt, or a combination of these inducers are based on remodelling of the pulmonary vasculature. This remodelling is driven by endothelial damage, inflammation, cytokine migration, and vasoconstriction. The degree of these processes differs per model, therefore the degree of pressure load differs subsequently. In contrast to these models, PAB induces fixed RV afterload and is therefore reproducible and not affected by therapeutic interventions. This allows for the study of interventions targeting the pressure-loaded RV without affecting the RV afterload. This model of PAB in mice shows a significant gradient across the PAB and enables evaluation of this substantial pressure load.

Dimensional evaluation by echocardiography is challenging due to the triangular shape of the RV wrapped around the LV, and its position immediately behind the sternum[41,42]. Echocardiography, both 2D and 3D, has shown to be inferior compared to CMR[51,52]. In pediatric cohorts with congenital heart diseases, echocardiographic volumetry shows lower reliability and systematic underestimation compared to

CMR[53,54]. Results regarding myocardial deformation measurements are still preliminary in this specific group of patients[55–57]. Of course, in clinical practice, echocardiography is a very accessible tool to identify abnormal loading conditions by recognition of shunts and valve insufficiencies in case of volume load, and stenosis and pulmonary hypertension by increased gradients and septal flattening in case of pressure load. Pressure-volume analysis by means of invasive heart catheterization is an available alternative for invasive hemodynamic and functional assessments. This technique is widely regarded indicative for load-independent ventricular function, but also comes with limitations that currently hamper the theoretical benchmark status of PV-loops in RV in small animals. For example, deriving reproducible and accurate volume and flow measurements is challenging in these small animals and many procedures require open-chest measurements. Furthermore, serial assessments are difficult if not unfeasible due to the invasive nature of the technique. Compared to both echocardiography and catheterization, assessment of volumes and function will be more accurate with CMR. In research, it is important for translatability to obtain results using modalities that can also be used for clinical practice. Therefore, development of standardized methods and optimization in experimental protocols is highly relevant.

The current protocol describes the use of self-gated CMR, which obviates the need for ECG triggering and respiratory gating. This method has been described previously in a report from the same institution, demonstrating good intra- and interobserver variability[58]for example, a myocardial infarction. Cardiac MRI is often used because it is noninvasive and provides high temporal and spatial resolution for the left and right ventricle. In animal cardiac MRI, the quality of the required electrocardiogram signal is variable and sometimes deteriorates over time, especially with infarcted hearts or cardiac hypertrophy. Therefore, we compared the self-gated IntraGateFLASH method with a prospectively triggered FLASH (fast low-angle shot. Another method that could be used if the self-gated method is unavailable, is prospective ECG triggering. However, a previous report from this institution demonstrated that the self-gated method provides less variability, better signal and contrast-to-noise ratios, and less arrhythmia-induced artifacts. Therefore, we recommend using the self-gated method, as stated in the current protocol.

Accurate assessment of RV pressure load is crucial in order to validate the PAB model. This can be performed by means of invasive heart catheterization, for example. However, disadvantages of such invasive procedures are that they are very hazardous and complex to perform serially or during the follow-up time of the study and are therefore generally performed just before termination. However, at termination, RV pressure is not only dependent on the tightness of the banding but becomes increasingly dependent on RV function. Whenever RV

failure occurs within the duration of PAB, as measured by decreased cardiac output, RV systolic pressure will decrease, biasing results. Such biases can be avoided or minimized by assessing RV pressure load at 2 weeks after PAB surgery, instead of at termination. By means of echocardiography, assessment of RV afterload at this time point can be performed reliably and safely. This allows grouping of the mice into groups with equal pressure load, which could be helpful for intervention studies. Also, repeated measurements are easily feasible.

The most critical step in the surgical protocol is the separation of the arteria pulmonalis from the aorta and the subsequent placement of the suture loop. This has to be performed gently in order not to cause any rupture, because this would result in fatal bleeding. PAB in mice requires that well-trained microsurgeons perform the actual banding, including knotting the suture, which should be done very carefully.

The current model aims to generate chronic RV pressure load, resulting in RV remodelling, RV dysfunction, and eventually RV failure. Therefore, adequate tightening of the PAB is important. During the development of the model, it has become apparent that small differences in tightness of the banding significantly affected the profile of RV adaptation: e.g., the use of a 25 G needle appeared to be "too tight", as it induced high rates of mortality during surgery. Needles <23 G were "too loose", as they did not induce the desired phenotype of RV remodelling and dysfunction.

The most critical step in the echocardiographic examination is adequate measurement of pulmonary flow velocity (step 3.3.7). One has to make sure that the angle of the probe is correct: the pulmonary artery has to be exactly vertically visible within the image. Otherwise, flow velocity, and therefore the PAB gradient, are underestimated.

It is important to try to limit the length of time of the procedures during the experiment, especially CMR. Furthermore, when analyzing the CMR images with postprocessing software, the researcher must become familiar with the manual segmentation and postprocessing guidelines before reproducible results can be obtained.

Using CMR as in the current protocol does not enable assessment of flow velocities over the PAB. Therefore, additional echocardiographic measurements using the Doppler mode are inevitable. Due to the PAB and the subsequent marked increase in PA flow, the signal is very clear, making determination of the PAB gradient by echocardiography convenient and reproducible. Notwithstanding, the extra echocardiographic measurements may involve more logistical arrangements. In general, inclusion or exclusion of papillary muscles and trabeculae affects volumes and subsequent functional parameters. Here, we chose to include papillary muscles and trabeculae in blood volumes (and thus exclude from myocardial mass) which

may underestimate the ejection fraction. Furthermore, the current protocol focuses on parameters used in clinical practice, representing global function. Parameters such as the tricuspid annular plane systolic excursion (TAPSE), fractional septum to free wall distance at the middle of the RV (fSFD), and fractional tricuspid annulus-apex distance change (fTAAD) were not analyzed.

A major advantage of CMR is the ability to perform noninvasive, serial testing within one subject with a relatively high accuracy of volumetric and functional measurements. Because it is a measurement after which the animal can survive, unlike open-chest pressure-volume analysis, for example, it allows for a follow-up after the measurements. Although we have focused on cardiac dimensions and function, future uses of this technique include CMR-derived tissue characterization or scar tissue assessment by means of late gadolinium enhancement. This enables reduction of histopathological assessments, which will lead to a reduction in animals required for studies. More CMR research may optimize tissue characterization in humans and reduce iatrogenic damage due to biopsies.

In conclusion, this protocol was created to provide guidance in the assessment of cardiac morphology and function in mice exposed to increased RV pressure load. The combination of PAB with CMR improves standardization and reproducibility. This makes it a very valuable technique for the study of signaling pathways involved in the failure of the pressure-loaded RV by the use of transgenic or knockout mice.

ACKNOWLEDGMENTS

We would like to thank P. Da Costa-Martins for her support with the animal experiments in this study.

DISCLOSURES

The University Medical Center Groningen has contracted with Actelion and Lilly for consultancy activities of R.M.F. Berger outside the content of this manuscript. The other authors declare that they have no competing interests.

REFERENCES

1. Norozi K, Wessel A, Alpers V, Arnhold JO, Geyer S, Zoege M, Buchhorn R. Incidence and Risk Distribution of Heart Failure in Adolescents and Adults With Congenital Heart Disease After Cardiac Surgery. *Am J Cardiol* 2006;97:1238–1243.
2. Borgdorff MAJ, Koop AMC, Bloks VW, Dickinson MG, Steendijk P, Sillje HHW, Wiechen MPH van, Berger RMF, Bartelds B. Clinical symptoms of right ventricular failure in experimental chronic pressure load are associated with progressive diastolic dysfunction. *J Mol Cell Cardiol* Elsevier Ltd; 2015;79:244–253.
3. Koop AMC, Hagdorn QAJ, Bossers GPL, Leusden T van, Gerding A, Weeghel M van, Vaz FM, Koonen DPY, Silljé HHW, Berger RMF, Bartelds B. Right ventricular pressure overload alters cardiac lipid composition. *Int J Cardiol* Elsevier B.V.; 2019;
4. Faber MJ, Dalinghaus M, Lankhuizen IM, Steendijk P, Hop WC, Schoemaker RG, Duncker DJ, Lamers JM, Helbing WA. Right and left ventricular function after chronic pulmonary artery banding in rats assessed with biventricular pressure-volume loops. *Am J Physiol Hear Circ Physiol* 2006;291:H1580-6.
5. Bogaard HJ, Natarajan R, Henderson SC, Long CS, Kraskauskas D, Smithson L, Ockaili R, McCord JM, Voelkel NF. Chronic pulmonary artery pressure elevation is insufficient to explain right heart failure. *Circulation* 2009;120:1951–1960.
6. Samson N, Paulin R. Epigenetics, inflammation and metabolism in right heart failure associated with pulmonary hypertension. *Pulm Circ* 2017;7:572–587.
7. Rumsey WL, Abbott B, Bertelsen D, Mallamaci M, Hagan K, Nelson D, Erecinska M. Adaptation to hypoxia alters energy metabolism in rat heart. *Am J Physiol - Hear Circ Physiol* W.L. Rumsey, Zeneca Pharmaceuticals, Wilmington, DE 19850-5437, United States; 1999;276:H71–H80.
8. Drozd K, Ahmadi A, Deng Y, Jiang B, Petryk J, Thorn S, Stewart D, Beanlands R, DeKemp RA, DaSilva JN, Mielniczuk LM. Effects of an endothelin receptor antagonist, Macitentan, on right ventricular substrate utilization and function in a Sugen 5416/hypoxia rat model of severe pulmonary arterial hypertension. *J Nucl Cardiol* L.M. Mielniczuk, Division of Cardiology, Department of Medicine, University of Ottawa Heart Institute, Ottawa, Canada; 2016;1–11.
9. Gomez-Arroyo J, Mizuno S, Szczepanek K, Tassell B Van, Natarajan R, Remedios CG Dos, Drake JI, Farkas L, Kraskauskas D, Wijesinghe DS, Chalfant CE, Bigbee J, Abbate A, Lesnefsky EJ, Bogaard HJ, Voelkel NF. Metabolic gene remodeling and mitochondrial dysfunction in failing right ventricular hypertrophy secondary to pulmonary arterial hypertension. *Circ Hear Fail* N.F. Voelkel, Victoria Johnson Center for Lung Obstructive Disease Research, Virginia Commonwealth University, Richmond, VA 23298, United States; 2013;6:136–144.
10. Bruns DR, Dale Brown R, Stenmark KR, Buttrick PM, Walker LA. Mitochondrial integrity in a neonatal bovine model of right ventricular dysfunction. *Am J Physiol - Lung Cell Mol Physiol* L.A. Walker, Univ. of Colorado-Denver, Dept. of Medicine, Cardiology, Aurora, United States; 2015;308:L158–L167.
11. Zhang W-H, Qiu M-H, Wang X-J, Sun K, Zheng Y, Jing Z-C. Up-regulation of hexokinase1 in the right ventricle of monocrotaline induced pulmonary hypertension. *Respir Res* Y. Zheng, First Hospital of Jilin University, Center of Cardiovascular Disease, Changchun, China; 2014;15.

12. Paulin R, Sutendra G, Gurtu V, Dromparis P, Haromy A, Provencher S, Bonnet S, Michelakis ED. A miR-208-Mef2 axis drives the decompensation of right ventricular function in pulmonary hypertension. *Circ R*es 2015;116:56–69.
13. Sutendra G, Dromparis P, Paulin R, Zervopoulos S, Haromy A, Nagendran J, Michelakis ED. A metabolic remodeling in right ventricular hypertrophy is associated with decreased angiogenesis and a transition from a compensated to a decompensated state in pulmonary hypertension. *J Mol Med* E.D. Michelakis, Department of Medicine, University of Alberta, Edmonton, AB T6G 2B7, Canada; 2013;91:1315–1327.
14. Balestra GM, Mik EG, Eerbeek O, Specht PAC, Laarse WJ van der, Zuurbier CJ. Increased in vivo mitochondrial oxygenation with right ventricular failure induced by pulmonary arterial hypertension: Mitochondrial inhibition as driver of cardiac failure? *Respir Res* C.J. Zuurbier, Department of Anesthesiology, Laboratory of Experimental Intensive Care and Anesthesiology, AMC, Amsterdam, Netherlands; 2015;16.
15. Piao L, Fang YH, Cadete VJJ, Wietholt C, Urboniene D, Toth PT, Marsboom G, Zhang HJ, Haber I, Rehman J, Lopaschuk GD, Archer SL. The inhibition of pyruvate dehydrogenase kinase improves impaired cardiac function and electrical remodeling in two models of right ventricular hypertrophy: Resuscitating the hibernating right ventricle. *J Mol Med* 2010;88:47–60.
16. Piao L, Sidhu VK, Fang Y-H, Ryan JJ, Parikh KS, Hong Z, Toth PT, Morrow E, Kutty S, Lopaschuk GD, Archer SL. FOXO1-mediated upregulation of pyruvate dehydrogenase kinase-4 (PDK4) decreases glucose oxidation and impairs right ventricular function in pulmonary hypertension: therapeutic benefits of dichloroacetate. *J Mol Med* S.L. Archer, Department of Medicine, Queen's University Kingston, Kingston, K7L 3N6, ON, Canada; 2013;91:333–346.
17. Feen DE Van Der, Weij M, Smit-Van Oosten A, Jorna LM, Hagdorn QAJ, Bartelds B, Berger RMF. Shunt surgery, right heart catheterization, and vascular morphometry in a rat model for flow-induced pulmonary arterial hypertension. *J Vis Exp* 2017;2017:1–11.
18. Sheikh AM, Barrett C, Villamizar N, Alzate O, Valente AM, Herlong JR, Craig D, Lodge A, Lawson J, Milano C, Jaggers J. Right ventricular hypertrophy with early dysfunction: A proteomics study in a neonatal model. *J Thorac Cardiovasc Surg* A.M. Sheikh, Department of Pediatric Cardiac Surgery, the Neuroproteomics Center, Durham, NC, United States; 2009;137:1146–1153.
19. Olivetti G, Ricci R, Lagrasta C, Maniga E, Sonnenblick EH, Anversa P. Cellular basis of wall remodeling in long-term pressure overload-induced right ventricular hypertrophy in rats. *Circ Res* Department of Pathology, University of Parma, 43100 Parma; 1988;**63**:648–657.
20. Lauva IK, Brody E, Tiger E, Kent RL, Copper G 4th, Marino TA. Control of myocardial tissue components and cardiocyte organelles in pressure-overload hypertrophy of the cat right ventricle. *Am J Anat* United States; 1986;177:71–80.
21. Fang Y-H, Piao L, Hong Z, Toth PT, Marsboom G, Bache-Wiig P, Rehman J, Archer SL. Therapeutic inhibition of fatty acid oxidation in right ventricular hypertrophy: Exploiting Randle's cycle. *J Mol Med* S.L. Archer, Medicine/Cardiology, University of Chicago, Chicago, IL 60637, United States; 2012;90:31–43.
22. Piao L, Fang Y-H, Parikh K, Ryan JJ, Toth PT, Archer SL. Cardiac glutaminolysis: A maladaptive cancer metabolism pathway in the right ventricle in pulmonary hypertension. *J Mol Med* S.L. Archer, Department of Medicine, Queen's University, Etherington Hall,

Kingston, ON K7L 3N6, Canada; 2013;91:1185–1197.

23. Sack MN, Disch DL, Rockman HA, Kelly DP. A role for Sp and nuclear receptor transcription factors in a cardiac hypertrophic growth program. *Proc Natl Acad Sci U S A* D.P. Kelly, Center for Cardiovascular Research, Box 8086, Washington Univ. Sch. of Medicine, St. Louis, MO 63110, United States; 1997;**94**:6438–6443.
24. Broderick TL, King TM. Upregulation of GLUT-4 in right ventricle of rats with monocrotaline-induced pulmonary hypertension. *Med Sci Monit* T. L. Broderick, Department of Physiology, Midwestern University, Glendale, AZ 85308, United States; 2008;14:BR261–BR264.
25. Enache I, Charles A-L, Bouitbir J, Favret F, Zoll J, Metzger D, Oswald-Mammosser M, Geny B, Charloux A. Skeletal muscle mitochondrial dysfunction precedes right ventricular impairment in experimental pulmonary hypertension. *Mol Cell Biochem* I. Enache, Service de Physiologie et d'Explorations Fonctionnelles, Pôle de Pathologie Thoracique, Centre Hospitalier Universitaire Strasbourg, Nouvel Hôpital Civil, 67091 Strasbourg, France; 2013;373:161–170.
26. Sun X-Q, Zhang R, Zhang H-D, Yuan P, Wang X-J, Zhao Q-H, Wang L, Jiang R, Jan Bogaard H, Jing Z-C. Reversal of right ventricular remodeling by dichloroacetate is related to inhibition of mitochondria-dependent apoptosis. *Hypertens Res* Z.-C. Jing, State Key Laboratory of Cardiovascular Disease, Fu Wai Hospital, National Center for Cardiovascular Disease, Peking Union Medical College, Chinese Academy Medical Science, Beijing, China; 2016;39:302–311.
27. Adrogue J V, Sharma S, Ngumbela K, Essop MF, Taegtmeyer H. Acclimatization to chronic hypobaric hypoxia is associated with a differential transcriptional profile between the right and left ventricle. *Mol Cell Biochem* H. Taegtmeyer, Department of Internal Medicine, Division of Cardiology, University of Texas Houston - Medical School, Houston, TX 77030, United States; 2005;278:71–78.
28. Sharma S, Taegtmeyer H, Adrogue J, Razeghi P, Sen S, Ngumbela K, Essop MF. Dynamic changes of gene expression in hypoxia-induced right ventricular hypertrophy. *Am J Physiol - Hear Circ Physiol* H. Taegtmeyer, Dept. of Internal Medicine, Division of Cardiology, Univ. of Texas-Houston Med. School, Houston, TX 77030, United States; 2004;286:H1185–H1192.
29. Nouette-Gaulain K, Malgat M, Rocher C, Savineau J-P, Marthan R, Mazat J-P, Sztark F. Time course of differential mitochondrial energy metabolism adaptation to chronic hypoxia in right and left ventricles. *Cardiovasc Res* F. Sztark, Laboratoire d'Anesthésiologie, E.A. Physiologie Mitochondriale, Universite Bordeaux 2, 33076 Bordordeaux, France; 2005;66:132–140.
30. Graham BB, Kumar R, Mickael C, Sanders L, Gebreab L, Huber KM, Perez M, Smith-Jones P, Serkova NJ, Tuder RM. Severe pulmonary hypertension is associated with altered right ventricle metabolic substrate uptake. *Am J Physiol - Lung Cell Mol Physiol* B.B. Graham, Division of Pulmonary Sciences and Critical Care Medicine, Univ. of Colorado Denver, Aurora, United States; 2015;309:L435–L440.
31. Liu A, Philip J, Vinnakota KC, Bergh F Van den, Tabima DM, Hacker T, Beard DA, Chesler NC. Estrogen maintains mitochondrial content and function in the right ventricle of rats with pulmonary hypertension. *Physiol Rep* 2017;5:1–12.
32. Kobr J, Slavik Z, Uemura H, Saeed I, Furck A, Pizingerová K, Fremuth J, Tonar Z. Right Ventricular Pressure Overload and Pathophysiology of Growing Porcine Biomodel. *Pediatr Cardiol* 2016;37:1498–1506.

33. Yerebakan C, Klopsch C, Niefeldt S, Zeisig V, Vollmar B, Liebold A, Sandica E, Steinhoff G. Acute and chronic response of the right ventricle to surgically induced pressure and volume overload – an analysis of pressure–volume relations☆. *Interact Cardiovasc Thorac Surg* 2010;10:519–525.
34. Gufler H, Niefeldt S, Boltze J, Prietz S, Klopsch C, Wagner S, Vollmar B, Yerebakan C. Right Ventricular Function After Pulmonary Artery Banding: Adaptive Processes Assessed by CMR and Conductance Catheter Measurements in Sheep. *J Cardiovasc Transl Res* Journal of Cardiovascular Translational Research; 2019;
35. Baicu CF, Li J, Zhang Y, Kasiganesan H, Cooper G, Zile MR, Bradshaw AD. Time course of right ventricular pressure-overload induced myocardial fibrosis: relationship to changes in fibroblast postsynthetic procollagen processing. *Am J Physiol Circ Physio*l 2012;303:H1128–H1134.
36. Manohar M, Parks CM, Busch MA, Tranquilli WJ, Bisgard GE, McPherron TA, Theodorakis MC. Regional myocardial blood flow and coronary vascular reserve in unanesthetized young calves exposed to a simulated altitude of 3500 m for 8-10 weeks. *Circ Res* 1982;50:714–726.
37. Fávaro GAG, Assad RS, Abduch MCD, Silva GJJ, Gomes GS, Andrade JL, Krieger JE, Moreira LFP. Reversible pulmonary trunk banding: VII. Stress echocardiographic assessment of rapid ventricular hypertrophy in young goats. *J Thorac Cardiovasc Surg* 2013;145.
38. Nielsen EA, Okumura K, Sun M, Hjortdal VE, Redington AN, Friedberg MK. Regional septal hinge-point injury contributes to adverse biventricular interactions in pulmonary hypertension. *Physiol Rep* 2017;5:1–13.
39. Borgdorff M a J, Bartelds B, Dickinson MG, Boersma B, Weij M, Zandvoort A, Silljé HHW, Steendijk P, Vroomen M De, Berger RMF. Sildenafil enhances systolic adaptation, but does not prevent diastolic dysfunction, in the pressure-loaded right ventricle. *Eur J Heart Fail* 2012;14:1067–1074.
40. Gold H, Prindle K, Levey G, Epstein S. Effects of experimental heart failure on the capacity of glucagon to augment myocardial contractility and activate adenyl cyclase. *J Clin Invest* 1970;49:999–1006.
41. Brittain EL, Hemnes AR, Keebler M, Lawson M, Byrd BF, DiSalvo T. Right ventricular plasticity and functional imaging. *Pulm Circ* 2012;2:309–326.
42. Jiang L, Siu SC, Handschumacher MD, Guererro JL, Antonio J, Prada V De, King ME, Picard MH, Weyman AE, Levine RA. Three-dimensional Echocardiography In Vivo Validation for Right Ventricular Volume and Function. 1994;89:2342–2350.
43. Markiewicz W, Sechtem U, Higgins CB. Evaluation of the right ventricle by magnetic resonance imaging. *Am Heart J* 1987;113:8–15.
44. Pattynama PMT, Lamb HJ, Velde EA Van der, Geest RJ Van der, Wall EE Van der, Roos A De. Reproducibility of MRI-derived measurements of right ventricular volumes and myocardial mass. *Magn Reson Imaging* 1995;13:53–63.
45. Wiesmann F, Gatehouse PD, Panting JR, Taylor AM, Firmin DN, Pennell DJ. Comparison of fast spiral, echo planar, and fast low-angle shot MRI for cardiac volumetry at .5T. *J Magn Reson Imaging* 1998;8:1033–1039.
46. Feen DE Van der, Kurakula K, Tremblay E, Boucherat O, Bossers GP, Szulcek R, Bourgeois A, Lampron M-C, Habbout K, Martineau S, Paulin R, Kulikowski E, Jahagirdar R, Schalij I,

Bogaard HJ, Bartelds B, Provencher S, Berger RMF, Bonnet S, Goumans M-J. Multicenter Preclinical Validation of BET Inhibition for the Treatment of Pulmonary Arterial Hypertension. *Am J Respir Crit Care Med* 2019;rccm.201812-2275OC.

47. Costa Martins PA da, Salic K, Gladka MM, Armand A-S, Leptidis S, Azzouzi H el, Hansen A, Coenen-de Roo CJ, Bierhuizen MF, Nagel R van der, Kuik J van, Weger R de, Bruin A de, Condorelli G, Arbones ML, Eschenhagen T, Windt LJ De. MicroRNA-199b targets the nuclear kinase Dyrk1a in an auto-amplification loop promoting calcineurin/NFAT signalling. *Nat Cell Biol* Nature Publishing Group; 2010;12:1220–1227.
48. Cheng H-W, Fisch S, Cheng S, Bauer M, Ngoy S, Qiu Y, Guan J, Mishra S, Mbah C, Liao R. Assessment of right ventricular structure and function in mouse model of pulmonary artery constriction by transthoracic echocardiography. *J Vis Exp* 2014;e51041.
49. Schulz-Menger J, Bluemke DA, Bremerich J, Flamm SD, Fogel MA, Friedrich MG, Kim RJ, Knobelsdorff-Brenkenhoff F Von, Kramer CM, Pennell DJ, Plein S, Nagel E. Standardized image interpretation and post processing in cardiovascular magnetic resonance: Society for Cardiovascular Magnetic Resonance (SCMR) Board of Trustees Task Force on Standardized Post Processing. *J Cardiovasc Magn Reson* 2013;15:1–19.
50. Hagdorn QAJ, Bossers GPL, Koop AMC, Piek A, Eijgenraam TR, Feen DE van der, Silljé HHW, Boer RA de, Berger RMF. A novel method optimizing the normalization of cardiac parameters in small animal models: The importance of dimensional indexing. *Am J Physiol - Hear Circ Physi*ol 2019;316:H1552–H1557.
51. Scherrer-Crosbie M, Steudel W, Hunziker PR, Foster GP, Garrido L, Liel-Cohen N, Zapol WM, Picard MH. Determination of Right Ventricular Structure and Function in Normoxic and Hypoxic Mice. *Circulati*on 2012;98:1015–1021.
52. Wiesmann F, Frydrychowicz A, Rautenberg J, Illinger R, Rommel E, Haase A, Neubauer S. Analysis of right ventricular function in healthy mice and a murine model of heart failure by in vivo MRI. *Am J Physiol Circ Physiol* 2002;283:H1065–H1071.
53. Lu X, Nadvoretskiy V, Bu L, Stolpen A, Ayres N, Pignatelli RH, Kovalchin JP, Grenier M, Klas B, Ge S. Accuracy and Reproducibility of Real-Time Three-Dimensional Echocardiography for Assessment of Right Ventricular Volumes and Ejection Fraction in Children. *J Am Soc Echocardiogr* 2008;21:84–89.
54. Soriano BD, Hoch M, Ithuralde A, Geva T, Powell AJ, Kussman BD, Graham DA, Tworetzky W, Marx GR. Matrix-array 3-dimensional echocardiographic assessment of volumes, mass, and ejection fraction in young pediatric patients with a functional single ventricle: A comparison study with cardiac magnetic resonance. Circulation 2008;117:1842–1848.
55. Damy T, Kallvikbacka-Bennett A, Goode K, Khaleva O, Lewinter C, Hobkirk J, Nikitin NP, Dubois-Randé JL, Hittinger L, Clark AL, Cleland JGF. Prevalence of, associations with, and prognostic value of tricuspid annular plane systolic excursion (TAPSE) among out-patients referred for the evaluation of heart failure. *J Card Fai*l 2012;18:216–225.
56. Kowalik E, Kowalski M, Rózański J, Kuśmierczyk M, Hoffman P. The impact of pulmonary regurgitation on right ventricular regional myocardial function: An echocardiographic study in adults after total repair of tetralogy of fallot. *J Am Soc Echocardiogr* 2011;24:1199–1204.
57. Koestenberger M, Nagel B, Ravekes W, Everett AD, Stueger HP, Heinzl B, Sorantin E, Cvirn G, Fritsch P, Gamillscheg A. Systolic right ventricular function in pediatric and adolescent patients with tetralogy of Fallot: Echocardiography versus magnetic resonance imaging. *J Am Soc Echocardiogr* Elsevier Inc; 2011;24:45–52.

58. Bovens SM, Boekhorst BCM te, Ouden K den, Kolk KWA van de, Nauerth A, Nederhoff MGJ, Pasterkamp G, Hove M ten, Echteld CJA van. Evaluation of infarcted murine heart function: Comparison of prospectively triggered with self-gated MRI. *NMR Biomed* 2011;24:307–315.

Supplemental table. Table of materials

Name of Material/ Equipment	Company	Catalog Number	Comments/ Description
Anesthesia induction chamber			
Isoflurane			
Isoflurane evaporator			
Ventilation mask			
20G cannula			
Heat mat			
Miniventilator for rodents	Hugo Sachs	model 687	
Buprenorphine			
Needle and syringe for subcutaneous injections			
Chloride-hexidine			
Sterile surgical instruments			
Blunt 25G needle			
monofilament polypropylene 6-0 sutures			
23G needle			
monofilament polypropylene 5-0 sutures			
pure polyglycolic acid 5-0 sutures			
Incubator (37˚C)			
Echocardiography machine	GE Healthcare, Waukesha, WI, USA		Vivid Dimension 7
14.0 MHz echocardiography transducer	GE Healthcare, Waukesha, WI, USA		
9.4T magnetic resonance scanner with 1,500 mT/m gradient set	Bruker BioSpin, Ellingen, Germany		
CMR post-processing software	Medis Medical Imaging Systems, Leiden, The Netherlands		Qmass version 7.6
Data visualisation and statistical software	GraphPad Prism Inc, La Jolla, CA, USA		software version 7.02
Eye ointment			
Pediatric electrocardiogram-stickers			

6

CHAPTER 6

Increased mir-199b expression contributes to right and left ventricular remodelling in a mouse model of right ventricular pressure overload

A.M.C. Koop*, R. F. Videira*, B. Duygu, L. Ottaviani, E. M. Poels, S. Leite, K. W. A. van de Kolk, G. J. du Marchie Sarvaas, B. Bartelds, A. P. Lourenço, D. S. Nascimento, P. Pinto-do-Ó, I. Falcão- Pires, M. J. Goumans, R.M.F. Berger, P. A. da Costa Martins
- Under revision, Journal of Molecular and Cellular Cardiology.

* These authors have equally contributed to the manuscript.

ABSTRACT

Background and aims

Despite its association with high mortality and morbidity, research on the pathophysiology of right ventricle (RV) failure has remained behind in regard to the left ventricle (LV). Similar to what happens in the LV, upon chronic pressure overload induced by pulmonary artery banding (PAB), calcineurin activation also contributes to RV remodelling. We have previously identified miR-199b as a pro-hypertrophic microRNA during LV remodelling that, in response to pressure overload, induces calcineurin/NFAT-signaling activity leading to exaggerated LV remodelling and cardiac dysfunction. In this study, we aimed at understanding the contribution of miR-199b to RV remodelling in response to pressure overload induced by pulmonary artery banding (PAB).

Methods and results

In the present study, wild-type (WT) and transgenic (TG) mice with cardiac-specific overexpression of miR-199b were subjected to six weeks of RV pressure overload induced by PAB. Echocardiographic and MRI derived hemodynamic parameters, and molecular remodelling were assessed for experimental groups and compared to sham-operated controls. Six weeks after PAB, levels of miR-199b increased in both WT and TG mice, resulting in significant differences in Nppb, Acta1 and Myh6 expression. The significantly higher miR-199b levels in the TG mice did not influence the Fulton index, but did result in higher relative cardiomyocyte surface area. RV function tended to be worse for TG mice, demonstrated by the inverse correlation for cardiac output and RV ejection fraction with miR-199b expression. Not only the RV was affected by RV pressure overload, but also LV remodelling showed extensive differences at the molecular level between WT and TG mice. Differently, in the LV, miR-199b overexpression was accompanied by decreased Dyrk1a and increased Rcan1-4 expression as previously described in LV pressure overload. Although miR-199b-induced calcineurin/NFAT activation mediates the inhibition of Dyrk1a in the LV, this does not apply for the pressure-loaded RV.

Conclusions

Increased expression levels of miR-199b in cardiomyocytes were associated with impaired RV function in RV pressure overload, whereas increased miR-199b expression without RV pressure overload was not sufficient to worsen RV function. In the LV, contrarily to the RV, upregulation of miR-199b in the LV leads Dyrk1a inhibition and activation of calcineurin/NFAT signaling, increasing LV susceptibility to RV stress. Altogether, these findings suggest a less prominent role for miR-199b in the RV compared to LV.

INTRODUCTION

Sustained pressure overload of the right ventricle (RV) is a major pathophysiological factor in several cardiovascular disorders, including pulmonary hypertension (PH).[1-3] It is noteworthy that RV failure due to pressure overload is the main determinant of the outcome of congenital heart diseases[4] and the most common cause of death in patients with severe pulmonary artery hypertension (PAH). Persistently increased RV afterload will eventually culminate in RV hypertrophy. Hypertrophic cardiac growth is believed to be an initial beneficial response to reduce wall stress, improve contractility, preserve cardiac output[5,6] and enhance capillary density in order to comply with the increased oxygen demand in the hypertrophied tissue.[7] However, as the disease progresses, the transition from RV adaptation to failure is inevitable.[3] RV failure, characterized as a progressive decrease in cardiac output, is accompanied by increased contractility, decreased diastolic function, and pathologic changes in capillary density and fibrosis.[8-10]

Notwithstanding its worse prognosis, the impact of right ventricular function on the outcome of cardiovascular diseases has been neglected due to its less obvious involvement in disease processes. As a consequence of being connected to low impedance pulmonary circulation, the RV has thinner walls, lower oxygen demand and lower wall stress compared to the LV.[11] Therefore, even minor alterations in total pulmonary resistance may have a great impact on RV function in contrast to LV, which is less affected by larger changes in afterload.[12,13]

The differences between the two ventricles range from molecular to structural and functional levels, and start as soon as cardiac embryonic development initiates. The primary heart field, by expressing T-box transcription factor 5 (Tbx5) and Heart- and neural crest derivatives-expressed protein 1 (Hand1), gives origin to the LV and the atria. Meanwhile, the secondary heart field leads to the development of the RV and RV outflow tract through expression of crucial RV-fate genes such as Heart- and neural-crest derivatives-expressed protein 2 (Hand2), Islet1 (Isl1) and fibroblast growth factor-10 (Fgf10).[14] These differences persist in to the adult heart and, because the healthy adult RV is connected to low-pressure high-volume system and the LV is associated with high-pressure system, during injury the RV is more sensitive to volume overload whereas the LV is more prone to pressure overload.[15]

Although RV and LV share common features of maladaptive remodelling such as hypertrophy, capillary rarefaction and fibrosis, they demonstrate particular types of hypertrophic growth. For example, RV pathological remodelling is usually associated with an eccentric hypertrophy (new sarcomeres are added *in-series*) and LV remodelling is commonly manifested by a concentric hypertrophy (new sarcomeres are added *in-parallel*).[16] Interestingly, pathological RV remodelling

seems to be reversible to some extent, as lung transplantation often results in decreased pulmonary pressure, smaller RV and normalized septal shape.[17-19] The functional and structural differences between RV and LV highlight the fact that the current comprehensive knowledge on LV function and pathology cannot be directly applied to RV and that a better understanding of RV function and RV failure pathology is crucial in order to develop efficient and specific therapeutics for this cardiac condition.

PAH is a complex disease with several etiologies and its remodelling can result from the interaction of different factors such as genetic background, epigenetic modifications and pathobiological environmental factors.[20] In the past decade, microRNAs emerged as small, non-coding RNA molecules with the ability to repress or degrade mRNAs and thereby to regulate gene expression during various cellular processes, in many different tissues, including the myocardium.[21] Numerous studies have elucidated the role of microRNAs throughout cardiovascular development and remodelling.[22,23] Abnormal expression and dysregulation of numerous miRNAs have been associated to the onset and development of PAH.[24-27] As most studies focus on the vascular alterations and presently, little is known about the changes in microRNA expression patterns in the RV upon remodelling. Nevertheless, differences between the LV and RV may be explained by miR-expression patterns as the prevalence of specific miRs in the resting RV is quantitatively different from that in the LV, and this difference is maintained during afterload stress.[28] This implies that not only the remodelling process itself but also its regulation may be ventricle-specific. Although the number of studies unraveling such processes in the RV is scarce, a recent report suggested that downregulation of miR-208 is associated with deterioration of RV function, (on MCT-induced PH model.[29] In the damaged RV, nuclear receptor corepressor 1 (NCoR1), a target of miR-208, is activated leading to acetylation of the enhancer factor-2 (Mef2) promotor and thus inhibiting Mef2 expression. During the transition from RV hypertrophy to RV failure, Mef2 inhibition results in suppression of crucial metabolic, angiogenic and contractile adaptation of the RV to pressure overload, rapid RV decompensation and subsequent heart failure.[29]

During LV remodelling, pathological hypertrophy is mediated by calcineurin activation and modulation of the calcineurin-nuclear factor of activated T-cells (NFAT) signaling activity, has shown to reduce LV hypertrophy and improve function.[30,31] Calcineurin activation has also reported to contribute to RV remodelling induced by pulmonary artery banding (PAB).[32] We have previously identified miR-199b as a pro-hypertrophic microRNA during LV remodelling, induced by banding of the aorta, which induces calcineurin/NFAT-signaling activity leading to exaggerated LV remodelling and cardiac dysfunction.[34] Since we have successfully targeted the miR199b/calcineurin/NFAT pathway in experimentally induced left-sided heart

failure,[33] and miR-199b has shown to be upregulated in PAB,[34] in this study we aim at understanding the contribution of miR-199b to RV remodelling in response to pressure overload induced by pulmonary artery banding (PAB).

MATERIAL AND METHODS

Animal models and Pulmonary Artery Banding Surgery

All animal experiments were performed conform the guidelines from Directive 2010/63/EU of the European Parliament on the protection of animals used for scientific purposes. The procedures were reviewed and approved by the Animal Care and Use Committee of the University of Maastricht and Animal Experiments Committee of the University of Groningen and were performed according to the rules formulated in the Dutch law on care and use of experimental animals (Projects 2012-035 and 2012-128).

Animal models employed in this study consist of mice carrying murine miR-199b transgene[33] under control of alpha-myosin heavy chain promoter (-MHC) in C57BL/6 background and non-TG littermates (WT). Pulmonary artery banding (PAB) was performed, as described below, in mice older than 8 weeks of both genders. Animals were anesthetized with isoflurane/air mixture (5% induction; 2–3% maintenance). Animals were intubated with a 20G plastic blunt needle and placed in a supine position on a heating pad (37˚C) and ventilated with room air using a Harvard miniventilator (model 687, Hugo Sachs, Germany; respiratory rate 180 breaths per minute and a tidal volume of 125 µL). The pulmonary artery was approached by a left lateral thoracotomy and banded with a 7-0 suture by tying over a 23G needle. Post-operative pain relief was provided with buprenorphine (0.01 mg/kg s.c.) twice daily for 2-3 consecutive days if necessary. Sham-operated animals underwent the same procedure without PAB. At the endpoints of all experiments, mice were anaesthetized by isoflurane and the hearts were harvested. All efforts were made to minimize suffering.

Hemodynamic analyses

Hemodynamic function was assessed by both echocardiography and cardiac magnetic resonance imaging (MRI) during anesthesia with 1.5-3% isoflurane in a 2:1 mixture of air (0.3L/min) and oxygen (0.15L/min) and warming at 37˚C. Echocardiography was performed using a Vivid Dimension 7 and i13L-transducer (GE Healthcare, Waukesha, WI, USA). Pulmonary artery banding gradient, right ventricular dimensions and tricuspid annular plane systolic excursion (TAPSE) were assessed with echocardiography at two, four and six weeks, from short-axis at aorta level,

parasternal long axis and four-chamber views respectively. MRI was performed at six weeks in a 9.4T MRI scanner (Bruker BioSpin, Ellingen, Germany) equipped with 1,500 mT/m gradient set. Respiratory and heart rate were derived using pressure pad placed under the chest of the mouse. The longitudinal axis of the right ventricle was determined with a two and four chamber scout scans, where after axes were adjusted to actual axes. Slices of longitudinal axis, four chamber views, and ten or eleven slices of the short-axis of one millimeter and no slice gap, were obtained. Slices were derived including complete apex and base of the right ventricle. Cine imaging was performed with a retrospectively-triggered (self-gated) gradient-echo sequence (Paravision 4.0 and IntraGate, Bruker Biopspin GmBH) with the following parameters: TR = 6.8 ms, TE = 1.3 ms, number of movie frames = 15, slice thickness = 1 mm, matrix = 256 x 256, field-of-view = 30 x 30 mm^2. The myocardium was manually segmented by drawing the epicardial and endocardial contours, excluding the papillary muscles using QMass (version MR 7.6, Medis Medical Imaging Systems, Leiden, The Netherlands). Semi-automatic segmentation was used to determine end-diastolic volume (EDV), end-systolic volume (ESV), and wall thickness (WT). Stroke volume (SV) was calculated as EDV-ESV. Ejection fraction (EF) was calculated as 100%(EDV - ESV)/EDV. Cardiac output (CO) was calculated manually as SV x mean observed heart rate. Septal flattening is expressed by eccentricity index, both end diastolic and systolic, which was calculated by dividing the diameter of the left ventricular diameter parallel to the intraventricular septum by the diameter perpendicular to the intraventricular septum derived from short-axis at mid-papillary level.

RNA isolation, cDNA conversion and Real-time RT-PCR

Total RNA was isolated from mouse heart tissue using TRIzol reagent (Invitrogen) according to manufacturer's instructions. Then RNA (1 mg) was reverse-transcribed with either M-MLV reverse transcriptase (Promega, Madison, WI, USA) or for miRNA transcript detection with miScript Reverse Transcription Kit (Qiagen). Real-time PCR was performed on a BioRad iCycler (Biorad) using SYBR Green (VWR). Transcript quantities were compared using the relative Ct method, where the amount of target normalized to the amount of endogenous control (L7 for mRNAs and U6 (miScript Primer Assays) for miRNAs) and relative to the control sample is given by $2^{-\Delta Ct}$. Primer sequences for mRNA detection are depicted in **table 1**.

Histology, Immunohistochemistry and immunofluorescence microscopy

For histological analysis, hearts were arrested in diastole, perfusion-fixed with 4% paraformaldehyde, embedded in paraffin and cut into 4-µm sections. Paraffin sections

were stained with hematoxylin and eosin (H&E) for routine histological analysis, Sirius Red for detection of fibrillar collagen and FITC-labelled wheat-germ-agglutinin antibody (WGA, Sigma, 1:100) to visualize and quantify the cell cross-sectional area. Isolectin B4 staining (GSI-biotin, Vector, 1:100) was performed to visualize the capillaries in cardiac tissue. Slides were visualized using a Zeiss Axioskop 2Plus with an AxioCamHRc. Modification of Isolectine B4 staining with additional fluorescence labeled-streptavidin (Dylight 595-conjugated streptavidin, Jackson Thermo, 1:100) and counterstaining with FITC-labeled WGA was performed to assess capillary to cardiomyocyte ratios. Collagen deposition, cell surface areas and capillary density were determined using ImageJ software. Slides were visualized using a Leica DM2000 and a Leica DM3000 microscope for bright field and fluorescence imaging, respectively.

Statistical Analysis

All data are presented as mean values ± standard error of mean (SEM), unless otherwise specified. The variables were analyzed using Student's t-test and analysis of variance (ANOVA) to assess statistical significance between groups. The significant effects evaluation was conducted using Tukey's multiple comparison tests, with an adjusted calculation of *p*-value. Probability values $p<0.05$ were considered statistically significant. The strength of relationship between cardiac output and miR-199b expression as well as between RVEF and miR-199b expression was assessed by Pearson product correlation coefficient formula. All analyses were done using GraphPad Prism software V5.04 (GraphPad software, Inc, La Jolla, CA, USA).

RESULTS

Cardiac expression of miR-199b in RV remodelling induced by PAB

To assess whether miR-199b is involved in RV failure, we subjected WT mice and TG mice with cardiac-specific overexpression of miR-199b (MHC-199b)[33] to sham or pulmonary artery banding (PAB) surgery for 6 weeks (**figure 1a**). Two weeks after PAB surgery, both WT and MHC-199b mice displayed a similar increase in PAB gradient (**figure 1b**) which slightly increases over time. Six-weeks after banding, both WT and MHC-199b showed similar PAB gradients indicating the same degree of pressure overload imposed on these groups. Real-time PCR revealed upregulation of miR-199b in WT mice after PAB (**figure 1c**). Despite the elevated miR-199b expression levels in MHC-199b sham-operated mice, MHC-199b PAB animals revealed increased levels of miR-199b upon six weeks of RV pressure overload (**figure 1c**), indicating that RV stress further induces miR-199b expression.

Cardiac-specific overexpression of miR-199b promotes RV remodelling induced by pressure overload

Hypertrophy of the RV was determined by the Fulton index, the ratio of right ventricular weight to left ventricular plus septum weight (RV/LV+S). An increased Fulton index was observed 6 weeks after PAB in both WT and MHC-199b animals, compared to sham (**figure 1d**). Despite the differences in miR-199b expression levels, animals from both groups developed similar degrees of RV hypertrophy when subjected to PAB (**figure 1d**). Histological analysis demonstrated, however, that besides displaying myocardial disarray (**figure 1e**), the banded TG hearts also display increased cross-sectional surface areas of cardiomyocytes when compared to banded-WT hearts (**figure 1e-g**). At six weeks post-PAB, the hearts of WT animals subjected to PAB displayed severe deposition of collagen and formation of fibrotic lesions which, however, did not differ from those found in the RV of TG mice (**figure 1h, 1i**).

miR-199b overexpression impairs RV function during pressure overload-induced RV remodelling

Although miR-199b TG mice do not display an obvious pathological baseline phenotype nor cardiac dysfunction, these animals were shown to be more sensitive to cardiac stress than WT mice.[33] MHC-199b mice, in the sham group did not show cardiac dilatation or dysfunction. Mice with a pressure-loaded RV, either TG or WT, developed RV dilatation as reflected by increased end-diastolic and end-systolic RV volumes (**figure 2a-c**). Whereas cardiac output remained preserved in WT animals subjected to PAB surgery (**figure 2d**), it decreased significantly in MHC-199b animals after six weeks of RV pressure overload. In fact, miR-199b expression is inversely related to cardiac output (**figure 2e**). When evaluating the effects of PAB on RV EF, we observed more pronounced effects since both WT and TG animals showed decreased ejection fraction (EF) after PAB (**figure 2f**). RVEF also negatively correlated with miR-199b expression levels (**figure 2g**). Similarly, the tricuspid annular plane systolic excursion (TAPSE) was also decreased upon RV pressure overload in both WT and MHC-199b, but more severely in the latter group (**figure 2h**). The slopes of TAPSE over time are indicative of progressive impairment of RV function in MHC-199b compared to WT mice (**figure 2i**). The observed cardiac phenotypes induced by PAB correlated with increased transcript abundance of cardiac stress genes, including atrial natriuretic factor (*Nppa*), brain natriuretic factor (*Nppb*) -skeletal actin (*Acta1*) and -myosin heavy chain (*Myh7*) (**figure 3a-d**). While -myosin heavy chain (*Myh6*) was decreased after PAB in both WT and MHC-199b hearts, the Myh6/Myh7 ratio is significantly lower in the TG animals,

miR-199b overexpression aggravates right ventricular hypertrophy and is associated with decreased cardiac function in right ventricular pressure load.

indicative of a stronger cardiac stress-induced MHC-isotype switch these animals (**figure 3d-e**).

Taken together, these results indicate that cardiac miR-199b overexpression sensitizes the RV to pressure overload by inducing stress marker gene expressi

Downstream effectors of miR-199b in RV remodelling

Next, we investigated the mechanisms by which miR-199b may induce exaggerated RV remodelling and dysfunction following chronic pressure overload. Our group has previously established that miR-199b exerts its pro-hypertrophic function in the pressure-overloaded LV by directly regulating the calcineurin/nuclear factor of activated T-cell (CnA/NFAT) pathway. As calcineurin activation also may contribute to RV remodelling induced by pulmonary artery banding[32] we assessed *Rcan1-4* transcript expression levels, a sensitive marker of cardiac NFAT activity, in PAB hearts. As expected, a significant upregulation of calcineurin/NFAT signaling was induced by RV pressure overload. However, no differences were observed between WT and MHC-199b hearts (**figure 3f**). Although we could observe lower levels of dual-specificity tyrosine-phosphorylation regulated kinase 1a (*Dyrk1a*), a previously validated target gene of miR-199b, these differences were not statistically significant (**figure 3g**).

We further assessed expression levels of transforming growth factor beta (*Tgfb*) as a growth factor involved in fibrosis and cardiomyocyte hypertrophy,[35] and as a potential target gene of the miR-199 family. Although we observed a clear increase in *Tgfb* mRNA in banded-hearts, no differences were observed between WT and MHC-199b mice (**figure 3h**). Similar results were obtained for *Endoglin*, a coreceptor for *Tgf*β-signaling (**figure 3i**). As we did not detect major differences regarding collagen deposition at the histological level between the WT and TG animals after PAB, we also assessed the expression levels of collagen type I alpha 1 chain (*Col1a1*) as a fibrosis-related gene. At the molecular level, we observed a clear upregulation of *Col1a1* in MHC-199b hearts compared to WT hearts when subjected to RV pressure overload (**figure 3j**).

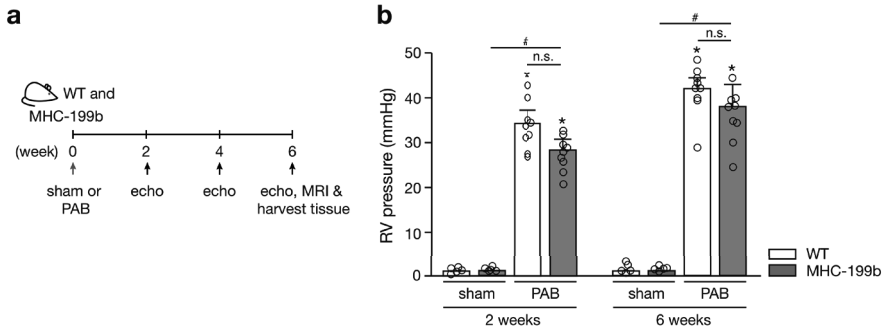

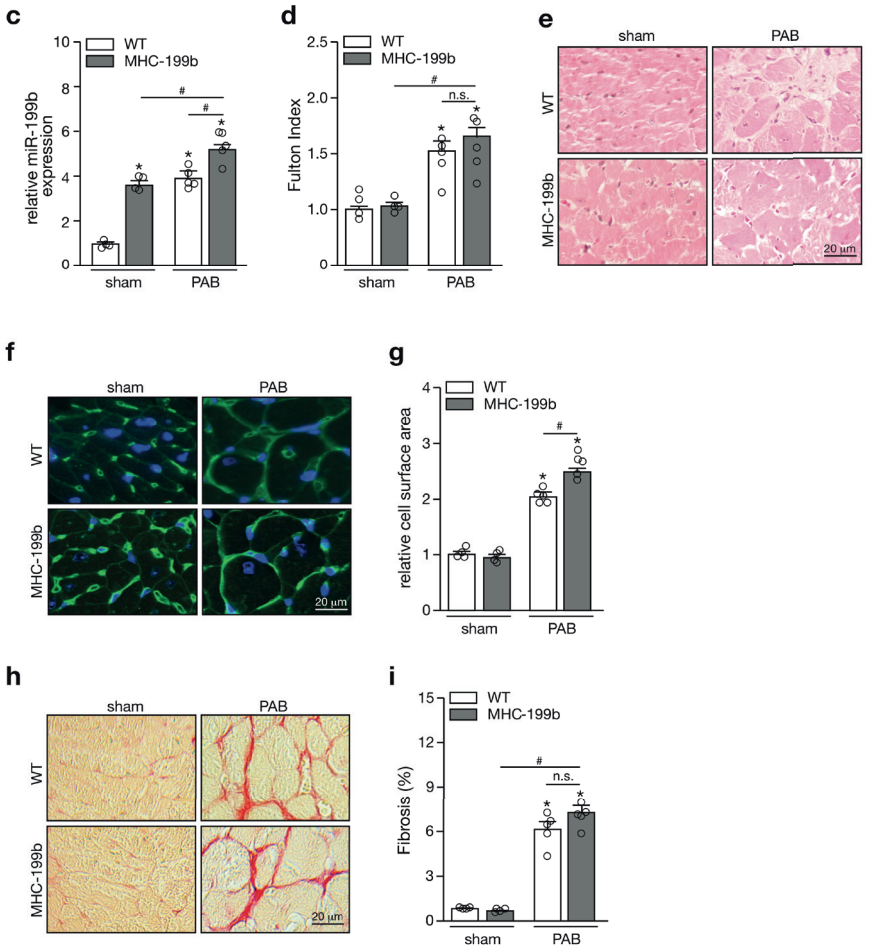

Figure 1. Assessment of right ventricular hypertrophy induced by PAB upon cardiac overexpression of miR-199b. a) Design of the in vivo study; b) Assessment of pulmonary artery banding gradient in wildtype (WT) and MHC-miR-199b Tg (MHC-199b) animals, by measuring RV pressure at 2 and 6 weeks after either sham or PAB surgery; c) Quantitative real-time PCR analysis of miR-199b expression in RV tissue from WT and MHC-199b animals either after sham or PAB surgery, n=5-8 hearts; d) Fulton's index values (ratio of right ventricular weight to left ventricular plus septal weight) of WT and MHC-199b animals either after sham or PAB surgery, n=5-8 hearts; e) High-magnification of representative images of histological sections stained for haematoxylin & eosin (H&E), black scale bar is equivalent to 20 mm; f) High-magnification of representative images of histological sections stained for wheat germ agglutinin (WGA), black scale bar is equivalent to 20 mm; g) Quantification of cell surface areas in f, n=30 microscopic field/heart, 3 hearts; h) High-magnification of representative images of histological sections stained for Sirius-red, black scale bar is equivalent to 20 mm; i) Quantification of collagen deposition in h, n=30 microscopic field/heart, 3 hearts. Statistical analysis using One-way ANOVA with Tukey's multiple comparisons test. *p<0.05 versus corresponding control group; #p<0.05 versus corresponding experimental group (error bars are s.e.m.).

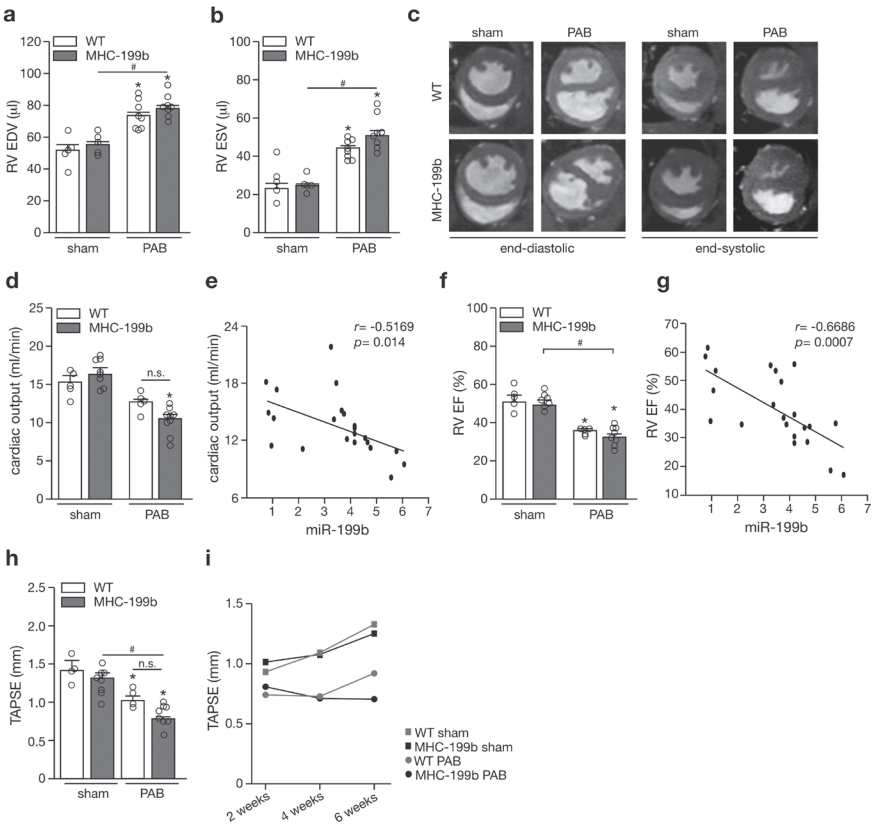

Figure 2. miR-199b overexpression impairs RV function during pressure overload-induced RV remodelling. Cardiac function was assessed in hearts from wildtype (WT) and MHC-miR-199b Tg (MHC-199b) animals, either after sham or PAB surgery, and followed by quantitative analysis. a) RV end-diastolic volumes (EDV) and b) RV end-systolic volumes, n=5-8 hearts; c) Representative MRI images of cardiac ventricular end-diastole and end-systole; d) Cardiac output, n=5-8 hearts; e) A Pearson's correlation was run to determine the relationship between cardiac miR-199b expression levels and cardiac output in 22 mice, independent of the treatment and genotype. f) RV ejection fraction (EF), n=5-8 hearts; g) A Pearson's correlation was run to determine the relationship between cardiac miR-199b expression levels and RV EF in 22 mice, independent of the treatment and genotype; h) echocardiographic tricuspid annular plane systolic excursion (TAPSE) measurements at the end of the study and i) every 2 weeks throughout the complete study, n=5-8 hearts. Statistical analysis using One-way ANOVA with Tukey's multiple comparisons test. *p<0.05 versus corresponding control group; #p<0.05 versus corresponding experimental group (error bars are s.e.m.).

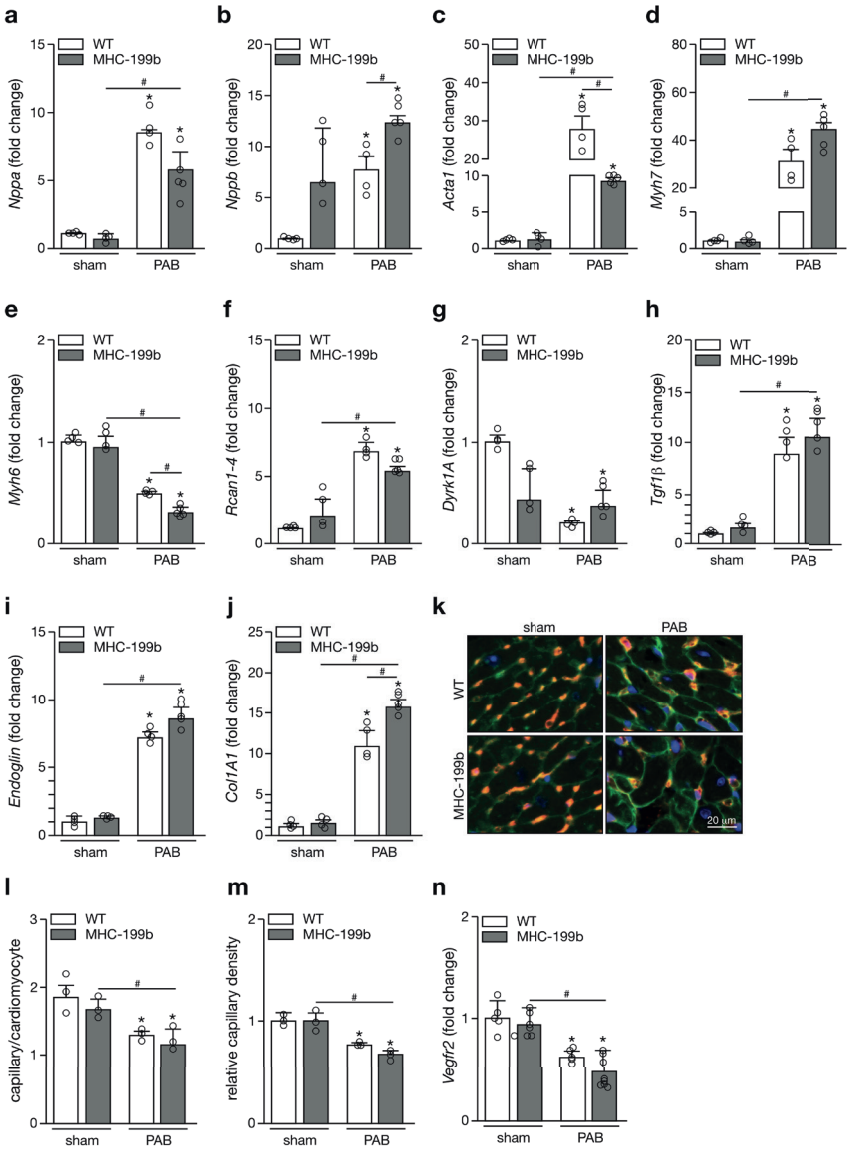

Figure 3. RV expression profile of cardiac hypertrophy-related genes. Quantitative real-time PCR analysis was performed to assess the expression levels of several genes known to be related to cardiac hypertrophy in RV tissue from wildtype (WT) and MHC-miR-199b Tg (MHC-199b) animals, either after sham or PAB surgery. a) natriuretic peptides atrial natriuretic factor (Nppa); b) brain natriuretic peptide (Nppb); c) -skeletal actin (Acta1); d) -myosin heavy chain (Myh7); e) a-myosin heavy chain (Myh6); f) regulator of Calcineurin 1 Isoform 4 (Rcan1-4); g) nuclear NFAT kinase dual-specificity tyrosine-(Y)-phosphorylation regulated kinase 1a (Dyrk1a); h) transforming growth factor beta (TGF-β); i) endoglin; j) collagen type I alpha 1 chain (COL1A1); k) Capillaries in RV sections of wildtype (WT) and MHC-miR-199b Tg (MHC-199b) animals, either after sham or PAB surgery, were identified by isolectin B4 immunohistochemistry (yellow). WGA marks cell membranes (green), and Hoechst stain identifies

nuclei (blue), black scale bar is equivalent to 20 mm; from the images obtained we determined l) capillaries per cardiomyocytes ratios and m) relative capillary density, density of WT-sham animals was set at 1; n=30 microscopic field/heart, 3 hearts; n) Quantitative real-time PCR analysis of vascular endothelial growth factor receptor 2 (Vegfr2) expression levels of hearts of RV from wildtype (WT) and MHC-miR-199b Tg (MHC-199b) animals, either after sham or PAB surgery. All PCR data are from 5-8 animals per group. Statistical analysis using One-way ANOVA with Tukey's multiple comparisons test. *p<0.05 versus corresponding control group; #p<0.05 versus corresponding experimental group (error bars are s.e.m.).

As RV capillary rarefaction is a phenomenon that leads to maladaptive RV remodelling, we assessed the capillary density of the RV in our different experimental groups. Histochemical analysis and respective quantification, as well as determination of vascular endothelial growth factor receptor 2 (*Vegfr2*) expression levels, reflected lower capillary density in both WT and MHC-199b after PAB, in agreement with similar endoglin levels, suggesting that increased miR-199b levels are not directly associated with RV microvascular remodelling (**figure 3k-n**).

Cardiac overexpression of miR-199b increases LV susceptibility to remodelling under RV stress conditions

As we have previously shown, miR-199b is upregulated during LV failure and its overexpression increases the sensitivity of the LV to cardiac stress, although indirectly, RV chronic stress can also affect LV remodelling and function.[36-38] Therefore, we also analyzed the changes in molecular profile and morphological adaptation of the LV under conditions of RV pressure overload in both WT and MHC-199b hearts. PAB was able to induce miRNA-199b expression in the LV of WT animals but not in the TG animals (**figure 4a**) when compared to the sham controls. PAB equally increased LV weight indicative of LV hypertrophic growth in the two genotypes (**figure 4b**). Histological analysis revealed increased fibrosis in the LV of TG animals subject to PAB, compared to WT (**figure 4c,d**), but no changes in cardiomyocyte hypertrophy were observed in the left myocardium (**figure 4e,f**). Furthermore, PAB did not induce capillary rarefaction in the LV, independently of the genotype (**figure 4g**). Surprisingly, there was not only a clear upregulation of cardiac stress genes such as *nppa*, *nppb* and *myh7* (**figure 4h-j**) in the LV of TG mice subjected to PAB, but we also observed increased levels of *Rcan 1-4* in the LV of both WT and MHC-199b after PAB, with a more pronounced effect in the TG animals (**figure 4k**). Congruent to this, left ventricular expression levels of *Dyrk1A* were reduced upon RV pressure overload, an effect that was more prominent in TG animals (**figure 4l**). RV pressure overload also induced *Tgfβ* expression in the LV with higher levels in the TG mice (**figure 4m**). No changes were observed in *Vegfr2* mRNA abundance which is consistent with no changes in LV capillary density (**figure 4n**).

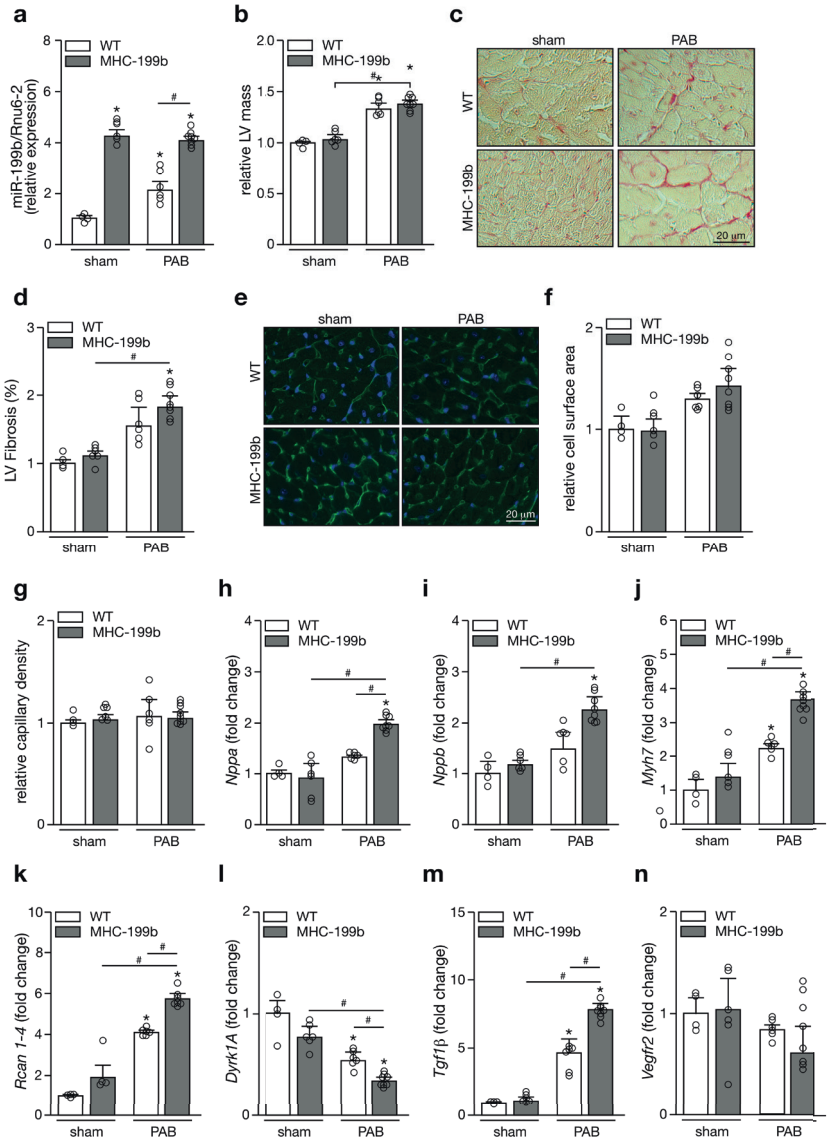

Figure 4. Assessment of left ventricular remodelling induced by PAB upon cardiac overexpression of miR-199b. a) Quantitative real-time PCR analysis of miR-199b expression in LV tissue from WT and MHC-199b animals either after sham or PAB surgery, n=5-8 hearts; b) relative LV mass, LV mass of WT sham was set as 1; c) High-magnification of representative images of histological sections stained for Sirius-red; d) Quantification of collagen deposition in c, n=30 microscopic field/heart, 3 hearts, black scale bar is equivalent to 20 mm; e) High-magnification of representative images of histological sections stained for wheat germ agglutinin (WGA); f) Quantification of cell surface areas in e, n=30 microscopic field/heart, 3 hearts; g) relative capillary density

was determined from histological sections stained for isolectin B4 immunohistochemistry and WGA (bars, 20 μm), density of WT-sham animals was set at 1, n=30 microscopic field/heart, 3 hearts; Quantitative real-time PCR analysis was performed to assess the expression levels of several genes known to be directly or indirectly related to cardiac hypertrophy in LV tissue from wildtype (WT) and MHC-miR-199b Tg (MHC-199b) animals, either after sham or PAB surgery: h) natriuretic peptides atrial natriuretic factor (Nppa); i) brain natriuretic peptide (Nppb); j) β-myosin heavy chain (Myh7); k) regulator of Calcineurin 1 Isoform 4 (Rcan1-4); l) nuclear NFAT kinase dual-specificity tyrosine-(Y)-phosphorylation regulated kinase 1a (Dyrk1a); m) transforming growth factor beta (TGF-β) and n) vascular endothelial growth factor receptor 2 (Vegfr2). All PCR data are from 5-8 animals per group. Statistical analysis using One-way ANOVA with Tukeys multiple comparisons test. ∗p<0.05 versus corresponding control group; #p<0.05 versus corresponding experimental group (error bars are s.e.m.).

Following the molecular and cellular changes, we also assessed how RV stress, together with increased miR-199b expression levels, influenced LV function. LV eccentricity index, defined as the ratio of the length of two perpendicular minor-axis diameters, one of which bisected and was perpendicular to the interventricular septum, was obtained at end-systole and end-diastole (**figure 5a,b**). While we could detect an abnormal motion of the interventricular septum which is in accordance with RV remodelling, this effect was not different between WT and TG animals (**figure 5a,b**). Both end-diastolic and systolic volumes decreased in the TG animals subjected to PAB but remained unchanged in WT (**figure 5c,d**). A similar pattern was observed for left ventricular stroke volume (LVSV) (**figure 5e**), suggesting affected function. However, this was not reflected in the LV EF, for which no differences were observed between the different groups (**figure 5f**). Altogether, this data confirms that the LV is susceptible to increased miR-199b levels, even under conditions of indirect stress such as RV pressure overload.

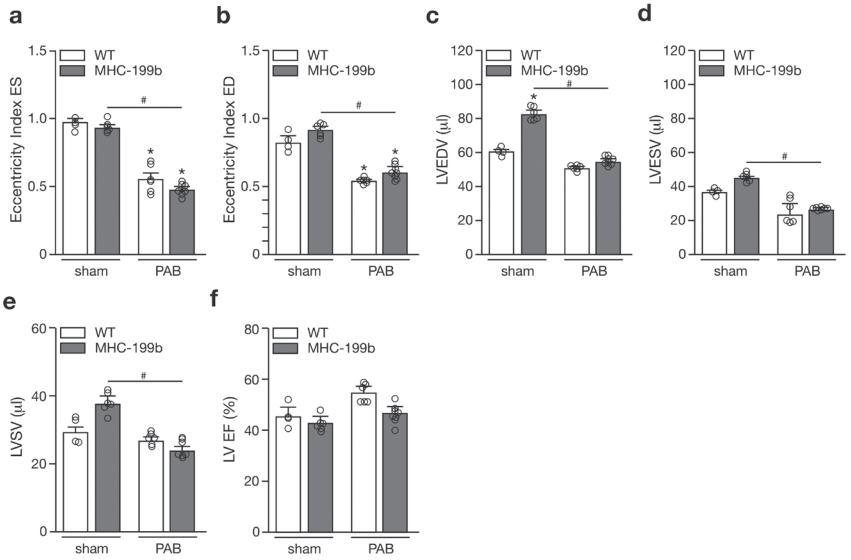

Figure 5. miR-199b overexpression sensitizes the LV to pressure overload of the RV. Cardiac function was assessed in hearts from wildtype (WT) and MHC-miR-199b Tg (MHC-199b) animals, either after sham or PAB surgery, and followed by quantitative analysis: a) eccentricity index at end-systole and b) end-diastole; c) left ventricle end-diastolic volume (LVEDV) and d) end-systolic volume (LVESV); e) left ventricular stroke volume (LVSV) and f) ejection fraction (EF). All data are from 5-8 animals per group. Statistical analysis using One-way ANOVA with Tukey's multiple comparisons test. *p<0.05 versus corresponding control group; #p<0.05 versus corresponding experimental group (error bars are s.e.m.).

DISCUSSION

We aimed at unraveling the contribution of miR-199b to the process towards cardiac remodelling upon RV pressure overload. PAB induced significant upregulation of miR-199b expression in the RV which was associated with worsened RV function. Although the effect of miR-199b on RV remodelling is reflected by cardiac hypertrophic growth and increased expression of cardiac stress markers, the RV responds differently to increased levels of miR-199b when compared to the LV. Increased miR-199b expression levels in the RV did not seem to affect Calcineurin/NFAT signaling as previously described for the LV.[33] However, this signaling cascade was affected in the LV of mice that were subjected to RV pressure overload. These data suggest distinct regulatory functions for miR-199b in the RV compared to the LV.

Abnormal microRNA expression patterns have been shown in experimental RV failure.[34] Studies based on animal models of chronic hypoxia- or monocrotaline-induced PAH mainly focused on alterations in microRNA expression patterns of the pulmonary artery smooth muscle or endothelial cells. In concordance, microRNAs

such as miR-17/92,[39,40] miR-27a,[41] miR-96,[42] miR-126,[27] miR-130,[43] miR-143/145[44] and miR-210[45], all known to be involved either in cell proliferation, vascular remodelling or apoptosis, were identified as playing important roles in the pathogenesis of PAH. miR-126 downregulation in the skeletal muscle of PAH patients is associated with a decrease in RV vascular endothelial growth factor (VEGF)-induced angiogenesis and in exercise tolerance.[27] Reestablishment of miR-126 levels resulted in improved RV function and increased microvascular density in experimental PAH.[27] Furthermore, Reddy and colleagues[34] identified miR-34a, miR-28, miR-93 and miR-148 to be upregulated in the pressure-overloaded RV and further inducing changes in oxidative metabolism, cell cycle and calcium homeostasis. Nevertheless, the differences between RV and LV response to pressure overload regarding microRNA-dependent regulatory mechanisms has not yet been explored. Thus, the present study provides evidence for distinct roles of a specific microRNA, depending on which chamber is under direct stress.

Our previous work and that from others has established that miR-199b is upregulated in both ventricles throughout the different remodelling stages induced by pressure overload.[33,34] Although common mechanisms are suggested to be involved in both RV and LV remodelling, the current study indicates their regulation to be different, as well as their vulnerability to distinctive types of stress. RV response to increased pressure load, as for the LV, also includes changes in myocardial hypertrophy and fibrosis, as well as adaptation of the cardiac capillary network.[46] In the present study, we show that increased levels of miR-199b in the pressure-overloaded RV result in increased hypertrophic growth of the RV when compared to wildtype animals under similar RV pressure. We were able to induce chronic pressure load of the RV progressively in time in both wildtype and TG mice. Decreased RV contractility in TG mice after 4 and 6 weeks of pressure overload reflected in the TAPSE, a measure of the longitudinal contraction of the RV. Furthermore, cardiac output and RV ejection fraction inversely correlated with miR-199b expression. Altogether, these data strongly suggest a pathologic effect of increased miR-199b levels on the hemodynamic function of the RV. Regarding fibrosis, while there was a significant increase in collagen deposition after PAB, no differences between WT and miR-199b TG animals were observed, at the histological level. Nevertheless, after RV pressure we observed increased transcript levels of collagen type I alpha 1 chain (*Col1A1*) in TG animals compared to wildtype, suggesting a more fibrotic profile of the TG RVs.

Similar to what we have previously described for the LV, we also observed increased NFAT activity in the stressed RV, which was reflected by increased transcript levels of RCAN1-4.[33] However, we could not directly correlate this with miR-199b expression levels. Upon RV pressure overload, a switch in myosin heavy chain (MHC) isoforms from the fast MHC to the slower and energetically favorable, MHC, is induced in

the RV.[47] In fact, we observed increased abundance of Myh7 transcripts and lower transcript levels of Myh6 in miR-199b TG animals subjected to RV pressure overload, also suggesting that RV hypertrophic growth under these conditions is a result of reactivation of the fetal gene program and consequent change in MHC/MHC ratio, rather than activation of Calcineurin/NFAT signaling.

Despite most attention being given to LV function, whereas RV function and disease have remained less explored, it is an established fact that there is a relationship between LV and RV function and that ventricular interaction plays an important role in the cardiac response to stress. While impairment of the RV might influence LV function,[48] RV function is one independent predictor of mortality and the development of heart failure in patients with LV dysfunction.[49] Abnormal motion of the interventricular septum can occur in right ventricular pressure overload and is reflected by changes in eccentricity index of left ventricular shape.[50] We observed clear changes in LV shape under RV pressure overload conditions, even though no changes were observed between the different genotypes. Other LV parameters such as LV end-diastolic and end-systolic volumes, as well as left ventricular stroke volume, were more affected in TG animals after RV pressure overload than in the wild-type animals under similar conditions, indicating greater susceptibility of the TG LV to RV stress. This is consistent with our previous findings showing that overexpression of miR-199b does not result in cardiac dysfunctional phenotypes in resting conditions but increases LV sensitivity to cardiac stress such as pressure overload induced by transverse aortic constriction (TAC).[33] Moreover, TG animals displayed increased LV fibrosis as well as increased abundance of fibrosis-related transcripts. Interestingly, RV stress showed a clear response of the LV by activation of the Calcineurin/NFAT signaling pathway, revealed by an increased RCAN1-4 mRNA and subsequent decrease in Dyrk1A levels, a previously identified target of miR-199b.[33]

Although the current study does not allow us to conclude on the contribution of miR-199b to RV remodelling towards RV failure, it does show that its overexpression sensitizes both ventricles to RV stress, with a more profound effect on the LV. Furthermore, studying RV dysfunction without significant failure allows for a better understanding of the cellular and molecular mechanisms preceding clinical failure, and thus target finding for early intervention. Perhaps more important, our study adds to the evidence that the stressed RV represents a qualitatively different substrate than the stressed LV and therefore, pharmacotherapy should be tailored accordingly.

Funding

SL was supported by a Foundation for Science and Technology of Portugal (FCT) grant (SFRH/BD/110404/2015). RMFB and BB were supported by the Sebald fund,

by the Netherlands CardioVascular Research Initiative: the Dutch Heart Foundation, Dutch Federation of University Medical Centers, the Netherlands Organisation for Health Research and Development and the Royal Netherlands Academy of Sciences (CVON-Phaedra 2012-08). PDCM was supported by a Dutch Heart Foundation grant (NHS2010B261) and a Foundation for Science and Technology of Portugal (FCT) grant (PTDC/BIM-MEC/4578/2014).

CONFLICT OF INTEREST

PDCM is one of the cofounders of Mirabilis Therapeutics.

REFERENCES

1. Simon MA. Assessment and treatment of right ventricular failure. *Nat Rev Cardiol* Nature Publishing Group; 2013;10:204–218.
2. Voelkel NF, Quaife RA, Leinwand LA, Barst RJ, McGoon MD, Meldrum DR, Dupuis J, Long CS, Rubin LJ, Smart FW, Suzuki YJ, Gladwin M, Denholm EM, Gail DB. Right ventricular function and failure: Report of a National Heart, Lung, and Blood Institute working group on cellular and molecular mechanisms of right heart failure. *Circulation* 2006;114:1883–1891.
3. Bogaard HJ, Abe K, Noordegmaf A V, Voelkel NF. The right ventricle under pressure. *Chest* N. F. Voelkel, Department oj Pulmonary Medicine and Critical Care, Virginia Commonwealth University, Sanger Hall, Richmond, VA 23284; 2009;135:794–804.
4. Norozi K, Wessel A, Alpers V, Arnhold JO, Geyer S, Zoege M, Buchhorn R. Incidence and Risk Distribution of Heart Failure in Adolescents and Adults With Congenital Heart Disease After Cardiac Surgery. *Am J Cardiol* 2006;97:1238–1243.
5. Borgdorff MAJ, Dickinson MG, Berger RMF, Bartelds B. Right ventricular failure due to chronic pressure load: What have we learned in animal models since the NIH working group statement? *Heart Fail Rev* M.A.J. Borgdorff, Department of Pediatric Cardiology, Center for Congenital Heart Diseases, Beatrix Children's Hospital, University Medical Center Groningen, Groningen, Netherlands; 2015;20:475–491.
6. Haddad F, Doyle R, Murphy DJ, Hunt SA. Right ventricular function in cardiovascular disease, part II: Pathophysiology, clinical importance, and management of right ventricular failure. *Circulation* 2008;117:1717–1731.
7. Sutendra G, Dromparis P, Paulin R, Zervopoulos S, Haromy A, Nagendran J, Michelakis ED. A metabolic remodeling in right ventricular hypertrophy is associated with decreased angiogenesis and a transition from a compensated to a decompensated state in pulmonary hypertension. *J Mol Med* E.D. Michelakis, Department of Medicine, University of Alberta, Edmonton, AB T6G 2B7, Canada; 2013;91:1315–1327.
8. Borgdorff MAJ, Koop AMC, Bloks VW, Dickinson MG, Steendijk P, Sillje HHW, Wiechen MPH van, Berger RMF, Bartelds B. Clinical symptoms of right ventricular failure in experimental chronic pressure load are associated with progressive diastolic dysfunction. *J Mol Cell Cardiol* Elsevier Ltd; 2015;79:244–253.
9. Bogaard HJ, Natarajan R, Henderson SC, Long CS, Kraskauskas D, Smithson L, Ockaili R, McCord JM, Voelkel NF. Chronic pulmonary artery pressure elevation is insufficient to explain right heart failure. *Circulation* 2009;120:1951–1960.
10. Guglin M, Verma S. Right side of heart failure. *Heart Fail Rev* 2012;17:511–527.
11. Friedberg MK, Redington AN. Right versus left ventricular failure: Differences, similarities, and interactions. *Circula*tion 2014;129:1033–1044.
12. MacNee W. State of the Art Pathophysiology of Cor Pulmonale in Chronic Obstrudive. *Am J Respir Crit Care Med* 1994;150:833–852.
13. Vonk Noordegraaf A, Westerhof BE, Westerhof N. The Relationship Between the Right Ventricle and its Load in Pulmonary Hypertension. *J Am Coll Cardiol* 2017;69:236–243.
14. Meilhac SM, Esner M, Kelly RG, Nicolas JF, Buckingham ME. The clonal origin of myocardial cells in different regions of the embryonic mouse heart. *Dev Cell* 2004;6:685–698.

15. Mihl C, Dassen WRM, Kuipers H. Cardiac remodelling: Concentric versus eccentric hypertrophy in strength and endurance athletes. *Netherlands Hear J* 2008;16:129–133.
16. Tabibiazar R, Wagner RA, Liao A, Quertermous T. Transcriptional Profiling of the Heart Reveals Chamber-Specific Gene Expression Patterns. *Circ Res* 2003;93:1193–1201.
17. Katz WE, Gasior TA, Quinlan JJ, Lazar JM, Firestone L, Griffith BP, Gorcsan J. Immediate effects of lung transplantation on right ventricular morphology and function in patients with variable degrees of pulmonary hypertension. *J Am Coll Cardiol* Elsevier Masson SAS; 1996;27:384–391.
18. Schulman L, Leibowitz D, Anandarangam T, DiTullio M, McGregor C, Smith C, Homma S. Variability of right ventricular functional recovery after lung transplantation. *Transplantation* 1996;62:622–625.
19. Gorter TM, Verschuuren EAM, Veldhuisen DJ Van, Hoendermis ES, Erasmus ME, Bogaard HJ, Vonk Noordegraaf A, Berger RMF, Melle JP Van, Willems TP. Right ventricular recovery after bilateral lung transplantation for pulmonary arterial hypertension. *Interact Cardiovasc Thorac Surg* 2017;24:890–897.
20. Tuder RM, Archer SL, Dorfmuller P, Erzurum SC, Guignabert C, Michelakis E, Rabinovitch M, Schermuly R, Stenmark KR, Morrell NW. Relevant issues in the pathology and pathobiology of pulmonary hypertension. *Turk Kardiyol Dern Ars* Turkey; 2014;42 Suppl 1:5–16.
21. Ha M, Kim VN. Regulation of microRNA biogenesis. *Nat Rev Mol Cell Biol* Nature Publishing Group; 2014;15:509–524.
22. Espinoza-Lewis R, Wang D-Z. MicroRNAs in Heart Development. *Curr Top Dev Biol* 2016;100:279–317.
23. Divakaran V, Mann DL. The Emerging Role of MicroRNAs in Cardiac Remodeling and Heart Failure. *Circ Res* 2008;103:1072–1083.
24. Iacobazzi D, Suleiman M-S, Ghorbel M, George S, Caputo M, Tulloh R. Cellular and molecular basis of RV hypertrophy in congenital heart disease. *Heart* 2015;heartjnl-2015-308348.
25. Drake JI, Bogaard HJ, Mizuno S, Clifton B, Xie B, Gao Y, Dumur CI, Fawcett P, Voelkel NF, Natarajan R. Molecular signature of a right heart failure program in chronic severe pulmonary hypertension. *Am J Respir Cell Mol Biol* 2011;45:1239–1247.
26. Joshi SR, Dhagia V, Gairhe S, Edwards JG, McMurtry IF, Gupte SA. Microrna-140 is elevated and mitofusin-1 is downregulated in the right ventricle of the sugen5416/hypoxia/normoxia model of pulmonary arterial hypertension. *Am J Physiol - Hear Circ Physiol* S.A. Gupte, Department of Pharmacology, New York Medical College, Valhalla, United States; 2016;311:H689–H698.
27. Potus F, Ruffenach G, Dahou A, Thebault C, Breuils-Bonnet S, Tremblay È, Nadeau V, Paradis R, Graydon C, Wong R, Johnson I, Paulin R, Lajoie AC, Perron J, Charbonneau E, Joubert P, Pibarot P, Michelakis ED, Provencher S, Bonnet S. Downregulation of miR-126 Contributes to the Failing Right Ventricle in Pulmonary Arterial Hypertension. *Circulation* 2015;132:932–943.
28. Reddy S, Bernstein D. Molecular mechanisms of right ventricular failure. *Circulation* S. Reddy, Department of Pediatrics (Cardiology), Stanford Cardiovascular Institute, Stanford University, Lucile Packard Children's Hospital, Palo Alto, United States; 2015;132:1734–1742.

29. Paulin R, Sutendra G, Gurtu V, Dromparis P, Haromy A, Provencher S, Bonnet S, Michelakis ED. A miR-208-Mef2 axis drives the decompensation of right ventricular function in pulmonary hypertension. *Circ Res* E.D. Michelakis, Department of Medicine, Cardiology, University of Alberta, Edmonton, Canada; 2015;116:56–69.

30. Wilkins BJ, Dai YS, Bueno OF, Parsons SA, Xu J, Plank DM, Jones F, Kimball TR, Molkentin JD. Calcineurin/NFAT Coupling Participates in Pathological, but not Physiological, Cardiac Hypertrophy. *Circ Res* 2004;94:110–118.

31. Rooij E Van, Doevendans PA, Crijns HJGM, Heeneman S, Lips DJ, Bilsen M Van, Williams RS, Olson EN, Bassel-Duby R, Rothermel BA, Windt LJ De. MCIP1 overexpression suppresses left ventricular remodeling and sustains cardiac function after myocardial infarction. *Circ Res* 2004;94:e18–e26.

32. Bartelds B, Borgdorff M a., Smit-Van Oosten A, Takens J, Boersma B, Nederhoff MG, Elzenga NJ, Gilst WH Van, Windt LJ De, Berger RMF. Differential responses of the right ventricle to abnormal loading conditions in mice: Pressure vs. volume load. *Eur J Heart Fail* 2011;13:1275–1282.

33. Costa Martins PA da, Salic K, Gladka MM, Armand A-S, Leptidis S, Azzouzi H el, Hansen A, Coenen-de Roo CJ, Bierhuizen MF, Nagel R van der, Kuik J van, Weger R de, Bruin A de, Condorelli G, Arbones ML, Eschenhagen T, Windt LJ De. MicroRNA-199b targets the nuclear kinase Dyrk1a in an auto-amplification loop promoting calcineurin/NFAT signalling. *Nat Cell Biol* Nature Publishing Group; 2010;12:1220–1227.

34. Reddy S, Zhao M, Hu D-Q, Fajardo G, Hu S, Ghosh Z, Rajagopalan V, Wu JC, Bernstein D. Dynamic microRNA expression during the transition from right ventricular hypertrophy to failure. *Physiol Genomics* 2012;44:562–575.

35. Goumans M, Dijke P Ten. TGF- Signaling in Control of Cardiovascular Function. *Cold Spring Harb Perspect Biol* 2018;10:pii:a022210.

36. Dell'Italia LJ. The forgotten left ventricle in right ventricular pressure overload. *J Am Coll Cardiol* Elsevier Inc.; 2011;57:929–930.

37. Hardziyenka M, Campian ME, Reesink HJ, Surie S, Bouma BJ, Groenink M, Klemens CA, Beekman L, Remme CA, Bresser P, Tan HL. Right ventricular failure following chronic pressure overload is associated with reduction in left ventricular mass: Evidence for atrophic remodeling. *J Am Coll Cardiol* Elsevier Inc.; 2011;57:921–928.

38. Louie EK, Lin SS, Reynertson SI, Brundage BH, Levitsky S, Rich S. Pressure and Volume Loading of the Right Ventricle Have Opposite Effects on Left Ventricular Ejection Fraction. *Circulation* 1995;92:819–824.

39. Brock M, Trenkmann M, Gay RE, Michel BA, Gay S, Fischler M, Ulrich S, Speich R, Huber LC. Interleukin-6 modulates the expression of the bone morphogenic protein receptor type ii through a novel STAT3-microRNA cluster 17/92 pathway. *Circ Res* 2009;104:1184–1191.

40. Caruso P, MacLean MR, Khanin R, McClure J, Soon E, Southgate M, MacDonald RA, Greig JA, Robertson KE, Masson R, Denby L, Dempsie Y, Long L, Morrell NW, Baker AH. Dynamic changes in lung MicroRNA profiles during the development of pulmonary hypertension due to chronic hypoxia and monocrotaline. *Arterioscler Thromb Vasc Biol* 2010;30:716–723.

41. Kang BY, Park KK, Green DE, Bijli KM, Searles CD, Sutliff RL, Michael Hart C. Hypoxia mediates mutual repression between microRNA-27a and PPAR in the pulmonary vasculature. PLoS One. 2013.

42. Wallace E, Morrell NW, Yang XD, Long L, Stevens H, Nilsen M, Loughlin L, Mair KM, Baker AH, MacLean MR. A sex-specific microRNA-96/5-hydroxytryptamine 1B axis influences development of pulmonary hypertension. *Am J Respir Crit Care Med* 2015;191:1432–1442.

43. Bertero T, Lu Y, Annis S, Hale A, Bhat B, Saggar R, Saggar R, Wallace WD, Ross DJ, Vargas SO, Graham BB, Kumar R, Black SM, Fratz S, Fineman JR, West JD, Haley KJ, Waxman AB, Chau BN, Cottrill KA, Chan SY. Systems-level regulation of MicroRNA networks by miR-130/301 promotes pulmonary hypertension. *J Clin Inv*est 2014;124:3514–3528.

44. Caruso P, Dempsie Y, Stevens HC, McDonald RA, Long L, Lu R, White K, Mair KM, McClure JD, Southwood M, Upton P, Xin M, Rooij E Van, Olson EN, Morrell NW, MacLean MR, Baker AH. A role for miR-145 in pulmonary arterial hypertension: Evidence from mouse models and patient samples. *Circ Res* 2012;111:290–300.

45. Gou D, Ramchandran R, Peng X, Yao L, Kang K, Sarkar J, Wang Z, Zhou G, Usha Raj J. Mir-210 has an antiapoptotic effect in pulmonary artery smooth muscle cells during hypoxia. *Am J Physiol - Lung Cell Mol Physiol* 2012;303:682–691.

46. Ryan JJ, Huston J, Kutty S, Hatton ND, Bowman L, Tian L, Herr JE, Johri AM, Archer SL. Right Ventricular Adaptation and Failure in Pulmonary Arterial Hypertension. *Can J Cardiol* Canadian Cardiovascular Society; 2015;31:391–406.

47. Lowes BD, Minobe W, Abraham WT, Rizeq MN, Bohlmeyer TJ, Quaife RA, Roden RL, Dutcher DL, Robertson AO, Voelkel NF, Badesch DB, Groves BM, Gilbert EM, Bristow MR. Changes in gene expression in the intact human heart: Downregulation of -myosin heavy chain in hypertrophied, failing ventricular myocardium. *J Clin Inves*t 1997;100:2315–2324.

48. Hill MF, Singal PK. Right and Left Myocardial Antioxidant Responses During Heart Failure Subsequent to Myocardial Infarction. *Circulation* 1997;96:2414–2420.

49. Zornoff LAM, Skali H, Pfeffer MA, John Sutton M St., Rouleau JL, Lamas GA, Plappert T, Rouleau JR, Moyé LA, Lewis SJ, Braunwald E, Solomon SD. Right ventricular dysfunction and risk of heart failure and mortality after myocardial infarction. *J Am Coll Cardiol* 2002;39:1450–1455.

50. Ryan T, Petrovic O, Dillon JC, Feigenbaum H, Conley MJ, Armstrong WF. An echocardiographic index for separation of right ventricular volume and pressure overload. *J Am Coll Cardiol* 1985;5:918–927.

SUPPLEMENTAL MATERIAL

Table 1. Sequences of primers used for real-time RT-PCR

Gene name	Sequence
Nppa	5'-TCTTCCTCGTCTTGGCCTTT-3'
	5'-CCAGGTGGTCTAGCAGGTTC-3'
Nppb	5'-TGGGAGGTCACTCCTATCCT-3'
	5'-GGCCATTTCCTCCGACTTT-3'
Acta1	5'-CCGGGAGAAGATGACTCAAA-3'
	5'-GTAGTACGGCCGGAAGCATA-3'
Myh7	5'-CGGACCTTGGAAGACCAGAT-3'
	5'-GACAGCTCCCCATTCTCTGT-3'
Myh6	5'-CCAACACCAACCTGTCCAAGT-3'
	5'-AGAGGTTATTCCTCGTCGTGCAT-3'
Rcan1.4	5'-GCTTGACTGAGAGAGCGAGTC-3'
	5'-CCACACAAGCAATCAGGGAGC-3'
Dyrk1A	5'-AAGTTATCTGAAGCCTTCTGC-3'
	5'-CATGGTATGCTACATGGAAGGC-3'
TGF1β	5'-GCAGCACGTGGAGCTGTA-3'
	5'-CAGCCGGTTGCTGAGGTA-3'
Endoglin	5'-CTTCCAAGGACAGCCAAGAG-3'
	5'-GTGGTTGCCATTCAAGTGTG-3'
Col1A1	5'-GAAGCACGTCTGGTTTGGA-3'
	5'-ACTCGAACGGGAATCCATC-3'
Vegfr2	5'-AGCACTGGTCCTATGGGTTG-3'
	5'-GGTTCTGCCATTTGATCCA-3'

6

7

CHAPTER 7

The adult heart requires baseline expression of the transcription factor Hand2 to withstand right ventricular pressure overload

A.M.C. Koop*, R.F. Videira*, L. Ottaviani, E.M. Poels, M.M. Kocken, P. Mendes-Ferreira, K.W.A. van de Kolk, G.J. Du Marchie Sarvaas, A. Lourenço, D.S. Nascimento, L.J. de Windt, I. Falcão-Pires, R.M.F. Berger, P.A. da Costa Martins

- Submitted, Cardiovascular Research.

* These authors have equally contributed to the manuscript.

ABSTRACT

Background and aims

Research on the pathophysiology of right ventricular (RV) failure has, in spite of the associated high mortality and morbidity, lagged behind compared to the left ventricle (LV). Despite its association with high mortality and morbidity, attention to the pathophysiology of right ventricular (RV) failure has lagged behind compared to the left ventricle (LV). Previous work from our lab revealed that the embryonic basic helix-loop-helix transcription factor heart and neural crest derivatives expressed-2 (Hand2) is re-expressed in the adult heart and activates a 'fetal gene program' contributing to pathological cardiac remodelling under conditions of LV pressure overload. As such, ablation of cardiac expression of Hand2 conferred protection to cardiac stress and abrogated the maladaptive effects that were observed upon increased expression levels. In this study, we aimed to understand the contribution of Hand2 to RV remodelling in response to pressure overload induced by pulmonary artery banding (PAB).

Methods and results

In the present study, Hand2F/F and MCM- Hand2F/F mice were treated with tamoxifen (control and knockout, respectively) and subjected to six weeks of RV pressure overload induced by PAB. Echocardiographic- and MRI-derived hemodynamic parameters as well as molecular remodelling were assessed for all experimental groups and compared to sham-operated controls. Six weeks after PAB, levels of Hand2 expression increased in the control banded animals but, as expected, remained absent in the knockout hearts. Despite the dramatic differences in Hand2 expression, pressure overload resulted in impaired cardiac function independently of the genotype. In fact, Hand2 depletion seems to sensitize the RV to pressure overload as these mice develop more hypertrophy and more severe cardiac dysfunction. The LV of RV-pressure overloaded hearts was also dramatically affected as reflected by changes in shape, decreased LV mass and impaired cardiac function. RNA sequencing revealed a distinct set of genes that are dysregulated in the pressure-overloaded RV, compared to the previously described pressure-overloaded LV.

Conclusions

Cardiac-specific depletion of Hand2 is associated with severe cardiac dysfunction in conditions of RV pressure overload. While inhibiting Hand2 expression can prevent cardiac dysfunction in conditions of LV pressure overload, the same does not hold true for conditions of RV pressure overload. This study highlights the need to better understand the molecular mechanisms driving pathological remodelling of the RV in contrast to the LV, in order to better diagnose and treat patients with RV or LV failure.

INTRODUCTION

Heart failure (HF), roughly described as the inability of the heart to pump blood, is a leading cause of morbidity and mortality worldwide, currently affecting more than 26 million people.[1] Commonly, HF is classified in left (LV) and right ventricular (RV) failure, depending on which ventricle is failing. The majority of the studies are focused on LV failure, whereas RV failure has received less attention. Therefore, it is not surprising that the knowledge on LV failure is greater and more accurate than on RV failure. Likewise, most of the therapies for HF are directed to the LV and commonly also administered to patients suffering from RV failure. As RV failure remains associated with poor prognosis,[2] new RV specific therapies are urgently needed. However, our limited understanding on RV molecular pathophysiological mechanisms remains an obstacle in the development of new and more efficient drugs.

The RV has not been systematically investigated on the cellular and molecular level most likely because of the widely held opinion that the conditions governing RV and LV failure are identical or very similar and, as such, most concepts of RV failure have been shaped by the studies of the LV. However, embryological and physiological differences exist between both ventricles that support the hypothesis that gene expression patterns and their consequences differ between RV and LV failure. In fact, from embryonic development to the adult organism, both ventricles are exposed to different stimuli, including different hemodynamic forces and unique patterns of gene expression. RV is characterized by thinner walls, continuous coronary flow and is classically connected to a low-resistance pulmonary circulation, rendering it more sensitive to pressure-overload than volume-overload.[3,4]

The vertebrate heart forms from two populations of cardiac progenitor cells: the primary and the secondary heart field. The primary heart field gives rise to the cardiac crescent, left ventricle and atria.[5-7] The secondary heart field gives rise to the outflow tract, the right ventricle and atria.[5,8] During these embryological processes, transcription factors are locally expressed in the developing heart and while some can be found in both the primary and secondary heart fields, others show specific expression patterns in just one of them. T-box 5 (*TBX5*) and the basic helix-loop-helix transcription factor heart and neural crest derivatives expressed-1 (*HAND1*) are both expressed in the primary heart field, while heart and neural crest derivatives expressed-2 (*HAND2*), islet-1 (*ISL1*), fibroblast growth factor-8 (*FGF8*), fibroblast growth factor-10 (*FGF10*) and paired-like homeodomain-2 (*PITX2*) are expressed in the secondary heart field.[9,10] In mice, loss-of-function of these transcription factors revealed their importance during development of the heart. Without expression of *Hand1*, formation of the left ventricle is disrupted due to a proliferation defect, and the mutants die from extraembryonic effects.[11-13] In contrast, *Hand2* mutants show right-ventricular deficient vascularization and hypoplasia.[14,15] From embryonic day

7.75, *Hand2* expression becomes limited to heart tube segments that will develop in the future RV, but, after E10.5, *Hand2* expression is disrupted and its levels decline drastically in the heart.[15-16] Interestingly, two studies reported that individuals with pulmonary stenosis and congenital heart disease carry a loss-of-function mutation of the *HAND2* gene,[17-18] suggesting *HAND2* as a potential key player in RV failure pathology. Furthermore, previous work from our lab revealed that *Hand2* re-expression in the adult mouse heart activates a 'fetal gene program' and contributes to pathological cardiac remodelling under conditions of LV pressure overload. *Hand2* overexpression induces hypertrophic growth of the LV and bi-chamber dilation, again suggesting a role for this transcription factor in adult RV remodelling.[19] In agreement, ablation of cardiac expression of *Hand2* conferred protection to cardiac stress and abrogated the maladaptive effects that were observed upon increased expression levels.

RV failure is a complex condition with an important impact on cardiovascular disease that still lacks accurate understanding and consequently, an efficient treatment. Here, we aim to elucidate the molecular mechanisms underlying RV failure, and decipher the intricate role of Hand2 on RV hypertrophy, by functional and molecular characterization of hearts from mice with cardiac-specific *Hand2* ablation and that were exposed to conditions of RV pressure overload.

MATERIAL AND METHODS

Experimental procedures were reviewed and approved by the Institutional Animal Care and Use Committees and authorized by the Animal Experimental Committee of the local government in accordance to the Dutch law (DEC 2012-172) and European Directive 2010/63/EU. In addition, the investigation conforms to the Guide for the Care and Use of Laboratory Animals published by the US National Institutes of Health (NIH Publication No. 85-23, revised 1985).

Animal models and Pulmonary Artery Banding Surgery

Mice harboring a floxed allele of *Hand2* (*Hand2*$^{F/F}$) in a B6129F1 background were described previously,[20] and crossbred with mice harboring a tamoxifen-regulated form of Cre recombinase (MerCreMer) under control of the murine *Myh6* promoter (MHC–MerCreMer; MCM mice)[21] in a B6129F1 background to generate MCM–*Hand2*$^{F/F}$ mice. *Hand2*$^{F/F}$ and MCM–*Hand2*$^{F/F}$ were treated with either vehicle (10/90 v/v ethanol/peanut oil, Sigma P2144) or tamoxifen (45 mg kg^{-1} per day) by daily intraperitoneal injections for 5 consecutive days. Both male and female, adult MCM–*Hand2*$^{F/F}$ mice and *Hand2*$^{F/F}$ mice (10-12 weeks of age) were used for functional and histological analyses.

Pulmonary artery banding (PAB) was performed, as described below, in mice older than 8 weeks from both genders. Animals were anesthetized with isofluorane/air mixture (5% induction; 2–3% maintenance), and subsequently analgesia with buprenorphine (0.01 mg/kg s.c.) was injected. Animals were placed in a supine position on a heating pad (37˚C) and intubated with a 20G catheter and ventilated with room air using a Harvard mini-ventilator (model 687, Hugo Sachs, Germany; respiratory rate 180 breaths per minute and a tidal volume of 125 µL). The pulmonary artery was approached by a left lateral thoracotomy and banded with a 7-0 suture by tying over a 23G needle. Post-operative pain relief was provided with buprenorphine (0.01 mg/kg s.c.) twice daily for 2-3 consecutive days if necessary. Sham-operated animals underwent the same procedure without PAB. All protocols were reviewed and approved by the Animal Care and Use Committee of the University of Maastricht and Animal Experiments Committee of the University of Groningen and were performed according to the rules formulated in the Dutch law on care and use of experimental animals.

Hemodynamic analyses

Hemodynamic function was assessed at day 5 and week 6 after sham or PAB surgery, by cardiac magnetic resonance imaging (MRI) during anesthesia with isoflurane (induction 5%; 1.5-3% maintenance) and warming at 37˚C. Echocardiography to assess the pulmonary artery banding gradient was performed using a Vivid Dimension 7

and i13L-transducer (GE Healthcare, Waukesha, WI, USA) from a short-axis view at aortic level, at day 5 and week 6 after sham or PAB surgery. MRI was performed by using a vertical 9.4T 89-mm diameter bore scanner (Bruker BioSpin, Etllingen, Germany) equipped with 1,500 mT/m gradienset (Bruker BioSpin GmbH, Ellingen, Germany). Respiratory and heart rate were derived using a pressure pad placed under the chest of the mouse. The longitudinal axis of the RV was determined with two and four chamber scout scans, where after axes were adjusted to actual axes. Slices of longitudinal axis, four chamber view, and ten or eleven slices of the short-axis of one millimeter and no slice gap were obtained. Slices were derived including complete apex and base of the right ventricle. Cine imaging was performed with a retrospectively-triggered (self-gated) gradient-echo sequence (Paravision 4.0 and IntraGate, Bruker Biopspin GmBH) with the following settings: TR=6.8 ms, TE= 1.9 ms, number of movie frames= 15, slice thickness= 1 mm, matrix= 256 x 256 and field of view= 30 x 30. The myocardium was manually segmented by drawing the epicardial and endocardial contours, excluding the papillary muscles using QMass (version MR 7.6, Medis Medical Imaging Systems, Leiden, The Netherlands). Semiautomatic segmentation was used to determine end-diastolic volume (EDV), end-systolic volume (ESV), and wall thickness (WT). Stroke volume (SV) was calculated as EDV-ESV. Ejection fraction (EF) was calculated as (EDV - ESV)/EDVX100. Cardiac output (CO) was calculated manually as SV x mean observed heart rate. Septal flattening is expressed by the eccentricity index, both end diastolic and systolic, which was calculated by dividing the diameter of the left ventricular diameter parallel to the intraventricular septum by the diameter perpendicular to the intraventricular septum derived from short-axis at the mid-papillary level.

RNA isolation, cDNA conversion and Real-time RT-PCR

Total RNA was isolated from mouse heart tissue using Direct-zol™ reagent (ZYMO) according to manufacturer's instructions. RNA (1 ug) was then reverse-transcribed with either M-MLV reverse transcriptase (Promega, Madison, WI, USA). Quantitative real-time polymerase chain reaction (qPCR) was performed on a BioRad iCycler (Biorad) using SYBR Green reagent (VWR). Transcript quantities were compared using the relative Ct method, where the amount of target normalized to the amount of endogenous control (L7 for mRNAs) and relative to the control sample is given by $2^{-\Delta Ct}$. Primer sequences for mRNA detection are depicted in **supplemental table 1**.

Histology, Immunohistochemistry and immunofluorescence

For histological analysis, hearts were perfusion-fixed with 4% paraformaldehyde, embedded in paraffin and cut into 4-µm sections. Paraffin sections were stained

with hematoxylin and eosin (H&E) for routine histological analysis, Sirius Red for detection of fibrillar collagen and FITC-labelled wheat-germ-agglutinin (WGA, Sigma) to visualize and quantify the cell cross-sectional area (CSA). Modification of Isolectine B4 staining with additional fluorescence labeled-streptavidin (Dylight 595-conjugated streptavidin, Jackson Thermo, 1:100) and counterstaining with FITC-labeled WGA was performed to assess capillary to cardiomyocyte ratios. Collagen deposition, cell CSA and capillary density were determined using ImageJ software. Slides were visualized using a Leica DM2000 and a Leica DM3000 microscope for bright field and fluorescence imaging, respectively

Library construction and sequencing

Total RNA was extracted using Direct-zol™ reagent (ZYMO), following the manufacturer's procedure. The total RNA quality and quantity were analysed by a Bioanalyzer 2100 and RNA 6000 Nano LabChip Kit (Agilent, CA, USA) with RIN number >7.0. Approximately 10 mg of total RNA was used to remove ribosomal RNA according to the manuscript of the Epicentre Ribo-Zero Gold Kit (Illumina, San Diego, USA). Following purification, the ribo-minus RNA fractions is fragmented into small pieces using divalent cations under elevated temperature. Then the cleaved RNA fragments were reverse-transcribed to create the final cDNA library in accordance with a strand-specific library preparation by dUTP method. The average insert size for the paired-end libraries was 300±50 bp. And then we performed the pair-end 2×150bp sequencing on an illumina Hiseq 4000 platform housed in the LC Sciences (Hangzhou, China) following the vendor's recommended protocol.

Bioinformatics analysis

For transcripts assembly, firstly, Cutadapt[22] and perl scripts in house were used to remove the reads that contained adaptor contamination, low quality bases and undetermined bases. Then sequence quality was verified using FastQC (http://www.bioinformatics. babraham.ac.uk/projects/fastqc/). We used Bowtie2[23] and Tophat2[24] to map reads to the genome of Mus musculus (Version: v88). The mapped reads of each sample were assembled using StringTie.[25] Then, all transcriptomes from 6 samples were merged to reconstruct a comprehensive transcriptome using perl scripts and gffcompare (https://github.com/ gpertea/gffcompare/). After the final transcriptome was generated, StringTie[25] and Ballgown[26] was used to estimate the expression levels of all transcripts. To analyze the differential expression StringTie[25] was used to perform expression level for mRNAs by calculating FPKM (FPKM=[total_exon_fragments/mapped_reads(millions) *exon_length(kB)]). The differentially expressed mRNAs were selected with log2 (fold change) >1 or log2 (fold change)

<-1 and with parametric F-test comparing nested linear models (p value < 0.05) by R package Ballgown.[26]

Statistical Analysis

All data are presented as mean ± standard error of mean (SEM). The variables were analyzed using Student's t-test and two-way analysis of variance (ANOVA) to assess statistical significance between groups (IBM SPSS Statistics for Macintosh, Version 25.0, released 2017; IBM Corp). The evaluation of significant effects evaluation was conducted using Tukey's multiple comparison tests, with an adjusted calculation of *p*-value. Probability values $p<0.05$ were considered statistically significant.

RESULTS

Cardiac-specific deletion of Hand2 augments RV susceptibility to increased pressure overload induced by PAB

To assess the contribution of Hand2 to the response of the RV to pressure overload, we induced deletion of a floxed *Hand2* (*Hand2*$^{F/F}$) allele using a tamoxifen-inducible Cre recombinase protein fused to two mutant oestrogen-receptor ligand-binding domains [F] under control of the cardiac-specific a-myosin heavy chain promoter (MCM-*Hand2*$^{F/F}$) in adult mice, as described by us before.[19] *Hand2*$^{F/F}$ (control) and MCM-*Hand2*$^{F/F}$ (knockout) mice were subjected to sham or pulmonary artery banding (PAB) surgery for 6 weeks, a period during which cardiac function was assessed by echocardiography at day 5 and MRI at weeks 2 and 6 (**figure 1a**). Whereas 5 days after PAB surgery, both *Hand2*$^{F/F}$ and *MCM-Hand2*$^{F/F}$ mice displayed a similar increase in PA gradients (**figure 1b**), the knockout mice showed a slight decrease in pressure 6 weeks after banding, even though it was not statistically significant. In control mice, RV pressure overload induced myocardial *Hand2* expression by 3.5-fold in the RV and 3-fold in the LV (**figure 1c**). Elevated expression of *Hand2* in control mice subjected to PAB, is accompanied by impaired RV function as reflected by functional parameters, assessed by MRI at week 6 (**figure 1d-1k, table 1**). These results suggest that lowering *Hand2* expression could protect the heart from RV pressure overload, as also shown previously for mouse models of LV pressure overload.[19] Hand2 silencing, however, resulted in further impairment of RV remodelling and function as reflected by increased RV end-diastolic and end-systolic volumes (EDV and ESV, respectively; **figure 1e and 1f, table 1**) and a subsequent decrease in RV ejection fraction (RV EF; **figure 1g, table 2**). Impaired RV function was also associated with increased RV mass (**figure 1i and 1j, table 1**). These data suggest an increase in sensitivity of the RV to pressure overload when *Hand2* is silenced.

Although elevated expression of Hand2 in control mice subjected to PAB is accompanied by impaired RV function, Hand2 silencing resulted in further impairment of right ventricular remodelling and function.

Table 1. MRI assessment of right ventricle function parameters of Hand2F/F and MCM-Hand2F/F mice at 2 and 6 weeks of sham or PAB

	Hand2$^{F/F}$				MCM- Hand2$^{F/F}$			
	sham		PAB		sham		PAB	
	2 weeks	6 weeks	2 weeks	6 weeks	2 weeks	6 weeks	2 weeks	6 weeks
Stroke volume (μl)	27.0±3.2	21.1±1.1	24.0±2.1	24.9±2.4	26.9±2.3	23.8±4.0	25.9±1.8	23.1±2.8
Cardiac output (ml/min)	14.1±1.3	11.1±1.3	10.0±0.9*	10.4±0.8*	12.9±0.8	13.3±1.3	11.9±0.6	10.6±1.0*
ED volume (μl)	71.2±8.9	72.0±6.8	84.1±12.5	91.7±13.5	66.5±3.1	68.8±6.1	116.9±7.4*#	117.8±10.7*#
ES volume (μl)	44.1±5.8	50.9±6.1	60.1±14.4	66.7±12.7*	39.5±3.9	45.1±2.5	91.0±6.2*#	94.7±10.2*#
ED mass (mg)	22.6±1.7	22.3±4.7	30.1±3.2*	32.9±3.8*	22.2±2.8	23.2±2.0	33.9±2.6*	37.8±2.0*
ES mass (mg)	20.4±2.1	24.3±2.2	29.9±4.9	36.3±4.7*	19.9±2.4	21.6±1.4	34.4±1.2*	37.6±3.1*
EF (%)	38.1±1.9	38.2±3.8	28.6±2.0	26.1±2.4*	40.9±3.0	34.8±2.3	22.3±1.3*#	19.4±2.1*#

Data are expressed as means ± SEM. ED, end-diastole; ES, end-systole; RV, right ventricle; EF, ejection fraction. *, indicates $p<0.05$ vs sham group; #, indicates $p<0.05$ *vs* experimental group. n.s.=5-10 animals per group

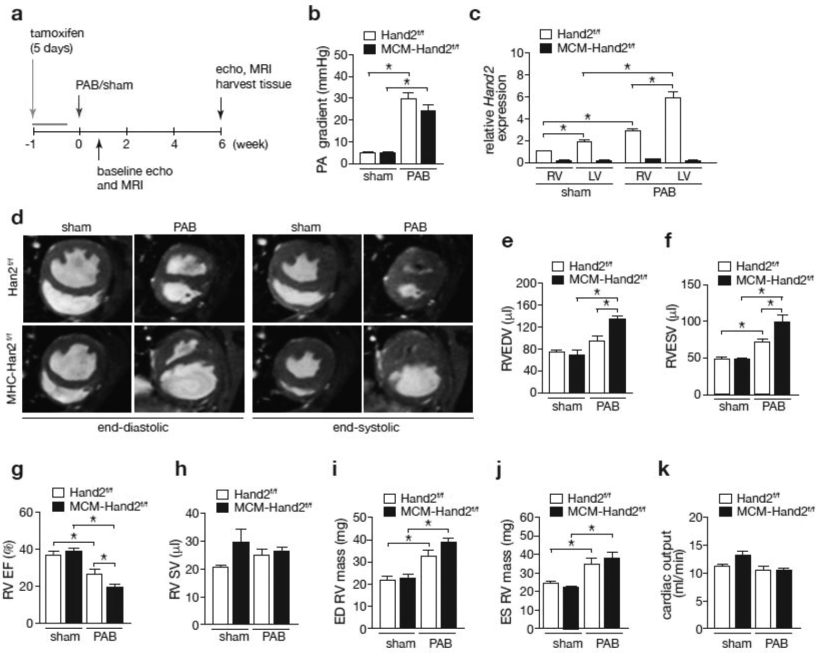

Figure 1. Cardiac specific depletion of Hand2 sensitizes the RV to pressure overload. a) Design of the in vivo study; b) Assessment of pulmonary artery pressure gradient in control (Hand2F/F) and knockout (MCM-Hand2F/F) mice 5 days after either sham or PAB surgery; c) Quantitative real-time PCR analysis of Hand2 expression in RV tissue from Hand2F/F and MCM-Hand2F/F animals either after sham or PAB surgery; d) Representative images of short-axis plan in end-diastole and end-systole hearts obtained by cardiac resonance image from Hand2F/F and MCM-Hand2F/F animals either after sham or PAB surgery Cardiac function was assessed in hearts from Hand2F/F and MCM-Hand2F/F animals either after sham or PAB surgery, and followed by quantitative analysis: e) RV end-diastolic volumes (EDV) and f) RV end-systolic volumes (ESV); g) RV ejection fraction (EF); h) RV stroke volume; i) RV end-diastolic mass; j) RV end-systolic mass; k) Cardiac output. Data are from 5-10 animals per group; $*p < 0.05$ between indicated groups (error bars are s.e.m.).

Cardiac-specific silencing of Hand2 exacerbates hypertrophic growth of the RV in response to pressure overload

Hypertrophy of the right heart was assessed by the Fulton index, the ratio of right ventricular weight to left ventricular plus septum weight (RV/LV+S). Whereas an increased Fulton index was observed 6 weeks after PAB in both control and knockout animals, compared to sham (**figure 2a, table 2**), the effect was more profound in the absence of *Hand2* expression. These observations were confirmed by increased CSA of cardiomyocytes derived from banded-knockout hearts when compared banded-control hearts (**figure 2b and 2c)**. Hypertrophic RV remodelling was associated with significantly increased mRNA expression of hypertrophic "fetal" cardiac genes encoding natriuretic peptides atrial natriuretic factor (*Nppa*) and brain natriuretic peptide (*Nppb*), alpha-skeletal actin 1 (*Acta1*) and a-myosin heavy chain (*Myh7*) (**figure 2d-g**). Furthermore, an increase in mRNA levels of regulator of calcineurin isoform 4 (*RCAN1.4*) confirms activation of calcineurin/NFAT signaling in the RV response to pressure overload which was not affected by *Hand2* silencing (**figure 2h**). At 6 weeks post-PAB, both control and *Hand2* knockout animals displayed similar levels of collagen deposition and formation of fibrotic lesions (**figure 2i,j**). In line, no significant differences were observed for mRNA expression levels of the profibrotic markers collagen type I (*Col1A*), transforming growth factor beta (*Tgfb)* and endoglin (*Eng)* between the banded animals (**figure 2k-m**). Remarkably, despite silencing of Hand2 resulting in lower levels of profibrotic markers in the RV of sham animals, these levels significantly rose to control levels upon subjection to PAB.

As RV capillary rarefaction is a phenomenon that leads to maladaptive RV remodelling, we assessed the capillary to myocyte ratio of the RV in our different experimental groups. While histochemical analysis and respective quantification reflected higher capillary to myocyte ratio in control mice subjected to RV stress, a significant decrease was observed in Hand2 knockout animals, under the same conditions (**figure 2n**). Vascular endothelial growth factor receptor 2 (*Vegfr2*) expression levels, revealed angiogenic favoring patterns with increased expression levels in the knockout compared to control animals, either subjected to sham or PAB. Although knockout PAB animals showed increased *Vegfr2* expression (compared to controls), this pattern was insufficient to promote adequate angiogenesis (**figure 2n**), and RV stress in the absence of Hand2 expression resulted in inhibition of *Vegfr2* (compared to sham, **figure 2o**).

Taken together, these data indicate that silencing of Hand2 induces exacerbated hypertrophy while also impairing microvascular remodelling under conditions of RV pressure overload.

Table 2. Morphometric characteristics of Hand2F/F and MCM-Hand2F/F mice subjected to 6 weeks of sham or PAB

	Hand2$^{F/F}$		MCM- Hand2$^{F/F}$	
	sham	PAB	sham	PAB
n	5	6	6	10
HW/BW (mg/g)	5.6±0.5	7.3±0.7*	5.9±0.7	7.9±0.3*
HW/TL (mg/mm)	7.9±0.5	9.2±0.4	7.9±0.6	10.0±0.4*
RVW (mg)	29.2±2.1	39.3±1.1*	26.5±3.1	44.4±3.9*
IVS+LV (mg)	127.1±7.1	151.8±9.0*	138.3±5.2	150.2±10.3*
Fulton index	0.18±0.02	0.25±0.01*	0.19±0.03	0.30±0.02*#

Data are expressed as means ± SEM. HW, heart weight; BW, body weight; TL, tibia length; RVW, right ventricle weight; IVS, intraventricular septum; LV, left ventricle. *, indicates p<0.05 vs sham group; #, indicates p<0.05 vs experimental group. n.s.=5-10 animals per group.

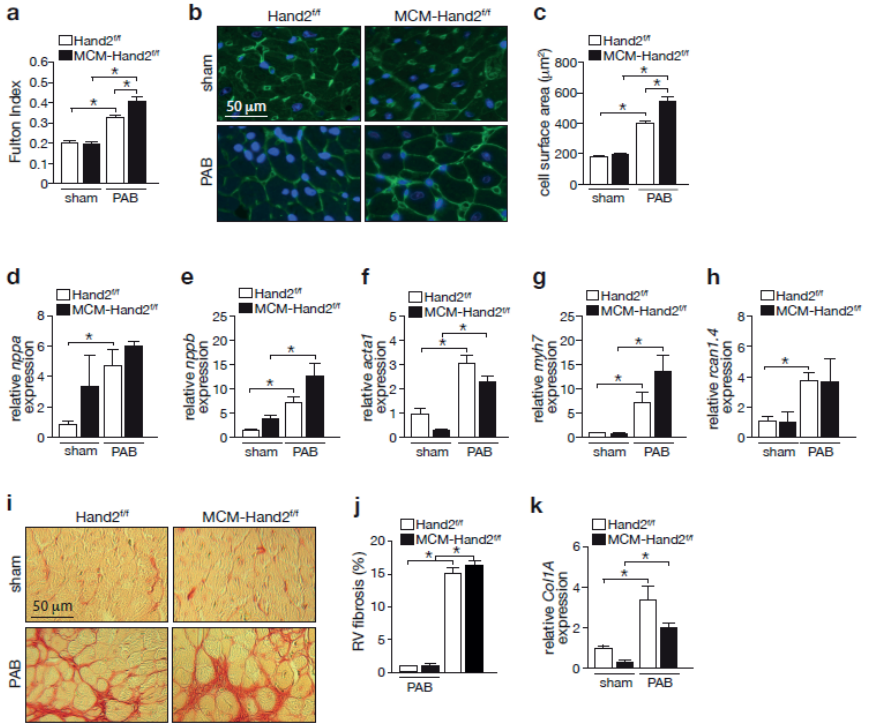

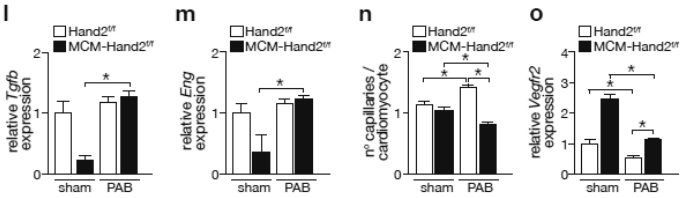

Figure 2. Assessment of right ventricular remodelling induced by PAB upon cardiac depletion of Hand2. a) Fulton's index values (ratio of right ventricular weight to left ventricular plus septal weight) of Hand2F/F and MCM-Hand2F/F animals either after sham or PAB surgery; b) High-magnification of representative images of histological sections stained for wheat germ agglutinin (WGA); c) Quantification of CSA in b, n=30 microscopic field/heart, 3 hearts. Quantitative real-time PCR analysis was performed to assess the expression levels of several genes known to be related to cardiac hypertrophy in RV tissue from Hand2F/F and MCM-Hand2F/F animals either after sham or PAB surgery: d) natriuretic peptides atrial natriuretic factor (Nppa); e) brain natriuretic peptide (Nppb); f) -skeletal actin (Acta1); g) -myosin heavy chain (Myh7); h) regulator of Calcineurin 1 Isoform 4 (Rcan1-4); i) High-magnification of representative images of histological sections stained for Sirius Red; j) Quantification of collagen deposition in i, n=30 microscopic field/heart, 3 hearts. Quantitative real-time PCR analysis of k) collagen type I alpha 1 chain (Col1A1); l) transforming growth factor beta (TGF-β) and m) endoglin; n) Capillaries in RV sections of Hand2F/F and MCM-Hand2F/F animals subjected to either sham or PAB surgery were identified by isolectin B4 immunohistochemistry combined with WGA and, from the images obtained, we determined the ratio of capillaries per cardiomyocyte ratios; o) Quantitative real-time PCR analysis of vascular endothelial growth factor receptor 2 (Vegfr2) expression levels in the RV of Hand2F/F and MCM-Hand2F/F animals, subjected to either sham or PAB surgery. Data are from 5-10 animals per group; $*p < 0.05$ between indicated groups (error bars are s.e.m.).

Effects of cardiac silencing of Hand2 in the function and morphology of the LV under conditions of right ventricular pressure overload

Based on interventricular interaction, any changes in RV shape will have consequences for the LV. While we observed increased eccentricity for the banded animals at both end-diastole and end-systole, no differences were observed between control and knockout mice (**figure 3a and 3b**). Increased LV eccentricity index reflects increased pressure of the RV and represents septal flattening which affects LV function and remodelling. Pressure overloaded animals, independent of the genotype, displayed decreased LV end-diastolic and -systolic volumes and subsequent decrease in stroke volumes and cardiac output (**table 3**). No changes in systolic function were observed, as reflected by preserved LV ejection fraction throughout the different experimental groups (**table 3**). Whereas animals subjected to PAB seem to display larger cardiomyocytes, this effect was not significant in the control or knockout mice (**figure 3c**). In agreement, a clear upregulation of the stress cardiac genes *Nppa*, *Nppb* and *Myh7* in the LV of control-banded animals was observed but the expression levels remained at baseline in banded-knockout animals (**figure 3d-f**). A significant downregulation in *Acta1* mRNA expression levels in the LV, after PAB, was observed independent of the genotype and in contrast to the RV (**figure 3g**). While a clear increase in *Rcan1.4* was observed in the LV of

control hearts upon RV pressure overload, *Rcan1.4* mRNA levels were significantly decreased in the knockout LVs, under similar conditions, compared to the control LVs (**figure 3h**). Although increased collagen deposition and fibrotic lesions were observed in the LVs of the control mice subjected to PAB, this was not observed in knockout animals (**figure 3i**). Similar results were obtained regarding mRNA levels for *Col1A*, *Tgfβ* and *Eng* in the LV tissue (**figure 3j-l**).

When assessing the capillary density of the LV in our different experimental groups we observed higher capillary density in the control mice compared to the knockout animals, in both sham and PAB groups, despite a decrease in the overloaded groups (**figure 3m**). The lower capillary density observed at baseline in the Hand2 knockout animals was even more reduced upon RV stress (**figure 3m**). This was in line with the expression profile of *Vegfr2*, which although not significant did show a trend to decrease in the absence of Hand2, either at baseline or under RV stress conditions (**figure 3n**).

Silencing of Hand2 seems to ameliorate the molecular maladaptive response of the left ventricle to right ventricular stress.

These data suggest that RV pressure overload results in deformation of the LV with preserved LV function. Furthermore, while silencing of Hand2 seems to ameliorate the molecular maladaptive response of the LV to RV stress, vascular remodelling remains slightly impaired.

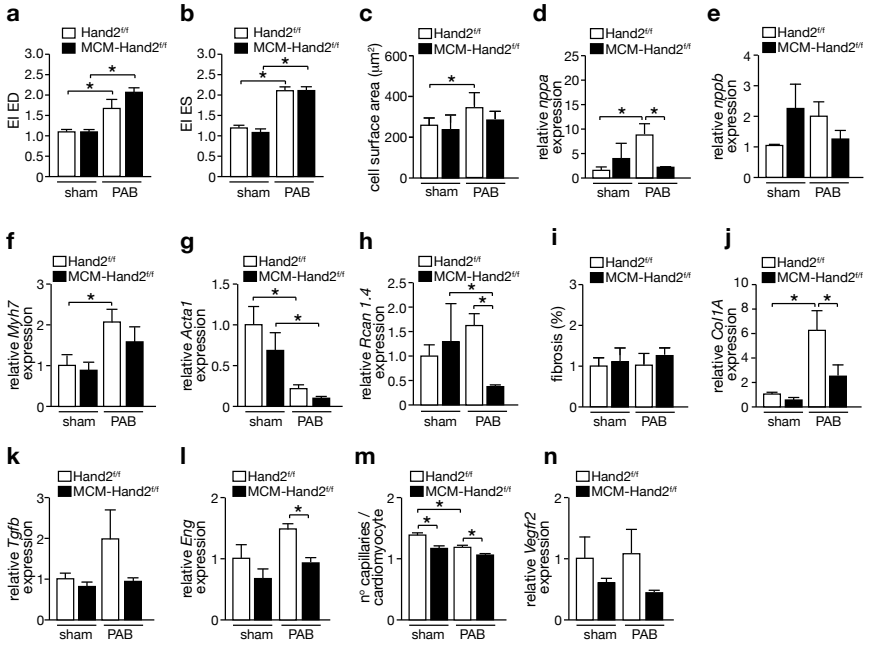

Figure 3. Assessment of left ventricular remodelling induced by PAB upon cardiac depletion of Hand2. a) Assessment of left ventricular eccentricity index at end-diastole and b) end-systole; c) Quantification of cardiomyocyte CSA from images of histological sections stained for wheat germ agglutinin (WGA), n=30 microscopic field/heart, 3 hearts. Quantitative real-time PCR analysis was performed to assess the expression levels of several genes known to be related to cardiac hypertrophy in RV tissue from Hand2F/F and MCM-Hand2F/F animals either after sham or PAB surgery: d) natriuretic peptides atrial natriuretic factor (Nppa); e) brain natriuretic peptide (Nppb); f) -myosin heavy chain (Myh7); g) -skeletal actin (Acta1); h) regulator of Calcineurin 1 Isoform 4 (Rcan1-4); i) Quantification of collagen deposition from images of histological sections stained for Sirius Red, n=30 microscopic field/heart, 3 hearts. Quantitative real-time PCR analysis of j) collagen type I alpha 1 chain (Col1A1); k) transforming growth factor beta (TGF-β) and l) endoglin; m) Capillaries in RV sections of Hand2F/F and MCM-Hand2F/F animals subjected to either sham or PAB surgery were identified by isolectin B4 immunohistochemistry combined with WGA and, from the images obtained, we determined the ratio of capillaries per cardiomyocyte ratios; n) Quantitative real-time PCR analysis of vascular endothelial growth factor receptor 2 (Vegfr2) expression levels in the RV of Hand2F/F and MCM-Hand2F/F animals, subjected to either sham or PAB surgery. Data are from 5-10 animals per group; $*p < 0.05$ between indicated groups (error bars are s.e.m.).

Mechanisms underlying pressure overload-induced RV pathological remodelling

During RV failure, pathological remodelling is activated, as observed by an increase in cardiomyocyte hypertrophy and fibrosis, followed by a decline in cardiac function. To obtain more insight into the molecular and cellular mechanisms driving RV remodelling induced by pressure overload, we performed total RNA sequencing in RV tissue derived from control ($Hand2^{F/F}$) animals subjected to either sham or PAB surgery. Transcriptomic analysis revealed 1399 genes to be differentially expressed,

either up- or downregulated, between the two groups (**figure 4a, supplemental table 2**). Generation of a heatmap representing the 100 most differentially expressed transcripts between the experimental groups disclosed 17 downregulated and 83 upregulated genes in the banded WT animals (**figure 4b**). Among the top upregulated, we found several collagens and fibrotic related genes (Collagen type VIII, type IV and type XVI alpha 1 chain, *Col8a1*, *Col4a1* and *Col16a1*; Periostin, *Postn*; and Transforming growth factor beta-3, *Tgfβ3*) but also hypertrophic (Natriuretic peptide A and B, *Nppa* and *Nppb*, respectively; Myocilin, *Myoc*) and inflammatory genes (Interleukin 17 receptor C, *Il17rc* and Chemokine C-motif ligand 21A serine, *Ccl21a*) (**figure 4b**). After compiling our list of PAB-associated genes, we undertook a gene ontology enrichment analysis of this gene set, processing genes in terms of their associated molecular function. The top 20 GO terms based on biological processes and ranked by fold-enrichment are shown in **figure 4c**. This top-rank included biological processes such as "extracellular matrix-receptor interaction, collagen trimer, neutrophil chemotaxis, cell adhesion and chemokine signaling, receptor binding and activity. The KEGG pathway analysis results revealed that the differentially expressed genes were highly associated with several pathways, including "TNF-signaling pathway", "hypertrophic cardiomyopathy", "dilated cardiomyopathy", "ECM-receptor interaction" as well as "chemokine signaling" (**figure 4d**). These results indicate that cardiac remodelling induced by PAB involves genes that are directly related to fibrosis, ECM remodelling, vascular function and inflammation, in agreement with the RV and LV phenotypes observed in mice that were subjected to PAB.

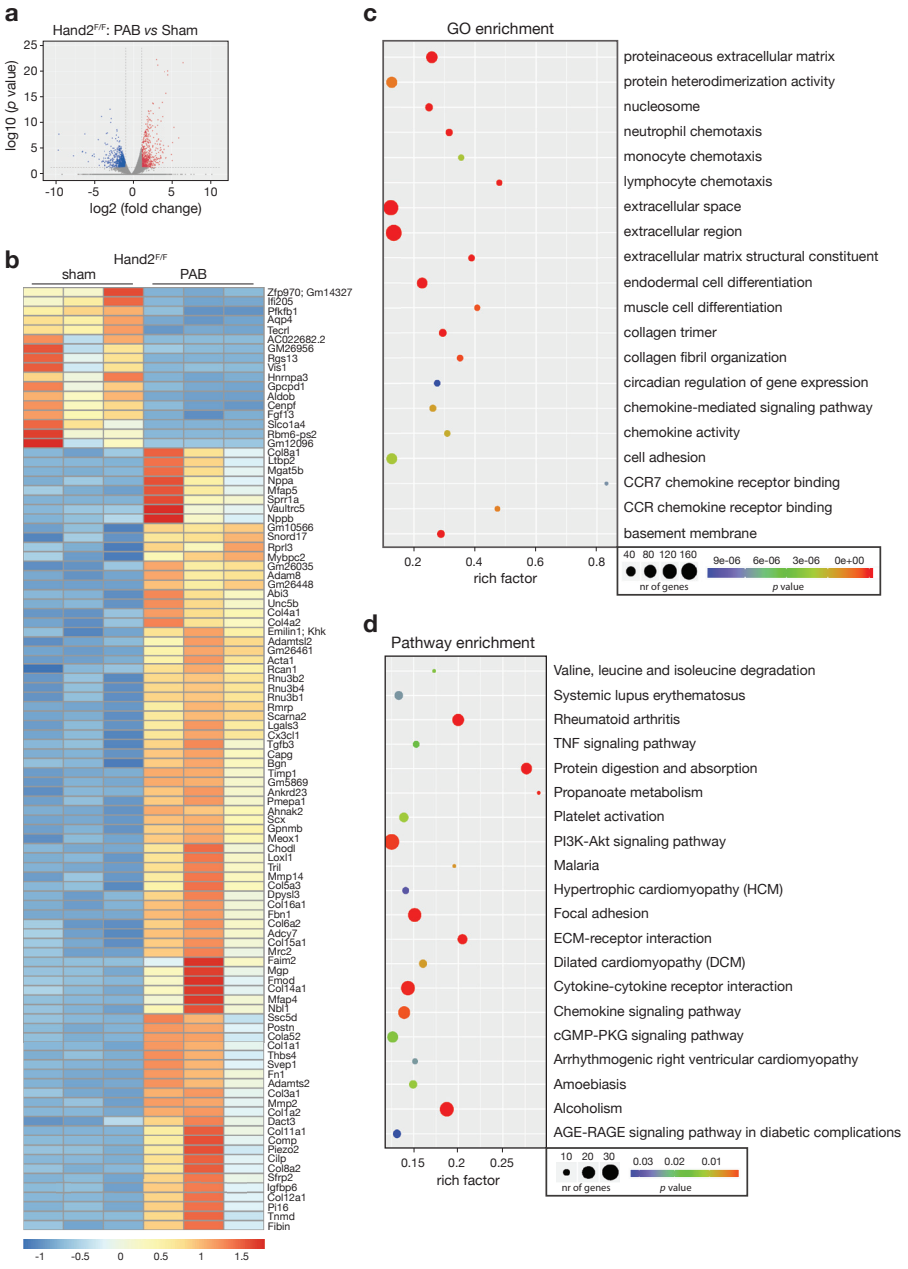

Figure 4. Transcriptional changes in the pressure-overloaded RV. RNA-sequencing was performed to assess the transcriptomic changes in RV tissue from control (Hand2F/F) animals subjected to either sham or PAB surgery for 6 weeks. a) Volcano plot representation of differential expression of genes in the RV of sham and

banded animals. Red and blue points mark the genes with significantly increased or decreased expression, respectively, in Hand2F/F sham to Hand2F/F PAB (FDR<0.01). The x-axis shows log2-fold expression changes and the y-axis the log10-fold likelihood of a gene being differentially expressed; b) Heatmap of the 100 top differentially expressed genes in the RV tissue of Hand2F/F sham compared to Hand2F/F PAB showing log2 FPKM (color scale) values of dysregulated genes, with red and blue colors representing increased and decreased expression, respectively; c) Number of differentially expressed genes enriched in GO terms with p value and rich factor shown in a scatterplot. The summarized GO terms are related to the biological processes upon pulmonary artery banding in the heart. Rich factor=number of differentially expressed genes in GO term/total number of genes in GO term. The larger the rich factor, the higher enrichment is. Circle size is proportional to the frequency of the GO term, whereas color indicates the log10 p value (red higher, blue lower); d) KEGG pathway analysis of differentially expressed genes with p value and rich factor shown in a scatterplot. Differentially enriched pathways in the RV tissue of control animals subjected to PAB, in comparison to sham.

Mechanisms underlying the role of Hand2 in pressure overload-induced RV pathological remodelling

Next, and to better understand how RV remodelling induced by pressure overload is affected by Hand2 silencing, we performed RNA-sequencing to assess the transcriptomic changes in total RNA from RV tissue derived from control or knockout animals subjected to PAB. Transcriptome analysis identified 1783 transcripts potentially regulated by Hand2 (**figure 5a, supplemental table 3**). Generation of a heatmap representing the 100 most differentially expressed transcripts between the 2 experimental groups revealed 33 downregulated and 67 upregulated genes in the RV of Hand2 knockout mice (**figure 5b, table 5**). Upon silencing of Hand2, RV stress resulted in downregulation of genes that are mostly associated with cellular components related to nucleic acid binding, regulation of transcription and transcription factor activity (U3B small nuclear RNA 2, *Rnu3b2*; GINS complex subunit 2, *Gins2*; Telomerase RNA component, *Terc*; Transcription factor 7, *TCF7*) and cell adhesion genes (a desintegrin and metallopeptidase domain 8, *Adam8*; Angiopoietin-like protein 4, *Angptl4*; Rho GDP dissociation inhibitor alpha, *Arhgdia*; Ankyrin repeat domain 63, *Ankrd63*; Ephrin B3, *Efnb3*) (**figure 5b,c**). In turn, the upregulated genes are associated with hypertrophy (*Nppb*; Myotrophin, *Mtpn*; Distrophin, *Dmd*) and cell cycle inhibitors (Interferon activated gene 205, *Ifi205*; cell division cycle 73, *CDC73*) (**figure 5b, 5c**). Interestingly, genes such as Bone morphogenetic protein receptor, type II (*Bmpr2*), Rho-associated coiled-coil containing protein kinase 2 (*Rock2*) and Tissue inhibitor of metalloproteinase 3 (*Timp3*), previously associated with pulmonary hypertension (PH), showed an even higher expression in the absence of Hand2. Furthermore, ontology (GO) and pathway (KEGG) enrichment analysis associated the observed gene expression patterns with regulation of transcription, muscle cell differentiation, cellular response to hypoxia, as well as with development of different types of cancer and different signaling pathways in cancer, platelet activation, p53 signaling pathway and cell communication through gap junctions (**figure 5c, 5d**). These results reveal the role of Hand2 in specific molecular and cellular processes that key in the response of the RV to pressure overload.

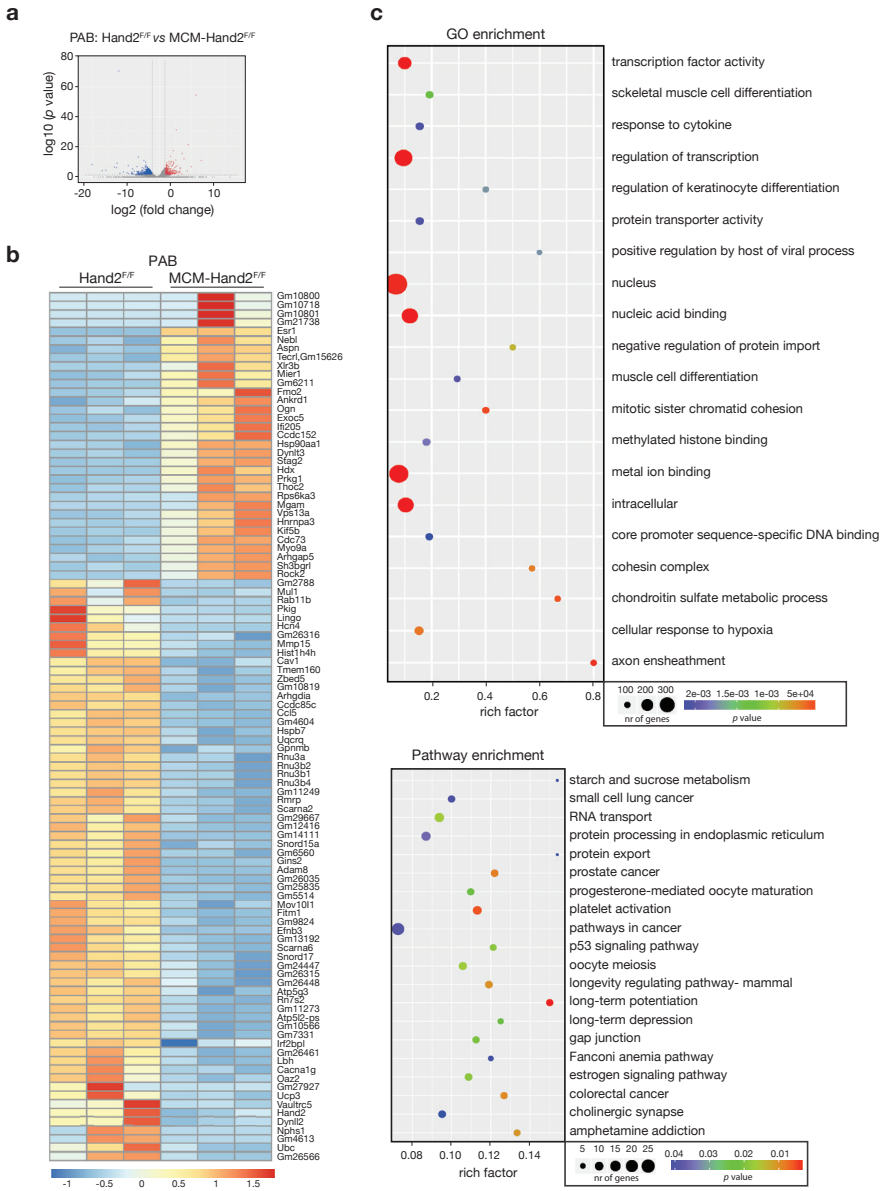

Figure 5. Hand2-dependent transcriptional changes in the pressure-overloaded RV. RNA-sequencing was performed to assess the transcriptomic changes in RV tissue from control (Hand2F/F) and knockout (MCM-Hand2F/F) animals subjected to PAB. a) Volcano plot representation of differential expression of genes in the RV of Hand2F/F versus MCM-Hand2F/F. Red and blue points mark the genes with significantly increased or decreased expression, respectively (FDR<0.01). The x-axis shows log2fold-expression changes and the y-axis the log10fold-likelihood of a gene being differentially expressed; b) Heatmap of the 100 top differentially expressed genes in the RV tissue of Hand2F/F sham compared to Hand2F/F PAB showing log2 FPKM (color scale) values of dysregulated genes, with red and blue colors representing increased

and decreased expression, respectively; c) Number of differentially expressed genes enriched in GO terms with p value and rich factor shown in a scatterplot. The summarized GO terms are related to the biological processes upon pulmonary artery banding in the heart. Rich factor=number of differentially expressed genes in GO term/total number of genes in GO term. The larger the rich factor, the higher enrichment is. Circle size is proportional to the frequency of the GO term, whereas color indicates the log10 p value (red higher, blue lower); d) KEGG pathway analysis of differentially expressed genes with p value and rich factor shown in a scatterplot. Differentially enriched pathways in the RV tissue of knockout animals subjected to PAB, in comparison to control animals subjected to PAB.

Table 3. MRI assessment of left ventricle function parameters of Hand2F/F and MCM-Hand2F/F mice at 2 and 6 weeks of sham or PAB

	$Hand2^{F/F}$				$MCM\text{-}Hand2^{F/F}$			
	sham		PAB		sham		PAB	
	2 weeks	6 weeks	2 weeks	6 weeks	2 weeks	6 weeks	2 weeks	6 weeks
Stroke volume (μl)	35.2±0.9	32.3±2.0	27.3±3.9	23.3±1.3*	38.6±2.7	35.6±2.4	21.7±1.8*	22.1±1.4*
Cardiac output (ml/min)	18.4±0.4	16.9±1.8	11.4±1.7*	9.8±0.5*	18.6±0.8	17.1±1.2	9.9±0.7*	10.2±0.6*
ED volume (μl)	92.7±2.8	91.5±7.7	58.9±9.4*	53.7±4.9*	86.3±2.8	84.5±4.5	47.5±2.8*	52.2±4.7*
ES volume (μl)	57.5±3.4	59.3±6.1	31.6±6.2*	30.4±3.9*	47.7±2.8	48.8±3.2	25.7±1.7*	30.0±4.4*
ED mass (mg)	53.7±7.1	53.0±1.5	38.3±4.1*	39.3±3.2*	54.1±3.2	59.1±3.2	37.8±1.9*	40.3±1.5*
ES mass (mg)	59.1±4.5	57.7±6.7	43.2±3.8	42.8±4.1	60.3±4.0	63.4±4.6	40.2±2.1*	43.0±2.2*
EF (%)	38.1±1.9	35.5±1.7	47.4±3.8	44.0±2.0	44.6±2.5	42.3±1.9	45.5±2.6	42.4±3.0

Data are expressed as means ± SEM. ED, end-diastole; ES, end-systole; LV, left ventricle; EF, ejection fraction. *, indicates $p<0.05$ vs sham group; #, indicates $p<0.05$ *vs* experimental group. n.s.=5-10 animals per group

DISCUSSION

Here, we aimed to unravel the role of Hand2 in right ventricular remodelling and establish whether this transcription factor has a similar contribution to the remodelling of both ventricles in response to pressure overload. We demonstrated that RV pressure overload, by subjecting control animals ($Hand2^{F/F}$) to PAB, results in increased *Hand2* expression levels in both RV and LV ventricles, with the LV revealing higher levels of expression compared to the RV. Although *Hand2* is known to be expressed throughout the atrial and ventricular myocardium with its highest expression in the developing RV, these results are in line with our previous work where we have shown, in adult hearts, higher *Hand2* expression levels in the LV compared to the RV in both resting and stress conditions.[19] Whereas Hand2 participation in adult myocardial remodelling has not been thoroughly studied and understood, our studies indicate that ventricular pressure overload, either on the right or left side, induces *Hand2* expression in both ventricles, with the LV showing the highest levels. However, this contrasts with a study in mice and rats where induction of cardiac hypertrophy either by phenylephrine treatment for 3-5 days or aortic banding for 5, 14 and 21 days resulted in reduced *Hand1* and *Hand2* RV expression levels.[27] In this study we assessed Hand2 expression at 6 weeks after PAB and therefore we cannot exclude a different expression pattern in the first days/weeks after banding as first

response to the sudden cardiac stress.

As previously observed by us,[19] one would expect that correcting the expression levels of Hand2, which is elevated in disease, would reduce maladaptation and confer protection. Nevertheless, a loss of function mutation in the Hand2 gene results in increased RV volumes at both end-diastole and end-systole, as well as decreased ejection fraction and cardiac output in mice subjected to RV pressure overload, compared to controls, indicating an inability of the RV to adapt to pressure overload. Impaired cardiac function was associated with increased hypertrophic growth of the RV, reflected by increased heart weight to body weight ratios, increased Fulton index as well as elevated cardiomyocyte CSA. While collagen deposition reached similar levels in both control and *Hand2*-knockout mice subjected to RV stress, absence of *Hand2* inhibits expression of fibrosis-related genes markers early in the disease process. TGFβ signaling is involved in tissue repair and scar formation[28] and not only it is an important regulator of vascular remodelling and inflammation of the lung[29] and kidney,[30] it also regulates hypertrophy and fibrosis in the heart.[31-33] While endoglin is an established regulator of vascular remodelling,[34,35] it also plays a critical role in the development of fibrosis by serving as a coreceptor for TGFb signaling.[36,37] Their expression profiles confirm the similar collagen deposition observed in the banded animals, independently of the genotype and the fact that the Hand2 knockout hearts display more severe hypertrophic phenotypes. These results, together with the observed increase in some of the hypertrophic gene markers, strongly suggest that absence of *Hand2* expression, under pressure overload of the RV, drives cardiac remodelling towards a more hypertrophic phenotype, without exaggerated fibrosis. Nevertheless, such a phenotype is characterized by a stronger impairment of cardiac function as reflected by the altered functional parameters measured by MRI.

Due to the pericardium and the common ventricular septum (ventricular interdependence), alterations in loading conditions of the RV are known to influence septal reconfiguration and motion towards the LV[38,39] and, in this way, affect left ventricular performance by altering the LV pressure-volume curve.[40,41] Assessing the eccentricity index of the LV shape reflects the abnormal motion of the intraventricular septum depending on the type of right ventricular overload, whether systolic or diastolic.[42] In our study, animals that were subjected to PAB revealed an index significantly greater than 1.0 at both systole and diastole which confirms right pressure overload[42] and subsequent abnormal leftward septal motion and configuration. But was the LV affected? In control mice, RV pressure overload did affect the LV as cardiomyocyte hypertrophy and mRNA expression of hypertrophic markers and pro-fibrotic genes were increased. In the absence of *Hand2* expression, the hypertrophic response was lost, with decreased cardiomyocyte CSA and associated gene expression. Whereas these results indicate some degree of

protection, conferred by depletion of Hand2, analysis of LV function by MRI, revealed a decrease in LV volumes as well as in LV mass, reduced stroke volumes and cardiac output, explained by decreased preloading of the LV due to right-sided pressure overload. Previous studies have shown that impaired cardiac function is not always accompanied by transcriptional activation of the "classical" marker genes associated either with hypertrophy or fibrosis and that it only happens once hypertrophy and/or fibrosis start to develop.[43-44] The fact that control mice subjected to RV pressure overload developed LV cardiomyocyte hypertrophy, but *Hand2* knockout hearts did not, might be explained by the absence/presence of transcriptional alterations of hypertrophic markers. In those studies, it was speculated that the absence of transcriptional deregulation and no alterations at the cellular level, such as hypertrophy and/or fibrosis, could facilitate recovery of cardiac function by specific treatments[43-45] or eventually reversing the stress. If this is the case in our study, remains to be clarified.

As LV diastolic filling is diminished in patients, and animal models, with pulmonary hypertension,[46-49] this may cause a decrease in preloading of the LV and atrophy, and ultimately heart failure. In fact, reduction in LV mass was reported in disorders that are associated with chronic RV pressure overload, dysfunction and altered LV diastolic filling.[50,51] LV atrophy is characterized by less prominent transcriptional changes in hypertrophic genes. This supports our findings in the *Hand2*-depleted animals subjected to PAB where we observed decreased LV mass, no hypertrophy and no dramatic changes in hypertrophic gene expression. Whether the LV under these conditions becomes atrophic remains to be investigated as we would have to look at the IVS and LV separately as well as analyses the cardiomyocyte length and width in more detail.

We have previously identified differentially expressed transcripts of cardiac *Hand2* target genes in pressure overloaded LVs from Hand2 $^{F/F}$ and MCM-Hand2 $^{F/F}$ animals.[19] Besides identifying several genes that had not previously been associated with cardiac hypertrophy, we also noticed a variety of genes involved in TGFβ signaling as well as genes with defined functions during embryonic cardiac development.[19] Although RV remodelling due to increased pressure load is associated with increased expression of genes known to be involved in hypertrophy, fibrosis and angiogenesis, most of those genes were not affected by silencing of Hand2. Unbiased approached gene analysis of Hand2 KO hearts, subjected to RV pressure overload, revealed dysregulation of several other cardiac hypertrophy-associated genes, cell cycle inhibitors and cellular components related to nucleic acid binding, regulation of transcription and transcription factor activity, as well as cell adhesion genes.

While in the pressure-overloaded RVs of Hand2 KO animals we observed differential

expression of several pro-fibrotic and extracellular matrix component genes, genes involved in angiogenesis and endothelial cell function, sarcomere cytoskeleton genes, proinflammatory genes and also genes associated with cardiac hypertrophy and diastolic function; genes that are associated with embryonic development were not very prominent, in contrast to what we observed in the overloaded LVs, and suggesting that the set of *Hand2* target genes that are employed during response of the adult RV to pressure overload are very distinct from the ones engaged during cardiac embryonic development.

Altogether, our data indicate that *Hand2* depletion does not confer cardiac protection to RV pressure overload but in contrast, sensitizes the RV to stress. Furthermore, it indicates that modulation of Hand2 expression has opposite effects in each of the ventricles and also supports the notion that each ventricle responds to stress in very dissimilar ways, involving different signaling pathways and different cellular processes. While inhibiting *Hand2* expression can prevent cardiac dysfunction in conditions of LV pressure overload, the same does not hold true for conditions of RV pressure overload, emphasizing that it is imperative to better understand the molecular mechanisms driving pathological remodelling of the RV in contrast to the LV, in order to better diagnose and treat patients with RV or LV failure.

ACKNOWLEDGEMENTS

R.F.V. and P.D.C.M. were supported by a Foundation for Science and Technology of Portugal (FCT) grant (PTDC/BIM-MEC/4578/2014). P.D.C.M. was further supported by a Dutch Heart Foundation grant (NHS2010B261).

REFERENCES

1. Ambrosy AP, Fonarow GC, Butler J, Chioncel O, Greene SJ, Vaduganathan M, Nodari S, Lam CSP, Sato N, Shah AN, Gheorghiade M. The global health and economic burden of hospitalizations for heart failure: Lessons learned from hospitalized heart failure registries. *J Am Coll Cardiol* Elsevier Inc; 2014;63:1123–1133.
2. Marques-Alves P, Baptista R, Silva AM Da, Pêgo M, Castro G. Real-world, long-term survival of incident patients with pulmonary arterial hypertension. *Rev Port Pneumol (English Ed* 2017;23:124–131.
3. Dell'Italia LJ. The forgotten left ventricle in right ventricular pressure overload. *J Am Coll Cardiol* Elsevier Inc.; 2011;57:929–930.
4. Simon MA. Assessment and treatment of right ventricular failure. *Nat Rev Cardiol* Nature Publishing Group; 2013;10:204–218.
5. Abu-Issa R, Kirby ML. Heart Field: From Mesoderm to Heart Tube. *Annu Rev Cell Dev Biol* 2007;23:45–68.
6. Buckingham M, Meilhac S, Zaffran S. Building the mammalian heart from two sources of myocardial cells. *Nat Rev Genet* 2005;6:826–835.
7. Garry DJ, Olson EN. A Common Progenitor at the Heart of Development. *Cell* 2006;127: 1101–1104.
8. Meilhac SM, Esner M, Kelly RG, Nicolas JF, Buckingham ME. The clonal origin of myocardial cells in different regions of the embryonic mouse heart. *Dev Cell* 2004;6:685–698.
9. Cai CL, Liang X, Shi Y, Chu PH, Pfaff SL, Chen J, Evans S. Isl1 identifies a cardiac progenitor population that proliferates prior to differentiation and contributes a majority of cells to the heart. *Dev Cell* 2003;5:877–889.
10. Kelly RG, Brown NA, Buckingham ME. The Arterial Pole of the Mouse Heart Forms from Fgf10-Expressing Cells in Pharyngeal Mesoderm. *Dev C*ell 2001;1:435–440.
11. Firulli AB, Mcfadden DG, Lin Q, Srivastava D, Olson EN. Heart and extra-embryonic mesodermal defects in mouse embryos lacking the bHLH transcription factor Hand1. *Nat Genet* 1998;18:266–270.
12. Riley P, Anson-cartwright L, Crossu C. The Hand1 bHLH transcription factor is essential for placentation and cardiac morphogenesis. *Nat Genet* 1998;18:271–275.
13. McFadden DG, Charité J, Richardson JA, Srivastava D, Firulli AB, Olson EN. A GATA-dependent right ventricular enhancer controls dHAND transcription in the developing heart. *Development* 2000;127:5331–5341.
14. Srivastava D, Cserjesi P, Olson EN. A subclass of bHLH proteins required for cardiac morphogenesis. *Science (80-)* 1995;270:1995–1999.
15. Srivastava D, Thomas T, Lin Q, Kirby ML, Brown D, Olson EN. Regulation of cardiac mesodermal and neural crest development by the bHLH transcription factor, dHAND. *Nat Genet* 1997;16:154–160.
16. Zaffran S, Kelly RG, Meilhac SM, Buckingham ME, Brown NA. Right ventricular myocardium derives from the anterior heart field. *Circ R*es 2004;95:261–268.
17. Shen L, Li XF, Shen AD, Wang Q, Liu CX, Guo YJ, Song ZJ, Li ZZ. Transcription factor HAND2 mutations in sporadic chinese patients with congenital heart disease. *Chin Med J*

(Engl) 2010;123:1623–1627.

18. Sun Y-M, Wang J, Qiu X-B, Yuan F, Li R-G, Xu Y-J, Qu X-K, Shi H-Y, Hou X-M, Huang R-T, Xue S, Yang Y-Q. A HAND2 loss-of-function mutation causes familial ventricular septal defect and pulmonary stenosis. *G3 Genes, Genomes, Genet* J. Wang, Department of Cardiology, Jing'an District Central Hospital, Shanghai, China; 2016;6:987–992.
19. Dirkx E, Gladka MM, Philippen LE, Armand A, Kinet V, Leptidis S, Azzouzi H, Salic K, Bourajjaj M, Silva GJJ, Olieslagers S, Nagel R Van Der, Weger R De, Bitsch N, Kisters N, Seyen S, Morikawa Y, Chanoine C, Heymans S, Volders PGA, Thum T, Dimmeler S, Cserjesi P, Eschenhagen T, Paula A, Martins C, Windt LJ De, Azzouzi H El, Salic K, Bourajjaj M, et al. Nfat and miR-25 cooperate to reactivate the transcription factor Hand2 in heart failure. *Nat Cell Biol* Nature Publishing Group; 2013;15:1282–1293.
20. Morikawa Y, D'Autréaux F, Gershon MD, Cserjesi P. Hand2 determines the noradrenergic phenotype in the mouse sympathetic nervous system. *Dev Biol* 2007;307:114–126.
21. Sohal DS, Nghiem M, Crackower MA, Witt SA, Kimball TR, Tymitz KM, Penninger JM, Molkentin JD. Temporally regulated and tissue-specific gene manipulations in the adult and embryonic heart using a tamoxifen-inducible Cre protein. *Circ Res* 2001;
22. Martin M. Cutadapt removes adapter sequences from high-throughput sequencing reads. *EMBnet.journal* 2011;
23. Langmead B, Salzberg SL. Fast gapped-read alignment with Bowtie 2. *Nat Methods* 2012;9:357–359.
24. Kim D, Pertea G, Trapnell C, Pimentel H, Kelley R, Salzberg SL. TopHat2: Accurate alignment of transcriptomes in the presence of insertions, deletions and gene fusions. *Genome Biol* 2013;14:R36.
25. Pertea M, Pertea GM, Antonescu CM, Chang TC, Mendell JT, Salzberg SL. StringTie enables improved reconstruction of a transcriptome from RNA-seq reads. *Nat Biotechnol* 2015;33:290–295.
26. Frazee AC, Pertea G, Jaffe AE, Langmead B, Salzberg SL, Leek JT. Ballgown bridges the gap between transcriptome assembly and expression analysis. *Nat Biotechnol* 2015;33:243–246.
27. Thattaliyath BD, Firulli BA, Firulli AB. The basic-helix-loop-helix transcription factor HAND2 directly regulates transcription of the Atrial Naturetic Peptide gene. *J Mol Cell Cardiol* 2002;34:1335–1344.
28. Massagué J. TGF-beta signal transduction. *Annu Rev Biochem* 1998;67:753–791.
29. Coward WR, Saini G, Jenkins G. The pathogenesis of idiopathic pulmonary fibrosis. *Ther Adv Respir Dis* 2010;4:367–388.
30. López-Hernández FJ, López-Novoa JM. Role of TGF-β in chronic kidney disease: An integration of tubular, glomerular and vascular effects. *Cell Tissue Res* 2012;347:141–154.
31. Dijke P Ten, Arthur HM. Extracellular control of TGF signalling in vascular development and disease. *Nat Rev Mol Cell Biol* 2007;8:857–869.
32. Liang H, Zhang C, Ban T, Liu Y, Mei L, Piao X, Zhao D, Lu Y, Chu W, Yang B. A novel reciprocal loop between microRNA-21 and TGFRIII is involved in cardiac fibrosis. *Int J Biochem Cell Biol* 2012;44:2152–2160.
33. Goumans M, Dijke P Ten. TGF-β Signaling in Control of Cardiovascular Function. *Cold*

Spring Harb Perspect Biol 2018;10:pii:a022210.

34. Li DY, Sorensen LK, Brooke BS, Urness LD, Davis EC, Taylor DG, Boak BB, Wendel DP. Defective angiogenesis in mice lacking endoglin. *Science (80-)* 1999;284:1534–1537.
35. Hawinkels LJAC, Kuiper P, Wiercinska E, Verspaget HW, Liu Z, Pardali E, Sier CFM, Dijke P Ten. Matrix metalloproteinase-14 (MT1-MMP)-mediated endoglin shedding inhibits tumor angiogenesis. *Cancer Res* 2010;70:4141–4150.
36. Chen K, Mehta JL, Li D, Joseph L, Joseph J. Transforming growth factor receptor endoglin is expressed in cardiac fibroblasts and modulates profibrogenic actions of angiotensin II. *Circ Res* 2004;95:1167–1173.
37. Shyu K-G, Wang B-W, Chen W-J, Kuan P, Hung C-R. Mechanism of the inhibitory effect of atorvastatin on endoglin expression induced by transforming growth factor-beta1 in cultured cardiac fibroblasts. *Eur J Heart Fail* 2010;12:219–226.
38. Weyman a E, Wann S, Feigenbaum H, Dillon JC. Mechanism of abnormal septal motion in patients with right ventricular volume overload: a cross-sectional echocardiographic study. *Circulation* 1976;54:179–186.
39. Weber KT, Janicki JS, Shroff S, Fishman AP. Contractile mechanics and interaction of the right and left ventricles. *Am J Cardiol* 1981;47:686–695.
40. Bemis CE, Serur JR, Borkenhagen D, Sonnenblick EH, Urschel CW. Influence of right ventricular filling pressure on left ventricular pressure and dimension. *Circ Res* 1974;34: 498–504.
41. Li KS, Santamore WP. Contribution of each wall to biventricular function. *Cardiovasc Res* 1993;27:792–800.
42. Ryan T, Petrovic O, Dillon JC, Feigenbaum H, Conley MJ, Armstrong WF. An echocardiographic index for separation of right ventricular volume and pressure overload. *J Am Coll Cardio*l 1985;5:918–927.
43. Grubb DR, Crook B, Ma Y, Luo J, Qian HW, Gao XM, Kiriazis H, Du XJ, Gregorevic P, Woodcock EA. The atypical 'b' splice variant of phospholipase C1 promotes cardiac contractile dysfunction. *J Mol Cell C*ardiol 2015;84:95–103.
44. Rowell J, Koitabashi N, Kass DA, Barth AS. Dynamic gene expression patterns in animal models of early and late heart failure reveal biphasic-bidirectional transcriptional activation of signaling pathways. *Physiol Genomi*cs 2014;46:799–787.
45. Matkovich SJ, Grubb DR, McMullen JR, Woodcock EA. Chronic Contractile Dysfunction without Hypertrophy Does Not Provoke a Compensatory Transcriptional Response in Mouse Hearts. *PLoS One* 2016;11:e0158317.
46. Marcus JT, Vonk Noordegraaf A, Roeleveld RJ, Postmus PE, Heethaar RM, Rossum a C Van, Boonstra A. Impaired left ventricular filling due to right ventricular pressure overload in primary pulmonary hypertension: noninvasive monitoring using MRI. *Chest* 2001;119: 1761–1765.
47. Schena M, Clini E, Errera D, Quadri A. Echo-Doppler evaluation of left ventricular impairment in chronic cor pulmonale. *Chest* 1996;109:1446–1451.
48. Krayenbuehl H, Turina J, Hess O. Left ventricular function in chronic pulmonary hypertension. *Am J Cardiol* 1978;41:1150–1158.

49. Lazar J, Flores A, Grandis D, Orie J, Schulman D. Effects of chronic right ventricular pressure overload on left ventricular diastolic function. *Am J Cardiol* 1993;72:1179–1182.

50. Sutinen S, Pääkkö P, Tienari J. Weights of the body and cardiac ventricles in pulmonary emphysema. *Virchows Arch A Pathol Anat Histopathol* 1985;407:249–257.

51. Gorter TM, Veldhuisen DJ Van, Bauersachs J, Borlaug BA, Celutkiene J, Coats AJS, Crespo-Leiro MG, Guazzi M, Harjola V-P, Heymans S, Hill L, Lainscak M, Lam CSP, Lund LH, Lyon AR, Mebazaa A, Mueller C, Paulus WJ, Boer RA De. Right heart dysfunction and failure in heart failure with preserved ejection fraction: mechanisms and management. Position statement on behalf of the Heart Failure Association of the European Society of Cardiology. *Eur J Heart Fail* 2017;20:16–37.

SUPPLEMENTAL MATERIAL

Supplemental table 1. Sequence of primers used for quantitative real-time PCR

Gene Name	Primer Sequence
ACTA-1	FW-5'CCGGGAGAAGATGACTCAAA3'
	RV-5'GTAGTACGGCCGGAAGCATA3'
COL1A1	FW- 5'CCAATGGTGCTCCTGGTATT3'
	RV-5'GGTTCACCACTGTTACCCTT3'
DYRK1A	FW-5'CACGCTGTATGAGCAGAGAT3'
	RV-GTCCTCCTGTTTCTACTCCAAG3'
ENG	FW-5'AACACGTGCAGACTCTCCA3'
	RV-5'ATCACCTCATTGCTGACCAC3'
MYH6	FW-5'TCGAAAGGAAGCTGGCAGA3'
	RV-5'GTCATTGGCATGGACAGCA3'
MYH7	FW-5'CGGACCTTGGAAGACCAGAT3'
	RV-5'GACAGCTCCCCATTCTCTGT3'
NPPA	FW- 5'GGTGTCCAACACAGATCTGA'3
	RV-5'CTTCCTCAGTCTGCTCACT'3
NPPB	FW-5'TGGGAGGTCACTCCTATCCT3'
	RV-5'GGCCATTTCCTCCGACTTT3'
RCAN-1-4	FW-5' CCCTGGTTTCACTTTCGC3'
	RV-5'AAGGAACCTACAGCCTCT3'
TGFβR1	FW-5'GGTGGTATACTGAGACACCTTG3'
	RV-5'CCCAAGGAAAGGTAGGTGATAG3'
VEGFR2	FW-5'GTTAAGCGGGCCAATGAAGG3'
	RV-5' CGGCCAAGAGGTTTTCCTAGTT3'
L7	FW-5'GAAGCTCATCTATGAGAAGGC3'
	RV-5'AAGACGAAGGAGCTGCAGAAC3'

Supplemental table 2. List of genes significant differentenly expressed between sham versus PAB revealed by ranscriptomic analysis.

Due to excessive length, table not added to the manuscript.

Supplemental table 3. List of genes significant differentenly expressed between Hand2F/F versus MCM-Hand2F/F revealed by ranscriptomic analysis.

Due to excessive length, table not added to the manuscript.

7

8

CHAPTER 8

Multi-biomarker assessment in children with congenital heart disease and various types of increased right ventricular load

A.M.C. Koop*, M. G. Haarman*, E.T. Liem, D. van de Weerd, A. Wendt, G. du Marchie Sarvaas, R.A. de Boer, H.L. Hillege, R.M.F. Berger

* These authors contributed equally to the manuscript.

ABSTRACT

Background

Over the last decades, the population of patients with congenital heart disease (CHD) and pulmonary hypertension (PH) has increased due to improved treatment options. In many of these patients the right ventricle (RV) remains persistently exposed to pressure, volume or combined overload, leading to RV remodelling including fibrosis, hypertrophy, dilatation and eventually RV failure. Early recognition of such remodelling processes may enable preservation of cardiac function and functional status by targeted interventions. This study aimed to explore whether multi-biomarker assessment can help in early identification of RV remodelling and its functional consequences in children with CHD and PH.

Methods

One-hundred and twenty-five children (median age 9.6 years (IQR 5.0-14.2), 53% male) with (a history of) various types of RV overload underwent clinical, echocardiographic, and laboratory assessment of eight selected blood-derived biomarkers, reflecting various remodelling processes.

Results

Blood-derived multi-biomarker profiles were associated with both type and severity of RV overload. N-terminal pro-B-Type natriuretic peptide (NT-proBNP) and endothelin-1 (ET-1) were increased in children with RV pressure overload compared to a reference group with no residual overload, whereas none of the biomarkers were increased in children with RV volume overload. High sensitive Troponin T, NT-proBNP, ET-1, Mid-Regional Pro-Adrenomedullin, myeloperoxidase, and growth differentiation factor-15 were associated with RV hypertrophy. NT-proBNP inversely correlated with systolic RV function.

Conclusions

This study outlines the concept of the use of multi-biomarker assessment for early recognition of RV remodelling and activation of molecular processes of RV adaptation in relation to type and degree of RV overload and function.

INTRODUCTION

Over the past decades, survival of children with congenital heart disease (CHD) and pulmonary hypertension (PH) has improved markedly due to advances in treatment strategies. This increased survival has led to an expanding population of children and grown-up patients with congenital heart disease (GUCH).[1,2] However, in many patients residual lesions are present, which lead to deterioration of cardiac and physical function over time. Overload of the right ventricle (RV), either primary or residual, leading to chronic cardiac adaptation, is an important determinant in the development of RV failure in patients with CHD and PH. RV adaptation to abnormal loading includes cardiac remodelling processes, such as hypertrophy, inflammation and fibrosis, that precede deterioration of ventricular function.[1,3] Identifying abnormal load and consequent remodelling processes in early stages of the disease could optimize timing of (re-)interventions aimed at preservation of cardiac function.

In acquired left ventricular (LV) disease, blood-derived biomarkers have shown to be of value in clinical practice.[4–6] Ventricular adaptation and remodelling is a process of injury and repair, which includes myocardial stretch and injury, inflammation, metabolic changes and connective tissue deposition. These processes are accompanied by elevated plasma levels of compounds from the various involved pathways.[6–9] Biomarkers as N-Terminal pro-B-Type natriuretic peptide (NT-proBNP), midregional proadrenomedullin (MR-proADM) and neprilysin are known to be released in abnormal loading conditions and to address activation of renin angiotensin-aldosterone system (RAAS). Increases in NT-proBNP will stimulate natriuresis, diuresis and vasodilation, and MR-proADM has natriuretic and vasodilatory effects in response to activation of the sympathetic nervous system.[10] Serum levels of galectin-3, growth differentiation factor-15 (GDF-15) and myeloperoxidase (MPO) have been suggested to reflect ventricular remodelling characterized by oxidative stress, inflammation and fibrosis.[11–16] Endothelin-1 (ET-1) is a vasoconstrictive and inotropic agent with also mitogenic abilities, released both intra- and extracardiacally, initially serving cardiovascular adaptation.[17] Troponin T, a myofilament, is released to the bloodstream when cardiomyocyte injury and decay occurs. These biomarkers are likely to be of value, not only in patients with LV-diseases, but also in those with a stressed RV. To date, however, these biomarkers have been insufficiently studied in adaptive processes of the RV in children with CHD or PH.[18–24]

In this study a multi-biomarker approach was chosen for the characterization of RV adaptation and remodelling in response to abnormal loading in children with various congenital heart defects or PH. A selected set of plasma biomarkers was used related to various pathophysiological processes involved in cardiac adaptation and remodelling. We investigated the biomarkers profiles in children with different types and degree of RV overload in relation to echocardiographic RV function

and remodelling. Based on the findings in this study, the discussion presents a conceptual algorithm illustrating the potential use of a multi-biomarker approach in clinical practice, which may direct and facilitate follow-up of children with CHD.

METHODS

Study design and population

A prospective, cross-sectional observational cohort study was performed (registered at ClinicalTrials.gov; Unique identifier: NCT04130243). Consecutive children aged 0-18 years with (a history of) RV overload who visited the outpatient clinic of the Center for Congenital Heart Disease at the University Medical Center Groningen, the Netherlands, between December 2017 and November 2018 and in whom the patient or parents/caregivers provided written informed consent, were included.

Overload of the RV was categorized as either increased pressure, volume or combined volume/pressure overload. The degree of (residual) overload was scored as mild-to-moderate or severe. A group of children with a history of RV overload, but no actual residual RV overload, was included as a reference group. Detailed information regarding categorization is described in the supplemental material.

Patients aged >18 years, children with a concomitant musculoskeletal disease, children under examination for non-diagnosed disease at time of investigation, and children with significant left-sided cardiac lesions were excluded from this study. Ethical approval for this study was obtained from the Medical Ethics Review Board of the University Medical Center Groningen and written informed consent from the children (and/or their guardians) was given at enrollment (reference-number 2017/190).

Echocardiography

All children underwent two-dimensional transthoracic echocardiography performed on a GE Vivid E9 or E95 machine (GE Healthcare, Boston, United States of America). Echocardiography was performed as part of clinical follow-up and performed according to the pediatric guidelines of the American Society of Echocardiography and included measurement of tricuspid annular plane systolic excursion (TAPSE).[25] Systolic RV function was qualitatively assessed by eyeballing and scored as good, moderate or poor. Similarly, the presence of RV hypertrophy (RVH) and RV dilatation were assessed and scored as either present or not present. Continuous wave Doppler was used to measure maximum velocities of tricuspid (TR) and pulmonary

valve regurgitation, if present. Two experienced echocardiographers (DvdW and AW) independently performed post-hoc analyses on these images.

Blood sampling and biomarker assays

Blood samples and echocardiography were obtained on the same day. Blood samples were collected in EDTA or heparin tubes and centrifuged. NT-proBNP and galectin 3 were analyzed immediately. Plasma for measuring GDF-15, MR-proADM, MPO, neprilysin and ET-1 was stored at -80˚C (median storage period: 6.3 months (interquartile range; IQR: 4.4-7.3)), where after analysis took place. All samples were subjected to one freeze-thaw cycle. For detailed description of biomarker assays, see supplemental material.

Statistics

Data are presented as medians with interquartile ranges (IQR) or frequencies (as percentage). The clinical characteristics, echocardiographic variables and biomarker plasma levels of children with either no residual RV overload, pressure, volume or combined residual RV overload were compared using Kruskal Wallis or Chi-squared test when appropriate. For pairwise testing post-hoc correction was performed with Bonferroni correction. To study differences in biomarker levels between mild-moderate and severe overload, the ratios were calculated of the plasma levels of these biomarkers in patients with mild-to-moderate overload and severe overload, respectively, to the levels in patients with no residual overload.

The differences in plasma level of all eight biomarkers in children with good, moderate or poor systolic RV function were analyzed using Kruskal Wallis test. The differences in plasma level of the biomarkers in children with and without RVH and RV dilation were analyzed using Mann Whitney U test. Receiver operating characteristic (ROC) curves were plotted to analyze the ability of the different biomarkers in identifying RV dilatation and/or RVH. To identify a cut-off value the highest sum of specificity and sensitivity were used.

Spearman correlation analysis was used to study the correlation between TAPSE and the eight different biomarkers. Analyses were adjusted for age and sex. Statistical analysis was performed using IBM SPSS version 23.0 (Armonk, NY, USA). All statistical tests were two-tailed and a p-value of <0.05 is considered statistically significant.

RESULTS

Clinical and echocardiographic characteristics

One-hundred and twenty-five children with (a history of) RV overload were included in this study. Anatomical diagnoses included tetralogy of Fallot (TOF) (61%), PH (20%), and atrial septal defect (ASD) (5%). Diagnosis with TOF embodied TOF, corrected TOF, pulmonary atresia and pulmonary stenosis. Children with PH had either PH associated with CHD (n=14) or PH not associated with CHD (n=11) and were classified according to the most recent Nice classification.[26–28] Fourteen percent of the children had other diagnoses (e.g. RV-pulmonary artery (PA) conduit stenosis) (**table 1**).

Fifty-six children (44%) were assigned to the group of RV pressure overload, 25 children (20%) to the group of RV volume overload and 28 children (23%) to the group of combined overload of the RV (predominantly volume overload, n=11; predominantly pressure overload, n=2; type of loading equally distributed n=15). Sixteen children (13%) with corrected CHD had no residual RV overload and formed the reference. Patient characteristics, including functional status and echocardiographic parameters, stratified for the type of RV overload are summarized in **table 1**.

Biomarker plasma levels in relation to the type of RV overload

Plasma levels of NT-proBNP and ET-1 were significantly higher in the children with RV pressure overload compared to the reference group. Plasma ET-1 levels were also significantly higher when compared to the combined RV overload group (**table 2**).

Biomarker plasma levels in relation to the severity of RV overload

By expressing plasma levels of each biomarker as a ratio to the respective values in the reference group, we obtained multi-biomarkers profiles for patients according to type and degree of RV overload (**figure 1**). Biomarker plasma levels were most pronouncedly increased in children with RV pressure overload, and less in those with RV volume overload or those with combined RV overload. Plasma levels of NT-proBNP and ET-1 increased with the severity of RV pressure overload, while hsTnT and GDF-15 were significantly increased only in children with severe RV pressure overload. GDF-15 serum levels showed a trend of increase in children with mild-moderate RV pressure overload (**figure 1a**). Children exposed to RV volume overload showed a different multi-biomarker profile, characterized by smaller differences in biomarker plasma levels in relation to the degree of overload, that failed to reach statistical significance (**figure 1b**). The plasma level of neprilysin in children with abnormal RV loading in contrast to other investigated biomarkers, tended to decrease, independent of the type of overload.

Plasma levels of NT-proBNP and ET-1 increased with the severity of RV pressure overload.

Biomarker plasma levels in relation to RV remodelling and function

In the total study population, 51 children showed RVH with echocardiography, whereas 71 children did not. In three children RVH could not be assessed due to insufficient quality of the images. Plasma levels of hsTnT, NT-proBNP, MR-proADM, GDF-15, MPO and ET-1 were increased in children with RVH compared to those without RVH (**figure 2a**). The predictive value of these six biomarkers were expressed by ROC curves and revealed the following cut-off values and max area under the curve (AUC): NT-proBNP 147 ng/L (AUC 0.76, p<0.001; sensitivity 64% and specificity 78%), ET-1 1.36 pg/ml (AUC 0.74, p<0.001; sensitivity 80% and specificity 58%), hsTnT 5.5 ng/l (AUC 0.62, p=0.031; sensitivity 50% and specificity 69%), MR-proADM 0.448 nmol/l (AUC 0.65, p=0.006; sensitivity 45% and specificity 89%), GDF-15 321 pg/ml (AUC 0.67, p=0.002; sensitivity 82% and specificity 49%), and MPO 37.5 ng/ml (AUC 0.68, p=0.002; sensitivity 49% and specificity 83%).

Plasma levels of hsTnT, NT-proBNP, MR-proADM, GDF-15, MPO and ET-1 are associated with right ventricular hypertrophy in children with increased right ventricular pressure load.

Echocardiographic assessment showed 73 children to have RV dilatation, whereas 49 children did not. In three children RV dilatation could not be assessed. Biomarker plasma levels did not differ significantly between children with and without RV dilatation (**figure 2b**).

Echocardiographic assessment revealed a good systolic RV function (eyeballing) in 86% of the children, a moderate systolic RV function in 12% and poor systolic RV function in 2%. The median (IQR) z-score TAPSE was -2.1 (-3.8 to -0.5).29 Stratification for type of RV overload is shown in **table 1.** RV function did not differ between groups. Although none of the biomarkers levels showed a correlation with subjective assessment of systolic RV function (**figure 2c**), Spearman correlation analysis of the eight biomarkers revealed NT-proBNP to correlate inversely with RV function expressed as TAPSE (**table 3**).

Table 1. Clinical characteristics

	All patients		Pressure overload		Volume overload	
	n	*Median (IQR), n (%)*	*n*	*Median (IQR), n (%)*	*n*	*Median (IQR), n (%)*
Patient characteristics						
Age	125	9.6 (5.0-14.2)	56	9.2 (2.8-14.0)	25	8.9 (5.2-14.7)
Sex, male	125	66 (53)	56	24 (43)	25	14 (56)
BSA	122	1.07 (0.72-1.51)	53	1.03 (0.63-1.46)	25	0.94 (0.74-1.68)
WHO-FC/NYHA	125		56		25	
I		94 (75)		31 (55)		23 (92)
II		25 (20)		19 (34)		2 (8)
III		5 (4)		5 (9)		0 (0)
IV		1 (1)		1 (2)		0 (0)
Diagnosis	125		56		25	
TOF (+/- PA), PS		77 (61)		29 (52)		19 (76)
PH		25 (20)		23 (41)		0 (0)
ASDI & ASDII		6 (5)		0 (0)		4 (16)
Other*		17 (14)		4 (7)		2 (8)
Echocardiographic parameters						
RV function						
RV function eyeballing	124		55		24	
Good		106 (86)		44 (80)		23 (92)
Moderate		15 (12)		10 (18)		1 (4)
Poor		3 (2)		1 (2)		1 (4)
TAPSE, mm	117	16.0 (13.3-19.1)	53	16.0 (13.0-20.0)	23	16.0 (13.0-19.0)
RV remodelling						
RVH, yes	122	51 (42)	53	38 (72)	25	2 (8)
RV dilatation, yes	122	73 (60)	54	29 (54)	25	21 (84)
Severity of overload	125		56		25	
None		16 (13)		0 (0)		0 (0)
Mild-moderate		57 (46)		29 (52)		14 (56)
Severe		52 (42)		27 (48)		11 (44)

BSA: body surface area; WHO-FC: World Health Organization Functional Class; NYHA: New York Heart Association; TOF: Tetralogy of Fallot; PA: pulmonary atresia; PS: pulmonary stenosis; PH: pulmonary hypertension; ASDI: atrial septal defect type I; ASDII: atrial septal defect type II; RV: right ventricular; TAPSE: tricuspid annular plane systolic excursion; RVH: right ventricular hypertrophy. * other diagnoses included RV-PA conduit stenosis with signs of RV overload. ǂ significant difference between no residual overload and pressure overload. ǂ significant difference between combined overload and pressure overload § significant difference between pressure overload and volume overload. || significant difference between no residual overload and combined overload. # significant difference between no residual overload and volume overload ** p-value from Kruskal Wallis or Chi-squared test

Combined overload		No overload		
n	*Median (IQR), n (%)*	*n*	*Median (IQR), n (%)*	P-value**
28	9.8 (6.1-14.3)	16	11.0 (7.9-14.7)	0.489
28	19 (68)	16	9 (56)	0.176
28	1.10 (0.75-1.53)	16	1.22 (1.03-1.61)	0.350
28		16		**0.005†**
	24 (86)		16 (100)	
	4 (14)		0 (0)	
	0 (0)		0 (0)	
	0 (0)		0 (0)	
28		16		**<0.001†§||#**
	24 (86)		5 (31)	
	2 (7)		0 (0)	
	0 (0)		2 (13)	
	2 (7)		9 (56)	
28		16		0.562
	25 (89)		14 (88)	
	2 (7)		2 (12)	
	1 (4)		0 (0)	
26	15.0 (12.8-19.0)	15	16.0 (15.0-18.0)	0.662
28	11 (39)	16	0 (0)	**<0.001†‡§||**
28	20 (71)	15	3 (20)	**<0.001#||**
28		16		**<0.001†||#**
	0 (0)		16 (100)	
	14 (50)		0 (0)	
	14 (50)		0 (0)	

Table 2. Levels of biomarkers per type of RV overload

		All patients		Pressure overload		Volume overload
Biomarkers	*n*	*Median (IQR)*	*n*	*Median (IQR)*	*n*	*Median (IQR)*
hs TnT, ng/l	124	5.0 (4.0-7.0)	55	6.0 (4.0-7.0)	25	5.0 (4.0-6.0)
NT-proBNP, ng/l	124	113 (62-209)	55	143 (75-251)	25	86 (56-179)
Galectin-3, ng/ml	125	12.4 (10.6-15.5)	56	12.8 (10.2-16.6)	25	11.9 (10.2-14.8)
MR-proADM, nmol/l	125	0.389 (0.340-0.451)	56	0.398 (0.344-0.508)	25	0.374 (0.340-0.436)
GDF-15, pg/ml	124	352 (281-454)	55	384 (299-524)	25	349 (263-452)
MPO, ng/ml	125	27.3 (19.2-41.5)	56	31.1 (22.2-49.0)	25	25.3 (18.2-35.5)
ET-1, pg/ml	124	1.46 (1.19-1.95)	55	1.67 (1.36-2.74)	25	1.32 (1.10-1.79)
Neprilysin, ng/ml	124	0.81 (0.00-6.38)	55	0.69 (0.03-10.07)	25	1.20 (0.22-14.54)

hs TnT: high-sensitive Troponin T; NT-proBNP: N-terminal pro-B-Type natriuretic peptide; ET-1: Endothelin-1; MR-proADM: midregional proadrenomedullin; MPO: myeloperoxidase; GDF-15: growth differentiation factor 15. * significant difference between no residual overload and pressure overload. † significant difference between combined overload and pressure overload. ‡ p-value from Kruskal Wallis test

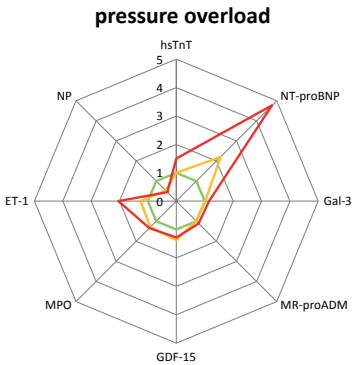

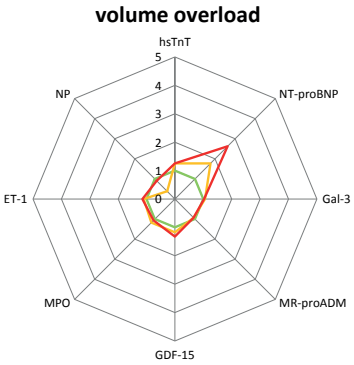

	no residual load *(n=16)*	mild-moderate overload *(n=29)*	severe overload *(n=27)*	*p-value*	mild-moderate overload *(n=15)*	severe overload *(n=12)*	*p-value*
hsTnT	4.0 (0.8-5.0)	4.0 (3.0-6.0)	6.0 (5.0-8.0)	**0.001*†**	5.0 (4.0-6.0)	5.0 (4.0-9.5)	0.228
NT-proBNP	48 (33-128)	106 (63-149)	229 (112-314)	**<0.001*†**	85 (57-162)	126 (48-357)	0.164
Gal-3	11.8 (9.6-13.5)	12.0 (10.2-15.9)	13.6 (10.0-16.8)	0.193	12.5 (9.7-14.9)	12.1 (10.4-16.2)	0.728
MR-proADM	0.395 (0.324-0.427)	0.388 (0.325-0.492)	0.439 (0.363-0.524)	0.147	0.368 (0.339-0.444)	0.368 (0.342-0.412)	0.924
GDF-15	284 (250-392)	391 (276-607)	364 (329-495)	**0.021***	333 (285-433)	376 (251-458)	0.333
MPO	23.2 (17.1-29.4)	29.9 (21.4-42.1)	31.2 (23.4-61.5)	0.078	27.3 (19.9-35.3)	24.8 (17.0-49.2)	0.834
ET-1	1.17 (0.85-1.45)	1.48 (1.33-1.89)	2.39 (1.48-3.05)	**<0.001*‡**	1.29 (1.09-1.86)	1.34 (1.13-1.81)	0.15
NP	1.38 (0.00-7.24)	0.74 (0.13-11.63)	0.62 (0.00-10.07)	0.900	0.53 (0.16-22.78)	1.25 (0.02-10.41)	0.965

Figure 1. Patterns of changes in plasma levels in the combined panel of eight biomarkers according to type and degree of RV overload compared with no residual RV overload. NT-proBNP: N-Terminal pro-B-Type natriuretic peptide; MR-proADM: midregional proadrenomedullin; Gal-3: galectin-3; GDF-15: growth differentiation factor 15; MPO: myeloperoxidase; ET-1: endothelin-1; hsTnT: high sensitive Troponin T; NP: neprilysin.

Combined overload		No overload		
n	*Median (IQR)*	*n*	*Median (IQR)*	P-value‡
28	5.0 (3.3-6.8)	16	4.0 (0.8-5.0)	0.190
28	129 (65-190)	16	48 (33-129)	**0.015***
28	12.6 (11.6-15.5)	16	11.8 (9.6-13.5)	0.296
28	0.380 (0.333-0.435)	16	0.395 (0.324-0.427)	0.201
28	342 (280-452)	16	284 (250-392)	0.050
28	26.8 (18.6-47.0)	16	23.2 (17.1-29.4)	0.128
28	1.33 (1.17-1.71)	16	1.17 (0.85-1.45)	**<0.001*†**
28	0.44 (0.00-2.30)	16	1.38 (0.00-7.24)	0.447

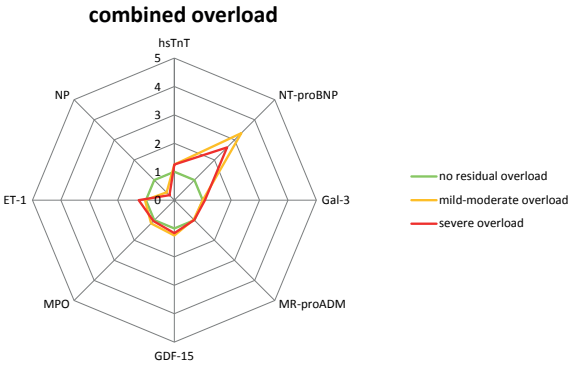

mild-moderate overload *(n=13)*	severe overload *(n=13)*	*p-value*
5.0 (3.5-6.5)	5.0 (2.0-8.0)	0.604
160 (66-237)	126 (67-175)	**0.027‡**
11.8 (11.6-14.7)	12.7 (11.3-15.7)	0.345
0.381 (0.316-0.460)	0.390 (0.348-0.434)	0.861
354 (276-492)	330 (276-397)	0.344
26.9 (19.5-53.9)	24.2 (14.2-41.5)	0.496
1.21 (1.14-1.54)	1.47 (1.21-1.82)	0.087
0.53 (0.00-6.45)	0.34 (0.00-1.70)	0.657

* no residual vs. severe overload
† mild-moderate vs. severe overload
‡ no residual vs. mild-moderate overload

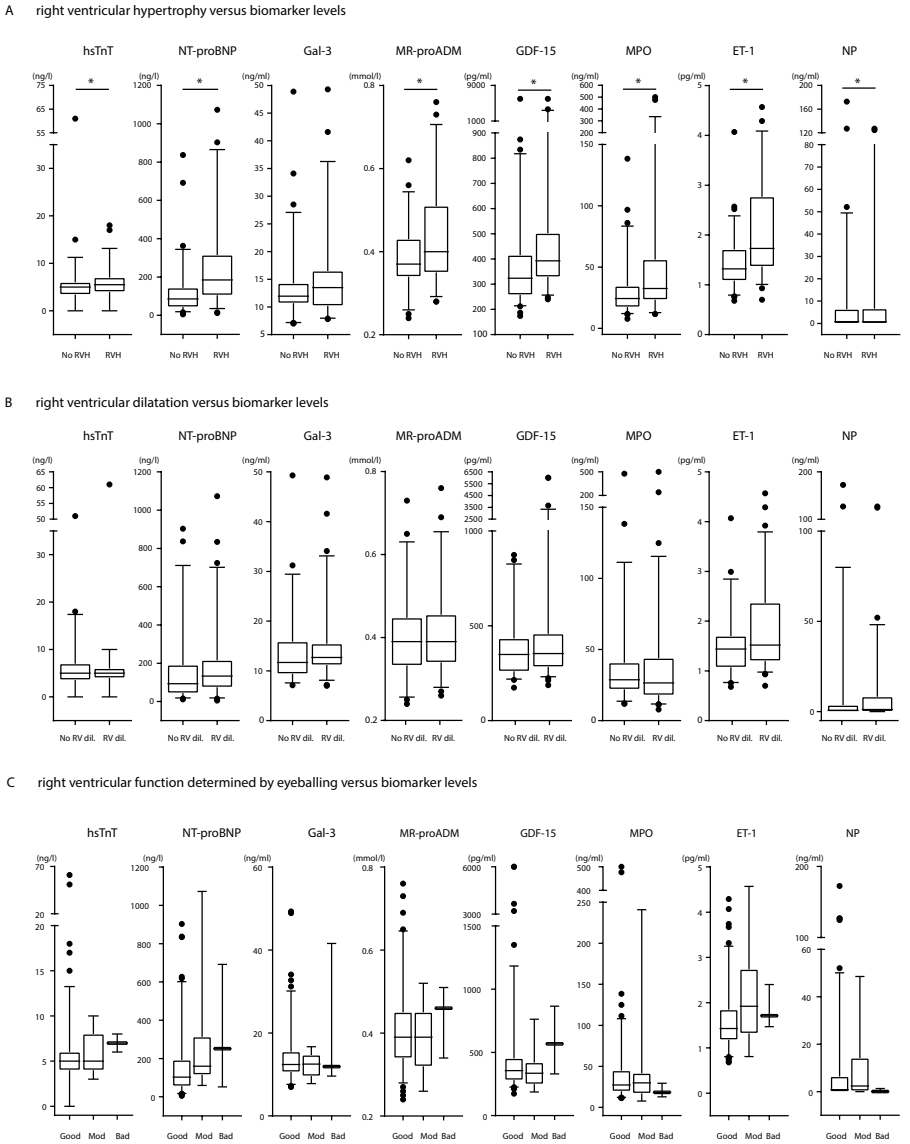

Figure 2. Relation between the plasma levels of the eight biomarkers and right ventricular hypertrophy (**A**), right ventricular dilatation (**B**) and subjective assessment of right ventricular function (**C**). NT-proBNP: N-Terminal pro-B-Type natriuretic peptide; MR-proADM: midregional proadrenomedullin; Gal-3: galectin-3; GDF-15: growth differentiation factor 15; MPO: myeloperoxidase; ET-1: endothelin-1; hsTnT: high sensitive Troponin T; NP: neprilysin; RVH: right ventricular hypertrophy; RV dil.: right ventricular dilatation; mod: moderate.

Table 3. Correlation between serum biomarker levels and tricuspid annular plane systolic excursion assessed in all patients

Biomarker	TAPSE (r)	P-value
hs TnT, ng/l	-0.159	0.087
NT-proBNP, ng/l	-0.365	**<0.001***
Galectin-3, ng/ml	-0.079	0.395
MR-proADM, nmol/l	-0.009	0.920
GDF-15, pg/ml	0.003	0.976
MPO, ng/ml	-0.145	0.118
ET-1, pg/ml	0.010	0.911
Neprilysin, ng/ml	0.055	0.560

TAPSE: tricuspid annular plane systolic excursion; hs TnT: high-sensitive Troponin T; NT-proBNP: N-terminal pro-B-Type natriuretic peptide; MR-proADM: midregional proadrenomedullin; GDF-15: growth differentiation factor 15; MPO: myeloperoxidase; ET-1: Endothelin-1; * remained significant after adjusting for age and sex.

DISCUSSION

The aim of this study was to investigate multi-biomarker serum profiles in children with different RV overload conditions in order to identify degree of RV load, RV remodelling and RV function, also in early stages of disease. In children with CHD, multi-biomarker profiles - defined by changes in the plasma levels of a panel of eight selected circulating biomarkers - were associated with both the type and the degree of RV overload. Although the direction of changes in plasma levels of this panel of selected biomarkers seemed comparable in the different types of RV overload, RV pressure overload was associated with the most prominent changes in biomarker plasma levels, that correlated with echocardiographic RV function and remodelling. NT-proBNP and ET-1 plasma levels were able to identify the presence and degree of RV pressure overload, but not volume overload. An increase in hsTnT serum level showed to indicate severe RV pressure overload. In RV volume overload, no association between this biomarker profile and the severity of overload could be demonstrated. Increased plasma levels of a spectrum of biomarkers, hsTnT, NT-proBNP, MR-proADM, GDF-15, MPO and ET-1 were associated with RVH, were the associated trends of the various biomarker plasma levels with severity of pressure overload and RVH may reflect timing of the molecular processes activated during RV adaptation. Since each biomarker represents specific pathways involved in ventricular remodelling, the altered biomarker profile might eventually be used to characterize RV condition, its stage of adaptation and serve as pillar in directing follow-up and therapeutic interventions. In **figure 3**, we present a hypothetical algorithm to recognize abnormal RV loading, RV remodelling and associated processes.

Pressure and volume overload are distinct entities with distinct injury and remodelling patterns which could explain the differences in multi biomarker serum profiles in children with either pressure or volume overload of the RV. Pressure overload induces initial concentric hypertrophy progressing towards eccentric hypertrophy (dilatation) in more advanced disease, whereas volume overload will induce dilatation without the preceding stage of concentric hypertrophy.[30,31] Although underlying mechanisms remain to be unraveled, one may speculate that different types of overload activate various signaling cascades in various degrees, which in turn lead to load-specific RV remodelling. This study in children with CHD and/or PH suggests that pathophysiological pathways, known from LV remodelling, are more extensively activated in RV pressure overload than in volume or combined overload.

It is well known that volume overload is initially better, or longer, tolerated by the RV than pressure load. Failure of the RV due to severe volume load (e.g. corrected TOF) in general takes longer than failure to severe pressure load (e.g. severe right outflow tract obstruction or PH). The fact that isolated RV volume overload in this pediatric study did not induce pronounced elevation of biomarkers may be due to the young age of the patients and relative short existence of RV overload when compared to adults with long standing volume loaded RV's. In other words: in this pediatric study, the duration and impact of volume overload might have been too short to induce significant changes in biomarker plasma levels. Previous studies that reported increased levels of NT-proBNP in pediatric patients with repaired TOF included patients with combined RV overload instead of isolated volume overload.[32,33] In line with our results, a previous study in children with repaired TOF with isolated volume overload also failed to demonstrate an association with plasma levels of NT-proBNP.[33] Along the same line of reasoning: elevated levels of hsTnT have been shown in patients with CHD and are clinically relevant, because of its relation with increased risk for cardiovascular events, as death, heart failure and hospitalization.[34] However, in patients with RV volume load the actual relation between hsTnT plasma level and worse RV function and remodelling has been shown only in adult patients with repaired TOF.[35]

Timely identification of type and severity of RV pressure overload and the adaptive status of the RV is believed to be of important in pursuing preservation of functional status. Pressure overload is a debilitating condition for the thin walled RV and is known to induce rapid deterioration of RV function, especially in acute onset or severe pressure overload. The current study shows that in children with CHD, NT-proBNP is a marker of RV pressure overload and its severity. NT-proBNP is released by cardiomyocytes due to myocardial stretch, resulting in RAAS activation with increased natriuresis, diuresis and vasodilation, and widely used as a marker of cardiac decompensation. The current study assessed NT-proBNP as part of the multi-biomarker panel and showed that NT-proBNP was highly affected by pressure overload compared to other biomarkers. The progressively increased plasma levels in RV pressure overload were also found for ET-1 and reflect a state of progressive inotropic and mitogenic abilities. Increased plasma levels of ET-1 have been related to PAH and ET-1 has been shown to be involved in the pathogenesis of this disease.[36,37] In the current study ET-1 was increased predominantly in patients with PAH (data not shown), indicating that increased ET-1 plasma levels in children with CHD may increase awareness for the presence of PAH. In addition to a measure for the severity of RV pressure load, NT-proBNP can serve as a surrogate of systolic RV function, as demonstrated by its correlation with TAPSE, that was independent of age and sex. This is in line with studies in patients with TOF, a systemic RV, and PH.[38–41] If hsTnT is increased simultaneously, this indicates severe RV pressure overload accompanied with cell decay, a consideration that may direct to expeditious interventions. In adults with PAH due to CHD, increased plasma levels of cardiac troponin are shown to be associated with poor outcome[42,43] and hsTnT has been identified as a marker for risk stratification.[44] To our knowledge, we are the first to explicitly relate cardiac troponin to the degree of RV pressure overload in children with CHD.

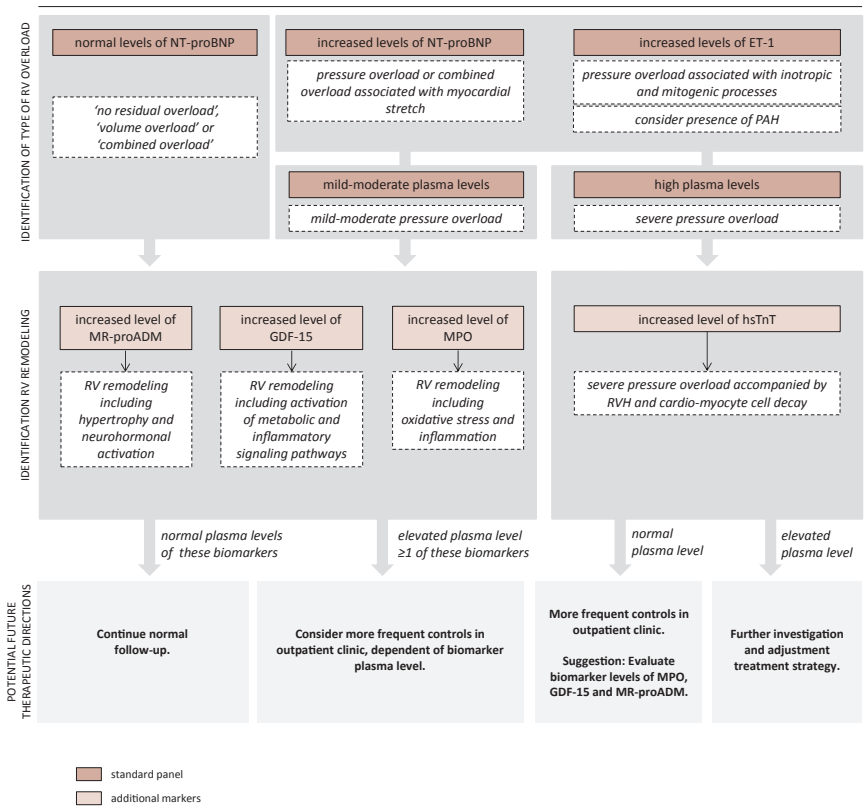

Figure 3. Conceptual algorithm of potential clinical use of a blood-derived multi-biomarker approach to characterize right ventricular disease in children with congenital heart disease or pulmonary hypertension and to guide medical management decisions. NT-proBNP: N-Terminal pro-B-Type natriuretic peptide; MR-proADM: midregional proadrenomedullin; GDF-15: growth differentiation factor 15; MPO: myeloperoxidase; ET-1: endothelin-1; hsTnT: high sensitive Troponin T; PAH: pulmonary arterial hypertension; RV: right ventricle; RVH: right ventricular hypertrophy.

The presence of RV remodelling in the form of RVH was associated with a change in plasma level of six biomarkers in the investigated multi-biomarker profile, suggesting the involvement of several remodelling pathways or processes. RVH is known as adaptation mechanism to increased pressure overload and is present already in early phases of abnormal RV loading.[45,46] The data of this study suggest activation of molecular processes involved in myocardial stretch, neurohormonal activation, metabolism, inflammation and oxidative stress, leading to fibrosis and cell decay. Plasma levels of MR-proADM and MPO were not related to type and degree of RV overload, but significantly increased in the presence of RVH. Increased plasma levels of MR-proADM in adult patients with chronic LV heart failure have been associated

with worse functional status and decreased one-year survival rates.[47] Experimental studies showed that upregulation of adrenomedullin inhibited cardiac hypertrophy by the regulation of cardiac growth as an autocrine or a paracrine factor.[48] Infusion of adrenomedullin as therapy in rats with PH lowered vascular resistance in the lung and heart via nitric oxide generation in the vasculature.[49] Based on these finding, one may speculate that MR-proADM in children with RVH is upregulated to counteract hypertrophy on cardiac and pulmonary level. MPO is known to be released into the extracellular fluid during inflammatory activity and oxidative stress and is involved in the pathogenesis of several major chronic diseases including rheumatoid arthritis, liver diseases, diabetes, cancer and also cardiovascular diseases.[50] Elevated plasma levels of MPO have been shown to predict the development of congestive heart failure, the need for heart transplantation or mortality in a variety of pathologic conditions.[51–53] In children with uncorrected TOF, myocardial fibrosis has been described already at a young age (mean (SD) age 0.7±0.2 years).[54] In the current study, the increased plasma MPO plasma levels in the children with RVH are in line with the occurrence of oxidative stress and subsequent fibrosis early in experimental RV pressure overload in rats subjected to pulmonary artery banding.[45,46,55] Galectin-3 has been reported extensively as a biomarker in heart failure to be involved in cell adhesion, inflammation and tissue fibrosis.[56–60] In the current study galectin-3 plasma levels however did not correlate with increased RV pressure overload nor with RV remodelling. GDF-15 also has a role in metabolism, inflammation and fibrosis. In acquired heart disease serum levels of GDF-15 are used in risk stratification and prognostic utility for atrial fibrillation,[61] myocardial infarction,[62] and heart failure.[63,64] In patients with CHD GDF-15 has been positively related to NYHA class,[64,65] and in those with a Fontan circulation, GDF-15 has shown to be an early marker of decreased heart function and to predict hospitalization and death.[38] In the current study in children with different abnormal loading conditions of the RV, GDF-15 correlated with the severity of RV pressure overload and RVH a potential role for GDF-15 in the characterization of early RV disease in children with preserved functional status.

Whereas other plasma levels of the studied biomarkers increased or remained stable, neprilysin showed decreasing trends in pressure, volume and combined overload, among the different degrees of overload. Neprilysin is known to be activated to counteract in the vasoconstriction and sodium retention cascade activated by the RAAS and the sympathetic nervous system, by the degradation of natriuretic peptides and vasoactive compounds. Recently published data showed that patients with heart failure with preserved ejection fraction (HFpEF) had lower neprilysin levels compared to controls,[66] while increased plasma levels of neprilysin are associated with heart failure in patients with reduced ejection fraction (HFrEF) and with increased mortality.[67] Combing these data with the current findings may suggest that the phenotype of the majority of the included children is comparable to these of patients with HFpEF.

In this study, a concept of a multi-biomarker approach has been outlined by assessing plasma levels of a panel of eight biomarkers in order to guide follow-up and eventually treatment strategies including optimization of timing of surgical or medicinal interventions. This serves the goal to prevent adverse processes of RV remodelling, such as metabolic and neuro-endocrine dysregulation, oxidative stress injury and fibrosis, and by that preserve RV function in time. The authors emphasize that an algorithm as shown in **figure 3** is conceptual and hypothetical, requires further validation before clinical use and here solely serves the purpose of illustrating the potential value of blood-derived multi-biomarker profiles in children with CHD and abnormal RV loading conditions. Data regarding these biomarkers are still sparse and future research is needed to further elucidate the role of such multi-biomarkers profiles in pediatric heart disease. Since the current cohort predominantly included children with preserved functional class, this algorithm focuses on early detection of RV disease in this group of patients. Once validated, an algorithm like this may offer advances for children with CHD in remote areas, where advanced diagnostic tools to evaluate cardiac function are not available. Eventually, integrating the use of plasma biomarkers with the characterization of RV remodelling and metabolic processes in the RV by advanced imaging techniques, including single photon emission computed tomography, may further improve the clinical assessment of adaptive and mal-adaptive RV-responses to chronic abnormal loading conditions.

LIMITATIONS

This prospective study contains the completeness of both clinical and echocardiographic data in a relatively large pediatric cohort. However, the number of children per group for different types of RV overload was still modest which limited multivariate analyses. As this was a cross-sectional study, the prognostic value of the multi-biomarker approach on outcome and the use of the biomarker profile for treatment decisions could not be assessed. Larger, prospective cohort studies with longer follow-up are needed to investigate these additional and important questions.

CONCLUSION

In this pediatric cohort consisting of children with a(n) (history of) abnormal RV loading conditions due to CHD or PH and with predominantly preserved functional status, plasma levels of NT-proBNP and ET-1 were increased in RV pressure overload in general, whereas hsTnT was identified as a marker for severe RV pressure overload. RVH was accompanied by increased levels of hsTnT, NT-proBNP, MR-proADM, GDF-15, MPO and ET-1, suggesting accompany of neuro-endocrine, inflammatory and metabolic processes. This study illustrates the potential use of an accessible,

blood-derived multi-biomarker approach in pediatric patients with CHD that may contribute to the characterization of RV adaptation to abnormal loading conditions and, eventually, aims for early recognition of adverse processes in RV remodelling and guidance in decisions on treatment strategies.

SOURCE OF FUNDING

This study was funded in part by the Sebald fund.

DISCLOSURES

The University Medical Center Groningen, which employs Dr. RA de Boer has received research grants and/or fees from AstraZeneca, Abbott, Bristol-Myers Squibb, Novartis, Novo Nordisk, and Roche. Dr. RA de Boer received speaker fees from Abbott, AstraZeneca, Novartis, and Roche.

The University Medical Center Groningen contracts with Actelion, Lilly, GSK and Pfizer and received fees for steering committee and advisory board activities by Dr. RMF Berger.

REFERENCES

1. Norozi K, Zoege M, Buchhorn R, Wessel A, Geyer S. The Influence of Congenital Heart Disease on Psychological. *Congenit Heart Dis* 2006;1:282–288.
2. Warnes CA, Bhatt AB, Daniels CJ, Gillam LD, Stout KK. COCATS 4 task force 14: Training in the care of adult patients with congenital heart disease. *J Am Coll Cardiol* Elsevier Inc; 2015;65:1887–1898.
3. Kato TS, Armstrong HF, Schulze PC, Lippel M, Amano A, Farr M, Bacchetta M, Bartels MN, Tullio MR Di, Homma S, Mancini D. Left and right ventricular functional dynamics determined by echocardiograms before and after lung transplantation. *Am J Cardiol* Elsevier Inc.; 2015;116:652–659.
4. Boer R a de, Daniels LB, Maisel AS, Januzzi JL. State of the art: newer biomarkers in heart failure. *Eur J Heart Fail* 2015;17:559–569.
5. Mueller C, McDonald K, Boer RA de, Maisel A, Cleland JGF, Kozhuharov N, Coats AJS, Metra M, Mebazaa A, Ruschitzka F, Lainscak M, Filippatos G, Seferovic PM, Meijers WC, Bayes-Genis A, Mueller T, Richards M, Januzzi JL. Heart Failure Association of the European Society of Cardiology practical guidance on the use of natriuretic peptide concentrations. *Eur J Heart Fail* 2019;21:715–731.
6. Chow SL, Maisel AS, Anand I, Bozkurt B, Boer RA de, Felker GM, Fonarow GC, Greenberg B, Januzzi JL, Kiernan MS, Liu PP, Wang TJ, Yancy CW, Zile MR, American Heart Association Clinical Pharmacology Committee of the Council on Clinical Cardiology; Council on Basic Cardiovascular Sciences; Council on Cardiovascular Disease in the Young; Council on Cardiovascular and Stroke Nursing; Council on Cardiopulm P and RC on E and PC on FG and TB and C on Q of C and OR. Role of Biomarkers for the Prevention, Assessment, and Management of Heart Failure: A Scientific Statement From the American Heart Association. *Circulation* 2017;135:e1054–e1091.
7. Hartupee J, Mann DL. Positioning of inflammatory biomarkers in the heart failure landscape. *J Cardiovasc Transl Res* 2013;6:485–492.
8. Sawada Y, Suda M, Yokoyama H, Kanda T, Sakamaki T, Tanaka S, Nagai R, Abe S, Takeuchi T. Stretch-induced hypertrophic growth of cardiocytes and processing of brain-type natriuretic peptide are controlled by proprotein-processing endoprotease furin. *J Biol Chem* 1997;272:20545–20554.
9. Jumean MF, Kiernan MS. Determinants of survival following hospitalization for acute heart failure. *Curr Heart Fail Rep* 2014;11:201–211.
10. Frank Peacock W. Novel biomarkers in acute heart failure: MR-pro-adrenomedullin. *Clin Chem Lab Med* 2014;52:1433–1435.
11. Besler C, Lang D, Urban D, Rommel KP, Roeder M Von, Fengler K, Blazek S, Kandolf R, Klingel K, Thiele H, Linke A, Schuler G, Adams V, Lurz P. Plasma and cardiac galectin-3 in patients with heart failure reflects both inflammation and fibrosis: Implications for its use as a biomarker. *Circ Hear Fail* 2017;10:1–9.
12. Kempf T, Haehling S von, Peter T, Allhoff T, Cicoira M, Doehner W, Ponikowski P, Filippatos GS, Rozentryt P, Drexler H, Anker SD, Wollert KC. Prognostic Utility of Growth Differentiation Factor-15 in Patients With Chronic Heart Failure. *J Am Coll Car*diol 2007;50:1054–1060.

13. Calvier L, Legchenko E, Grimm L, Sallmon H, Hatch A, Plouffe BD, Schroeder C, Bauersachs J, Murthy SK, Hansmann G. Galectin-3 and aldosterone as potential tandem biomarkers in pulmonary arterial hypertension. *Heart* 2016;102:390–396.
14. Tang WHW, Tong W, Troughton RW, Martin MG, Shrestha K, Borowski A, Jasper S, Hazen SL, Klein AL. Prognostic Value and Echocardiographic Determinants of Plasma Myeloperoxidase Levels in Chronic Heart Failure. *J Am Coll Cardiol* 2007;49:2364–2370.
15. Maisel A, Mueller C, Nowak R, Peacock WF, Landsberg JW, Ponikowski P, Mockel M, Hogan C, Wu AHB, Richards M, Clopton P, Filippatos GS, Somma S Di, Anand I, Ng L, Daniels LB, Neath SX, Christenson R, Potocki M, McCord J, Terracciano G, Kremastinos D, Hartmann O, Haehling S von, Bergmann A, Morgenthaler NG, Anker SD. Mid-Region Pro-Hormone Markers for Diagnosis and Prognosis in Acute Dyspnea. Results From the BACH (Biomarkers in Acute Heart Failure) Trial. *J Am Coll Cardiol* Elsevier Inc.; 2010;55:2062–2076.
16. Volpe M, Carnovali M, Mastromarino V. The natriuretic peptides system in the pathophysiology of heart failure: from molecular basis to treatment. *Clin Sci (Lond)* 2016;130:57–77.
17. McMurray JJ, Ray SG, Abdullah I, Dargie HJ, Morton JJ. Plasma endothelin in chronic heart failure. *Circulation* 1992;85:1374–1379.
18. Koch A, Zink S, Singer H. B-type natriuretic peptide in paediatric patients with congenital heart disease. *Eur Heart J* 2006;27:861–866.
19. Albada ME Van, Loot FG, Fokkema R, Roofthooft MTR, Berger RMF. Biological serum markers in the management of pediatric pulmonary arterial hypertension. *Pediatr Res* 2008;63:321–327.
20. Loon RLE van, Roofthooft MTR, Delhaas T, Osch-Gevers M van, Harkel ADJ ten, Strengers JLM, Backx A, Hillege HL, Berger RMF. Outcome of Pediatric Patients With Pulmonary Arterial Hypertension in the Era of New Medical Therapies. *Am J Cardiol* Elsevier Inc.; 2010;106:117–124.
21. Takatsuki S, Wagner BD, Ivy DD. B-type natriuretic peptide and amino-terminal pro-B-type natriuretic peptide in pediatric patients with pulmonary arterial hypertension. *Congenit Heart Dis* 2012;7:259–267.
22. Ploegstra M-J, Douwes JM, Roofthooft MTR, Zijlstra WMH, Hillege HL, Berger RMF. Identification of treatment goals in paediatric pulmonary arterial hypertension. *Eur Respir J* 2014;1616–1626.
23. Fernandes BA, Maher KO, Deshpande SR. Cardiac biomarkers in pediatric heart disease: A state of art review. *World J Cardiol* 2016;8:719.
24. Baum H, Hinze A, Bartels P, Neumeier D. Reference values for cardiac troponins T and I in healthy neonates. *Clin Biochem* 2004;37:1079–1082.
25. Lopez L, Colan SD, Frommelt PC, Ensing GJ, Kendall K, Younoszai AK, Lai WW, Geva T. Recommendations for Quantification Methods During the Performance of a Pediatric Echocardiogram: A Report From the Pediatric Measurements Writing Group of the American Society of Echocardiography Pediatric and Congenital Heart Disease Council. *J Am Soc Echocardiogr* Elsevier Inc; 2010;23:465–495.
26. Simonneau G, Montani D, Celermajer DS, Denton CP, Gatzoulis MA, Krowka M, Williams PG, Souza R. Haemodynamic definitions and updated clinical classification of pulmonary hypertension. *Eur Respir J* 2019;53.

27. Rosenzweig EB, Abman SH, Adatia I, Beghetti M, Bonnet D, Haworth S, Ivy DD, Berger RMF. Paediatric pulmonary arterial hypertension: updates on definition, classification, diagnostics and management. *Eur Respir J* 2019;53.

28. Simonneau G, Gatzoulis MA, Adatia I, Celermajer D, Denton C, Ghofrani A, Gomez Sanchez MA, Krishna Kumar R, Landzberg M, Machado RF, Olschewski H, Robbins IM, Souza R. Updated clinical classification of pulmonary hypertension. *J Am Coll Cardiol* 2013;62.

29. Koestenberger M, Ravekes W, Everett AD, Stueger HP, Heinzl B, Gamillscheg A, Cvirn G, Boysen A, Fandl A, Nagel B. Right Ventricular Function in Infants, Children and Adolescents: Reference Values of the Tricuspid Annular Plane Systolic Excursion (TAPSE) in 640 Healthy Patients and Calculation of z Score Values. *J Am Soc Echocardiogr* 2009;**22**:715–719.

30. Rossi MA, Carillo S V. Cardiac hypertrophy due to pressure and volume overload: distinctly different biological phenomena? *Int J Cardiol* 1991;31:133–141.

31. Grossman W. Cardiac hypertrophy: Useful adaptation or pathologic process? *Am J Med* 1980;69:576–584.

32. Hirono K, Sekine M, Shiba N, Hayashi S, Nakaoka H, Ibuki K, Saito K, Watanabe K, Ozawa S, Higuma T, Yoshimura N, Kitajima I, Ichida F. N-terminal pro-Brain Natriuretic Peptide as a Predictor of Reoperation in Children With Surgically Corrected Tetralogy of Fallot. *Circ J* 2013;78:693–700.

33. Berg J van den, Strengers JLM, Wielopolski PA, Hop WC, Meijboom FJ, Rijke YB de, Boomsma F, Bogers AJJC, Pattynama PMT, Helbing WA. Assessment of biventricular functional reserve and NT-proBNP levels in patients with RV volume overload after repair of tetralogy of Fallot at young age. *Int J Cardiol* Elsevier Ireland Ltd; 2009;133:364–370.

34. Baggen VJM, Baart SJ, Bosch AE van den, Eindhoven JA, Witsenburg M, Cuypers JAAE, RoosHesselink JW, Boersma E. Prognostic Value of Serial NTerminal ProBType Natriuretic Peptide Measurements in Adults With Congenital Heart Disease. *J Am Heart Assoc* 2018;**7**.

35. Lai CTM, Wong SJ, Ip JJK, Wong WK, Tsang KC, Lam WWM, Cheung YF. Plasma Levels of High Sensitivity Cardiac Troponin T in Adults with Repaired Tetralogy of Fallot. *Sci Rep* Nature Publishing Group; 2015;5:1–8.

36. Dupuis J, Cernacek P, Tardif JC, Stewart DJ, Gosselin G, Dyrda I, Bonan R, Crepeau J. Reduced pulmonary clearance of endothelin-1 in pulmonary hypertension. *Am Heart J* 1998;135:614–620.

37. Stangl K, Dschietzig T, Richter C, Laule M, Stangl V, Tanis E, Baumann G, Felix SB. Pulmonary release and coronary and peripheral consumption of big endothelin and endothelin-1 in severe heart failure: acute effects of vasodilator therapy. *Circulation* 2000;102:1132–1138.

38. Meyer SL, Wolff D, Ridderbos FS, Eshuis G, Hillege H, Willems TP, Ebels T, Melle JP van, Berger RMF. GDF15 (Growth Differentiation Factor 15) Is Associated With Hospitalization and Mortality in Patients With a Fontan Circulation. *J Am Heart Assoc* 2020;15.

39. Eindhoven JA, Bosch AE Van Den, Jansen PR, Boersma E, Roos-Hesselink JW. The Usefulness of brain natriuretic peptide in complex congenital heart disease: A systematic review. *J Am Coll Cardiol* Elsevier Inc.; 2012;60:2140–2149.

40. Gan CT, McCann GP, Marcus JT, Wolferen SA van, Twisk JW, Boonstra A, Postmus PE, Vonk-Noordegraaf A. NT-proBNP reflects right ventricular structure and function in pulmonary hypertension. *Eur Respir J* 2006;28:1190–1194.

41. Norozi K, Buchhorn R, Kaiser C, Hess G, Grunewald RW, Binder L, Wessel A. Plasma

N-terminal pro-brain natriuretic peptide as a marker of right ventricular dysfunction in patients with tetralogy of Fallot after surgical repair. *Chest* The American College of Chest Physicians; 2005;128:2563–2570.

42. Torbicki A, Kurzyna M, Kuca P, Fijałkowska A, Sikora J, Florczyk M, Pruszczyk P, Burakowski J, Wawrzyńska L. Detectable serum cardiac troponin T as a marker of poor prognosis among patients with chronic precapillary pulmonary hypertension. *Circulation* 2003;108:844–848.
43. Schuuring MJ, Riel ACMJ van, Vis JC, Duffels MG, Straalen JP van, Boekholdt SM, Tijssen JGP, Mulder BJM, Bouma BJ. High-sensitivity troponin T is associated with poor outcome in adults with pulmonary arterial hypertension due to congenital heart disease. *Congenit Heart Dis* 2013;8:520–526.
44. Zelniker T, Uhlmann L, Spaich S, Friedrich J, Preusch MR, Meyer FJ, Katus HA, Giannitsis E. Novel biomarkers for risk stratification in pulmonary arterial hypertension. *ERJ open Res* 2015;1:1–9.
45. Koop AMC, Hagdorn QAJ, Bossers GPL, Leusden T van, Gerding A, Weeghel M van, Vaz FM, Koonen DPY, Silljé HHW, Berger RMF, Bartelds B. Right ventricular pressure overload alters cardiac lipid composition. *Int J Cardiol* Elsevier B.V.; 2019;287:96–105.
46. Borgdorff MAJ, Koop AMC, Bloks VW, Dickinson MG, Steendijk P, Sillje HHW, Wiechen MPH van, Berger RMF, Bartelds B. Clinical symptoms of right ventricular failure in experimental chronic pressure load are associated with progressive diastolic dysfunction. *J Mol Cell Cardiol* Elsevier Ltd; 2015;79:244–253.
47. Haehling S Von, Filippatos GS, Papassotiriou J, Cicoira M, Jankowska EA, Doehner W, Rozentryt P, Vassanelli C, Struck J, Banasiak W, Ponikowski P, Kremastinos D, Bergmann A, Morgenthaler NG, Anker SD. Mid-regional pro-adrenomedullin as a novel predictor of mortality in patients with chronic heart failure. *Eur J Heart Fail* 2010;12:484–491.
48. Tsuruda T, Kato J, Kitamura K, Kuwasako K, Imamura T, Koiwaya Y, Tsuji T, Kangawa K, Eto T. Adrenomedullin: a possible autocrine or paracrine inhibitor of hypertrophy of cardiomyocytes. *Hypertension* 1998;31:505–510.
49. Hinson JP, Kapas S, Smith DM. Adrenomedullin, a multifunctional regulatory peptide. *Endocr Rev* 2000;21:138–167.
50. Khan A, Alsahli M, Rahmani A. Myeloperoxidase as an Active Disease Biomarker: Recent Biochemical and Pathological Perspectives. *Med Sci* 2018;6:33.
51. Baldus S, Heeschen C, Meinertz T, Zeiher AM, Eiserich JP, Münzel T, Simoons ML, Hamm CW. Myeloperoxidase serum levels predict risk in patients with acute coronary syndromes. *Circulation* 2003;108:1440–1445.
52. Tang WHW, Brennan ML, Philip K, Tong W, Mann S, Lente F Van, Hazen SL. Plasma Myeloperoxidase Levels in Patients With Chronic Heart Failure. *Am J Cardiol* 2006;98: 796–799.
53. Tang WHW, Tong W, Troughton RW, Martin MG, Shrestha K, Borowski A, Jasper S, Hazen SL, Klein AL. Prognostic Value and Echocardiographic Determinants of Plasma Myeloperoxidase Levels in Chronic Heart Failure. *J Am Coll Cardi*ol 2007;49:2364–2370.
54. Peters THF, Sharma HS, Yilmaz E, Bogers AJJC. Quantitative analysis of collagens and fibronectin expression in human right ventricular hypertrophy. *Ann N Y Acad Sci* 1999;874:278–285.

55. Borgdorff MA, Bartelds B, Dickinson MG, Wiechen MPH van, Steendijk P, Vroomen M de, Berger RMF. Sildenafil treatment in established right ventricular dysfunction improves diastolic function and attenuates interstitial fibrosis independent from afterload. *Am J Physiol Circ Physiol* 2014;307:H361–H369.

56. Velde AR Van Der, Gullestad L, Ueland T, Aukrust P, Guo Y, Adourian A, Muntendam P, Veldhuisen DJ Van, Boer RA De. Prognostic value of changes in galectin-3 levels over time in patients with heart failure data from CORONA and COACH. *Circ Hear Fail* 2013;6:219–226.

57. Boer RA De, Lok DJA, Jaarsma T, Meer P Van Der, Voors AA, Hillege HL, Veldhuisen DJ Van. Predictive value of plasma galectin-3 levels in heart failure with reduced and preserved ejection fraction. *Ann Med* 2011;43:60–68.

58. Chen A, Hou W, Zhang Y, Chen Y, He B. Prognostic value of serum galectin-3 in patients with heart failure: a meta-analysis. *Int J Cardiol* Elsevier Ireland Ltd; 2015;182:168–170.

59. Dumic J, Dabelic S, Flögel M. Galectin-3: An open-ended story. *Biochim Biophys Acta - Gen Subj* 2006;1760:616–635.

60. Henderson NC, Sethi T. The regulation of inflammation by galectin-3. *Immunol Rev* 2009;230:160–171.

61. Marín F, Roldán V. Biomarkers: GDF-15 and risk stratification in atrial fibrillation. *Nat Rev Cardiol* Nature Publishing Group; 2015;12:8–9.

62. Dominguez-Rodriguez A, Abreu-Gonzalez P, Avanzas P. Relation of growth-differentiation factor 15 to left ventricular remodeling in ST-segment elevation myocardial infarction. *Am J Cardiol* Elsevier Inc.; 2011;108:955–958.

63. Li J, Li Q, Jia W, Liu K, Qi X, Cui Y, Huang A. Additional diagnostic value of growth differentiation factor-15 (GDF-15) to N-Terminal B-Type natriuretic peptide (NT-proBNP) in patients with different stages of heart failure. *Med Sci Monit* 2018;24:4992–4999.

64. Norozi K, Buchhorn R, Yasin A, Geyer S, Binder L, Seabrook JA, Wessel A. Growth differentiation factor 15: An additional diagnostic tool for the risk stratification of developing heart failure in patients with operated congenital heart defects? *Am Heart J* Mosby, Inc.; 2011;162:131–135.

65. Eindhoven JA, Bosch AE Van Den, Oemrawsingh RM, Baggen VJ, Kardys I, Cuypers JA, Witsenburg M, Schaik RH Van, Roos-Hesselink JW, Boersma E. Release of growth-differentiation factor 15 and associations with cardiac function in adult patients with congenital heart disease. *Int J Cardiol* Elsevier Ireland Ltd; 2016;202:246–251.

66. Lyle MA, Iyer SR, Redfield MM, Reddy YNV, Felker GM, Cappola TP, Hernandez AF, Scott CG, Burnett JC, Pereira NL. Circulating Neprilysin in Patients With Heart Failure and Preserved Ejection Fraction. *JACC Hear Fail* 2020;8:70–80.

67. Bayés-Genís A, Barallat J, Galán A, Antonio M De, Domingo M, Zamora E, Urrutia A, Lupón J. Soluble neprilysin is predictive of cardiovascular death and heart failure hospitalization in heart failure patients. *J Am Coll Cardiol* 2015;65:657–665.

SUPPLEMENTAL METHODS

Specification of categorization criteria of type and degree of loading

Categorization and scoring was performed based on the combination of anatomical diagnosis, repair status and actual echocardiographic assessment. The degree of RV pressure overload was scored as none, mild-to-moderate or severe based on the estimated RV pressure either estimated by the maximum velocity (Vmax) of a tricuspid regurgitation (mild-to-moderate <2.8 m/s and severe >2.8 m/s) or by Vmax over the pulmonary valve in children with sub- or supravalvular pulmonary stenosis (mild-to-moderate: 2-4 m/s; severe: >4 m/s).[1] In children with PAH, the diagnosis had previously been confirmed by right heart catheterization or, in case of clinical instability, by echocardiography.[2] In children with pulmonary regurgitation (PR) the degree of volume overload was scored based on the degree of PR, as determined by the magnitude/extent, localization, and the vena contracta of the regurgitant jet. Mild-to-moderate PR was defined as a relatively broad jet originating in the main pulmonary artery just above valvular closure lines. Severe PR was defined as a voluminous diastolic retrograde jet originating from the branch pulmonary arteries.[3] In children with an ASD, the magnitude of the left-to-right shunt and thus RV volume overload was estimated by RV size on echocardiography and classified as mild-to-moderate or severe.

Biomarker assays

NT-proBNP was measured using the *Elecsys* (Roche, Basel, Switzerland) assay and galectin-3 with the *Architect platform* (Abbott, Chicago, United States). High sensitive Troponin T (hsTnT) was measured with *Elecsys* (Roche, Basel, Switzerland) in lithium heparin anticoagulated tubes. GDF-15 (*DGD150*, R&D Systems, Abingdon, United Kingdom), MR-proADM (*82992*, Thermo Scientific Brahms, Henningsdorf, Germany), MPO (*DMYE00B*, R&D Systems, Abingdon, United Kingdom), neprilysin (*EHMME*, Thermo Scientific, Frederick, United States of America) and ET-1 (*DET100*, R&D Systems, Abingdon, United Kingdom) were determined in one badge using Kryptor or ELISA assays using EDTA plasma.

9

CHAPTER 9

General discussion

A.M.C. Koop

In the last decades, the impact of right ventricular (RV) function on clinical status has become increasingly clear.[1-4] The RV is no longer considered as a mirrored copy of the left ventricle (LV) due to many differences in embryonic origin, anatomy and physiology.[5] Hereby, the need for further understanding of the etiology of RV failure in different forms of heart failure has been recognized.[6] Recently, in 2018, this need has been translated in a scientific statement focusing on right sided heart failure.[7] However, as outlined in the introduction, underlying biological pathways involved in the development from adaptive RV remodelling towards RV failure are not specified yet. This complicates targeted invention enabling the preservation of RV function. The aim of this thesis was to identify factors of RV remodelling due to abnormal loading conditions, with a specific focus on RV metabolism and molecular mechanisms of remodelling by the use of animal models. Additionally, we performed multi-biomarker analysis in order to identify RV disease in 125 children with congenital heart disease or pulmonary hypertension. The biomarker panel represents various activated RV adaptation processes earlier studied in this thesis. In the current chapter we discuss the main findings and potential directions for further research, which may contribute to future clinical implications.

Clinical right ventricular failure is characterized by diastolic dysfunction

Up till now, in clinical practice, the assessment of RV function is still predominately based on systolic function by the echocardiographic derived parameter tricuspid annular plane systolic excursion (TAPSE).[5] However, in LV disease it has become increasingly clear that diastolic dysfunction is also an important predictor of prognosis and mortality.[8,9] Moreover, the assumption that 'RV failure is systolic failure' has also been challenged by various experimental and clinical studies, showing a deterioration of clinical function associated with increased contractility.[10-15] In chapter 2, we have shown that clinical RV failure is associated with impaired diastolic function, whereas preserved diastolic function was observed in RV dysfunction with preserved clinical function. Hereby, we conclude that RV diastolic function may play an important role in the development of clinical RV failure. Assessment of RV diastolic function predominantly relies on invasive measurements. Also we defined diastolic function by end-diastolic elastance measured by heart catheterization (chapter 2). Due to upcoming techniques, assessing RV diastolic function may become more accessible with new echocardiographic and cardiac magnetic resonance parameters.[16] We suggest further validation of these parameters in conditions of RV pressure overload.

Metabolic shifts in the pressure loaded right ventricle

It is known for decades that cardiac metabolism plays a central role in the development of heart failure, due to reduced substrate uptake or oxidation. This has resulted in energy sparing treatment as beta-blockers, ACE-inhibitors and angiotensin II blockers in left sided heart failure.[17,18] From the LV we know that fatty acid oxidation gradually decreases in conditions of increased afterload,[19-21] whereas glucose and lactate utilization initially increases.[22,23] This metabolic switch is part of reactivation of the fetal gene program, possibly due to the fact that the stressed heart is exposed to lower oxygen conditions similar to fetal conditions.[24] In these conditions, glucose utilization is preferred because less oxygen is needed to generate one molecule of ATP compared to fatty acid utilization. Moreover, the use of glucose for ATP production by glycolysis concerns anaerobic metabolism. In more progressive stages of cardiac dysfunction glucose utilization decreases,[24,25] suggesting that the increased glucose utilization serves as an adaptive mechanism. Although these insights are known for many decades, up till now no therapy directly targeting cardiac metabolism has not been implemented to the clinic yet.

Increased glucose utilization in the pressure loaded right ventricle may serve as a adaptive mechanism.

As **chapter 3** describes, studies in animal models and patients have shown that RV glucose uptake increases in conditions of increased RV afterload. This was illustrated by increased FDG-uptake and increased levels of expression of glucose transporter 1.[26-36] Also increased glycolysis was observed by increased expression of hexokinase 1 and glycolytic flux measured with Seahorse or Langendorf.[28,33,35,37,38] Because of the diversity of models used, encompassing various stages of RV disease and different ways of characterization, it was impossible to relate these metabolic alternations to clinical function. Based on these results we were unable to speculate about the role of the eventual decreases of glucose utilization and its potential role in the development towards clinical RV failure. Nevertheless, in **chapter 2**, we found at genetic level that fatty acid metabolism was downregulated in both compensated RV dysfunction and clinical RV failure, whereas downregulation of glycolysis and gluconeogenesis was specifically decreased in animals with clinical RV failure. On one hand, this raises the question whether the metabolic shift towards glycolysis serves as a(n) (temporary) adaptation mechanism. On the other hand, various therapeutic agents aiming to reduce glycolysis by activation of glucose oxidation through indirect activation of pyruvate dehydrogenase, show positive effects on both mitochondrial and cardiac function.[34,39,40] To evaluate the early stages of RV disease, **chapter 4** assessed mitochondrial respiratory capacity, as representative of RV oxidative metabolism, in conditions of RV pressure overload at three time points before any clinical signs of RV failure occurred. Here, we found a relative increase in the mitochondrial respiratory

capacity of glucose oxidation compared to fatty acid oxidation after mild depression of both in very early stages of RV pressure load. Albeit not all significant, negative trends of mitochondrial respiratory capacity for fatty acids (**chapter 4**), and medium-chain acyl-CoA dehydrogenase (MCAD) (**chapter 3** and **4**) were found. However, our meta-analyzes (**chapter 2**) revealed ambiguous results for mitochondrial respiratory capacity of fatty acids in various animal models.

To conclude, based our findings on metabolic alternations, further research should test the hypotheses whether 1) disappearance of increased glucose utilization and/or glycolysis will eventually lead to the development of RV failure and 2) increased RV pressure load itself negatively affects the mitochondrial activity for fatty acid oxidation.

The role of intracardiac lipids in the pressure loaded right ventricle

As shown in models of pulmonary arterial hypertension, we hypothesized that a decrease in fatty acid metabolism would result in the accumulation of toxic lipids in the pressure loaded RV. Surprisingly, in **chapter 4** we found no clear evidence of decreased fatty acid metabolism and neither we found accumulation of toxic lipids in response to increased pressure load. However, a firm decrease of poly-unsatured intracardiac lipids was measured, especially tetralinoleoylcardiolipin which forms an essential component of inner mitochondrial membrane. Interestingly, this occurs before significant deterioration of mitochondrial respiratory function and before the progression of RV dysfunction towards clinical RV failure. These findings may suggest cardiac lipid alternations due to early presence of low amounts of oxidative stress.

Our findings may indicate that cardiac lipid alternations are the result of early presence of low levels of oxidative stress.

Poly-unsaturated lipids are vulnerable to oxidative stress because their hydrogen atoms are easily taken by hydroxyl radicals due to their presence close to multiple double bounds. There may be also other players affecting cardiac lipid content, like insufficient uptake or defects in the formation of lipids. However, we found no abnormalities at gene level of the enzymes of the cardiolipin synthesis pathway. We hypothesize that poly-unsaturated fatty acids serve as a defence mechanism against oxidative stress via their capacity to quench oxygen radicals. The decrease of poly-unsaturated fatty acids, especially the decrease of cardiolipins, may be one of the first signs of functional metabolic deterioration in the stressed RV. Pilot experiments in our laboratory showed that therapy with the synthetic analogue of resveratrol, also known as a BET-bromodomain inhibitor, in rats subjected to pulmonary artery banding (PAB) was accompanied with preservation of intracardiac lipids and cardiac function, with the absence of a fetal switch and changes in metabolism. The preservation of intracardiac lipids, especially poly-unsaturated lipids, may result in longer beneficial adaptation before pathologic remodelling occurs. Upcoming research should focus

on the relation between epigenetics, by means of BET-bromodomain inhibition, intracardiac lipid content and cardiac function.

Molecular mechanisms of ventricular remodelling differ between the left and right ventricle

RV adaptation concerns similar processes as LV adaptation, encompassing hypertrophy, angiogenesis and fibrosis.[41,42] Indeed, as part of characterization of the model, we identified these processes in our models of PAB and studied the potential underlying molecular mechanisms. These mechanisms appeared to be different in the RV compared to previously identified molecular mechanism in the LV (**chapter 6** and **7**). Ventricular hypertrophy is accompanied with intracellular signaling cascades encompassing calcineurin and its downstream transcriptional effector nuclear factor activated T-cells (NFAT), in both the LV[43-46] and RV[47,48] (**chapter 2**, **4**, **6** and **7**). In the stressed LV, NFAT is phosphorylated by dual-specificity tyrosine-phosphorylation regulated kinase 1a (Dyrk1a), which contributes to nuclear export and hereby halts cardiac remodelling.[49,50] MicroRNA 199b (miR-199b) has been identified as regulator of Dyrk1a expression in the pressure loaded LV.[51] In **chapter 6**, we found that in the pressure loaded RV, similar as in the pressure loaded LV, the level of miR-199b expression is inversely correlated to ventricular function. However, miR-199b expression level was not inversely correlated with Dyrk1a and no correlation with Rcan1.4, as representative of NFAT activation, was found. This indicates a distinct response mechanism of the pressure loaded RV compared to the LV, as has been indicated by Reddy and colleagues before.[51] In the latter study, microarray analysis showed RV specific alternations of microRNA's upon increased pressure load. Especially microRNA's known to be involved in apoptosis, energy availability and calciumhandling appeared to be RV specific.[52] The potentially diverse functions of microRNA's in the different ventricles should be further determined.

bHLH transcription factor heart and neural crest derivatives expressed transcript 2 (Hand2) is embryonically essential to give rise to a healthy RV.[54-56] However, in the LV, Hand 2 is also known to be involved in pathological remodelling in the LV.[53] In the current thesis, we demonstrate that Hand2 is not only essential for the RV during fetal life, but also during adulthood to resist conditions of increased RV pressure load. Where Hand2 in the LV acts on signaling cascades in hypertrophy, i.e. calcineurin-NFAT signalling, RNA sequencing of RV-tissue showed that Hand2 depletion will lead to downregulation of extracellular matrix, collagen organization and angiogenesis. Again, we hereby illustrated the distinct molecular mechanisms in the different ventricles in increased afterload conditions during adulthood.

The effect of interventricular interdependence on LV molecular mechanisms

As has been recognized since the early twentieth century, the LV and RV are inextricably linked by the various mechanisms as part of ventricular interdependence. Both systolic and diastolic function of the ventricles are affected by the other ventricle.[57-59] Not only the presence of asynchronicity or regional inhomogeneity will influence cardiac output,[60,61] but also the interplay of end systolic and diastolic volumes with the end systolic and diastolic pressures in both ventricles will affect cardiac elastance.[62,63] Furthermore, LV atrophy has been described as result of reduced RV stroke volume in conditions of RV pressure overload.[64] In the presence of these hemodynamic and morphologic findings, it is not surprising that underlying LV molecular mechanisms are affected by RV pressure overload as well. In **chapter 6** we found that in the LV the calcineurin-NFAT signaling was affected in conditions of RV pressure overload. In addition, the miR-199b-Dyrk1a feedback loop seemed identical to what has previously been found in the pressure loaded LV.[51] Also **chapter 7** demonstrates activation of molecular mechanisms of LV remodelling. Again, the reaction of Hand2 on calcineurin-NFAT signaling in the LV exposed to conditions of RV pressure load is comparable to changes in the LV in conditions of LV pressure load. These findings address that the activation of pathologic remodelling of the LV already occurs in early stages of RV disease. This contributes to the relevance for early interventions in patients with a pressure overloaded RV.

Activation of pathologic left ventricular remodelling already occurs in early stage of RV disease.

Models of right ventricular pressure load

To measure the effect of increased pressure load on the RV, several models have been used. These models include models of pulmonary arterial hypertension in rats subjected to hypoxia[30,32,37,65,66], SUGEN and hypoxia[26,26,33,67] or monocrotoline[34-36, 38, 40, 68-71], and fawn hooded rats[39]. Other models concern rats or (transgenic) mice subjected to increased fixed afterload by PAB.[28, 33, 35, 72-75] However, the stimulus used to induce increased RV pressure will have substantial effects on the etiology and severity of disease. The differences between the models are driven by the level of endothelial damage, inflammation, cytokine migration, and vasoconstriction.[76] In the current thesis, we choose to specifically characterize models of PAB. This model represents a condition of fixed afterload, including both compensated RV dysfunction and clinical RV failure. Since it concerns a mechanical stimulus, other organs will not directly be affected by the stimulus, enabling the evaluation of the net effect of increased RV pressure load. Of course different PAB-models may represent different tightness of bandings, with subsequent differences of functional status and mortality.

This makes adequate pressure measurements necessary before cardiac function is affected influencing the pressure gradient across the PAB. Intermodel comparison (i.e. models of pulmonary arterial hypertension versus fixed afterload by pulmonary artery banding or clipping) of the degree of pressure load is challenging since right ventricular systolic pressure is not always measured and different derivatives have to be used in the different models (pulmonary artery acceleration time (PAAT) versus PAB-gradient respectively). This, in combination with the different disease etiology, makes that caution is advised when drawing any model-transcending conclusions. In the current thesis, we attempted to do so in **chapter 3** regarding metabolic outcome parameters. Integrating the results of multiple experiments and models is most optimal when experimental methods are standardized. Publication of protocols, as we did in **chapter 5**, may help to reduce affiliation related bias and hopefully stimulates joint publications by different research groups.

Characterization of the various models will be necessary to enable differentiation between common denominators as the result of RV pressure load and effects of the specific stimulus.

Translating experimental findings to clinical practice

The use of biomarkers in clinical practice has been rapidly expanded over the last years. Both biomarkers derived from blood and several imaging techniques may contribute to early diagnosis and offer guidance in the follow-up of patients with chronic disease.[77-79] These markers serve as a surrogate of pathophysiological processes. In heart failure, well-known biomarkers are NT-proBNP and troponine, representing myocardial stretch and decay respectively.[81-84] The selection of biomarkers is expanding, adding markers for processes as neuroendocrine activation, inflammation, metabolism and fibrosis.[80, 85-89] This may help to increase the recognition of cardiac remodelling in early stages of cardiac stress. Although their potential use is more and more clarified, clinical implementation remains sparse. This doesn't hold back the research studying the additional value of these biomarkers. Combing multiple biomarkers, and hereby creating subsequent biomarker profiles, is a promising technique to develop more advanced characterizations of particular groups of patients. This has been done for heart failure with preserved, mid-range and reduced ejection fraction (HFpEF, HFmrEF, and HFrEF respectively), deriving more insights in processes of molecular remodelling in the heterogeneous group of patients with HFmrEF.[90] In **chapter 8** we performed multi-biomarker analysis in children with (a history of) abnormal loading conditions and profiled plasma-derived biomarker expression according to type and degree of loading. Although the pattern of the biomarker profiles seemed to be comparable, the expression level of the biomarkers differed between the groups representing different levels of molecular remodelling. In addition, NT-proBNP and ET-1 enable identification

of RV pressure load, whereas hsTnT enables identification of severe RV pressure load specifically. NT-proBNP, hsTnT, MR-proADM, GDF-15, MPO and ET-1 were associated with RVH, which may reflect activation of broad spectrum of molecular processes, including processes involved in the RAAS-system, cardiomyocyte decay, inflammation, metabolism, oxidative stress and fibrosis. Based on the results, we suggested a hypothetical algorithm to recognize abnormal RV loading and remodelling, leading to potential therapeutic directions. The study in **chapter 8** included predominantly children with preserved functional class, so this algorithm may contribute after validation to early detection of RV disease in this specific group of patients. Combining the use of plasma derived biomarkers with the advanced imaging technique in order to assess morphologic alternations and metabolic processes, may further enable early recognition of RV adaptation. This may initiate early interventions in order to prevent progression of RV disease.

Development of biomarker based algorithms may contribute to the early detection of right ventricular disease.

Concluding remarks and future prospects

This thesis emphasizes the differences, and at the same time the interplay, between the RV and LV, where the molecular processes identified in the LV cannot be copied to the RV. This implies that all the pathological processes involved in LV adaptation also should be studied in the RV. Furthermore, this thesis demonstrates that the affected metabolic processes in the abnormally loaded RV depend on the experimental model used and the associated disease etiologies. These findings stress the dynamic character of metabolic processes, which makes standardization of experimental methods pivotal to draw robust conclusions. Increased pressure affects metabolic processes in the RV, therefore metabolic biomarkers or metabolites, such as intracardiac lipids, may serve as markers of RV adaptation. This would allow implementation of metabolic profiling, as an unbiased approach to define the state of the loaded RV in clinical practice. We showed that blood derived biomarkers reflect RV adaptation in early RV disease before the occurrence of clinical signs. These techniques will enable the possibility for early interventions in order to preserve RV function in conditions of increased pressure load.

REFERENCES

1. Gorter TM, Hoendermis ES, Veldhuizen DJ van, Voors AA, Lam CSP, Geelhoed B, Willems TP, Melle JP Van. Right ventricular dysfunction in heart failure with preserved ejection fraction: a systematic review and meta-analysis. *Eur J Heart Fail* 2016;18:1472–1487.
2. Norozi K, Wessel A, Alpers V, Arnhold JO, Geyer S, Zoege M, Buchhorn R. Incidence and Risk Distribution of Heart Failure in Adolescents and Adults With Congenital Heart Disease After Cardiac Surgery. *Am J Cardiol* 2006;97:1238–1243.
3. Wolferen SA Van, Marcus JT, Boonstra A, Marques KMJ, Bronzwaer JGF, Spreeuwenberg MD, Postmus PE, Vonk-Noordegraaf A. Prognostic value of right ventricular mass, volume, and function in idiopathic pulmonary arterial hypertension. *Eur Heart J* 2007;28:1250–1257.
4. Ghio S, Gavazzi A, Campana C, Inserra C, Klersy C, Sebastiani R, Arbustini E, Recusani F, Tavazzi L. Independent and Additive Prognostic Value of Right Ventricular Systolic Function and Pulmonary Artery Pressure in Patients With Chronic Heart Failure. *J Am Coll Cardiol* Elsevier Masson SAS; 2001;37:183–188.
5. Haddad F, Hunt SA, Rosenthal DN, Murphy DJ. Right ventricular function in cardiovascular disease, part I: Anatomy, physiology, aging, and functional assessment of the right ventricle. *Circulation* 2008;117:1436–1448.
6. Voelkel NF, Quaife RA, Leinwand LA, Barst RJ, McGoon MD, Meldrum DR, Dupuis J, Long CS, Rubin LJ, Smart FW, Suzuki YJ, Gladwin M, Denholm EM, Gail DB. Right ventricular function and failure: Report of a National Heart, Lung, and Blood Institute working group on cellular and molecular mechanisms of right heart failure. *Circulation* 2006;114:1883–1891.
7. Konstam MA, Kiernan MS, Bernstein D, Bozkurt B, Jacob M, Kapur NK, Kociol RD, Lewis EF, Mehra MR, Pagani FD, Raval AN, Ward C. Evaluation and Management of Right-Sided Heart Failure: A Scientific Statement From the American Heart Association. Circulation. 2018.
8. Rihal CS, Nishimura RA, Hatle LK, Bailey KR, Tajik AJ. Systolic and diastolic dysfunction in patients with clinical diagnosis of dilated cardiomyopathy: Relation to symptoms and prognosis. *Circulation* 1994;90:2772–2779.
9. Pinamonti B, Lenarda A Di, Sinagra G, Camerini F. Restrictive left ventricular filling pattern in dilated cardiomyopathy assessed by doppler echocardiography: Clinical, echocardiographic and hemodynamic correlations and prognostic implications. *J Am Coll Cardiol* 1993;22:808–815.
10. Gaynor SL, Maniar HS, Bloch JB, Steendijk P, Moon MR. Right atrial and ventricular adaptation to chronic right ventricular pressure overload. *Circulation* 2005;112:212–218.
11. Man FS De, Handoko ML, Ballegoij JJM Van, Schalij I, Bogaards SJP, Postmus PE, Velden J Van Der, Westerhof N, Paulus WJ, Vonk-Noordegraaf A. Bisoprolol delays progression towards right heart failure in experimental pulmonary hypertension. *Circ Hear Fail* 2012;5:97–105.
12. Borgdorff M a J, Bartelds B, Dickinson MG, Steendijk P, Vroomen M de, Berger RMF. Distinct loading conditions reveal various patterns of right ventricular adaptation. *Am J Physiol Heart Circ Physio*l 2013;305:H354-64.
13. Borgdorff M a. J, Dickinson MG, Berger RMF, Bartelds B. Right ventricular failure due to chronic pressure load: What have we learned in animal models since the NIH working group statement? *Heart Fail Rev* Springer US; 2015;475–491.

14. Trip P, Rain S, Handoko ML, DerBruggen C Van, Bogaard HJ, Marcus JT, Boonstra A, Westerhof N, Vonk-Noordegraaf A, S De Man F. Clinical relevance of right ventricular diastolic stiffness in pulmonary hypertension. *Eur Respir J* 2015;45:1603–1612.
15. Rain S, Handoko ML, Trip P, Gan CT-J, Westerhof N, Stienen GJ, Paulus WJ, Ottenheijm CAC, Marcus JT, Dorfmüller P, Guignabert C, Humbert M, Macdonald P, Remedios C Dos, Postmus PE, Saripalli C, Hidalgo CG, Granzier HL, Vonk-Noordegraaf A, Velden J Van Der, Man FS De. Right ventricular diastolic impairment in patients with pulmonary arterial hypertension. *Circulation* F.S. De Man, Department of Pulmonology, VU University Medical Center, Institute for Cardiovascular Research, 1081 HV Amsterdam, Netherlands; 2013;128:2016–2025.
16. Chamsi-Pasha MA, Zhan Y, Debs D, Shah DJ. CMR in the Evaluation of Diastolic Dysfunction and Phenotyping of HFpEF: Current Role and Future Perspectives. *JACC Cardiovasc Imaging* Elsevier; 2020;13:283–296.
17. Cohn JN, Tognoni G. A Randomized Trial of the Angiotensin-Receptor Blocker Valsartan in Chronic Heart Failure. *N Engl J Med* 2001;345:1667–1675.
18. Pfeffer MA, Swedberg K, Granger CB, Held P, McMurray JJV, Michelson EL, Olofsson B, Östergren J, Yusuf S. Effects of candesartan on mortality and morbidity in patients with chronic heart failure: The CHARM-overall programme. *Lancet* 2003;362:759–766.
19. Stanley WC, Recchia FA, Lopaschuk GD. Myocardial substrate metabolism in the normal and failing heart. *Physiol Rev* 2005;85:1093–1129.
20. Osorio JC, Stanley WC, Linke A, Castellari M, Diep QN, Panchal AR, Hintze TH, Lopaschuk GD, Recchia FA. Impaired myocardial fatty acid oxidation and reduced protein expression of retinoid X receptor- in pacing-induced heart failure. *Circulation* 2002;106:606–612.
21. Chandler MP, Kerner J, Huang H, Vazquez E, Reszko A, Martini WZ, Hoppel CL, Imai M, Rastogi S, Sabbah HN, Stanley WC. Moderate severity heart failure does not involve a downregulation of myocardial fatty acid oxidation. *Am J Physiol - Hear Circ Physiol* 2004;287:1538–1543.
22. Remondino A, Rosenblatt-Velin N, Montessuit C, Tardy I, Papageorgiou I, Dorsaz PA, Jorge-Costa M, Lerch R. Altered expression of proteins of metabolic regulation during remodeling of the left ventricle after myocardial infarction. *J Mol Cell Cardiol* 2000;32:2025–2034.
23. Nascimben L, Ingwall JS, Lorell BH, Pinz I, Schultz V, Tornheim K, Tian R. Mechanisms for increased glycolysis in the hypertrophied rat heart. *Hypertension* 2004;44:662–667.
24. Razeghi P, Young ME, Alcorn JL, Moravec CS, Frazier OH, Taegtmeyer H. Metabolic gene expression in fetal and failing human heart. *Circulation* 2001;104:2923–2931.
25. Taylor M, Wallhaus TR, Degrado TR, Russell DC, Stanko P, Nickles RJ, Stone CK. An evaluation of myocardial fatty acid and glucose uptake using PET with [18F]fluoro-6-thia-heptadecanoic acid and [18F]FDG in patients with congestive heart failure. *J Nucl Med* 2001;42:55–62.
26. Graham BB, Kumar R, Mickael C, Sanders L, Gebreab L, Huber KM, Perez M, Smith-Jones P, Serkova NJ, Tuder RM. Severe pulmonary hypertension is associated with altered right ventricle metabolic substrate uptake. *Am J Physiol - Lung Cell Mol Physiol* B.B. Graham, Division of Pulmonary Sciences and Critical Care Medicine, Univ. of Colorado Denver, Aurora, United States; 2015;309:L435–L440.

27. Drozd K, Ahmadi A, Deng Y, Jiang B, Petryk J, Thorn S, Stewart D, Beanlands R, DeKemp RA, DaSilva JN, Mielniczuk LM. Effects of an endothelin receptor antagonist, Macitentan, on right ventricular substrate utilization and function in a Sugen 5416/hypoxia rat model of severe pulmonary arterial hypertension. *J Nucl Cardiol* L.M. Mielniczuk, Division of Cardiology, Department of Medicine, University of Ottawa Heart Institute, Ottawa, Canada; 2016;1–11.

28. Bruggen CE van der, Happé CM, Dorfmüller P, Trip P, Spruijt OA, Rol N, Hoevenaars FP, Houweling AC, Girerd B, Marcus JT, Mercier O, Humbert M, Handoko ML, Velden J van der, Vonk Noordegraaf A, Bogaard HJ, Goumans M-J, Man FS de. Bone Morphogenetic Protein Receptor Type 2 Mutation in Pulmonary Arterial HypertensionCLINICAL PERSPECTIVE. *Circulation* 2016;133:1747–1760.

29. Adrogue J V, Sharma S, Ngumbela K, Essop MF, Taegtmeyer H. Acclimatization to chronic hypobaric hypoxia is associated with a differential transcriptional profile between the right and left ventricle. *Mol Cell Biochem* H. Taegtmeyer, Department of Internal Medicine, Division of Cardiology, University of Texas Houston - Medical School, Houston, TX 77030, United States; 2005;278:71–78.

30. Sivitz WI, Lund DD, Yorek B, Grover-McKay M, Schmid PG. Pretranslational regulation of two cardiac glucose transporters in rats exposed to hypobaric hypoxia. *Am J Physiol - Endocrinol Metab* W.I. Sivitz, Dept. of Internal Medicine, Univ. of Iowa Hospitals and Clinics, Iowa City, IA 52246, United States; 1992;263:E562–E569.

31. Sharma S, Taegtmeyer H, Adrogue J, Razeghi P, Sen S, Ngumbela K, Essop MF. Dynamic changes of gene expression in hypoxia-induced right ventricular hypertrophy. *Am J Physiol - Hear Circ Physiol* H. Taegtmeyer, Dept. of Internal Medicine, Division of Cardiology, Univ. of Texas-Houston Med. School, Houston, TX 77030, United States; 2004;286:H1185–H1192.

32. Gomez-Arroyo J, Mizuno S, Szczepanek K, Tassell B Van, Natarajan R, Remedios CG Dos, Drake JI, Farkas L, Kraskauskas D, Wijesinghe DS, Chalfant CE, Bigbee J, Abbate A, Lesnefsky EJ, Bogaard HJ, Voelkel NF. Metabolic gene remodeling and mitochondrial dysfunction in failing right ventricular hypertrophy secondary to pulmonary arterial hypertension. *Circ Hear Fail* N.F. Voelkel, Victoria Johnson Center for Lung Obstructive Disease Research, Virginia Commonwealth University, Richmond, VA 23298, United States; 2013;6:136–144.

33. Piao L, Fang YH, Cadete VJJ, Wietholt C, Urboniene D, Toth PT, Marsboom G, Zhang HJ, Haber I, Rehman J, Lopaschuk GD, Archer SL. The inhibition of pyruvate dehydrogenase kinase improves impaired cardiac function and electrical remodeling in two models of right ventricular hypertrophy: Resuscitating the hibernating right ventricle. *J Mol Med* 2010;88:47–60.

34. Piao L, Fang Y-H, Parikh K, Ryan JJ, Toth PT, Archer SL. Cardiac glutaminolysis: A maladaptive cancer metabolism pathway in the right ventricle in pulmonary hypertension. *J Mol Med* S.L. Archer, Department of Medicine, Queen's University, Etherington Hall, Kingston, ON K7L 3N6, Canada; 2013;91:1185–1197.

35. Balestra GM, Mik EG, Eerbeek O, Specht PAC, Laarse WJ van der, Zuurbier CJ. Increased in vivo mitochondrial oxygenation with right ventricular failure induced by pulmonary arterial hypertension: Mitochondrial inhibition as driver of cardiac failure? *Respir Res* C.J. Zuurbier, Department of Anesthesiology, Laboratory of Experimental Intensive Care and Anesthesiology, AMC, Amsterdam, Netherlands; 2015;16.

36. Fang Y-H, Piao L, Hong Z, Toth PT, Marsboom G, Bache-Wiig P, Rehman J, Archer SL. Therapeutic inhibition of fatty acid oxidation in right ventricular hypertrophy: Exploiting Randle's cycle. *J Mol Med* S.L. Archer, Medicine/Cardiology, University of Chicago, Chicago, IL 60637, United States; 2012;90:31–43.

37. Rumsey WL, Abbott B, Bertelsen D, Mallamaci M, Hagan K, Nelson D, Erecinska M. Adaptation to hypoxia alters energy metabolism in rat heart. *Am J Physiol - Hear Circ Physiol* W.L. Rumsey, Zeneca Pharmaceuticals, Wilmington, DE 19850-5437, United States; 1999;276:H71–H80.

38. Zhang W-H, Qiu M-H, Wang X-J, Sun K, Zheng Y, Jing Z-C. Up-regulation of hexokinase1 in the right ventricle of monocrotaline induced pulmonary hypertension. *Respir Res* Y. Zheng, First Hospital of Jilin University, Center of Cardiovascular Disease, Changchun, China; 2014;15.

39. Piao L, Sidhu VK, Fang YH, Ryan JJ, Parikh KS, Hong Z, Toth PT, Morrow E, Kutty S, Lopaschuk GD, Archer SL. FOXO1-mediated upregulation of pyruvate dehydrogenase kinase-4 (PDK4) decreases glucose oxidation and impairs right ventricular function in pulmonary hypertension: therapeutic benefits of dichloroacetate. *J Mol Med* 2012;29:1–14.

40. Sun X-Q, Zhang R, Zhang H-D, Yuan P, Wang X-J, Zhao Q-H, Wang L, Jiang R, Jan Bogaard H, Jing Z-C. Reversal of right ventricular remodeling by dichloroacetate is related to inhibition of mitochondria-dependent apoptosis. *Hypertens Res* Z.-C. Jing, State Key Laboratory of Cardiovascular Disease, Fu Wai Hospital, National Center for Cardiovascular Disease, Peking Union Medical College, Chinese Academy Medical Science, Beijing, China; 2016;39:302–311.

41. Ryan JJ, Huston J, Kutty S, Hatton ND, Bowman L, Tian L, Herr JE, Johri AM, Archer SL. Right Ventricular Adaptation and Failure in Pulmonary Arterial Hypertension. *Can J Cardiol* Canadian Cardiovascular Society; 2015;31:391–406.

42. Opie LH, Commerford PJ, Gersh BJ, Pfeffer MA. Controversies in ventricular remodelling. *Lancet* 2006;367:1315; author reply 1315-6.

43. Molkentin JD, Lu JR, Antos CL, Markham B, Richardson J, Robbins J, Grant SR, Olson EN. A calcineurin-dependent transcriptional pathway for cardiac hypertrophy. *Cell* 1998;93:215–228.

44. Bourajjaj M, Armand AS, Costa Martins PA Da, Weijts B, Nagel R Van Der, Heeneman S, Wehrens XH, Windt LJ De. NFATc2 is a necessary mediator of calcineurin-dependent cardiac hypertrophy and heart failure. *J Biol Chem* 2008;283:22295–22303.

45. Windt LJ De, Lim HW, Bueno OF, Liang Q, Delling U, Braz JC, Glascock BJ, Kimball TR, Monte F del, Hajjar RJ, Molkentin JD. Targeted inhibition of calcineurin in pressure-overload cardiac hypertrophy in vivo. *Proc Natl Acad Sci* 2001;98:3322–3327.

46. Wilkins BJ, Windt LJ De, Bueno OF, Braz JC, Glascock BJ, Kimball TF, Molkentin JD. Targeted Disruption of NFATc3, but Not NFATc4, Reveals an Intrinsic Defect in Calcineurin-Mediated Cardiac Hypertrophic Growth. *Mol Cell Biol* 2002;22:7603–7613.

47. Bartelds B, Borgdorff M a., Smit-Van Oosten A, Takens J, Boersma B, Nederhoff MG, Elzenga NJ, Gilst WH Van, Windt LJ De, Berger RMF. Differential responses of the right ventricle to abnormal loading conditions in mice: Pressure vs. volume load. *Eur J Heart Fail* 2011;13:1275–1282.

48. Nagendran J, Gurtu V, Fu DZ, Dyck JRB, Haromy A, Ross DB, Rebeyka IM, Michelakis ED. A dynamic and chamber-specific mitochondrial remodeling in right ventricular hypertrophy can be therapeutically targeted. *J Thorac Cardiovasc Surg* E.D. Michelakis, Pulmonary Hypertension Program, Department of Medicine, University of Alberta, Edmonton, Alta., Canada; 2008;136:168-178.e3.

49. Arron JR, Winslow MM, Polleri A, Chang CP, Wu H, Gao X, Neilson JR, Chen L, Heit JJ, Kim SK, Yamasaki N, Miyakawa T, Francke U, Graef IA, Crabtree GR. NFAT dysregulation by increased dosage of DSCR1 and DYRK1A on chromosome 21. *Nature* 2006;441:595–600.

50. Gwack Y, Sharma S, Nardone J, Tanasa B, Iuga A, Srikanth S, Okamura H, Bolton D, Feske S, Hogan PG, Rao A. A genome-wide Drosophila RNAi screen identifies DYRK-family kinases as regulators of NFAT. *Nature* 2006;441:646–650.

51. Costa Martins PA da, Salic K, Gladka MM, Armand A-S, Leptidis S, Azzouzi H el, Hansen A, Coenen-de Roo CJ, Bierhuizen MF, Nagel R van der, Kuik J van, Weger R de, Bruin A de, Condorelli G, Arbones ML, Eschenhagen T, Windt LJ De. MicroRNA-199b targets the nuclear kinase Dyrk1a in an auto-amplification loop promoting calcineurin/NFAT signalling. *Nat Cell Biol* Nature Publishing Group; 2010;12:1220–1227.

52. Reddy S, Zhao M, Hu D-Q, Fajardo G, Hu S, Ghosh Z, Rajagopalan V, Wu JC, Bernstein D. Dynamic microRNA expression during the transition from right ventricular hypertrophy to failure. *Physiol Genomics* 2012;44:562–575.

53. Srivastava D, Thomas T, Lin Q, Kirby ML, Brown D, Olson EN. Regulation of cardiac mesodermal and neural crest development by the bHLH transcription factor, dHAND. *Nat Genet* 1997;16:154–160.

54. Shen L, Li XF, Shen AD, Wang Q, Liu CX, Guo YJ, Song ZJ, Li ZZ. Transcription factor HAND2 mutations in sporadic chinese patients with congenital heart disease. *Chin Med J (Engl)* 2010;123:1623–1627.

55. Sun Y-M, Wang J, Qiu X-B, Yuan F, Li R-G, Xu Y-J, Qu X-K, Shi H-Y, Hou X-M, Huang R-T, Xue S, Yang Y-Q. A HAND2 loss-of-function mutation causes familial ventricular septal defect and pulmonary stenosis. *G3 Genes, Genomes, Genet* J. Wang, Department of Cardiology, Jing'an District Central Hospital, Shanghai, China; 2016;6:987–992.

56. Dirkx E, Gladka MM, Philippen LE, Armand A, Kinet V, Leptidis S, Azzouzi H, Salic K, Bourajjaj M, Silva GJJ, Olieslagers S, Nagel R Van Der, Weger R De, Bitsch N, Kisters N, Seyen S, Morikawa Y, Chanoine C, Heymans S, Volders PGA, Thum T, Dimmeler S, Cserjesi P, Eschenhagen T, Paula A, Martins C, Windt LJ De, Azzouzi H El, Salic K, Bourajjaj M, et al. Nfat and miR-25 cooperate to reactivate the transcription factor Hand2 in heart failure. *Nat Cell Biol* Nature Publishing Group; 2013;15:1282–1293.

57. Kasner M, Westermann D, Steendijk P, Drose S, Poller W, Schultheiss HP, Tschöpe C. Left ventricular dysfunction induced by nonsevere idiopathic pulmonary arterial hypertension: A pressure-volume relationship study. *Am J Respir Crit Care M*ed 2012;186:181–189.

58. Damiano RJ, Follette P La, Cox JL, Lowe JE, Santamore WP. Significant left ventricular contribution to right ventricular systolic function. *Am J Physiol - Hear Circ Physiol* 1991;261.

59. Goldstein JA, Harada A, Yagi Y, Barzilai B, Cox JL. Hemodynamic importance of systolic ventricular interaction, augmented right atrial contractility and atrioventricular synchorny in acute right ventricular dysfunction. *J Am Coll Cardiol* 1990;**16**:181–189.

60. Marcus JT, Gan CTJ, Zwanenburg JJM, Boonstra A, Allaart CP, Götte MJW, Vonk-Noordegraaf A. Interventricular Mechanical Asynchrony in Pulmonary Arterial Hypertension. Left-to-Right Delay in Peak Shortening Is Related to Right Ventricular Overload and Left Ventricular Underfilling. *J Am Coll Cardiol* 2008;51:750–757.

61. Smith BCF, Dobson G, Dawson D, Charalampopoulos A, Grapsa J, Nihoyannopoulos P. Three-dimensional speckle tracking of the right ventricle: Toward optimal quantification of right ventricular dysfunction in pulmonary hypertension. *J Am Coll Cardio*l 2014;64:41–51.

62. Taylor RR, Covell JW, Sonnenblick EH, Ross J. Dependence of ventricular distensibility on filling of the opposite ventricle. *Am J Physiol* 1967;213:711–718.

63. Bemis CE, Serur JR, Borkenhagen D, Sonnenblick EH, Urschel CW. Influence of right ventricular filling pressure on left ventricular pressure and dimension. *Circ Res* 1974;34:498–504.

64. Hardziyenka M, Campian ME, Reesink HJ, Surie S, Bouma BJ, Groenink M, Klemens CA, Beekman L, Remme CA, Bresser P, Tan HL. Right ventricular failure following chronic pressure overload is associated with reduction in left ventricular mass: Evidence for atrophic remodeling. *J Am Coll Cardiol* Elsevier Inc.; 2011;57:921–928.

65. Bruns DR, Dale Brown R, Stenmark KR, Buttrick PM, Walker LA. Mitochondrial integrity in a neonatal bovine model of right ventricular dysfunction. *Am J Physiol - Lung Cell Mol Physiol* L.A. Walker, Univ. of Colorado-Denver, Dept. of Medicine, Cardiology, Aurora, United States; 2015;308:L158–L167.

66. Nouette-Gaulain K, Malgat M, Rocher C, Savineau J-P, Marthan R, Mazat J-P, Sztark F. Time course of differential mitochondrial energy metabolism adaptation to chronic hypoxia in right and left ventricles. *Cardiovasc Res* F. Sztark, Laboratoire d'Anesthésiologie, E.A. Physiologie Mitochondriale, Universite Bordeaux 2, 33076 Bordordeaux, France; 2005;66:132–140.

67. Liu A, Philip J, Vinnakota KC, Bergh F Van den, Tabima DM, Hacker T, Beard DA, Chesler NC. Estrogen maintains mitochondrial content and function in the right ventricle of rats with pulmonary hypertension. *Physiol Rep* 2017;5:1–12.

68. Broderick TL, King TM. Upregulation of GLUT-4 in right ventricle of rats with monocrotaline-induced pulmonary hypertension. *Med Sci Monit* T. L. Broderick, Department of Physiology, Midwestern University, Glendale, AZ 85308, United States; 2008;14:BR261–BR264.

69. Enache I, Charles A-L, Bouitbir J, Favret F, Zoll J, Metzger D, Oswald-Mammosser M, Geny B, Charloux A. Skeletal muscle mitochondrial dysfunction precedes right ventricular impairment in experimental pulmonary hypertension. *Mol Cell Biochem* I. Enache, Service de Physiologie et d'Explorations Fonctionnelles, Pôle de Pathologie Thoracique, Centre Hospitalier Universitaire Strasbourg, Nouvel Hôpital Civil, 67091 Strasbourg, France; 2013;373:161–170.

70. Sutendra G, Dromparis P, Paulin R, Zervopoulos S, Haromy A, Nagendran J, Michelakis ED. A metabolic remodeling in right ventricular hypertrophy is associated with decreased angiogenesis and a transition from a compensated to a decompensated state in pulmonary hypertension. *J Mol Med* E.D. Michelakis, Department of Medicine, University of Alberta, Edmonton, AB T6G 2B7, Canada; 2013;91:1315–1327.

71. Paulin R, Sutendra G, Gurtu V, Dromparis P, Haromy A, Provencher S, Bonnet S, Michelakis ED. A miR-208-Mef2 axis drives the decompensation of right ventricular function in pulmonary hypertension. *Circ Res* 2015;116:56–69.

72. Lauva IK, Brody E, Tiger E, Kent RL, Copper G 4th, Marino TA. Control of myocardial tissue components and cardiocyte organelles in pressure-overload hypertrophy of the cat right ventricle. *Am J Anat* United States; 1986;177:71–80.

73. Olivetti G, Ricci R, Lagrasta C, Maniga E, Sonnenblick EH, Anversa P. Cellular basis of wall remodeling in long-term pressure overload-induced right ventricular hypertrophy in rats. *Circ Res* Department of Pathology, University of Parma, 43100 Parma; 1988;**63**:648–657.

74. Sack MN, Disch DL, Rockman HA, Kelly DP. A role for Sp and nuclear receptor transcription factors in a cardiac hypertrophic growth program. *Proc Natl Acad Sci U S A* D.P. Kelly, Center for Cardiovascular Research, Box 8086, Washington Univ. Sch. of Medicine, St. Louis, MO 63110, United States; 1997;94:6438–6443.

75. Sheikh AM, Barrett C, Villamizar N, Alzate O, Valente AM, Herlong JR, Craig D, Lodge A, Lawson J, Milano C, Jaggers J. Right ventricular hypertrophy with early dysfunction: A proteomics study in a neonatal model. *J Thorac Cardiovasc Surg* A.M. Sheikh, Department of Pediatric Cardiac Surgery, the Neuroproteomics Center, Durham, NC, United States; 2009;137:1146–1153.

76. Stenmark KR, Meyrick B, Galie N, Mooi WJ, McMurtry IF. Animal models of pulmonary arterial hypertension: the hope for etiological discovery and pharmacological cure. *Am J Physiol Lung Cell Mol Physiol* 2009;297:L1013-32.

77. Chow SL, Maisel AS, Anand I, Bozkurt B, Boer RA De, Felker GM, Fonarow GC, Greenberg B, Januzzi JL, Kiernan MS, Liu PP, Wang TJ, Yancy CW, Zile MR. Role of biomarkers for the prevention, assessment, and management of heart failure: A scientific statement from the American Heart Association. Circulation. 2017.

78. Liu CH, Abrams ND, Carrick DM, Chander P, Dwyer J, Hamlet MRJ, Macchiarini F, Prabhudas M, Shen GL, Tandon P, Vedamony MM. Biomarkers of chronic inflammation in disease development and prevention: Challenges and opportunities. *Nat Immunol* Nature Publishing Group; 2017;18:1175–1180.

79. deSouza NM, Achten E, Alberich-Bayarri A, Bamberg F, Boellaard R, Clément O, Fournier L, Gallagher F, Golay X, Heussel CP, Jackson EF, Manniesing R, Mayerhofer ME, Neri E, O'Connor J, Oguz KK, Persson A, Smits M, Beek EJR van, Zech CJ. Validated imaging biomarkers as decision-making tools in clinical trials and routine practice: current status and recommendations from the EIBALL* subcommittee of the European Society of Radiology (ESR). *Insights Imaging* Insights into Imaging; 2019;10.

80. Daniels LB, Maisel AS. Natriuretic Peptides. *J Am Coll Cardiol* 2007;50:2357–2368.

81. Horwich TB, Patel J, MacLellan WR, Fonarow GC. Cardiac troponin I is associated with impaired hemodynamics, progressive left ventricular dysfunction, and increased mortality rates in advanced heart failure. *Circulation* 2003;108:833–838.

82. Hudson MP, O'Connor CM, Gattis WA, Tasissa G, Hasselblad V, Holleman CM, Gaulden LH, Sedor F, Ohman EM. Implications of elevated cardiac troponin t in ambulatory patients with heart failure: A prospective analysis. *Am Heart J* 2004;147:546–552.

83. Vecchia L La, Mezzena G, Zanolla L, Paccanaro M, Varotto L, Bonanno C, Ometto R. Cardiac Troponin I as diagnostic and prognostic marker in severe heart failure. *J Hear Lung Transplant* 2000;19:644–652.

84. Jensen MK, Bertoia ML, Cahill LE, Agarwal I, Rimm EB, Mukamal KJ. Novel metabolic biomarkers of cardiovascular disease. *Nat Rev Endocrinol* Nature Publishing Group; 2014;10:659–672.

85. Calvier L, Legchenko E, Grimm L, Sallmon H, Hatch A, Plouffe BD, Schroeder C, Bauersachs J, Murthy SK, Hansmann G. Galectin-3 and aldosterone as potential tandem biomarkers in pulmonary arterial hypertension. *Heart* 2016;102:390–396.

86. Tang WHW, Brennan ML, Philip K, Tong W, Mann S, Lente F Van, Hazen SL. Plasma Myeloperoxidase Levels in Patients With Chronic Heart Failure. *Am J Cardiol* 2006;98: 796–799.

87. Besler C, Lang D, Urban D, Rommel KP, Roeder M Von, Fengler K, Blazek S, Kandolf R, Klingel K, Thiele H, Linke A, Schuler G, Adams V, Lurz P. Plasma and cardiac galectin-3 in patients with heart failure reflects both inflammation and fibrosis: Implications for its use as a biomarker. *Circ Hear Fail* 2017;10:1–9.

88. Kempf T, Haehling S von, Peter T, Allhoff T, Cicoira M, Doehner W, Ponikowski P, Filippatos GS, Rozentryt P, Drexler H, Anker SD, Wollert KC. Prognostic Utility of Growth Differentiation Factor-15 in Patients With Chronic Heart Failure. *J Am Coll Car*diol 2007;50:1054–1060.

89. Maisel A, Mueller C, Nowak R, Peacock WF, Landsberg JW, Ponikowski P, Mockel M, Hogan C, Wu AHB, Richards M, Clopton P, Filippatos GS, Somma S Di, Anand I, Ng L, Daniels LB, Neath SX, Christenson R, Potocki M, McCord J, Terracciano G, Kremastinos D, Hartmann O, Haehling S von, Bergmann A, Morgenthaler NG, Anker SD. Mid-Region Pro-Hormone Markers for Diagnosis and Prognosis in Acute Dyspnea. Results From the BACH (Biomarkers in Acute Heart Failure) Trial. *J Am Coll Cardiol* Elsevier Inc.; 2010;55:2062–2076.

90. Tromp J, Khan MAF, Mentz RJ, O'Connor CM, Metra M, Dittrich HC, Ponikowski P, Teerlink JR, Cotter G, Davison B, Cleland JGF, Givertz MM, Bloomfield DM, Veldhuisen DJ Van, Hillege HL, Voors AA, Meer P van der. Biomarker Profiles of Acute Heart Failure Patients With a Mid-Range Ejection Fraction. *JACC Hear Fail* 2017;5:507–517.

APPENDICES

NEDERLANDSE SAMENVATTING

Hartfalen treft meer dan 26 miljoen mensen wereldwijd en is een van de meest voorkomende doodsoorzaken in de westerse wereld. Hoewel de medische zorg en de wetenschap zich decennia lang met name gefocust hebben op de linkerhelft van het hart, als pomp van de systeemcirculatie, is er de afgelopen 20 jaar in toenemende mate aandacht voor de rechterhelft van het hart. De rechter hartkamer pompt bloed naar de longen waar bloed voorzien wordt van zuurstof en vervult hiermee een essentiële functie voor het menselijk lichaam. Daarnaast blijkt dat de functie van beide hartkamers niet individueel te bekijken is aangezien zij de gemeenschappelijke tussenwand (het septum), die een belangrijke rol speelt bij het verpompen van bloed, delen. Wanneer de functie van de rechter hartkamer verslechtert, zullen er op termijn lichamelijke klachten ontstaan zoals vocht in de benen of buik, verminderde eetlust, vermoeidheid en een verminderd inspanningsvermogen. Er is dan sprake van rechter hartkamer falen. Progressieve verslechtering van de rechter hartkamer functie zal uiteindelijk leiden tot het overlijden van de patiënt.

Een belangrijke oorzaak van rechter hartkamer falen is chronische abnormale belasting, zoals het geval is bij pulmonale hypertensie, aangeboren hartafwijkingen en linker hartkamer falen. Chronische abnormale belasting leidt tot structurele en functionele veranderingen in de hartspier. Middels deze veranderingen wordt gepoogd de hartfunctie te behouden. Echter, een gedeelte van deze veranderingen zal op termijn een averechts effect hebben op de hartfunctie. Hoewel veel mechanismen reeds onderzocht zijn in de linker hartkamer, zijn deze niet een-op-een te vertalen naar de rechter hartkamer vanwege de verschillen in embryonale oorsprong, anatomie en functie. Het onderscheid tussen de adaptieve en pathologische mechanismen van de rechter hartkamer als reactie op abnormale belasting is in mindere mate onderzocht en hiermee onvoldoende bekend.

In dit proefschrift wordt ingegaan op verschillende mechanismen die betrokken zijn bij chronische abnormale belasting van de rechter hartkamer en hoe herkenning van deze processen in de patiëntenpopulatie zou kunnen plaatsvinden. In **hoofdstuk 1** wordt verder ingegaan op de doelen van dit proefschrift en het kader waarbinnen deze doelen werden gesteld.

In **hoofdstuk 2** karakteriseerden we twee groepen ratten die blootgesteld werden aan drukbelasting van de rechter hartkamer. De drukbelasting werd gerealiseerd door het chirurgisch plaatsen van een bandje om de longslagader. Bij alle ratten was er sprake van een verslechterde rechter hartkamer functie, maar bij de helft van de ratten ging dit samen met lichamelijke klachten. Functionele en moleculaire parameters van ratten met zogenoemd klinisch rechter hartkamer falen (aanwezigheid van lichamelijke klachten) enerzijds en ratten met alleen

rechter hartkamer dysfunctie (afwezigheid van lichamelijke klachten) anderzijds, werden tegen elkaar afgezet. Klinisch rechter hartkamer falen werd gekenmerkt door een toegenomen contractiliteit (knijpkracht) en een verminderde diastolische functie (ontspanning). Op genniveau werd in beide groepen voornamelijk een toename gezien van processen betrokken bij celgroei, proliferatie en inflammatie (onstekingsprocessen). Ook werd ten gevolge van drukbelasting in rechter hartkamer een vermindering van genexpressie gezien van genen betrokken bij het oxidatieve (zuurstofrijke) metabolisme. Vermindering van expressie van genen betrokken bij glycolyse (suikerverbranding zonder zuurstof) trad specifiek op in de groep met klinisch rechter hartkamer falen.

Rechter hartkamer falen wordt gekenmerkt door verminderde diastolische functie (ontspanning) en verminderde genexpressie van genen betrokken bij glycolyse (zuurstofarme suikerverbranding).

Naar aanleiding van de resultaten in **hoofdstuk 2** presenteren we in **hoofdstuk 3** een overzicht van de huidige literatuur betreffende metabolisme in de drukbelaste rechter hartkamer. Op basis van 31 studies, waarin bevindingen van verschillende diermodellen van rechter hartkamer drukbelasting en patiënten met pulmonale hypertensie uitgezet worden, lieten meta-analyses een toegenomen genexpressie van glucose transporter 1 (betrokken bij suikeropname) en hexokinase 1 (een regulator van glycolyse) zien. Bovendien was er sprake van toegenomen glycolyse in de drukbelaste rechter hartkamer. Ten aanzien van andere metabole processen, onder andere processen betrokken bij vetzuurmetabolisme en de capaciteit van de mitochondria (energieproducerende organellen) tot oxidatief metabolisme, werden verschillende resultaten in de verschillende studies gezien. Er werd getoetst of het type model - bij ieder model is de drukbelasting op een andere manier tot stand gebracht - mogelijk van invloed was op metabole veranderingen. Inderdaad werden er significante modelgerelateerde verschillen gezien betreffende het regulator gen *peroxisome proliferator-activated receptor gamma coactivator 1-alpha (PGC-1α)* en de mitochondriële capaciteit. De duur van de drukbelasting bleek van invloed op de genexpressie van carnitine palmitoyltransferase 1B (CPT1B) (betrokken bij mitochondriële vetopname) en PGC-1α (regulator van oxidatief vetzuur metabolisme en mitochondriële content). Dit hoofdstuk benadrukt dat het vetzuur- en het oxidatieve glucose metabolisme in de rechter hartkamer afhankelijk zijn van meerdere factoren dan alleen drukbelasting. Het verder in kaart brengen van de gebruikte modellen en geïncludeerde patiënten, en standaardisatie van onderzoeksmethoden zijn essentieel om valide uitspraken te kunnen doen over metabole veranderingen in de drukbelaste rechter hartkamer.

Zo karakteriseerden wij in **hoofdstuk 4** het verloop van verschillende histologische, functionele en metabole veranderingen door de tijd (na twee, vijf en twaalf weken) in een ratmodel van toegenomen rechter hartkamer drukbelasting ten gevolge van een longslagaderbandje. Naast de expressie van genen betrokken bij metabolisme en de mitochondriële capaciteit, beoordeelden we de aanwezige vetten in de drukbelaste rechter hartkamer ten opzichte van een onbelaste rechter hartkamer. Na twaalf weken drukbelasting, waarbij er sprake was van rechter hartkamer dysfunctie, observeerden we toegenomen oxidatieve capaciteit voor glucose en onveranderde oxidatieve capaciteit voor vetzuren. Tegelijkertijd was er sprake van een afname van meervoudig onverzadigde vetten, inclusief afname van tetralinoleoyl cardiolipine. Tetralinoleoyl cardiolipine is onderdeel van de binnenste mitochondriële membraam en speelt een essentiële rol in de oxidatieve functie. Deze studie suggereert dus dat tekortkoming van meervoudig onverzadigde vetzuren voorafgaat aan vermindering van mitochondriële functie en klinisch rechter hartkamer falen.

Er is sprake van toegenomen suikeropname en glycolyse in het geval van rechter hartkamer drukbelasting zonder tekenen van klinisch rechter hartkamer falen.

In **hoofdstuk 5** presenteren we een protocol waarin we de methode van het aanleggen van het longslagaderbandje en de beoordeling van de functie en morfologie van beide hartkamers middels 'cardiac magnetic resonance imaging' in muizen beschrijven. Dit protocol is toegepast in hoofdstuk 6 en 7.

De vermindering van meervoudig onverzadigde vetzuren, in het bijzonder tetralinoleoyl-cardiolipine, gaat vooraf aan de vermindering van mitochondriele functie en klinisch rechter hartkamer falen.

De processen die betrokken zijn bij celgroei en zijn toegenomen in drukbelasting (hoofdstuk 2), omvatten veelal hypertrofie (verdikking) van de hartspiercellen. Dit houdt in dat er celvergroting plaatsvindt waarmee gepoogd wordt te compenseren voor de toegenomen druk op de hartspier. Bij aanhoudende belasting wordt deze respons pathologisch; dit leidt tot disfunctioneren van de hartkamer. In **hoofdstuk 6** onderzochten we in een muismodel met drukbelasting van de rechter hartkamer het calcineurin/nuclear factor of activated T cells (NFAT) signaleringssysteem, wat in de linker hartkamer een pathologische rol speelt bij hypertrofie. Hierbij bestudeerden we de rol van *microRNA 199b* en *NFAT kinase dual-specificty-tyrosine-(Y)-phosphorylation (Dyrk1a)*, welke beide beschreven zijn als activators van het calcineurin/NFAT signaleringssysteem in de linker hartkamer. Er werd een

opregulatie gezien van *microRNA 199b* in de drukbelaste rechter hartkamer, welke negatief correleerde met de rechter hartkamer functie. Hoewel er activatie optrad van het calcineurin/NFAT signaleringssysteem in drukbelaste rechter hartkamer, bleek dit onafhankelijk plaats te vinden van de genexpressie van *microRNA 199b* en *Dyrk1a*. Een opvallende bevinding was dat in het geval van drukbelasting van de rechter hartkamer ook opregulatie van *microRNA 199b* in de linker hartkamer plaatsvond. Bovendien vond er hierbij wel remming van *Dyrk1a* plaats, conform eerdere bevindingen in studies naar de drukbelaste linker hartkamer. Hiermee benadrukt dit hoofdstuk de ongelijkheid van de regulatoire processen in de rechter en linker hartkamer van hypertrofie ten gevolge van rechter hartkamer drukbelasting.

Opregulatie van microRNA 199b is geassocieerd met verminderde rechter hartkamerfunctie in de drukbelaste rechter hartkamer.

De verschillen ten aanzien van rechter versus linker hartkamer hypertrofie, worden verder uitgewerkt in **hoofdstuk 7**. Hierbij wordt ingegaan op transcriptie factor *heart and neural crest derivatives expressed 2 (Hand2)*. In eerdere studies bleek verminderde expressie van *Hand2* in experimentele diermodellen tot doodgeboorte te leiden vanwege uitblijvende rechter hartkamer ontwikkeling. In patiënten met specifieke aangeboren hartafwijkingen bleek *Hand2*-expressie verminderd te zijn. Echter, in het kader van drukbelasting draagt toegenomen *Hand2*-expressie in de linker hartkamer bij aan pathologische hypertrofie, fibrose en hartkamer dysfunctie, terwijl verminderde *Hand2*-expressie deze processen afzwakt. Opvallend genoeg toont onze studie in de drukbelaste rechter hartkamer tegenovergestelde resultaten, waarbij remming van *Hand2* leidt tot toename van rechter hartkamer remodellering en verminderde functie. Deze studie toont aan dat *Hand2* na zes weken rechter hartkamer drukbelasting geen significante bijdrage levert aan de regulatie van reeds bekende genen die betrokken zijn bij hypertrofie, fibrose en angiogenese. Daarentegen identificeerde we met behulp van RNA sequencing veranderingen op genniveau die betrokken zijn bij de regulatie van transcriptie en celadhesie, die op hun beurt processen als hypertrofie, fibrose en angiogenese via andere genen reguleren. Verder onderzoek zal meer inzicht moeten geven in de betrokken signaleringsprocessen en het effect van deze genen op eiwitniveau.

Expressie van transcriptefactor Hand2 in de rechter hartkamer is nodig om weerstand te kunnen bieden aan toegenomen rechter hartkamer drukbelasting.

In **hoofdstuk 8** onderzochten we acht verschillende biomarkers in het bloed van 125 kinderen met een aangeboren hartafwijking of pulmonale hypertensie. Deze biomarkers zijn afgeleiden van processen zoals hypertrofie, fibrose en inflammatie, inclusief oxidatieve stress, en werden gerelateerd aan hun echocardiografische parameters. De profielen van de biomarkers tussen de verschillende soorten van

rechter hartkamerbelasting (druk, volume of gecombineerd) toonden grotendeels hetzelfde patroon, al waren de bloedwaarden in patiënten met een drukbelaste rechter hartkamer hoger dan in patiënten met een volume belaste rechter hartkamer. Dit onderzoek liet ons zien dat *N terminal- pro hormone brain natriuretic peptide* en *endotheline-1* in staat zijn drukbelasting te identificeren, dat *mid-regional pro-adrenomedullin*, *growth differentiation factor-15* en *myeloperioxidase* mogelijk in staat zijn vroege remodelleringsproccesen van de rechter hartkamer te herkennen en dat *high sensitive troponine* juist kan dienen als marker voor ernstige druk en ernstige remodellering.

Dit proefschrift onderstreept de verschillen, en tegelijkertijd het samenspel, tussen de rechter en linker hartkamer, waarbij de processen geïdentificeerd in de linker hartkamer niet een-op-een te vertalen zijn naar de rechter hartkamer. Dit betekent dat processen van adaptatie geïdentificeerd in de linker hartkamer, ook bestudeerd moeten worden in de rechter hartkamer. Daarnaast laat dit proefschrift zien dat metabole processen afhankelijk zijn van het gebruikte experimentele model en mogelijk dus ook de etiologie van de onderliggende ziekte. Onze bevindingen benadrukken het dynamische karakter van metabole processen, wat standaardisatie van experimentele modellen cruciaal maakt om robuuste conclusies te kunnen vormen. Ook laat dit proefschrift zien dat het in kaart brengen van het intracardiale vetprofiel zou kunnen bijdragen aan de identificatie van vroege ziekte van de rechter hartkamer. Tot slot doen we een voorzet voor het toekomstige gebruik van multi-biomarker bepalingen bij het herkennen van abnormale belasting en remodelleringsprocessen van de rechter hartkamer in kinderen met aangeboren hartafwijkingen. Alles tezamen genomen komt dit proefschrift tegemoet aan de vraag van verschillende 'scientific statements' om de kennis ten aanzien van de abnormaal belaste rechter hartkamer te vergroten, met als doel bij te kunnen dragen aan een gerichte behandeling die aangrijpt op rechter hartkamer specifieke processen.

ABOUT THE AUTHOR

Anne-Marie Koop was born in Houten, the Netherlands on the 7th of September 1990. In 2008, after finishing secondary education (Nature & Health) at the St. Bonifatius college in Utrecht, she started studying Biomedical Sciences at the University of Amsterdam. After obtaining her propodeuse, Anne-Marie was admitted by selection to study Medicine at the University of Groningen. During the second and third year of her bachelor, she was representative for students studying medicine, dentistry and human movement sciences as a student-member of the board of University Medical Center Groningen. During her studies she continued to participate actively in several local and national education and research committees. Since completing her bachelor in 2012, Anne-Marie started her research under guidance of professor R.M.F. Berger at the department of pediatric cardiology of the Beatrix Children's Hospital (University Medical Center Groningen), focussing on right ventricular adaptation. After her junior in Groningen and senior clerkships in Deventer, Anne-Marie was accepted for the MD-PhD program and started to extend her research in the end of 2015. Her research activities were interrupted by the junior residency which she performed in the department of pediatric cardiology and thoracic surgery in the Wilhelmina Children's Hospital in Utrecht and the department of cardiology of St. Antonius hospital in Nieuwegein in the summer of 2017. One year later Anne-Marie started working as medical doctor at the cardiology department of the Noordwest Ziekenhuisgroep in Alkmaar, which was followed by her work at the cardiology department of the Erasmus Medical Center in Rotterdam. In summer 2020, Anne-Marie finished her thesis.

ACKNOWLEDGEMENTS

Een proefschrift schrijven doe je niet alleen. Met hulp en aanmoediging van velen is het eindresultaat nu daar!

Prof. dr. Berger, beste Rolf, ik wil je bedanken voor de aanmoediging en je enthousiasme de afgelopen jaren, en het onuitputtelijke streven naar het beste resultaat. Tijdens dit onderzoekstraject heb ik altijd mijzelf kunnen zijn en hebben we in alle openheid kunnen samenwerken. Je weet jonge onderzoekers te motiveren en hen zoveel mogelijk hun eigen pad te laten uitstippelen. Ik bewonder je gedrevenheid en energie waarmee je, ondanks je overvolle agenda, wetenschap en klinische zorg (niemand komt aan jouw patiëntenzorg!) naar een hoger plan blijft tillen!

Dr. Silljé, beste Herman, wat fijn dat ik altijd een beroep heb kunnen doen op jouw expertise in het experimentele onderzoek en jouw Groningse nuchtere kijk op mijn experimenten en studies. Onze overleggen leidden altijd tot concrete plannen en gaven weer een stevige zet in de goede richting. Ontzettend veel dank voor je pragmatische inzet en nuttige bijdrage aan dit proefschrift. Het heeft mij heel erg geholpen!

Dr. Bartelds, beste Beatrijs, samen trapten we enkele jaren geleden dit onderzoekstraject af. Door jouw tussentijdse vertrek naar het Erasmus MC verliep de begeleiding anders dan gepland. Desondanks heb ik veel kunnen leren van je scherpe feedback op stukken en presentaties. Je kwaliteiten ten aanzien van interpreteren en overbrengen van resultaten zijn indrukwekkend, evenals de hoeveelheid parate kennis die jij hebt ten aanzien van de beschikbare literatuur. Dit heeft zeker geholpen de verschillende manuscripten extra kracht bij te zetten. Dank!

Dr. Koonen, beste Debby, wat fijn dat Beatrijs jou vlak voor aanvang voor mijn sollicitatie van dit MD-PhD traject toevalligerwijs trof! Het heeft geleid tot een mooi onderzoeksvoorstel en een hele fijne samenwerking. Dank voor je grote betrokkenheid en support tijdens de experimenten van het geplande project. Jij liet mij optimaal gebruik maken van de faciliteiten die jullie laboratorium kent en jouw contacten in den lande. Jouw inventieve ideeën, zoals de lipidomics, zijn onmisbaar gebleken!

Geachte leden van de leescommissie, prof. dr. Bogaard, prof. dr. Ebels en prof. dr. Kuipers, graag dank ik jullie voor het lezen en beoordelen van mijn proefschrift.

Professor Da Costa-Martins, dear Paula, although our first meeting and subsequent

collaboration came as a surprise for us both, it turned out to be a really nice surprise! I really appreciated our collaboration at distance with very nice catch-ups in Groningen, Maastricht and Paris. Working with you, as a professor in molecular biology, added very welcome new aspects to this thesis. I appreciate your honesty and integrity, and the way you guide your PhD students next to the busy job you have including all your teaching duties. Dank ook voor je oprechte interesse en openheid op persoonlijk vlak, dit maakt samenwerken met jou heel fijn!

Dr. Willems, beste Tineke, wat leuk dat wij op de valreep nog samen aan een stuk gewerkt hebben! Je betrokkenheid en kritische, maar enthousiaste verschijning op onze researchmeeting heb ik altijd erg gewaardeerd. Leuk dat beeldvorming middels CMR een steeds grotere rol inneemt binnen de Kindercardiologie, daar gaan vast nog heel veel mooie projecten uit voortkomen!

Professor Hillige, beste Hans, bedankt voor de methodologische en statische ondersteuning bij het biomarkerstuk.

Professor de Boer, beste Rudolf, dank voor de leerzame en realistische feedback tijdens PhD- en lunchmeetings. Je betrokkenheid bij het biomarkerstuk waardeer ik zeer.

Beste kindercardiologen van het Centrum voor Congenitale Hartafwijkingen, ook jullie wil ik bedanken voor jullie hulp en input voor de biomarkerstudie. Drs. Du Marchie-Sarvaas, beste Gideon, bedankt voor de hulp bij het ontwikkelen van onze muizen echocardiografie protocollen. Dr. Liem, lieve Eryn, al sinds mijn coschappen in Deventer heb je je opgesteld als mijn mentor, en ik weet – dit doe je niet alleen voor mij. Het voelde dan ook zo terecht dat ik jou de (democratisch gekozen) onderwijsprijs-nominatie mocht overhandigen. Je betrokkenheid als clinicus en opleider is bewonderingswaardig. Super leuk dat we als bekroning (binnenkort) een gezamenlijke publicatie hebben!

Beste Annemieke, Michel en Bianca, dank voor het uitvoeren van al de operaties op onze ratten en muizen, en de bereidheid tot zo nu en dan overname van zorg voor de dieren. Het feit dat jullie altijd zo laagdrempelig te benaderen waren, heeft veel onnodige stagnatie voorkomen. Heel fijn!

Beste Kees, dank voor je grote betrokkenheid bij de CMR studies in muizen. Dankzij jouw bereidheid tot flink door- en overwerken hebben we in korte tijd veel werk kunnen verzetten. Dank voor het intensief meedenken over hoe 'de muizen-RV' het beste in beeld te brengen was, wat zelfs heeft geresulteerd in publicatie van ons protocol.

Beste analisten van het laboratorium kindergeneeskunde, in het bijzonder Niels,

Daphne, Mirjam en Albert, bedankt dat ik altijd welkom was voor mijn analyses, dat ik altijd antilichamen en primers kon komen halen, en natuurlijk bedankt voor jullie hulp. Albert, jij hebt mij met veel geduld de basisbeginselen van metabolisme en de Oroboros bijgebracht. Aan jouw wijze woorden "gewoon doorgaan" heb ik veel gehad dit traject.

Beste analisten van de experimentele cardiologie, Janny, Silke, Inge, Marloes, Martin, en Reinier, bedankt voor jullie hulp en expertise de afgelopen jaren! En last but not least in dit rijtje, onze eigen analist van de kindercardiologie, Tom. Dank voor al je hulp! Onmisbaar voor ons als onderzoekers. We vroegen jou een all-rounder te zijn en hebben de lat zeker niet laag gelegd. Hopelijk heb ik je niet te veel stress bezorgd met het brede spectrum aan analyses. Gelukkig wist je altijd in (bijpassende) stijl te performen, waarbij de Western (met snor en cowboyhoed) toch wel de kroon spande.

Beste Monique, dank voor al je hulp bij het inplannen van de vele afspraken en logistieke adviezen bij de klinische studies!

Collega's van de experimentele cardiologie, een dynamische groep mensen, die hebben bijgedragen aan de stimulerende omgeving op de 4e etage van 3215. Iedereen bedankt voor de fijne samenwerking, in het bijzonder Martijn en Nils die als nestors zowel de goede sfeer als de experimentele activiteiten bewaken. Thomas, bedankt voor je hulp bij muizen MRI's. Lawin en Janneke, het was een feest om met jullie een van de *Wie is de Mol?* edities voor de promovendi van de cardiologie neer te zetten: tot in details uitgedachte spellen in het casino, bioscoopzalen, en het FC Groningen stadion – niets was te gek! Mooi om te zien dat we elkaar vonden in ons perfectionisme, wat blijkbaar verder gaat dan onderzoek alleen. Ook de overige collega's van de klinische tak, dank voor alle gezelligheid op de borrels en social events.

Dan de groep promovendi en studenten van de kindercardiologie, in het bijzonder Menno, Reinout, Djoeke, Willemijn, Mark-Jan, Diederik, Lysanne, Guido, Floris-Jan, Graziella, Quint, Sanne, Marlies, Sophie, Johan, Karel en Shari, dank voor de super fijne en gezellige samenwerking. Diederik, Guido, Quint en Johan, boys van de Rechterkamer, hoewel het soms intens was, zeker gedurende the Christmas Room of the Year periode, had ik het voor geen goud willen missen!

Died, met bewondering kijk ik naar jouw researchactiviteiten en de ontspannenheid waarmee je deze uitvoert. Er valt op verschillende fronten veel van jou te leren. Dank voor je hulp bij verschillende teksten en de interessante samenwerking aan de off-spin van een van jouw projecten, die dit boekje helaas niet meer heeft gehaald. To be continued?!

Guido, met jou samenwerken is eigenlijk gewoon plezier maken. Jij zorgde dat de bergen zwaar (en regelmatig saai) werk, licht werden – met of zonder een door jou gemaakte macro. Dank voor de wijze lessen die jij mij bijbracht en de bergen relativering die je af en toe op m'n bureau wist te storten op momenten dat ik dat zo hard nodig had. Patiëntjes en hun ouders mogen in hun handen knijpen met jou als dokter!

Quint, een fijne collega en vriend met vele talenten! Dank voor je hulp op verschillende essentiële momenten. Het begon al in 2015 met het inleveren van mijn MD-PhD aanvraag toen ik zelf voor coschappen in Zuid-Afrika was en we elkaar nog niet eens kenden, tot aan de laatste fase van dit traject waarin je me verschillende malen een duwtje in de rug hebt weten te geven. Wat heerlijk dat we nu allebei de eindstreep hebben gehaald. Op naar ons volgende doel!

Lieve Marlies, ik bewonder je om je professionaliteit en de precisie waarmee je alles doet. Onze samenwerking aan de biomarkerstudie liep dan ook gesmeerd. Ik ga de vele gezellige en toch ook doortastende telefoongesprekken missen!

Ook dank ik graag de verschillende collega's, cardiologen en arts-assistenten die ik tijdens mijn klinische werkzaamheden naast mijn promotietraject in het Noord West Ziekenhuisgroep in Alkmaar en het Erasmus Medisch Centrum in Rotterdam ben tegengekomen. Velen van jullie hebben mij weten te inspireren en te motiveren.

Mijn lieve familie, dank voor jullie interesse en de support die jullie mij op verschillende manieren hebben gegeven. Soof, thanks voor je hulp en bemoedigende woorden op verschillende belangrijke momenten. Tabitha, mijn 'grote' nicht, afgelopen jaar heb ik op verschillende manieren ervaren wat voor effect timing kan hebben: wij begin september 2019 samen op congres naar Parijs was daar een fijn voorbeeld van. Dank voor je luisterend oor, al de gezelligheid en being my biggest cheerleader. Je bent een groot voorbeeld in het verleggen van je grenzen en het altijd 'aiming for the best'!

Mijn oudste vriendinnetjes, Eef, Fred, Ge, Ims, Lies, Roos en Will (oftewel Chix United a.k.a. de chicks, hoe we onszelf met enige gêne nu toch al 15 jaar noemen), oud en vertrouwd, van wie ik enorm van kan genieten. Dank dat ik af en toe stoom bij jullie kon afblazen, waarna we vervolgens weer ouderwetse gezelligheid beleefden, en ik altijd voor alles bij jullie terecht kan. ♥

JC Royaal, "een grote diverse club", hoe we dat mooi wisten te verkopen in 2009. Dank voor alle gezellige momenten als afwisseling tussen het studeren en werken door de afgelopen tien jaar. Jullie weten hoe erg ik daar van kan genieten! Lieve Em,

dank voor je luisterend oor en wijze adviezen. Mijn clubbies uit de Riviera, Alex, Anne, Milou, Pi, en Sas, en jullie vriendjes, hoewel onze hechte vriendschap misschien topografisch bepaald leek te zijn, bewijzen we nu dat het niet zo is. Zoveel dank voor jullie steun, met bijzonder groot inlevingsvermogen, en alle lieve en gezellige acties voor elkaar, waar we zo goed in zijn. Ik ben zo nieuwsgierig hoe de komende jaren er voor ons uit gaan zien, ik kan niet wachten!

Ewout, jij mag niet ontbreken in deze lijst – oorspronkelijk mijn maatje binnen de groep faculteitsbestuurders en de academische raad, en door de jaren heen een hele waardevolle vriend. Nog steeds weet jij gesprekken keer op keer weer tot een hoger niveau te tillen met al je kennis, enthousiasme en oneindige integriteit. Dank voor je support, altijd!

OOTB. Out of the box. Dat waren we, en zijn we nog steeds (nu zelfs met vier meiden extra). Lieve Lau, Moo, Annetje, Milou en Kir, zo trots ben ik op ons hoe we het altijd op onze eigen manier doen en hoe we elkaar daarin gevonden hebben en steunen. Met jullie samenwonende was "work hard, play hard" één groot feest!

Cor en Floor! Hoewel we elkaar amper kenden, wisten we zeker dat we samen moesten wonen in Deventer. Het delen van verschillende hoogte- en verdrietige dieptepunten heeft onze vriendschap alleen maar sterker en waardevoller gemaakt. Dank voor jullie support al vanaf de eerste fases van mijn onderzoek, inclusief de sollicitatie voor dit MD-PhD traject - van Deventer tot in Zuid-Afrika!

Dan mijn lieve paranifmen, Sophie en Willemijn. Soof, wij wisselden onze coschappen en onderzoeksperioden, en dus ons bureau in de Rechterkamer, af. Zo liet de echte vriendschap zoals we die nu hebben nog even op zich wachten. Dat we het afgelopen jaar enkele maanden samen in Rotterdam en in het Erasmus MC hebben doorgebracht, is voor mij van ongekende betekenis geweest. Je bent een mooi mens (hoe jij dat zelf over anderen zou kunnen zeggen), van wie zoveel valt te leren en met wie zoveel te beleven valt. Dank voor alles! Will, onze medische carrière trapten wij eigenlijk samen af met ons profielstuk "de medische casusbeschrijving", waarna we samen via een omweggetje via onder andere de Universiteit van Amsterdam, via decentrale selectie in Groningen terecht kwamen. Het allebei in Amsterdam wonen en het promoveren heeft onze vriendschap des te sterker gemaakt. Dank voor alle gezelligheid die jij overal brengt, de eindeloze gesprekken en de spreekwoordelijke spiegels. Op naar heel veel fijne borrels waarbij we filosoferen over onze toekomst!

Last but not least, pap, mam en Pieter. Lieve Piet, ik ben zo trots op hoe je je de afgelopen jaren hebt ontwikkeld tot wie je nu bent. Geniet van wat je allemaal bereikt hebt! Lieve papa en mama, ik weet niet hoe ik jullie genoeg kan bedanken. Jullie doen de term 'onvoorwaardelijk' eer aan. Dank voor alle momenten die jullie de afgelopen dertig jaar voor mij klaar hebben gestaan. Bij elk nieuw ambitieus plan of elke (logistieke) uitdaging dachten jullie mee en faciliteerden waar nodig. Ik realiseer me maar al te goed dat dit geen vanzelfsprekendheid is, net zoals de fijne basis, al jullie mooie waarden, wijze lessen en motivatie die jullie Pieter en mij hebben meegegeven. Ik hou van jullie.